DISSERTATION

EVIDENCE FOR A BIOLOGICAL CONTROL ON EMISSIONS OF MARINE ICE NUCLEATING PARTICLES: LABORATORY, FIELD AND MODELING RESULTS

Submitted by

Christina Song McCluskey

Department of Atmospheric Science

In partial fulfillment of the requirements

For the Degree of Doctor of Philosophy

Colorado State University

Fort Collins, Colorado

Fall 2017

Doctoral Committee:

Advisor: Sonia M. Kreidenweis
Co-Advisor: Paul J. DeMott

Jeffrey L. Collett
Jeffrey R. Pierce
Donald L. Mykles

ABSTRACT

EVIDENCE FOR A BIOLOGICAL CONTROL ON EMISSIONS OF MARINE ICE NUCLEATING PARTICLES: LABORATORY, FIELD AND MODELING RESULTS

Numerical models poorly represent cloud phase (liquid or ice) partitioning in high latitude regions, resulting in uncertainties in climate sensitivity estimates. Over the last decade, new observations have revealed that supercooled liquid clouds are unexpectedly abundant over the Southern Ocean, compared with midlatitudes, leading to large hemispheric biases in radiation budget estimates in models that assume the incorrect phase is present. One hypothesis for the persistence of liquid clouds to low temperatures is a relative absence of sources of ice nucleating particles (INPs), particles required for the first freezing of supercooled liquid water droplets at temperatures between 0 ˚C and -38 ˚C. Sea spray aerosol (SSA) generated by bubble bursting at the ocean surface is a main source of particles in the remote marine boundary layer over oceans. Since soluble sea salt is not active as an INP, it is hypothesized that marine organic aerosol components arising from oceanic biological activity serve as the only local potential source of INPs in regions such as the Southern Ocean. However, knowledge regarding marine-derived INP abundance, composition, and production mechanisms is limited. Laboratory, field, and modeling studies were used to (1) confirm the hypothesized source of marine INP emissions associated with marine organic aerosol that arises from elevated oceanic biological productivity; (2) identify marine INP compositions and their activation temperatures; (3) determine the natural abundances and variability of the number concentrations of marine INPs (n_{INPs}); and (4) evaluate the current best model estimates of marine INPs against new observations.

Observations of seawater biology, aerosol composition and ice nucleation ability of bulk seawater, the sea surface microlayer (upper 50 μm of the ocean surface), and laboratory-generated SSA during simulated phytoplankton blooms revealed that emissions of INPs active at temperatures warmer than -22 °C increased during the decay of two phytoplankton blooms. Enrichment of organic matter in the sea surface microlayer and its subsequent control on transferring organic material into the aerosol phase was found to be an important factor in the release of INPs from the ocean surface. Integration of all size and compositional analyses led to two proposed classes of marine INPs: (A) ice nucleation active molecules and (B) ice nucleation active intact or fragmented microbes (e.g., diatoms or bacteria).

To investigate marine INPs present in nature, several field campaigns were carried out over oceans and at two remote coastal sites. Regarding their abundance and variability, the number concentrations of ice nucleating particles, n_{INPs}, active at temperatures warmer than -30 ˚C, ranged over three or more orders of magnitude at any particular temperature for samples collected in the marine boundary layer during six research voyages over the Pacific Ocean, spanning 70 ˚S to 60 ˚N over various seasons. n_{INPs} were greater and more variable in the Northern Hemisphere compared to the Southern Hemisphere. Factors that contributed to this variability were investigated in detail at a North Atlantic Ocean coastal site (Mace Head Research Station, MHD) and over the Southern Ocean (SO). At MHD, normalizing observations by aerosol surface area and limiting measurements to pristine marine air masses narrowed the variability in n_{INPs}. That subset of data was used to develop a parameterization for INPs in pristine sea spray organic aerosol over the North Atlantic Ocean. Higher n_{INPs} active at temperatures warmer than -22 °C were observed in pristine SSA during a period that was influenced by organic aerosol arising from offshore biological activity. The INPs observed

during this event comprised ice nucleation active microbes (marine INP class B), which were distinct from other marine organic INPs at MHD. These observations indicate that further research is required to incorporate the microbe INP type into parameterizations. Measurements of INPs in the SO marine boundary layer aerosol and in seawater samples were the first in this region in over four decades. Observed n_{INPs} were a factor of 100 lower than those historical measurements. n_{INPs} observed over the SO were less variable than MHD and INP composition included refractory, heat-stable organic (marine INP class A), and heat-labile materials (marine INP class B). These data serve as new observational constraints on n_{INPs} and their sources and compositions that can be applied to evaluate numerical modeling studies.

The database from this work was used in an exploratory study to evaluate current modeling approaches for predicting marine INPs. Simulations with the atmospheric component (CAM5) of the Department of Energy Community Earth System Model with implementation of a physically-based parameterization for sea spray organic aerosol were conducted for the MHD and SO study periods. Modeled aerosol mass, number and composition were used as input for two marine INP parameterizations that have been developed since the beginning of this work (circa 2014). Findings indicated that, for INPs active at -15 °C during the MHD study period, observed n_{INPs} were bounded by estimates derived from the two marine INP parameterizations. Periods with discrepancies between modeled estimates and observed n_{INPs} were explained by observational evidence that different classes of marine INPs were present at MHD, further supporting the need for additional studies regarding the emissions of different marine INP classes. Different INP types (e.g., marine organic, mineral dust) are active at different temperatures and the observations from this work clearly indicate that organic aerosol is an important factor for determining marine n_{INPs}. Thus, further evaluation of these parameterizations

for INPs active at a range of temperatures (0 to -27 °C) and against measurements over the Southern Ocean, where sea spray organic aerosol production may be quite different from other regions, will be conducted in the future with these simulations. This deeper analysis may reveal underlying limitations of the parameterizations and provide insights on how to further refine numerical representations of INPs in regional and global models.

ACKNOWLEDGEMENTS

I first want to acknowledge Drs. Paul DeMott and Sonia Kreidenweis, who have cultured a graduate student experience that has directed me towards a career in studying aerosol-cloud-interactions. I want to thank them for their support and encouragement in my participation in numerous field projects, conferences, and workshops, which has fostered countless professional connections in my scientific community. Most importantly, they are exceptional role models for how to advance scientific knowledge, which has been invaluable to my graduate training. It has been an absolute privilege to have their guidance in navigating the challenges that have been encountered in this work and to be in the presence of their passionate pursuit of sound science.

I would also like to extend a special thank you to my committee members, Drs. Jeffrey Collett, Jeffrey Pierce and Donald Mykles, for the productive conversations and suggestions in the work reported in this dissertation. I extend substantial gratitude to the Kreidenweis research group, past and present, for scientific conversations, support and encouragement. In particular, I would like to thank Drs. Thomas Hill, Ezra Levin, Anthony Prenni, and Gavin McMeeking for training me on numerous instruments. These members in addition to Drs. Kaitlyn Suski, and Gregory Schill have also provided invaluable contributions to my scientific and professional development. I would like to thank Sam Atwood and Dr. Bonne Hotmann for graciously taking the time to help me learn Python, which was critical for completing this work. Finally, I would like to thank the outstanding administrative staff in the CSU Department of Atmospheric Science for their support during field campaigns, conference meetings, and more: Shannon Irey, Annette Foster, Darby Nabors, Jaime Joseph, Jaime Schmidt and Heather Packard.

I would like to acknowledge the Center for Aerosol Impacts on the Chemistry of the Environment (CAICE), lead by Drs. Kimberly Prather and Vicki H. Grassian, for the resources and support to facilitate innovative experiments that are a substantial portion of the work presented in this dissertation. I would like to thank Drs. Paul DeMott, Thomas Hill, Francesca Malfatti and Camille Sultana, who were major contributors to the scientific findings that emerged from the CAICE experiments. Thank you to all of the CAICE graduated students, postdocs and principle investigators for the many scientific meetings and discussions. A special thanks is given to Dr. Doug Collins, Dr. Camille Sultana and Christopher Lee for leading the mesocosm experiments at the University of California – San Diego. Various CAICE research teams and the Scripps Institute of Oceanography hydraulics laboratory staff contributed to the organization and data collections during the phytoplankton bloom experiments. Finally, the laboratory studies were supported by CAICE (CHE-1305427), which is a National Science Foundation Center for Chemical Innovation.

I would like to thank Dr. Colin O'Dowd for extending an invitation to participate in measurements conducted at the Mace Head Research Station (MHD) in collaboration with the BACCHUS organization. Drs. Jurgita Ovadnevaite and Darius Ceburnis were critical in organizing the MHD project, including useful scientific discussions and logistical support. I also would like to acknowledge Dr. James Atkinson, Dr. Matteo Rinaldi, and Kirsten Folsom for their data contributions that were important contributions to the discoveries made at MHD. Jake Zaragoza and Anne Marie Rauker are also acknowledged for their very appreciated contributions to the ice spectrometer analyses. I also thank the principal investigators involved in this study, including Drs. Paul DeMott, Sonia Kreidenweis, Colin O'Dowd, Cristina Facchini, Benjamin Murray, Zamin Kanji, and Ulrike Lohmann. Travel for this project was supported by an

ACCESS travel award, granted by the CSU Department of Atmospheric Science. The research conducted at MHD received partial funding from the European Union's Seventh Framework Programme (FP7/2007-2013) project BACCHUS under grant agreement no. 603445 and the CNR (Italy) under Air-Sea Lab: Progetto Laboratori Congiunti.

For my explorations in the Southern Ocean, I want to acknowledge Dr. Alain Protat for inviting us to participate in CAPRICORN and for his enthusiastic leadership before, during and after the research voyage. I want to thank Dr. Ruhi Humphries for coordinating and accommodating many needs required for our scientific equipment. Several people helped to make this project possible, including Dr. Sebastian Moreau, Dr. Ian McRobert, Stephen Thomas, Will Ponsonby, Ben Baldwinson, Tegan Sime, Leigh Roberts, Dr. Petter Strutton, and the RV-Investigator Crew Members. Finally, I want to thank all of the voyage participants for the discussions and friendships that made this project incredibly beneficial scientifically, professionally and personally.

The modeling project that serves as the final chapter of this dissertation is in large part due to Dr. Susannah Burrow's passionate stance on collaborations between laboratory, field, and modeling scientists. Her willingness to allocate her time to train me on how to utilize the atmospheric component of the DOE Community Earth System Model as a scientific tool has been greatly appreciated. I would like to thank the Department of Energy Office of Science Graduate Student Research Program for providing the financial resources to make this project possible.

Finally, I want to thank my loving family and friends for their support and encouragement over the many years.

TABLE OF CONTENTS

ABSTRACT ii

ACKNOWLEDGEMENTS vi

CHAPTER 1: INTRODUCTION TO THE DISSERTATION 1

CHAPTER 2: SCIENTIFIC APPROACH 9

Section 2.1 Mesocosm laboratory study experimental details 10

2.1.a Sea spray aerosol generation in the laboratory 10

2.1.b Mesocosm biological conditions 11

Section 2.2 Overview of Field Study Experimental Details 13

2.2.a CalWater-2015 14

2.2.b Ship observations over the Pacific Ocean 15

2.2.c Mace Head Research Station (MHD) 16

2.2.d Southern Ocean/ CAPRICORN 17

Section 2.3 OCEANFILMS model preliminary comparison 18

Section 2.4 Instrumentation 20

2.4.a Measurements of ice nucleating particle number concentrations 22

2.4.a.i Continuous Flow Diffusion Chamber 22

2.4.a.ii Ice Spectrometer 28

2.4.a.iii Other ice nucleation measurement techniques 31

2.4.b Probing the composition of ice nucleating particles 34

2.4.b.i Collection and analysis of ice crystal residuals 34
2.4.b.ii Determining composition and size of ice nucleating material 37
2.4.c Aerosol size distributions 38
2.4.d Aerosol Composition 40
2.4.d.i Aerosol time of flight mass spectrometry (ATOFMS) 40
2.4.d.ii Aerosol Mass Spectrometer 41
2.4.d.iii Bulk aerosol organic carbon 41
2.4.e Particulate mass concentrations (TEOM) 42
2.4.f Ocean Biological Activity 42
2.4.f.i Enzyme activities 42
2.4.f.ii Abundance of microbes 43
2.4.f.iii Chlorophyll a 43
2.4.f.iv Screening for presence of INA bacteria using DNA-based methods 43
2.4.g HYSPLIT back trajectories 45
CHAPTER 3: LABORATORY STUDIES 46
Section 3.1 Biology and aerosol composition during CAICE laboratory studies 46
3.1.a MART study (Jan 2014) 46
3.1.a.i Bulk seawater and sea surface microlayer biology during the MART study 46
3.1.a.ii Aerosol Composition during the MART study 47
3.1.b IMPACTS study (Jan 2014) 50
3.1.b.i Bulk seawater and sea surface microlayer biology during IMPACTS 50
3.1.b.ii Aerosol Chemistry 51

Section 3.2 Results from MART and IMPACTS laboratory experiments 53

3.2.a Trends in INP number concentration (indirect evidence for marine INP identity)... 53

3.2.a.i MART 53

3.2.a.ii IMPACTS 57

3.2.a.iii Summary of dynamics in n_{INPs} during MART and IMPACTS studies 59

3.2.b Ice nucleating entities in seawater and sea surface microlayer..... 60

3.2.c Contributions of heat labile material to aerosol INP populations 61

3.2.d Characteristics of ice crystal residuals..... 62

Section 3.3 Discussion..... 71

3.3.a Ice nucleating material during MART study 71

3.3.b Ice nucleating material during IMPACTS study 73

3.3.c Two classes of marine INPs..... 75

3.3.d Evaluating existing parameterizations with laboratory-generated nascent SSA 76

Section 3.4 Summary of laboratory studies 79

CHAPTER 4: MEASUREMENTS OF MARINE INPS IN THE FIELD..... 82

Section 4.1 Overview of INP measurements made over remote oceans and coastal regions 82

4.1.a Results and Discussions 82

4.1.a.i CalWater-2015 82

4.1.a.ii INPs over the Pacific Ocean 85

4.1.b Main findings and future work 86

Section 4.2 Marine and Terrestrial Organic Ice Nucleating Particles in Pristine Marine to Continentally-Influenced Northeast Atlantic Air Masses 89
4.2.a Project overview 89
4.2.b Results and Discussion 89
4.2.b.i Organic aerosol events during the campaign 89
4.2.b.ii INP population influences at MHD 92
4.2.b.iii Heat sensitivity and organic make up of INPs 98
4.2.b.iv Predicting marine INPs at MHD 103
4.2.c Summary 109
Section 4.3 Ice nucleating particles over the Southern Ocean 111
4.3.a Study overview/approach 111
4.3.b Results and Discussion 113
4.3.b.i INPs measured during CAPRICORN 113
4.3.b.ii Characteristics of INPs observed during CAPRICORN 120
4.3.b.iii Southern Ocean INP source potential 124
4.3.b.iv Characteristics of Southern Ocean seawater INEs 125
4.3.c Summary 126
CHAPTER 5: MODEL PREDICTION OF MARINE INPS 129
Section 5.1 Model and observation comparison of wind conditions and aerosol mass concentrations at MHD 129
Section 5.2 Estimating n_{INPs} from model output 132

Section 5.3 Overview of simulated aerosol and estimated n_{INPs} at MHD 135

Section 5.4 Future work 138

CHAPTER 6: SUMMARY 139

REFERENCES 146

APPENDIX I. ICE SPECTROMETER MEASUREMENT DETAILS 155

APPENDIX II. AEROSOL CONCENTRATOR FACTORS 164

APPENDIX III. FREEZING POINT DEPRESSION EFFECTS 165

APPENDIX IV. HYSPLIT BACK TRAJECTORIES 167

APPENDIX V. INSTRUMENTATION CONTACT INFORMATION 168

CHAPTER 1: INTRODUCTION TO THE DISSERTATION

Aerosol-cloud interactions serve as an important source of uncertainty in the scientific understanding of the Earth's climate system and of weather systems that govern hydrological budgets in many areas (e.g., the California Sierra Nevada Mountain range; *Creamean et al.,* 2013). One way that aerosols can impact cloud processes is via action as ice nucleating particles (INPs, *Vali et al.,* 2015). Atmospheric INPs are required for heterogeneous ice nucleation of supercooled liquid cloud droplets. This study focuses on the immersion freezing mode of INPs, which has been shown to act as the most important mode for mixed phase clouds (*de Boer et al.,* 2011; *Murray et al.,* 2012). INPs are often characterized by their temperature-dependent ice nucleation ability, quantified by their number concentration (n_{INPs}) or nucleation site density (n_s) (*Kanji et al.,* 2017). As recently summarized by *Kanji et al.* (2017), there are many sources of INPs, including mineral dusts, biological particles, organic-rich soil dusts and others, and n_{INPs} can range over several orders of magnitude even at one temperature depending on the aerosol concentration, composition and mixing state (e.g., field measurements of n_{INPs} range from approximately 10^{-4} to 10^{1} per L of air for INPs active at -20 °C, *Kanji et al.,* 2017).

The action of INPs in a cloud in concert with the Wegener-Bergeron-Findeisen process (*Pruppacher and Klett,* 1997) leads to rapid changes in cloud phase (liquid/ice) partitioning (e.g., *Verheggen et al.,* 2007), thereby altering the precipitation potential, lifetime and optical properties of mixed-phased clouds. Numerical models poorly represent these ice phase transitions in mixed phase clouds; for example, an evaluation of 19 global climate models by *McCoy et al.* (2015) found that the temperature in which ice and liquid were diagnosed to be equal (50% ice and 50% liquid) ranged over 35 °C. Numerical models' failures to match

observed cloud phase partitioning in high latitude clouds result in significant modeled energy biases that impact climate sensitivity estimates (*Tan et al.,* 2016). In an evaluation of models that contributed to the Third Coupled Model Intercomparison Project (CMIP3), model biases were attributed to too few and too short lived clouds (*Trenberth and Fasullo,* 2009). More specifically, *Kay et al.* (2016) reported that the CAM5 model (atmospheric component of the NCAR Community Earth System Model) produced too many ice clouds and too few supercooled liquid clouds when compared to satellite observations and these biases maximize over the Southern Ocean. High latitudes are dominated by oceans, particularity in the Southern Hemisphere, where a high prevalence of supercooled liquid clouds (*Huang et al.,* 2015) and an absence of known important INP sources, such as mineral dust (e.g., *DeMott et al.*, 2015), lead to aerosol-cloud interactions that are different from mid-latitude Northern Hemisphere regions where terrestrial INPs strongly influence ice phase transitions. State-of-the-knowledge (circa 2013) aerosol transport modeling studies including oceanic INPs indicated that biogenic INPs associated with sea spray aerosol (SSA) resulting from wave breaking and bubble bursting at the ocean surface were most likely to play an important role in determining INP populations over remote oceans at high latitudes (*Burrows et al., 2013*). Most importantly, their exploratory study brought to light the numerous gaps in the current knowledge of marine INPs (defined here as INPs associated with primary sea spray aerosol). Studies of marine INPs are also important for elucidating pre-industrial aerosol properties, which currently represent a major source of uncertainty for estimating aerosol climate forcing (*Carslaw et al.,* 2013). Investigations of ambient remote boundary layer aerosol and laboratory-generated SSA, reported by *DeMott et al.* (2016), revealed that the ice nucleating ability of SSA was a few orders of magnitude lower than terrestrial sources, further motivating investigations of the factors that determine the abundance of marine

INPs. Few studies have explored the types of particles that contribute to heterogeneous ice nucleation in clouds that occur in areas without or with limited terrestrial aerosol influences and the mechanisms that control emission rates of INPs from the oceans beneath them are largely unknown.

An extensive survey of INPs present in the marine boundary layer was reported by *Bigg* (1973), which included 3 years of ship-based filter collections of ambient aerosol samples over the Southern Ocean south of Australia and thermal diffusion chamber processing of these samples at water saturation. Research voyages occurred during all seasons and annual average n_{INPs} were reported, demonstrating nearly 3 orders of magnitude variability in averaged surface level n_{INPs} spatially (3 to 250 m^{-3} of air measured at T = -15 °C). *Bigg* (1973) suggested that the observed variability in n_{INPs} was associated with aerosol from distant continents arriving to the ocean surface, although the source regions remained unidentified. Later, *Schnell and Vali* (1976) recognized that the highest n_{INPs} reported by *Bigg* (1973) were co-located with ocean convergence and upwelling zones that were postulated to contain relatively high levels of ocean biological activity. *Schnell and Vali* (1976) also found higher INP number concentrations per volume of phytoplankton-rich seawater compared to seawater with little phytoplankton biomass and they ultimately proposed that biogenic INPs may be emitted from biologically active ocean waters (*Schnell and Vali*, 1976). Since these historical investigations of marine INPs, knowledge regarding the processes that govern SSA emissions, composition and ice nucleation activity has advanced greatly.

SSA is produced from film and jet droplets (*Blanchard,* 1963*; Blanchard and Woodcock,* 1957, *Wang et al.*, 2017) that form during bubble bursting at the ocean surface following wave breaking. Spume droplets have been observed in high wind speeds (>10 m/s), where a relatively

small number of massive droplets (droplet radii up to few hundreds of μm) are torn off the wave crest. Most studies neglect spume droplets, due to their short residence time and low number concentrations (*Exton et al.,* 1985). Many source functions intended to represent the generation of SSA have been derived based on wind speed (*Grythe et al.*, 2014), where higher number concentrations of SSA are associated with higher wind speeds. Other source functions use Reynolds number, which includes influences of wave height, wind history, surface friction velocity, and viscosity (*Ovadnevaite et al.,* 2014). The atmospheric lifetime of SSA is estimated to be seconds to days, since larger particles (particle diameter, $D_p > 5$ μm) are quickly removed from the atmosphere by deposition processes. Accumulation mode particles ($D_p \sim 100$ nm) are likely have the longest residence times, while the smallest particles are lost more quickly through diffusion and coagulation (*Grythe et al.,* 2014). Modeling studies by *Burrows et al.,* (2013) indicate that SSA could be important contributors to INP populations at cloud level, particularly for Southern Ocean clouds that cap the marine boundary layer (cloud tops below 3 km, *Mace et al.,* 2007).

Comprising both sea salts and organic matter, SSA is an aerosolized mixture of both seawater (SW) and the sea surface microlayer (SML, the upper 50 to 250 μm of the ocean surface; *Zhang et al.,* 1998, *van Pinxteren et al.,* 2017), whose compositions are investigated as major factors that govern SSA composition. Organic matter in SW and the SML includes particulate organic matter (POM) and dissolved organic matter (DOM). Here and throughout this work, POM (or particulate organic carbon, POC) and DOM (or dissolved organic carbon, DOC) are operationally defined following oceanographic literature conventions, where DOM is the material that which passes through a porous filter and POM is the material that is retained by the filter (typical pore size of 0.7 μm, *Kirchman*, 2008). DOM may include small particles and

colloids, while POM comprises phytoplankton (both living and detritus). DOM is the dominant form of organic matter in the oceans (ratio of DOM:living plankton is 200:1), storing 700 Gt of carbon (*Kirchman,* 2008). The SML can be enriched with both POM and DOM relative to SW (*Wurl et al.,* 2011; *Cunliffe et al.,* 2013) and enrichments of surfactants in SML compared to SW have been observed over a range of latitudes (50 ˚S to 50 ˚N) for wind speeds up to 13 m s^{-1} (*Sabbaghzadeh et al.,* 2017). The compositions of SW and SML are continuously evolving, where zooplankton, phytoplankton, bacteria, viruses, macrogels, macromolecules and colloidal constituents coexist and interact through many biochemical pathways as part of the microbial loop (*Ducklow*, 1983; *Azam et al.,* 1983). Variations in SW and SML compositions are particularly large during phytoplankton blooms, where phytoplankton grow in response to light availability, influenced by season and surface water mixing, and nutrient inputs (e.g., dust deposition). Changes in phytoplankton biomass are most commonly detected using Chlorophyll a (Chl *a*), a photosynthetic pigment found in phytoplankton (including cyanobacteria).

To study SSA composition, field and laboratory approaches have been utilized. Laboratory tools for SSA generation, including a wave channel, a plunging waterfall, and a glass frit, have permitted isolated studies of SSA during simulated phytoplankton blooms, which are induced by nutrient additions to natural seawater. Such studies have illustrated that SSA size distributions must be similar to natural SSA size distributions in order to accurately represent SSA composition and mixing state (*Collins et al.,* 2016). As summarized by *Gantt et al.* (2011), the organic mass fraction of submicron SSA has been shown to increase from less than 0.2 during low biologically productive periods (*Barker and Zeitlin,* 1972*; Oppo et al.,* 1999*; O'Dowd et al.,* 2004) to over 0.8 during high biologically active periods, characterized from Chl *a* concentrations (*Hoffman and Duce,* 1974*; O'Dowd et al.,* 2004*; Rinaldi et al.,* 2009*; Miyazaki*

et al., 2010). Fragmented or intact microbes have also been identified in SSA (e.g., *Pósfai et al.,* 2003*; Leck and Bigg,* 2007*; Patterson et al.,* 2016). Many variables control the transfer of organic species from the ocean surface to the aerosol; known parameters include the species solubility (*Cochran et al.,* 2016; *van Pinxteren et al.,* 2017), biological productivity and wind speed (*Gantt et al.,* 2011; *Rinaldi et al.,* 2013). A comparison between modeled estimates of sea spray organic mass fraction (factoring in wind speed and Chl *a*) against observations indicated that additional variables, such as bacteria counts or sea surface temperature, should also be considered as parameters that govern sea spray organic matter emissions (*van Pinxteren et al.,* 2017). The thickness, composition, and relevance of the SML for SSA composition remains an active area of research. Film droplets, formed by the bursting of bubble caps, have long been assumed as the main contributor to submicron sea spray organic matter and to be closely linked to the SML composition (e.g., *Burrows et al.,* 2013). However, recent experiments by *Wang et al.* (2017) illustrated that both film and jet drops contribute to submicron sea spray organic matter and that their contributions vary under different levels of biological productivity.

Following these advancements in SSA composition understanding and development of tools for studying SSA, both laboratory and field measurements have considered many non-sea salt constituents of SSA as possible contenders for heterogeneous ice nucleation. The surface of a marine diatom species, *Thalassiosira pseudonana,* (*Knopf et al*., 2011) as well as its organic exudates (*Wilson et al., 2015*) have been shown to promote freezing at conditions relevant for mixed-phase clouds (T > -38 °C). Regarding the size of INPs, *Rosinski et al*. (1987) concluded that ice-forming nuclei were likely carbonaceous, though not cellular, and smaller than 0.5 μm. *Schnell and Vali* (1976) report that ice-forming nuclei were approximately 1 μm and were heat labile (heating at 100 °C). *Wilson et al.* (2015) found that the ice nucleating entities (INEs)

within selected SML samples collected from the North Atlantic and Arctic (near Greenland) oceans during summertime were smaller than 0.2 μm and were positively correlated with TOC mass concentrations in the SML. *Irish et al.* (2017) also found that INPs in SML samples collected in the summertime from Canadian Arctic waters were smaller than 0.2 μm and that they were heat labile (i.e., proteinaceous). Studies of SSA generated in the laboratory during mesocosm experiments (i.e., simulated phytoplankton blooms) have also demonstrated that n_{INPs} in SSA increase in association with changes in biological activity (*Prather et al*., 2013; *Wang et al*., 2015, *DeMott et al.,* 2016). While these studies provide evidence that the emissions of INPs from oceans are in fact linked to biological activity, knowledge on the composition of marine INPs that are emitted during phytoplankton blooms and conditions that favor their release remains unclear. Additionally, observations of INPs in the ambient marine boundary layer (MBL) were limited to measurements made at least 30 years prior to the time in which the presented studies began. Little was known regarding the factors that control the variability in ambient marine INP number and composition, restricting advancements in scientific understanding of the global distribution of this potentially important INP source.

The overarching objectives of the work presented as part of this dissertation were to 1) confirm the hypothesized increase in marine INP emissions associated with nascent marine organic aerosol that arises from elevated oceanic biological productivity; 2) characterize nascent and ambient marine INP composition; 3) determine factors that are important for emissions of INPs from oceans; and 4) determine the natural abundances and variability of marine INPs using ambient measurements in the marine boundary layer. There are challenges involved with studying marine INPs. Low n_{INPs} that are associated with SSA require large sampling volumes and low detection limits. Additionally, terrestrial aerosol sources that are strong sources of INPs

relative to marine sources must be avoided in order to capture representative marine aerosol samples. These challenges were met with a series of laboratory mesocosm experiments and field observations in remote marine environments, presented in Chapters 2 and 3, respectively. The final theme utilizes field observations and knowledge gained from laboratory studies to evaluate global model simulations of SSA and, more specifically, sea spray organic matter used as input to estimate global distributions of marine organic INPs. The combined contributions offer key advancements in scientific understanding of immersion freezing marine INPs, with subsequent implications for improving numerical representation of aerosol cloud interactions occurring in mixed-phased clouds over high latitude ocean regions.

CHAPTER 2: SCIENTIFIC APPROACH

As summarized in Chapter 1, many factors may contribute to the production of marine ice nucleating particles (INPs), such as biological productivity, sea surface conditions, environmental conditions (e.g., wind speed) and atmospheric transport. Additionally, non-marine aerosol during collection of marine samples may easily bias measurements because terrestrial particles have been shown to nucleate ice more readily for a given surface area of aerosol compared to particles from oceanic sources (*DeMott et al.,* 2016). In consideration of these challenges, the scientific approach of this dissertation was to 1) investigate the identity and abundance of INPs in freshly emitted SSA during two laboratory mesocosm experiments (Section 2.1); 2) survey the abundance, variability and characteristics of natural marine INPs and

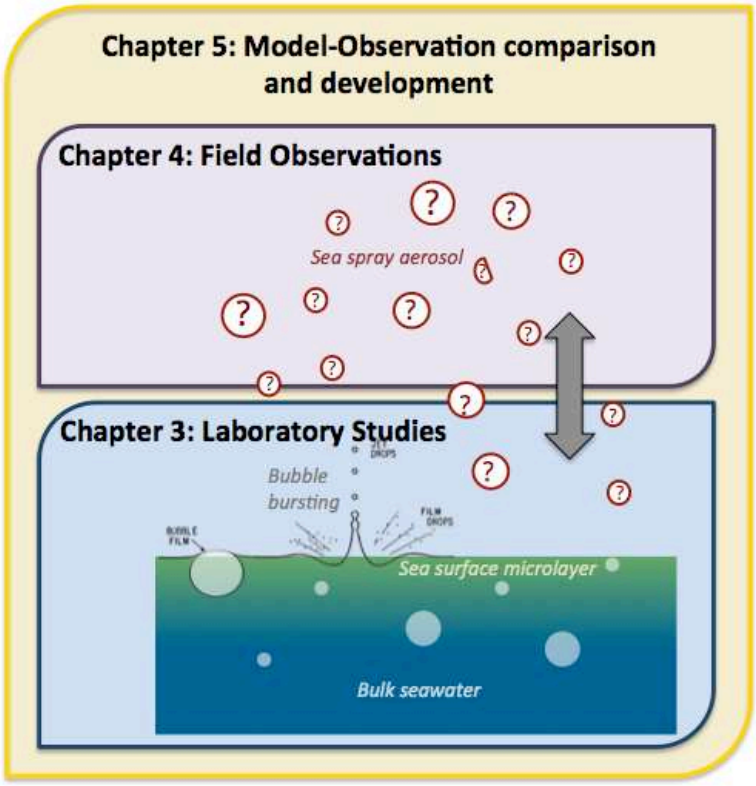

Figure 2.1-1. Schematic of scientific approach of this study for studying marine INPs.

marine organic aerosol at sites in remote oceanic and clean coastal regions (Section 2.2); and 3) utilize findings from laboratory and field studies to challenge a global aerosol transport model that includes a sophisticated representation of ocean organic aerosol emissions (Section 2.3). This approach is summarized in Figure 2.1-1. The instruments used to probe ice nucleation, composition, physical descriptors and biological properties of aerosol particles and seawater samples are described in Section 2.4.

Section 2.1 Mesocosm laboratory study experimental details

Laboratory studies were performed in order to probe the role in INP production of several key system components, including bulk seawater, the sea surface microlayer, and sea spray aerosol, during phytoplankton bloom conditions. Findings from these studies have been reported in *McCluskey et al.* (2017) and *McCluskey et al.* (submitted to *J. Atmos. Sci.*).

2.1.a Sea spray aerosol generation in the laboratory

Two mesocosm experiments, both performed at the Center for Aerosol Impacts on Chemistry of the Environment (CAICE) facilities at the University of California, San Diego at Scripps Institution of Oceanography (SIO), are described in this study. The first was performed using a Marine Aerosol Reference Tank (MART, Figure 2.1-2A, *Stokes et al.,* 2013). The MART is a 210 L Plexiglas tank that produces sea spray aerosol (SSA) using a plunging sheet of water, repeated at 4 s intervals by recirculating a portion of the contained seawater. The aerosol sampling port for the MART study is located approximately 15 cm from the surface of the seawater. The second set of data is from the Investigation into Marine PArticle Chemistry and Transfer Science (IMPACTS) campaign (*Wang et al.,* 2015) conducted at the SIO wave channel (Figure 2.1-2B, dimensions: 33 m long, 0.6 m deep and a volume of 13,000 L), which produces SSA via breaking waves (*Prather et al.,* 2013*; Collins et al.,* 2014). Aerosol measurements were

made from the main sampling manifold used by all investigators, unless otherwise stated. This manifold drew air from approximately 20 cm above the surface of the seawater and approximately 1.2 m downstream of the breaking wave. The particles produced by these two methods are considered nascent laboratory-generated SSA, and both methods produce similar bubble and aerosol particle size distributions (*Prather et al.,* 2013) and size-resolved chemical mixing states (*Collins et al.,* 2014*). DeMott et al.,* (2016) reported that INP number concentrations measured from these laboratory systems are similar to those observed in the ambient marine boundary layer when scaled by total particle number concentrations or total aerosol surface area.

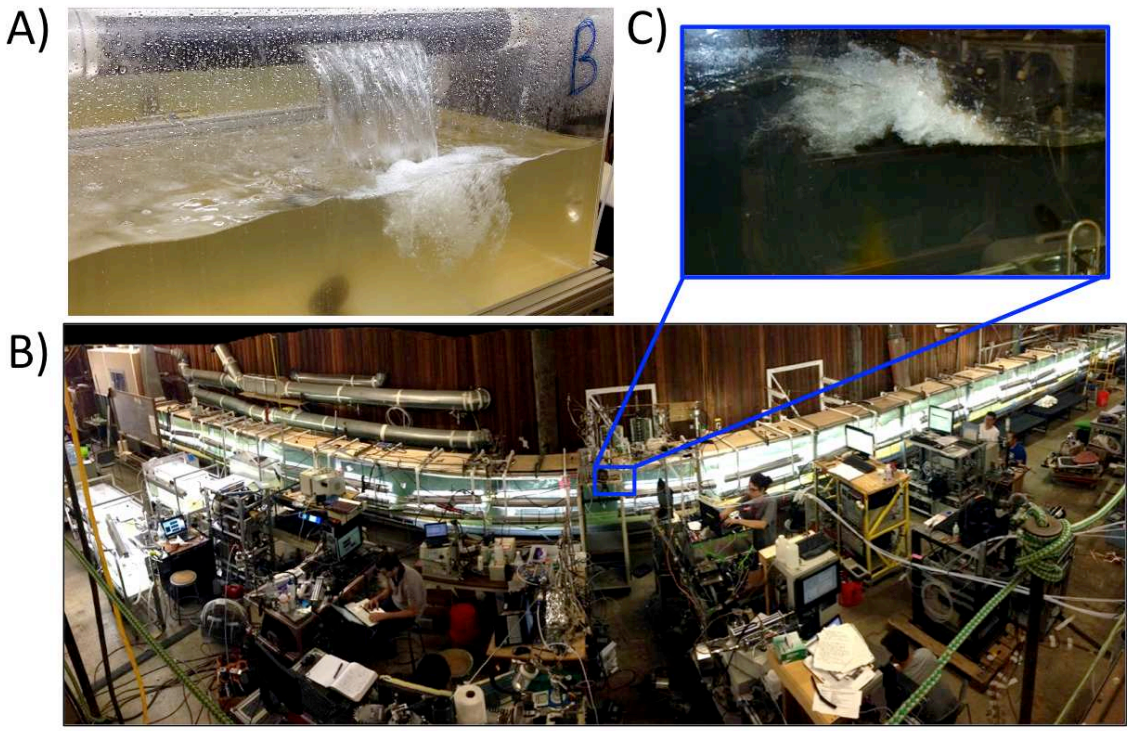

Figure 2.1-2. Pictures of the A) Marine Aerosol Reference Tank, B) Wave Flume (panoramic photo), and C) wave breaking in the waveflume.

2.1.b Mesocosm biological conditions

The two studies were performed during two different periods; measurements were made from 6 to 27 January 2014 for the MART study and from 3 July to 9 Aug 2014 for the

IMPACTS study. Experimental details have been previously described for the MART study (Tank E in *Lee et al.,* 2015) and the IMPACTS study (*Wang et al.,* 2015) and are repeated briefly here. For both experiments, seawater was collected at the Ellen Browning Scripps Memorial Pier (SIO in La Jolla, CA, 32° 52.00' N, 117° 15.40' W), located 275 m offshore. The seawater collection depths for the MART and IMPACTS studies were 0 m (i.e., sea surface) and approximately 4 m below the low tide level, respectively. Seawater for the MART and IMPACTS studies was collected on 5 January 2014 and 3 July 2014, respectively. The phytoplankton blooms were prompted by the addition of nutrients (f/2 algae growth medium with sodium metasilicate, ProLine Pentair Aquatic Eco-Systems, Apopka, FL) and tanks were equipped with 5700 K full spectrum lights (Full Spectrum Solutions, Model 205457). The concentration of Chl *a* in bulk seawater was monitored fluorometrically (Aquafluor, Turner Designs) several times a day as an indication of bloom growth. Control sampling was performed on the first day of each experiment following the nutrient addition (Day 0 for MART and IMPACTS were 6 January 2014 and 3 July 2014, respectively). During the MART study, SSA production commenced when Chl *a* started to increase exponentially. SSA was produced throughout the course of the IMPACTS experiment.

There were key differences between the two experiments that need to be considered while interpreting findings. Satellite-derived and field observations of Chl *a* concentrations during phytoplankton blooms have been reported at values of up to 5 μg L^{-1} (*Moore and Abbott,* 2000*, Mongin et al.,* 2011). Thus, the MART experiment is referred to in this study as a "denser" bloom, with Chl *a* concentrations reaching 39 μg L^{-1} (*Malfatti et al.,* in prep), whereas the IMPACTS study provided lower levels of Chl *a*, reaching approximately 5 μg L^{-1}. Additionally, these two experiments likely had diverse microbial communities due to different seawater

samples that were collected at different times of year. Although these mesocosms are considered unconstrained, they are both successions of naturally-occurring microbes in the collected seawater and could thus be used to achieve the goal of this study, which was to determine if there was a relationship between INPs and changes in biological productivity.

Section 2.2 Overview of Field Study Experimental Details

In addition to observing marine INPs in controlled environments available through CAICE facilities, observations of the factors affecting boundary layer marine INP concentrations are needed to validate laboratory-based findings and to determine the contribution of this potential INP source to ambient INP populations. To address this requirement, we have surveyed INP populations at various coastal and ocean locations, shown in Figure 2.2-1, analyzing environmental factors that can help to isolate the marine-derived INPs from other sources and using additional observations (e.g., Chl *a*) to link to the laboratory work. These field studies are explained in more detail below.

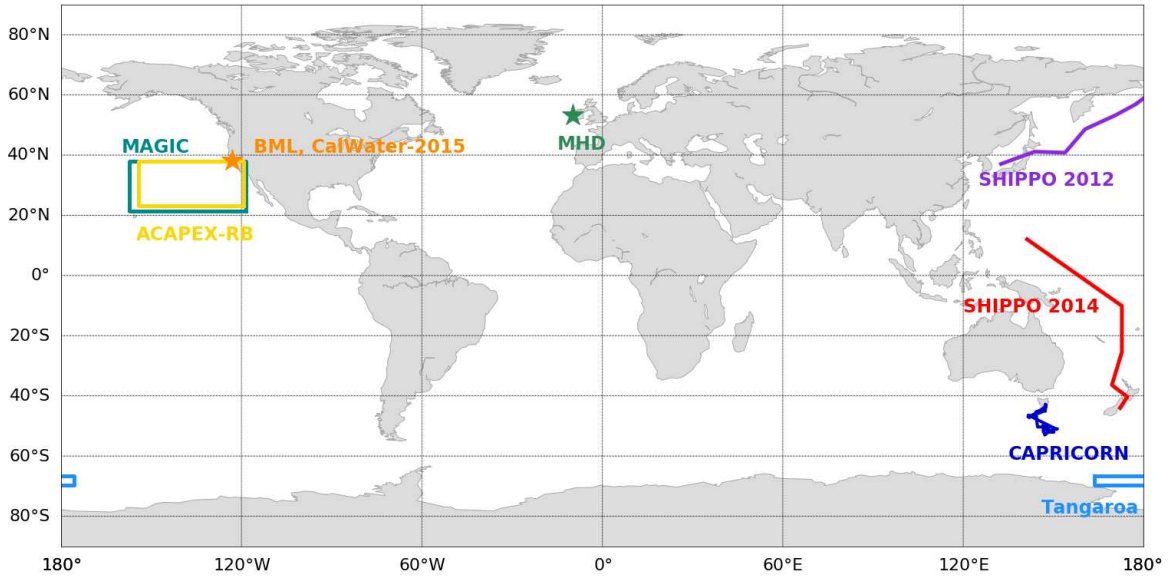

Figure 2.2-1. Locations of field observations sites (BML and MHD) and latitude and longitude bounds for the Tangaroa, MAGIC, and ACAPEX-RB ship campaigns. Also shown are the approximate tracks of the SHIPPO-2012, SHIPPO-2014, and CAPRICORN. Acronyms are defined in *Table 2.2-1*.

Table 2.2-1. Summary of field project names, platform, dates and location. Map of field location is provided in Figure *2.2-1*.

Acronym	Study	Platform	Date	Season	Location
BML, CalWater-2015	Bodega Marine Laboratory, CalWater-2015* campaign	Ground site	Jan-Feb 2015	Winter	38.3°N, 123 °W
MAGIC	Marine ARM GPCI** Investigation of Clouds	Horizon Spirit	Jun-Sept 2013	Winter-early fall	20 to 40˚N
ACAPEX-RB	ARM Cloud Aerosol Precipitation Experiment	Ron Brown	Jan-Feb 2015	Winter	20˚N to 40˚N
Tangaroa	New Zealand National Institute of Water and Atmospheric Research Southern Voyage	R/V Tangaroa	Feb 2015	Summer	43˚S to 72˚S
SHIPPO 2012 SHIPPO 2014	Ship-borne Pole-to-Pole experiment	R/V Araon	July 2012 April 2014	Summer Late fall	50˚N to 60˚N 44˚S to 10˚N
MHD	Mace Head Research Station	Ground Site	Aug 2015	Summer	53.3°N, 9.9°W
CAPRICORN	Clouds, Aerosols, Precipitation, Radiation, and atmospheric Composition Over the southeRn ocean	R/V Investigator	March 2016	Late summer	43˚S to 53˚S

* Precipitation, Aerosols and Pacific Atmospheric Rivers Experiment
**Global Energy and Water Cycle Experiment Cloud Systems Study Pacific Crosssection Intercomparison

2.2.a CalWater-2015

The University of California Davis Bodega Marine Laboratory (BML) is located on the coast of California (38.3 °N, 123 °W), situated north of Point Reyes National Seashore. Various aerosol and INP measurements were made from an instrument trailer, located at the BML approximately 100 m from the coastline, as part of the Calwater-2015 Precipitation, Aerosols and Pacific Atmospheric Rivers Experiment, summarized by *Martin et al.,* (2017). The primary objective of these measurements was to determine abundances of INPs in air masses intersecting BML, with particular focus on the contribution of SSA, mineral dust and anthropogenic aerosol.

In this work, we present measured n_{INPs} that were observed in aerosol collected during periods identified as marine background air masses and analyzed with the ice spectrometer (Section 2.4.a.ii).

2.2.b Ship observations over the Pacific Ocean

Filter collections of aerosol present in the MBL were collected during several ship campaigns, covering a large spatial range of the Pacific Ocean, shown in Figure 2.2-1. INP number concentrations (n_{INPs}) were measured from the collected filters with the ice spectrometer (IS, Colorado State University). The Marine Atmospheric Radiation Measurement (ARM) Global Energy and Water Cycle Experiment Cloud Systems Study Pacific Cross Section Intercomparison Investigation of Clouds (MAGIC, (www.archive.arm.gov/discovery/#v/results /s/fsite::mag)) study included aerosol and remote sensing observations during repeated transects of the Horizon Spirit cargo ship between Los Angeles, California and Honolulu, Hawaii from October 2012 to September 2013. Filter collections for INP measurements during MAGIC occurred from 22 June to 10 September 2013 and analyses of two samples from this campaign were previously reported by *DeMott et al.* (2016). The National Oceanic and Atmospheric Administration (NOAA) research vessel (RV) Ronald H. Brown was deployed during the DOE ARM Cloud Aerosol Precipitation Experiment (ACAPEX-RB, www.archive.arm.gov/discovery/ #v/results/s/fsite::acx), which occurred from 12 January 2015 to 12 February 2015, aligned with a portion of the CalWater-2015 campaign. The ACAPEX-RB ship measurements were made in a similar region of the Pacific Ocean as the MAGIC study and with a similar instrument suite. Measurements from the 2012 and 2014 voyages of the Ship-borne Pole-to-Pole experiment (SHIPPO) spanned the western Pacific Ocean from 44 ˚S to 60 ˚N and one 24-hour INP sample from this campaign was also included in *DeMott et al.* (2016). Spatial coverage of marine

boundary layer observations over the Pacific Ocean was extended to 72 °S in February 2015, when collections for INP measurements were made onboard the National Institute of Water and Atmospheric Research (NIWA) RV Tangaroa during a Southern Voyage.

2.2.c Mace Head Research Station (MHD)

In August 2015, various measurements were made as part of an INP detection inter-comparison project (*Atkinson et al.,* in prep) at the Mace Head Research Station (MHD, 53.32 °N, 9.90 °W). Measurements were made approximately 100 m inland from the coastline. Various offline and online techniques, including the ice spectrometer (IS, Colorado State University), Horizontal Ice Nuclei Counter – Evaporation (HINC-EV, ETH Zurich), and Dynamic Filter Processing Chamber (DFPC, National Research Council, Italy) were used to measure n_{INPs}. An aerodynamic particle sizer, scanning electrical mobility particle sizer, tapered element oscillating microbalance, and aerosol mass spectrometer were used to characterize aerosol size distributions, mass and composition (as detailed below). Meteorological conditions were also monitored, including wind speed and direction. All dates and times reported here are local unless otherwise stated.

Unique to the MHD study, two filters intended for analysis in the IS were collected daily at the top of the 10-meter mast: a CLEAN sector and an ALL filter. The pump for the CLEAN sector filter was powered using the MHD Clean Sector Sampler (*Rinaldi et al.,* 2009). This sampler supplies power to the sampling pump only when black carbon is less than 15 ng/m^3 and wind direction is between 180 to 300 degrees. The pump for the ALL filter was powered continuously during the total collection period. CLEAN sector filters represent aerosol from pristine marine air and ALL sector filters represent aerosol from all sources, as seen in Figure 2.2-2.

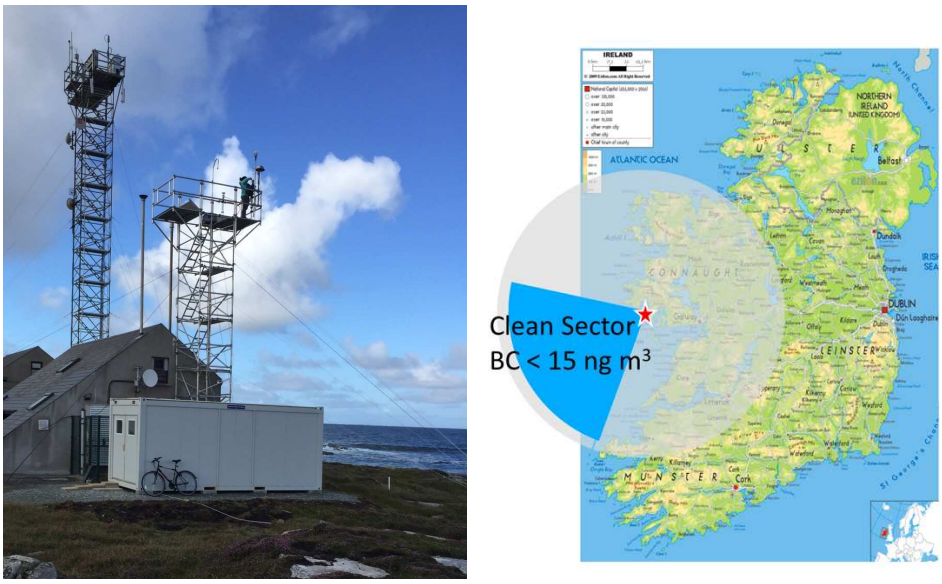

Figure 2.2-2. (left) Photo of observation station with 10-meter mast (shorter one in photo). (right) Map of the Mace Head Research station (red star) and a depiction of air mass arrival wind directions measured by the CLEAN sector versus ALL filters.

2.2.d Southern Ocean/ CAPRICORN

The Clouds, Aerosols, Precipitation, Radiation and atmospherIc Composition Over the southeRN ocean (CAPRICORN) voyage occurred from March 13 to April 15 in 2016 onboard Australia's RV Investigator, a research platform (commissioned in 2015) operated by the Commonwealth Science and Industrial Research Organization (CSIRO). The RV Investigator is equipped with a custom-designed air sampling inlet that is located approximately 14 m above sea level at the fore (front) of the ship. Both the IS and Continuous Flow Diffusion Chamber (CFDC) measured n_{INPs} during CAPRICORN and sampling details are provided below. The IS was also used to measure the ice nucleation behavior of SW samples, as described below.

Ship exhaust was characterized based on wind direction (Marine Wind Monitor, Model 05106, R.M. Young Company), condensation nuclei concentrations (CN, condensation particle counter, CPC Model 3776, TSI), and mass concentrations of black carbon (BC, Multiangle Absorption Photometer, MAAP Model 5012, Thermo Fisher Scientific). The protocol for

identification of exhaust contamination in the continuous sampling data was performed by Ruhi Humphries (CSIRO) and is considered preliminary in the presented work, with finalized identification in preparation for publication (*Humphries et al.* in prep). Briefly, the algorithm for identifying exhaust contamination identified periods with elevated BC concentrations (>0.07 μg L^{-1}) and high number concentrations of CN. Finally, radon (^{222}Rn, ANSTO 700 L two-filter ^{222}Rn detector, *Griffiths et al.,* 2016) was measured as a tracer for terrestrial air masses.

Section 2.3 OCEANFILMS model preliminary comparison

The atmospheric component (CAM5) of the DOE Community Earth System Model (CESM, version 1.2.1, *Hurrell et al.,* 2013) was used in this study as an aerosol transport and microphysics model (i.e., with nudged meteorology). Simulations were used to evaluate model estimates of aerosol concentrations, including marine aerosol and mineral dust, and subsequent predictions of n_{INPs}, with application of currently available INP relationships to aerosol parameters predicted by the model. The model ice microphyics are not altered in these model simulations.

Model details closely follow those by *Xu et al.* (2016), but are briefly described here. The model resolution is 1.9° latitude by 2.0° longitude and includes 30 vertical layers (surface to 3.6 hPa). Aerosol particles are represented by four aerosol modes as part of the Modal Aerosol Module (MAM4), summarized in Table 2.3-1. Aitken mode particles range in size from 20 to 80 nm in diameter (D_p). The MAM4 separates the accumulation mode aerosol particle population (80 nm < D_p < 1 μm) into soluble and insoluble species; insoluble species are aged into the soluble mode after being coated with condensed sulfate. Finally, coarse mode particles are represented with a size range of 1 to 10 μm. The model predicts total number mixing ratios and mode median diameter for each mode (each mode has a fixed width). Several aerosol particle

species are represented in these modes, also summarized in Table 2.3-1. Aerosol emissions in these simulations represent the year 2000. Emissions of anthropogenic SO_2, BC, and primary organic matter are from the Intergovernmental Panel on Climate Change AR5 (*Lamarque et al.,* 2010) and dust and sea salt aerosol emissions are calculated as a function of wind speed and temperature. Mass mixing ratios of each species are predicted for each aerosol mode and simulated aerosols are assumed to be internally mixed within each mode. That is, all particles described by a single MAM4 mode are assumed to have identical fractional composition and identical participation in particle evolution.

Particles evolve in the model through transport, particle phase transformations, and cloud microphysical processes. Transport of aerosol is determined based on resolved winds, turbulent mixing, and vertical velocity. Sedimentation and dry deposition are included in the model. Aerosol transformations include condensation and evaporation of trace gases (e.g., sulfate), homogeneous nucleation, particle coagulation, and chemical aging. Aqueous chemistry, particle activation and resuspension of particles from cloud evaporation are also represented in CAM5.

Table 2.3-1. Summary of aerosol modes in MAM4 and the aerosol species that comprise them.

Aerosol species	Aitken	Accumulation (soluble)	Accumulation (insoluble)	Coarse
SO_4	x	x		x
Secondary organic aerosol	x	x		
Particulate organic matter		x	x	
Black carbon		x	x	
Dust		x		x
Sea salt	x	x		x
Marine organic matter	x	x	x	

Sea salt emissions are simulated in CAM5 using two source functions: for sea salt particles with diameters smaller than 2.4 μm, emissions are based on sintered glass lab studies of synthetic seawater (*Martensson et al.,* 2003); for sea salt particles with diameters larger than 2.4

μm, emissions are based on white cap simulations from tank experiments with natural seawater (*Monahan,* 1986). Sea spray organic matter was simulated by the OCEANFILMS model, which is a mechanistic approach for connecting SSA composition to an ocean biogeochemical model (*Burrows et al.,* 2014; *Burrows et al.,* in prep). Monthly mean ocean surface concentrations of lipids, proteins, humic acid, and polysaccharides were estimated by a biogeochemical model (the Parallel Ocean Program, *Maltrud et al.,* 1998) that was used to simulate ocean general circulation and biogeochemical elemental cycling. These monthly mean concentrations are considered to represent a standard climatology of atmospheric boundary conditions (e.g., surface wind stress, solar radiation) for a generic year and are used for each simulation year. OCEANFILMS predicts the surface coverage of ocean bubble films and with a bubble film thickness of 0.1 μm to determine the organic mass fraction of SSA emissions.

The metric used to describe model and observation comparison is the modified normalized mean bias (B_n), which describes the mean fractional difference between the model and observation. B_n is calculated using the following expression:

$$B_n = \frac{2}{N}\sum_i \left|\frac{f_i - O_i}{f_i + O_i}\right|$$

where f_i is the modeled value, O_i is the observed value, and N is the number of data points included in the comparison. B_n can range from 2 to -2, where negative B_n indicates that the model biases to lower values compared to observations.

Section 2.4 Instrumentation

Numerous instruments were used to characterize ice nucleation, aerosol composition, particle size and ocean biology during the laboratory and field studies. A list of instrumentation and the size range of particles detected (if appropriate) is provided in Table 2.4-1.

Table 2.4-1. Summary of instrumentation used for aerosol sampling and collecting other relevant observational data in the studies referenced in this work: CAICE Marine aerosol reference tank (MART), Investigation into Marine PArticle Chemistry and Transfer Science (IMPACTS), CalWater-2015, Mace Head Research Station (MHD) and Clouds, Aerosols, Precipitation Radiation and atmospherIc Composition Over the southeRN ocean (CAPRICORN). Size ranges for particle measurement are listed when appropriate. The contact and affiliation of these instruments and data are provided in Appendix V.

		CAICE - MART	**CAICE - IMPACTS**	**CalWater-2015**	**MHD**	**CAPRICORN**
Ice Nucleation	CFDC	$D_{a,dry} < 1.5$ µm	$D_{a,dry} < 1.5$ µm****	$D_{a,dry} < 1.5$ µm****	-	$D_{a,dry} < 1.5$ µm****
	IS*	0.2 µm* < $D_{p,wet}$	0.05 µm* < $D_{p,dry}$ < 2.5 µm	0.2 µm* < $D_{p,wet}$	0.05 µm* < $D_{p,wet}$	0.2 µm* < $D_{p,wet}$
	HINC	-	-	-	$D_{p,dry}$ <2 µm	-
	DFPC	-	-	-	PM_1; PM_{10} (wet)	-
Aerosol Chemistry	ATOFMS	0.3 < D_{vac}** <3 µm	0.3 < D_{vac}** <3 µm	0.15 < D_{vac}** <3 µm	-	-
	Bulk TOC	TSP (wet)	$PM_{2.5}$; PM_{10} (wet)	-	-	-
	AMS	-	-	-	PM_1**	-
Particle Size	SMPS	yes	yes	yes	yes	yes
	APS	yes	yes	yes	yes	-
	TEOM	-	-		$PM_{2.5}$; PM_{10} (wet)	-
	Neph	-	-	-	-	Total Aerosol***
Ocean Biology	Chl *a*	Yes	Yes	-	Yes	Yes
	Enzyme act.	Yes	Yes	-	-	-
	HB counts	Yes	Yes	-	-	-

*lower size listed for IS sampling referrers to the filter pore size, however collection of smaller particles are expected, as discussed in the text
**vacuum diameter
*** RH <40 %
****Aerosol concentrator was used upstream of the CFDC.

2.4.a Measurements of ice nucleating particle number concentrations

Two main techniques were used to monitor concentrations of immersion freezing ice nucleating particles (INPs): The Colorado State University continuous flow diffusion chamber (CFDC, Section 2.4.a.i) and the CSU ice spectrometer (IS, Section 2.4.a.ii). Both instruments were utilized during the laboratory experiments and onboard the RV Investigator during CAPRICORN. Only IS data are reported for measurements made during Calwater2015 and CFDC data will be part of a future publication. Only IS filter collections (see below) were deployed was deployed during the field campaign at Mace Head research station and onboard other ships (MAGIC, ACAPEX-RB, SHIPPO 2014 and 2013, and Tangaroa). Two other ice nucleation instruments were used during the MHD study, which are briefly described in Section 2.4.a.iii.

2.4.a.i Continuous Flow Diffusion Chamber

The CFDC (*Rogers et al.,* 2001*; Schill et al.,* 2016) is an online instrument that was used to measure number concentrations of immersion-mode INPs (n_{INPs}). The CFDC comprises two upright ice-coated cylindrical columns, a cold "inner wall" and a warmer "outer wall", shown in Figure 2.4-1. A 1.12 cm gap exists between the two temperature-controlled and ice-coated walls, where a focused, laminar sample flow (1.5 Lpm, surrounded by 8.5 Lpm of filtered sheath flow) is exposed to cloud relevant conditions. The temperature gradient between the walls is typically set to create conditions supersaturated with respect to ice and water at the position of the sample lamina following the analytical equations given in *Rogers* (1998). The CFDC was operated at sample lamina supersaturations with respect to water (SS_w) of 3-7.5 % and temperatures ranging from -16 to -30 °C. During both studies, inline silica gel dryers were used to dry the aerosol sufficiently for sampling. Before entering the CFDC aerosol particles encounter an impactor with

an aerodynamic cutoff of 1.5 μm (for these studies only). Sampled air is then focused between sheath air and enters the upper region of the chamber. As aerosol is drawn through the first two-thirds of the chamber (the nucleation/growth region) particles are exposed to the large liquid water supersaturations and serve as condensation nuclei, collect water and grow in size. If a particle is active as an immersion-mode INP at the chamber conditions (and for a residence time of 4-5 s), an ice crystal will nucleate. The lower third of the column is a liquid evaporation region, where the ice-coated walls are set to equivalent temperatures and the supersaturation lowers to ice saturation (i.e., water subsaturation). At these conditions, the liquid droplets evaporate while the ice crystals continue to grow to the chamber exit, yielding a distribution of particles and hydrometeors that include evaporated droplets and haze particles (D_p < 1.5 μm), and ice crystals (D_p > ~4 μm). Finally, an optical particle counter (OPC) is used to measure the resulting particle size distribution, assigning those particles in the larger size mode (i.e., ice crystals) as equivalent to the INPs.

The reported n_{INPs} and their confidence intervals were determined following recent studies (*Schill et al.,* 2016; *DeMott et al.*, 2017). Background ice crystals in the CFDC are known to occur from ice crystals that grow on the chamber walls and periodically break away into the chamber flow. In these studies, instrument background was monitored by sampling filtered air for a minimum of 3 minutes every 10-20 minutes. Background ice crystal concentrations were interpolated for each time-averaged aerosol sampling point and subtracted from measured ice crystal concentrations to determine corrected n_{INPs}. Poisson counting statistics were used to determine standard deviations for background and sample ice crystal concentrations, which were added in quadrature to estimated n_{INPs} error. Statistically significant data were defined as those

with n_{INPs} more than 1.64 time greater than their error (Z statistic at 95% confidence interval for a one-tailed distribution).

The n_{INPs} present in SSA in the wave flume (IMPACTS) and ambient environments, particularly at warmer temperatures, were low and oftentimes below the detection limit of the CFDC. The detection limit of the CFDC varies between studies and sampling periods depending on conditions of the chamber, but minimum statistically significant n_{INPs} observed during this work was approximately 0.2 L^{-1}. During the IMPACTS and CAPRICORN study, an aerosol concentrator (MSP Corporation, Model 4240) was used upstream of the CFDC, similar to the sampling setup in previous studies by *Tobo et al.* (2013) and *DeMott et al.* (2017). The aerosol concentrator increases the detection limit of the CFDC by capturing most of the particles having aerodynamic diameters larger than 500 nm present in a sample flow of ~ 250 Lpm and concentrating them into 1.5 Lpm, thus enhancing the concentrations of these larger particles (D_p > 500 nm). Enhancement factors of up to 167 are possible in theory (*Romay et al.,* 2002*)*. Due to pre-existing damage to the aerosol concentrator, the concentrator was less effective during the IMPACTS study, and thus the concentrator factor (CF) was lower and variable (*Tobo et al.,* 2013). In *Tobo et al.* (2013) and *DeMott et al.* (2017), the CF was determined based on the ratio of n_{INPs} measured on and off the aerosol concentrator. However, this method was not possible on most occasions due to the low n_{INPs} measured without the aerosol concentrator during the IMPACTS and CAPRICORN studies. Thus, the CF was estimated and specified each day by taking the ratio of n_{500nm} measured by the CFDC with and without the concentrator. Throughout the IMPACTS study, the CF based on n_{500nm} ranged from 3.5 to 14.7 (CF_{avg} = 7.48 ± 3.38, Appendix II). In the few cases where n_{INPs} was successfully measured without the concentrator, the CF determine based on n_{INPs} was within a similar range ($CF_{avg,INPs}$ = 3.9 ± 1.7). During

CAPRICORN, CF based on n_{500nm} was higher and ranged from 46 to 130 (Appendix II). The measured n_{INPs} when sampling from the concentrator was then divided by this factor to correct to ambient conditions. This correction assumes that the majority of the INPs are within the larger size range of the aerosol distribution. Prior work has indicated that only modest underestimations (~2) of INPs occur if this assumption is violated and INPs are distributed across all size ranges (*Tobo et al.,* 2013). The correction would be most in error if there were a pronounced mode of INPs at sizes well below 500 nm, which is not the case in prior reported measurements of terrestrial INPs or for INPs measured at coastal sites (*Santachiara et al.,* 2009*; DeMott et al.,* 2010*; Mason et al.,* 2015). At present, the mode diameter of marine INPs in the atmosphere is unknown. Therefore, despite uncertainties introduced by concentrating aerosol and then correcting back to ambient concentrations, this methodology was applied here since observation of the low number concentrations of marine INPs at warm temperatures was not possible without the use of the aerosol concentrator. Separate measurements using a very different methodology (filter sampling followed by analysis in the IS) had some overlap with the CFDC data and offered one means of verifying the appropriateness of our continuous-sampling methodology.

Detailed descriptions of how the CFDC was set up during the laboratory studies (MART an IMPACTS) are provided by *McCluskey et al.,* (2017). Losses of larger particles in the sampling lines for both studies were estimated by calculating the ratio of number concentrations of particles with diameters > 500 nm and < 1.5 μm (n_{500nm}) measured by the CFDC OPC to n_{500nm} measured by the sizing suite (see Section 2.4.c). Losses of smaller particles due to diffusion were not assessed and are assumed to be negligible for particles larger than $D_p > 0.1$ μm (*Hinds,* 1999). Losses of particles with diameters smaller than 100 nm, while potentially 10% or greater,

are assumed to have insignificant contributions to uncertainties in both the INP population and the total aerosol surface area, and are thus not explicitly accounted for during this study.

CFDC measurements used in the CAPRICORN analysis were made from (1) a community sampling manifold that is located in the aerosol laboratory and (2) an independent inlet dedicated to the aerosol concentrator. The total distance from the RV Investigator sampling inlet to the aerosol laboratory manifold is approximately 8 m. Due to aerosol concentrator's large sampling volume and its likely influence on all sampling flows if drawn from the shared sampling manifold, it was placed on its own inlet (1 inch diameter stainless steal tubing) located next to the main sampling inlet. Attempts to determine particle losses due to sampling lines was limited to measurements of n_{500nm} from the sampling manifold compared to the aerosol concentrator manifold without the concentrator powered on (16 March 2015). The ratio of averaged n_{500nm} measured by the CFDC on the community sampling manifold (2.66 ±0.09 cm^{-3}) compared to the concentrator (0.79 ±0.5 cm^{-3}) was approximately 3. However, once the concentrator is turned on, a factor of 300 increase in flow through the sampling line was realized, which likely resulted in improved transmission efficiency of particles. Additionally, the collection efficiency of aerosol through the sampling inlets are likely dependent on wind direction, wind speed and ship motion. We note that the transmission of particles through the sampling manifolds onboard the RV Investigator have not been characterized and that this will be revisited during the next voyage planned for 2018. The data reported here are not corrected for sampling line losses and limited measurements indicate that these may be on the order of a factor of 3. Aerosol particles were collected on filters that were analyzed with the IS. Offline immersion freezing methods, including the IS, have been show to agree well with online

measurements of INPs in SSA (*DeMott et al.,* 2016 and work presented here) and thus provide a benchmark for the CFDC measurement made during CAPRICORN.

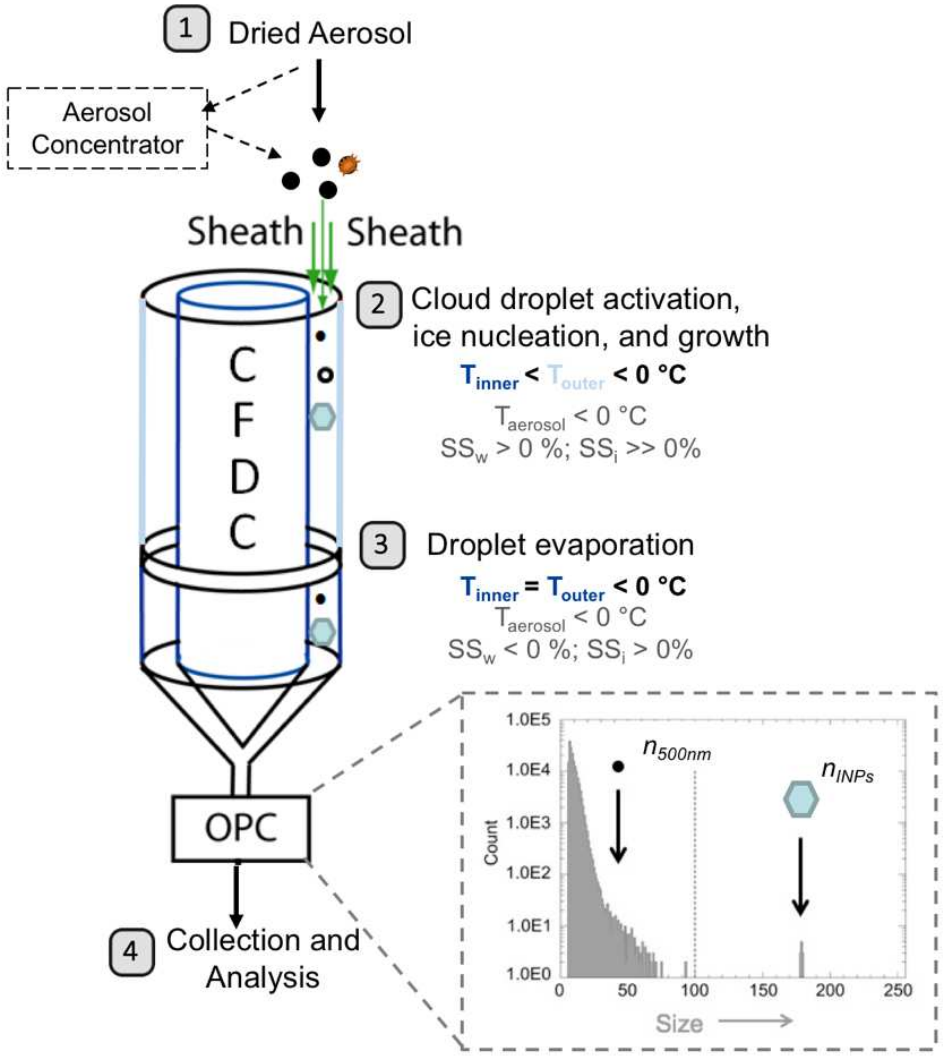

Figure 2.4-1. Schematic of the continuous flow diffusion chamber (CFDC) and sampling strategies. The inner wall and outer ice-coated walls are colored by their relative temperatures, where dark blue indicates coldest temperature, light blue indicates warmer temperature, and both walls are below zero (ice coated). The temperature control system and cooling fluid flow schematics are not shown. Supersaturation with respect to water (SS_w) and ice (SS_i) are also shown for each section of the chamber (1 and 2). The dashed lines around the aerosol concentrator indicate the optional addition of this portion of the sampling train. A typical measured distribution of hydrometeors as detected by the optical particle counter (OPC) is also provided to illustrate the separation of number counts of ice nucleating particles (n_{INPs}) and particles larger than 500 nm (n_{500nm}). The lower detection limit of the OPC (bin 6) is approximately 500 nm.

2.4.a.ii Ice Spectrometer

The second ice nucleation detection method is an offline method, where material is either collected onto filters or sampled in bulk, then immersed into liquid water for analysis with the ice spectrometer (*Hirunama et al., 2015*).

For aerosol particle collection, pre-sterilized Nuclepore^{TM} track-etched polycarbonate membrane filters (47 mm diameter, Whatman, GE Healthcare Life Sciences, Piscataway, NJ) with a pore size of 0.2 or 0.05 μm were used (Table 2.4-2). Details on flow rates and sampling setup are provided in *McCluskey et al.* (2017), *McCluskey et al.* (submitted to *J. Atmos. Sci*) and *McCluskey et al. a, b* (in prep) for the CAICE laboratory studies and field studies, respectively. The filter pre-cleaning protocol comprised soaking filters and dissassembled filter holders (separately) in 10% H_2O_2 for 10 and 60 minutes, respectively, and three rinses with deionized water (18 mΩ, 0.2 μm pore filtered, and for filters, a further rinse in deionized water that had been passed through an 0.02 μm pore Anotop syringe filter (Whatman)). Excess water on filter holders was removed with a compressed air can duster. Filters and filter holders were then placed on aluminum foil in a laminar flow hood to dry.

Typical accumulated sample volumes, filter pore sizes, and particle size ranges that were investigated for each project are provided in Table 2.4-1. During the IMPACTS and MART studies, particle losses associated with sampling lines upstream of the filter holder (47 mm aluminum filter housings, Pall Corporation) were estimated using a particle loss calculator (*von der Weiden et al.,* 2009), and used to determine the size range of particles collected and analyzed by the IS. During the IMPACTS study, a 3 m sampling line was used for the IS filter collection (same as the CFDC) and particle losses associated with this long line were determined using a particle loss calculator (*von der Weiden et al.,* 2009). Depositional losses were estimated to be

negligible (< 5%) for particles with diameters up to 2 μm and up to 30% for particles with diameter of 2.5 μm. Diffusional losses were also negligible (< 5%) for particles larger than 60 nm. Thus, the IMPACTS IS filters are assumed to be approximately $PM_{2.5}$. For all field campaign measurements, filters were exposed via open-faced filter holders. During the MHD study, filters were collected from a 10 m mast located at the observation station (Figure 2.2-2). CAPRICORN filters were collected from Deck 5 of the RV *Investigator*, which is approximately 23 m above the ocean surface (during calm conditions), shown in Figure *2.4-2*.

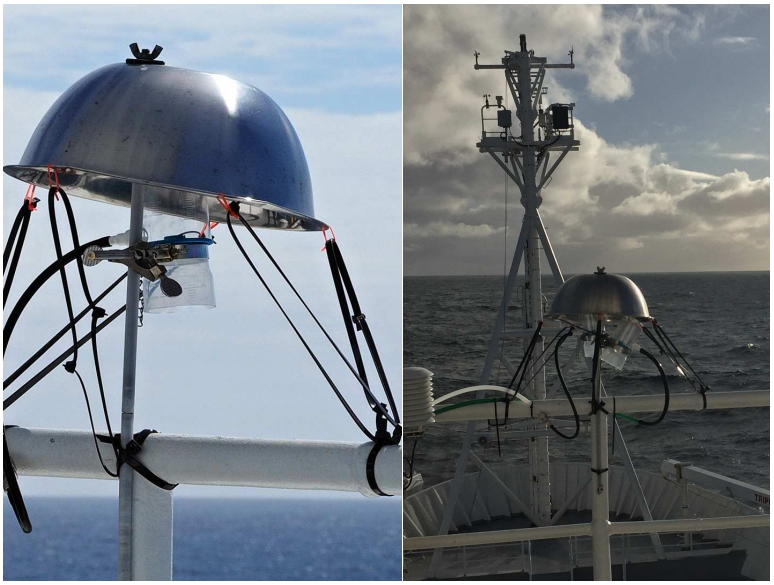

Figure 2.4-2. Photos of the open face filter units attached to railing onboard the RV Investigator during the CAPRICORN project

Blank filters were collected throughout each study to determine method contamination, shown in Appendix I. After sampling, filters were removed from the filter holders with clean plastic forceps, placed in sterile petri dishes, sealed with Parafilm and stored frozen (-20 °C) until they were processed). To release collected particles, filters were immersed in room temperature 5 mL deionized, 0.02 μm pore filtered water and shaken for 20 minutes, resulting in a sample solution ready for IS analysis.

The abundance and characteristics of ice nucleating entities (INEs, *Vali et al*., 2015) in the seawater and SML were also evaluated. Bulk seawater (SW) was collected for IS analyses during the CAICE studies. SW was also collected during CAPRICORN from thermosalinographs (SBE-38 CTD and SBE-21 TSG, SeaBird Inc.), or conductivity, temperature, and depth profilers (referred to as CTDs). 5-15 mL of SW were collected in sterile (Falcon) tubes, frozen and shipped to CSU. Surface microlayer (SML) samples were collected during CAICE studies using the glass plate method as described in *Cunliffe et al.,* (2013). Freezing point depression effects due to the ionic species in SW and SML samples, as contrasted with the pure water used for immersion freezing in the filter sample processing, are not accounted for in this study, as discussed in Appendix III.

Aliquots of suspended aerosol samples or bulk liquid samples, aliquots (typically 24-32 aliquots of 50-80 μL each) were placed into two, 96-well PCR trays (μCycler; Life Science Products, Frederick, CO) that were then placed into the aluminum blocks in the IS. A chiller was used to cool the blocks from 0 to -25 °C at a cooling rate of -0.33 °C min^{-1}, and the number of wells frozen were counted every 0.5 or 1 °C. Number concentrations of INPs per volume of liquid were determined as a function of temperature based on $-\ln(f)/V_a$, following *Vali et al.* (1971), where f is the fraction of unfrozen aliquots and V_a is the aliquot volume. The conversion to the equivalent ambient in-air concentration, n_{INPs}, was then obtained from the total volume used for rinsing and the volume of air collected. Blank filters were collected periodically throughout each study and INP measurements of the rinse water from these were analyzed and subtracted from the counts made on collected samples prior to computation of volumetric concentrations in air (Appendix U). Binomial sampling confidence intervals (95%) were used to

describe uncertainties associated with the IS (formula 2, *Agresti and Coull,* 1998). A comparison between the CFDC and IS techniques for detecting marine INPs is provided in Figure 2.4-3.

Table 2.4-2.Summary of IS filter collection details for each study

	CAICE - MART	CAICE - IMPACTS	CalWater - 2015	MHD	CAPRICORN
Filter holder	Inline	Inline	Open face	Open face	Open face
Pore size	0.2 µm	0.05 µm	0.05 µm	0.05 µm	0.2 µm
Approx. L of air	270-430	280-880	11000	6000	1300-3800
SW	Y	Y	-	-	Y
SML	Y	Y	-	-	-
Sampling height			~5 m AGL	10 m	23 m
Distance from shoreline			100 m inland	100 m inland	Open ocean

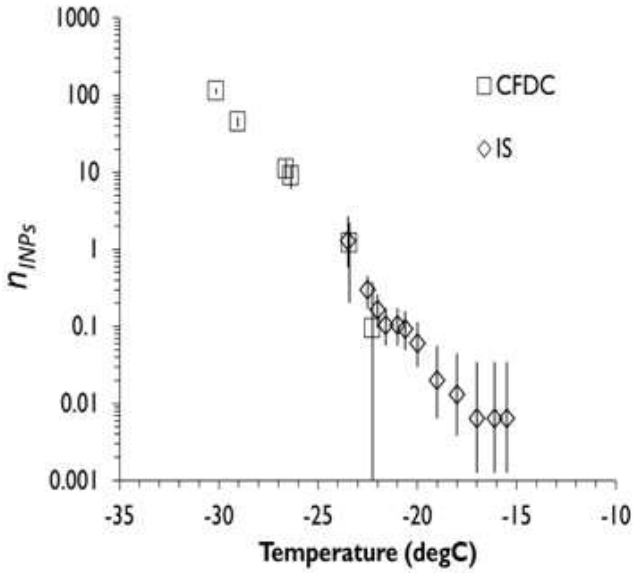

Figure 2.4-3. INP number concentrations per liter of air detected by the CFDC and IS laboratory studies of SSA (modified from *DeMott et al.,* 2016).

2.4.a.iii Other ice nucleation measurement techniques

The HINC-EV instrument was used in MHD studies. Constructed and operated by ETH Zürich, the HINC-EV is a horizontal CFDC closely resembling the University of Toronto CFDC (UT-CFDC, *Kanji and Abbatt*, 2009) and a chamber previously built at ETH Zurich (HINC, *Lacher et al.,* 2017). The principle difference between HINC and HINC-EVis the conversion of a portion of the chamber into an evaporation section. For more details on the horizontal CFDC

concept and UT-CFDC/HINC design please see *Kanji and Abbatt* (2009) and *Lacher et al.* (2017), respectively.

The HINC-EV consists of two horizontal parallel copper plates, an upper wall and a lower wall, which are temperature controlled by an external chiller. Humidity inside the chamber is provided by wet glass fiber filter papers on each wall, which are frozen into ice layers as the chamber is cooled. Supersaturation with respect to water (S_w) at the centerline of the chamber (a horizontal plane equidistant from the two chamber walls) is realized by inducing a temperature difference between the two chamber walls. The first section serves as a nucleation and growth section where ice will grow rapidly. The last 8.7 cm (equivalent to an aerosol residence time of 2.7 s) of HINC-EV is an evaporation section, kept at approximately ice saturation ($S_i = 1$) by maintaining the upper and lower walls at the same temperature.

Dried aerosol is introduced, and preconditioned to the centerline temperature, via an injector pipe at a distance of 18.7 cm from the HINC-EV outlet (corresponding to a growth section aerosol residence time of 5.7 s). The aerosol stream is surrounded by a sheath flow of particle-free pure nitrogen (zero grade - 99.998 % N_2), which is preconditioned to the chamber temperature and S_w prior to encountering the aerosol stream at the chamber head. The ratio of sheath air to sample air was 8:1. On leaving the injector, the aerosol stream is exposed to the centerline S_w and can act as either an INP (in the deposition and/or condensation depending on the centerline S_w) or a cloud condensation nuclei (CCN) and consequently as a possible immersion mode INP. In the evaporation section, activated CCN that are absent of immersion mode INPs evaporate, leaving an aerosol distribution containing dry particles and large ice particles. At the exit of the chamber, an optical particle counter measures the aerosol and ice particles; ice particles are counted by assuming that any nucleated INPs have grown to diameters

greater than 4 μm. During operation of HINC-EV, INPs are counted over 15 s and are reported here as averages over approximately 20 min. Filtered (particle-free) air is sampled for 10 min between each 20 min sample to quantify the amount of erroneous ice from the chamber rather than from aerosol. Ambient measurements that are less than one standard deviation of the background concentration are classified as below the limit of detection and thus assumed to be an unreliable representation of an ambient INP concentration (*Lacher et al.,* 2017).

During this study, ambient particles were sampled isokinetically from the top of the 10 m mast via a 100 mm diameter pipe. Before entering HINC-EV, aerosol was passed through approximately 3 m of horizontally oriented diffusion driers to remove the abundant ambient moisture that can result in erroneous freezing measurements and rapidly degrade instrument background noise. Before injection into HINC-EV, total aerosol concentration was measured using a condensation particle counter. Due to gravitational settling in the driers, the maximum particle size that entered the HINC-EV is estimated to be 2 μm (*Lacher et al.,* 2017). Finally, measurements at MHD were conducted at 243 K and S_w of 1.04, corresponding to S_i of 1.4. Uncertainties in chamber sampling conditions are estimated to be ± 0.4 K, S_w ± 0.02 and S_i ± 0.03.

Data from the Dynamic Filter Processing Chamber (DFPC) was also used in MHD studies. The DFPC is a replica of the diffusion chamber described by *Langer and Rogers* (1975). Atmospheric n_{INPs} active at -22 °C are detected via offline processing of membrane filters, following the procedure described in *Santachiara et al.* (2010) and *Belosi et al.,* (2017). Briefly, PM_1 and PM_{10} aerosol fractions were simultaneously sampled onto separate nitrocellulose membrane filters (Millipore HABG04700, nominal porosity 0.45 μm) by mounting different sampling heads (1 μm, and 10 μm cut-point-Standard EN 12341, TCR Tecora) in front of the

filters. Sampling was carried out only in the CLEAN sector. Samples were returned to CNR (at ambient temperature – i.e., not stored frozen) for analysis, where collected filters were placed onto a metal plate, previously covered with a smooth surface of Vaseline. Subsequently, the Vaseline was slightly heated (70 °C for 10 s) and rapidly cooled in order to fill the filter pores and create effective thermal contact. The metal plate was inserted into the DFPC, housed in a refrigerator, to detect and determine the concentration of aerosol particles active as INPs at different supersaturations with respect to ice and water. Five blanks (unsampled filters) were analyzed to account for contaminations during the INP quantification procedure and the results were corrected accordingly.

2.4.b Probing the composition of ice nucleating particles

To explore the composition and identity of marine INPs, we utilized several established methods and tools. First, we directly probed composition and size of the residual material from evaporated ice crystals downstream of the CFDC using a single-jet impactor and offline Scanning Electron Microscopy and Raman spectroscopy analyses. Offline treatments of bulk samples (filter collections, seawater samples) were performed to determine the heat sensitivity, size and organic nature of ice nucleating materials.

2.4.b.i Collection and analysis of ice crystal residuals

During the CAICE laboratory studies, the identity of ice crystal residuals (ICRs) was determined using the same basic approach as in *Prenni et al.* (2009). In this work, collections and analyses were limited to samples processed at cooler temperatures (T = -30 °C) due to the low n_{INPs} at other conditions, in order to maximize the numbers of particles available for analysis. Ice crystals were collected via use of a single jet impactor (2.9 μm 50% aerodynamic cutoff diameter, *Prenni et al.,* 2009) at the base of the CFDC. ICRs (i.e., evaporated ice crystals)

were analyzed using scanning electron microscopy (SEM), energy dispersive x-ray (EDX) analyses and micro-Raman spectroscopy. In each ICR collection period, approximately 5000 ice crystals were collected onto SEM grids (SPI Formvar®/Carbon Coated Transmission Electron Microscopy (TEM) grids, 200 mesh Cu) or onto substrates for application of micro-Raman spectroscopy (pre-cleaned quartz coverslips, Ted Pella Inc., part no. 26016) and a minimum of 50 ICRs were randomly selected and analyzed. These analyses provide direct measures of the composition and size of the material that possessed an ice nucleating entity and nucleated ice following condensation of droplets and immersion freezing at -30 °C (aerodynamic particle diameter, $D_a < 1.5$ μm, based on the cutpoint of the inlet impactor upstream of the CFDC). Although it is recognized that the statistical confidences will be limited due to the small sample size, the analyses of randomly-selected particles may reveal any major differences in relative contributions between the types of particles that comprised the ICRs.

Imagery (Quanta FEG MK2, SEM) and compositional (Oxford Instruments X-Max energy dispersive X-ray spectroscopy system (EDS)) analyses were performed at the Materials Characterization Laboratory in the Department of Geology and Geophysics (University of Wyoming, Laramie, WY). The spatial resolution of the SEM was 50 to 100 nm. ICRs were divided into three categories based on the morphology observed in the SEM imagery: "Crystalline with coatings" are particles such as a salt particle with visible significant coating; "Heterogeneous" particles are particles that resemble mixtures of constituents with various textures; and "Amorphous/unclassified" particles are particles that have indistinct morphology, oftentimes due to low resolution (i.e., $D_p <$ approximately 100 nm). These morphology categories are shown in Figure 2.4-4, where they are denoted as A, B, and C classes, respectively. The maximum dimensions (i.e., length along longest axis) of ICRs were also

measured from SEM imagery to estimate size distributions of collected ICRs, as demonstrated and reported in Figure 2.4-4. Particle and background spectra were collected for each ICR and utilized to infer qualitative chemical composition of ICRs. Spectral peaks that were elevated relative to background (particle-free areas) spectra were considered important contributors to the ICR spectra. Two ICR types are reported: ICRs containing carbon and oxygen (organics); and ICRs containing sodium chloride (salt). The numbers of ICRs that had these chemical signatures are reported for each morphology class and each ICR sample.

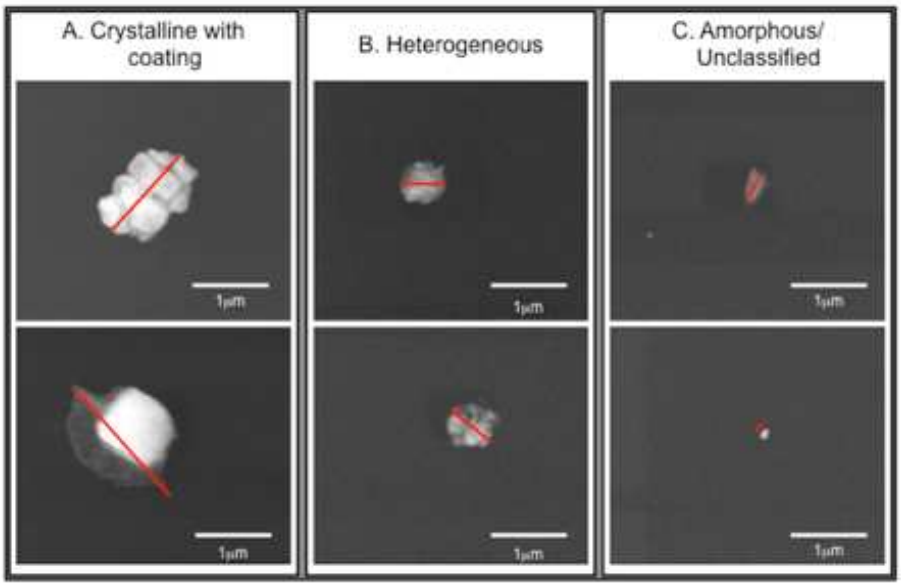

Figure 2.4-4. Example scanning electron microscopy images of each morphology group used to classify ice crystal residuals collected downstream of the continuous flow diffusion chamber. Red lines span the primary diameter of each particle to illustrate the measurement of ice crystal residual primary diameter. In the bottom right image, the red line is offset to allow visibility of the residual.

Raman microspectroscopy analysis was conducted on ICRs with diameters in excess of approximately 1 μm collected during the MART and IMPACTS studies. This size was chosen by the collaborator without consultation and future studies will advise collaborators to look at all sizes found on the substrate. Submicron aerosol particles collected on one day of the MART study following the methods of *Cochran et al.* (2017) are also shown for comparison. Briefly, spectra were acquired using a LabRam HR Evolution Raman Spectrometer (Horiba) equipped

with an Olympus BX41 optical microscope with 100X magnifications lens. Spectra in the range from 100-4000 cm^{-1} were acquired by taking the average signal from two exposures of 5-20 s using a 532 nm laser. Compositional information for these particles was based on comparisons to Raman spectra of standards as discussed in detail in *Cochran et al.* (2017).

2.4.b.ii Determining composition and size of ice nucleating material

To determine the contributions of biological material to the INP and ice nucleating entity (INE) populations, the aliquots comprising filter suspensions (aerosol), bulk seawater or SML were subjected to heat treatment. For the heat treatment, the sample solution was heated to 95 °C for 20 minutes, cooled to room temperature and dispersed into the IS wells for analysis. A reduction in IN activity under heating indicates the contribution of heat labile material to the INP population, which includes possible contributions from proteinaceous IN material. Heating will also alter the IN activity of some other classes of macromolecules by unfolding or degrading their structure, as suggested by *Pummer et al.* (2015).

Syringe filters were used to investigate the size range of the INE population in bulk seawater samples. The sample solution was pushed through a filter with a pore size of 0.2 μm (DISMIC-13 cp, Advantec; pre-rinsed with DI water to remove any INPs in the filter itself) and the filtrate was analyzed in the IS, revealing the contribution of INEs in the < 0.2 μm filtrate to the total INE population. This 0.2 μm size cut can be approximately associated with two groups of material in the marine biochemical system, where larger INEs (>0.2 μm) may be grazers, phytoplankton, and bacteria, and smaller INEs (< 0.2 μm) may be viruses, vesicles and dissolved organic carbon such as cellular debris and cell-free molecules (*Azam and Malfatti,,* 2007).

Aliquots from three aerosol filter suspensions from the IMPACTS study were also digested with hydrogen peroxide to decompose all organic INPs. 1 mL of the suspension was

combined with 0.5 mL of 30% H_2O_2 (Sigma Aldrich) to achieve a final concentration of 10%, then the mixture was immersed in water, and heated to 95 °C for 20 min while being illuminated with two, 26 W UVB fluorescent bulbs to generate hydroxyl radicals. To remove residual H_2O_2 to prevent otherwise significant freezing point depression due to its presence, catalase (Cat. number 100429, MP Biomedicals) was added to the cooled solution. Since catalase is itself decomposed by H_2O_2, while simultaneously catalyzing its disassociation into water and oxygen, the enzyme was added in several 20 μL aliquots, allowing several minutes between each, until no effervescence resulted upon its addition.

Method blanks were analyzed and revealed small changes in the background INP number concentrations associated with the heating, sizing and H_2O_2 tests (Appendix 1). Tests of significance between untreated and treated samples used Fisher's Exact Test (*Fisher,* 1922) to derive exact *p* values for the likelihood of the difference in proportions of wells frozen between samples at each temperature. The *p* value is given by:

$$p = \frac{(a+b)!\,(c+d)!\,(a+c)!\,(b+d)!}{a!\,b!\,c!\,d!\,n!}$$

where *a* and *b* are the numbers of wells frozen and unfrozen, respectively, in the untreated sample, and *c* and *d* are the same for the treated sample, at each temperature. *n* is the combined total number of aliquots being tested in both samples. In this study, values are considered statistically different if they have a *p* value of less than 0.05.

2.4.c Aerosol size distributions

In all studies, aerosol size distributions were monitored with a scanning mobility particle sizer (SMPS, TSI Model 3080, 0.014 μm < D_p < 0.75 μm) and an aerodynamic particle sizer (APS, TSI Model 3321, 0.54 μm < D_p). Different instruments (all the same instrument model, but different owners) were used for each campaign, but the basic approach is the same. Most of

the time, aerosol diffusion driers were used to dry aerosol upstream of the SMPS and APS to <20 % relative humidity and particles were assumed to be below their efflorescence relative humidity. If dryers were not present (e.g., CAPRICORN), corrections and assumptions were made to determine the best estimate of size distributions.

Several adjustments were applied to APS data: a size calibration was applied, the first three size bins of the APS were removed due to poor counting statistics, and the density of particulate matter in SSA was assumed to be 1.8 g cm^{-3}, based on *Zelenyuk et al.* (2007), to convert aerodynamic diameter to physical SSA diameter. The last 11 size bins were removed from the SMPS distributions after inversion, due to poor counting statistics and the SMPS impactor 50 % cutoff (D_{50} = 700 nm). These modified SMPS and APS data were used as the physical aerosol size distribution.

Measured size distributions were integrated over three different size ranges to account for changes in ice nucleating particle counts due to changes in aerosol concentrations. The total number concentration of particles with D_p < 1.5 μm, N_{tot}, calculated by summing the number concentrations of each bin up to this size from the merged size distribution, was used to normalize number concentrations determined from the CFDC (upper size limit of 1.5 μm). The total number concentration of particles with 0.5 μm < D_p < 1.5 μm, N_{500nm}, was calculated in the same manner as N_{tot}, where number concentrations of bins within this size range were added. Aerosol surface area was also calculated, assuming spherical particles, and the total surface area of particles, SA_{tot}, was used to calculate ice nucleation surface site density (n_s). SA_{tot} was calculated for bounded size distributions that were specific for each measurement technique to represent the size range of interest.

2.4.d Aerosol Composition

2.4.d.i Aerosol time of flight mass spectrometry (ATOFMS)

Size resolved dual-polarity mass spectra were generated for individual SSA particles having diameters between 0.25 and 3 μm during CAICE studies, utilizing an aerosol time-of-flight mass spectrometer (*Gard et al.,* 1997). Silica gel diffusional driers were utilized to dry the SSA particles before sampling, reducing the relative humidity of the sampled air to less than 15%. A Q-switched Nd:YAG laser pulse (266 nm wavelength, 8 ns, 700 μm spot size, 1.1-1.3 mJ pulse energy) desorbed and ionized the chemical components from each particle. Dual-polarity mass spectra were collected (mass-to-charge (*m/z*) range of -300 to 300) using a reflection time-of-flight mass spectrometer. Details of the ATOFMS mass spectral analyses can be found in *Sultana et al.* (2017a).

Briefly, four main spectral classifications were used in the CAICE studies to describe changes in the SSA composition. "BioSS" spectral signatures closely match those of previously described SSA particles that are likely microbe-containing (*Sultana et al.,* 2017b.); these spectra were dominated by potassium and phosphate ion markers and contained significant amounts of chloride ion signal and an array of organic nitrogen ion markers. The second biological spectral signature, "BioAg", is identified as spectra containing silver ion markers and often also contain markers identified in the "BioSS" spectra type. These spectral types are thought to be generated from bacterial cells that bioaccumulated silver nanoparticles from the wave flume during the IMPACTS study (*Guasco et al.,* 2014). The presence of organic particles is described by an abundance of the "Org" spectra type, whose spectral signatures include significant contributions from ions indicative of organic species. Finally, "SS" spectra type refers to particles containing sodium and sodium chloride ion markers with insignificant organics.

2.4.d.ii Aerosol Mass Spectrometer

Aerosol chemical composition was also measured in CAICE and MHD studies with an Aerodyne Research Inc. high resolution time-of-flight aerosol mass spectrometer (HR-ToF-AMS) which provides real-time size resolved composition of volatile and semi-volatile particulate matter (*DeCarlo et al.,* 2006). The HR-ToF-AMS quantifies non-refractory aerosol chemical composition, covering major inorganic species such as ammonium, sulphate, nitrate, plus organic species (*Jimenez et al.,* 2003) and sea salt mass (*Ovadnevaite et al.,* 2012) in the PM_1 size range (~100% transmission efficiency between 40-700 nm). A Nafion drier was installed in front of the HR-ToF-AMS sampling inlet to reduce relative humidity of the sample to <40%. The HR-ToF-AMS measurements were performed at a time resolution of 5 min and a vaporizer temperature of ~650 °C. The composition-dependent collection efficiencies (*Middlebrook et al.,* 2012) for the measurement periods discussed in this study ranged from 0.45 to 0.93. ToF-AMS HR Analysis 1.12G version was used for the high resolution data analysis.

2.4.d.iii Bulk aerosol organic carbon

Bulk aerosol organic carbon mass concentrations were measured during the CAICE laboratory experiments. During the MART experiment, total suspended SSA was collected from the headspace of the MART on 47 mm quartz fiber filters (QFF) (Pall, Life Sciences) at a flow rate of 3.5 Lpm using a custom-made single stage aerosol sampler. The QFF were pre-baked at 550 °C for 18 hours before sampling to remove contaminants, stored in aluminum foil-lined petri dishes sealed with Teflon tape, and kept at -20 °C before and after sample collection until analyzed. During IMPACTS, fine and coarse particulate matter ($PM_{2.5}$ and PM_{10}) were collected onto QFF with a dichotomous sampler (Anderson Instruments, Inc.) as described in *Cochran et al. (2016)*. For the MART and IMPACTS studies, the total organic carbon (TOC) content of SSA

was quantified by a 1.00 cm^2 sub-sample of QFF using a thermal optical analyzer (Sunset Laboratories) following the NIOSH Method 5040 (*Eller et al.,* 1999). The TOC concentration ($\mu g\ m^{-3}$) was calculated using the total filter area and sampled air volume, which was calculated using total sampling time and average flow rate.

2.4.e Particulate mass concentrations (TEOM)

Aerosol mass concentrations were monitored during the MHD study with a tempered element oscillating microbalance (TEOM, Thermo Scientific, Model 1405-DF), which measures fine ($PM_{2.5}$) and coarse ($PM_{2.5-10}$) particle mass fractions simultaneously. A virtual impactor is used to split the $PM_{2.5}$ from $PM_{2.5-10}$ and flow is dried below 20% RH by Nafion driers before arriving on the oscillating microbalances, which were kept at 30 °C. While low temperatures should have prevented volatilization of collected aerosol, slightly negative concentrations still occurred. Negative concentrations were observed after changes in air mass and particulate loading, particularly during rapid shifts from high aerosol loadings (polluted or high SSA) to low aerosol loadings (pristine air masses). The measurements were made at 6 min intervals and this time interval was sometimes insufficient to reach equilibrium, resulting in a mass drop and negative concentration. Leak checks have been routinely performed according to operational procedures. Detection limit and measurement precision was in the order of 1-2 $\mu g/m^3$ and the resolution was better than 1 $\mu g/m^3$.

2.4.f Ocean Biological Activity

2.4.f.i Enzyme activities

During the CAICE studies, daily seawater samples were collected and enzyme activities were determined following the fluorogenic substrate method of *Hoppe* (1983). Briefly, leucine amino-peptidase (LEU, protease) substrate and oleate (OLE, lipase) and stearate (STE, lipase)

substrates were added at saturation concentrations (20 μM) in the seawater sample and incubated for one hour. Fluorescence measurements were taken at the beginning and at the end of the incubation to assess the hydrolysis rate. Primary data on enzymatic activities and detailed descriptions for this method can be found in *Malfatti et al.* (in prep).

2.4.f.ii Abundance of microbes

During the CAICE studies, bacterial and viral abundances were measured in the bulk seawater and SSA according to Noble and Fuhrman (1998). Seawater and SSA collections were made every other day. SSA was impinged into 0.2 μm filtered autoclaved seawater in a 40 mL pre-combusted glass vial. Particles with $D_p > 1$ μm are preferentially collected with the impinging method. Primary abundance data of bacteria and viruses and detailed description of this method can be found in *Malfatti et al.* (in prep).

2.4.f.iii Chlorophyll a

During the CAICE experiments, Chl *a* concentrations in bulk seawater was monitored fluorometreically (Aquafluor, Turner Designs) several times a day as an indication of bloom growth. For the MHD study, daily Chlorophyll *a* concentrations were downloaded from MyOcean at 25 by 25 km resolution. Missing data due to cloud coverage were reconstructed using the Multichannel Singular Spectrum Analysis (MSSA) algorithm (*Ghil et al.,* 2002), following the same approach as *Rinaldi et al.* (2013). During CAPRICORN, SW samples collected from the CTDs were evaluated for Chl *a* concentrations using standard techniques (filtering and acetone extraction, *Holm-Hansen et al.,* 1965; *Lorenzen,* 1966) with a Turner Trilogy fluorometer, reported by *Moreau et al.,* (2017). Ocean color (satellite) was used to determine Chl *a* concentrations at the ocean surface during the campaign.

2.4.f.iv Screening for presence of INA bacteria using DNA-based methods

Standard and quantitative polymerase chain reactions (PCR) were used to probe samples for the presence of the *ina* (ice nucleation active) gene, the gene coding for the ice nucleating protein in the known species of IN bacteria (which we here term INB) (*Warren,* 1995).

For the IMPACTS study, DNA was extracted from bulk seawater and the SML. For the MART study, DNA was extracted from SSA collected on the 0.2 μm pore Nuclepore filters and from SML. For SSA samples, 0.75 or 1 mL of the same suspension used for INP determinations was processed, while for the SML DNA was extracted from 0.15 mL of the sample. Samples were centrifuged at 20,000 *g* for 10 min, and then all but 50 μL of the supernatant was removed. DNA was extracted from the residual aliquot using the PowerLyzer UltraClean microbial DNA isolation kit (MO BIO Laboratories), with bead beating using a FastPrep-24 instrument (MP Biomedicals) at setting 4 for 5 min, and employing the high recovery modification of the standard method as detailed in *Hill et al.* (2014).

For standard PCR, using primer pairs 3308f/3463r or 3341fb/3462r1, the reaction composition and PCR cycling conditions were as detailed in *Hill et al.* (2014), except that reactions did not include EvaGreen and that 40 cycles of amplification were used with annealing and extension at 54 °C. *Pseudomonas syringae* Cit7 DNA was used as the positive control. For the IMPACTS study, reactions were initiated with 1-70 ng DNA (concentration varied greatly among samples) extracted from bulk water samples on Days 0, 8, 15, 19, 24, 28, 34 and 36, while for the MART study ≤ 5 ng DNA per reaction was used, extracted from aerosol samples from Days 1, 12, 14, 16 and 20, and from the SML on Day 16. For qPCR, primer pair 3308f/3463r was used with reaction composition and PCR cycling conditions as detailed *in Hill et al.* (2014), with annealing and extension at 54 °C. Real-time PCR was performed on a Rotor-Gene 3000 (Corbett Research), using *P. syringae* Cit7 DNA for standards (see *Hill et al.,* 2014).

Only IMPACTS samples were tested, using 1-35 ng samples of DNA extracted from bulk seawater on Days 24, 34 and 36, and from SML on Days 19 and 34. Amplicons were assessed using 12 uL of the PCR reaction electrophoresed in 2% MetaPhor agarose gels (Cambrex) in 1× TAE buffer at 90 V for 45 min, using ethidium bromide for visualization. A 100 bp ladder (Promega) was used for sizing.

2.4.g HYSPLIT back trajectories

The origins of air masses during the MHD campaign were determined for focus periods based on back trajectories (72 hr, 500 m AGL) that were simulated using the National Oceanic and Atmospheric Administration (NOAA) HY-SPLIT model (*Stein et al.*, 2015, http://www.arl.noaa.gov/HYSPLIT_info.php). A detailed description of the back trajectory analyses is provided in Appendix IV.

CHAPTER 3: LABORATORY STUDIES

Chapter 3 reports on the findings from the CAICE laboratory experiments, as introduced in Chapter 2. These findings were published in two manuscripts: *McCluskey et al.* (2017 @ American Meteorological Society, used with permission) and *McCluskey et al.,* (submitted to *J. Atmos Sci)*. An introduction to the timeline of all data collected during both laboratory studies, excluding measurements of INPs, is provided in Section 3.1. In Section 3.2, results regarding variability in INP number concentrations and on the identity of INPs observed in the MART and IMPACTS studies are described. Section 3.3 concludes this chapter by reporting on the two main classes of marine INPs observed during these laboratory studies and an evaluation of the current approach used for predicting marine organic INPs. Finally, implications of these findings and suggestions for future research are summarized in Chapter 6.

Section 3.1 Biology and aerosol composition during CAICE laboratory studies

3.1.a MART study (Jan 2014)

3.1.a.i Bulk seawater and sea surface microlayer biology during the MART study

To describe biological activity of the bulk seawater, Chl *a* concentrations, counts of heterotrophic bacteria (HB), and enzyme activities are shown in Figure 3.1-1. During the MART experiment, an increase of phytoplankton biomass (Chl *a*) began on Day 8 and peaked on Day 11 (39 µg L^{-1}). A second bloom also occurred with its maximum in Chl *a* on Day 18 (up to 39 µg L^{-1}), as shown in Figure 3.1-1. Maxima in HB counts in SW were observed on Day 4 and Day 12. The maximum on Day 4 was likely associated with changes in the initial phytoplankton and bacterial communities in the seawater caused by the different environment of the MART tank with spiked nutrients. The second peak in HB counts present in seawater (Day 12) lagged the

initial increase in Chl *a* (Day 8) by 4 days and was likely associated with the increase in available organic material produced by the phytoplankton bloom.

The biological activity within mesocosms was also interpreted via the dynamics of enzyme activities in the bulk seawater, as illustrated in Figure 3.1-1. It can be seen that the decrease in Chl *a*, indicating the demise of the phytoplankton bloom, was immediately followed by a peak in protease (LEU) activity. The protease dynamics suggest an increase of proteins in the organic matter pool available for bacteria upon hydrolysis in order to satisfy their nitrogen requirements. Trends in lipase activity (i.e. enzymes that break down lipids) are also shown in Figure 3.1-1, where elevated lipase activity (OLE and STE), indicative of the presence of microbes possibly satisfying their carbon requirements, corresponded to periods of elevated bulk water HB counts, especially following the collapse of the primary bloom. Evidence for a sea surface microlayer (SML) is also apparent in Figure 3.1-1, where the abundance of HB in the SML mirrored the HB counts found in the SW. An enrichment of these microbes is apparent by the higher numbers of HB found in the SML compared to the bulk water at the collapse of the Chl *a* peak.

3.1.a.ii Aerosol Composition during the MART study

We first describe the presence of aerosolized microbes measured by an offline microscopy technique and an online single particle mass spectrometry technique. The transfer of microbes into the aerosol phase during the MART study can be inferred from Figure 3.1-1b, where HB counts in the aerosol ranged from 2×10^3 to 1×10^4 HB L^{-1} and coincided with periods when the SML contained elevated concentrations of HB (note: aerosol measurements of HB began on Day 10, *Malfatti et al.,* in prep). A maximum in aerosolized HB was observed on Day 18 by this offline technique. Using an ATOFMS, single particles with mass spectra

dominated by potassium, phosphate and organic nitrogen markers, similar to spectra generated from aerosolized microbes (*Fergenson et al.,* 2004; *Czerwieniec et al.,* 2005), were first identified and reported by *Sultana et al,* (2017b) and are reported for the MART study here (Figure 3.1-1d). It is maintained that this mass spectral type ($BioSS_{ATOFMS}$) is more likely to be generated by cells or cellular fragments desorbed and ionized within the ATOFMS without significant amounts of other material (e.g., organic species). Elevated number fractions of $BioSS_{ATOFMS}$ were observed on Days 11 to 13 of the MART study followed by a decline in the $BioSS_{ATOFMS}$ mass spectral type (Figure 3.1-1). In contrast, the offline bulk microscopy technique measured highest emissions of total heterotrophic bacteria on Days 16 and 18 (*Lee et al.,* 2015).

If microbes are emitted within sea spray droplets that contain significant amounts of dissolved organic material and are therefore already embedded in organic matrices, the ATOFMS is likely to generate mass spectra representative of the thick organic shell of the dried particle and not the embedded microbe within (*Sultana et al*., 2017b). *Sultana et al.* demonstrated this behavior by performing "depth profiling" of SSA by varying laser power. Thus, this cellular-like mass spectral type ($BioSS_{ATOFMS}$) could serve as an indicator for successful transfer of particulate cellular material into the aerosol phase with minimal amounts of extracellular organic material. Increasing transfer of non-cellular organic material into the aerosol phase could explain the discrepancy between the ATOFMS and offline microscopy measurements of HB. Notably, contrasting the relative trends between the two methods provides information on the organic coating present on particles.

As demonstrated in Figure 3.1-1e, variable total organic carbon was detected in the total suspended aerosol; concentrations were not correlated with other biological indicators. However,

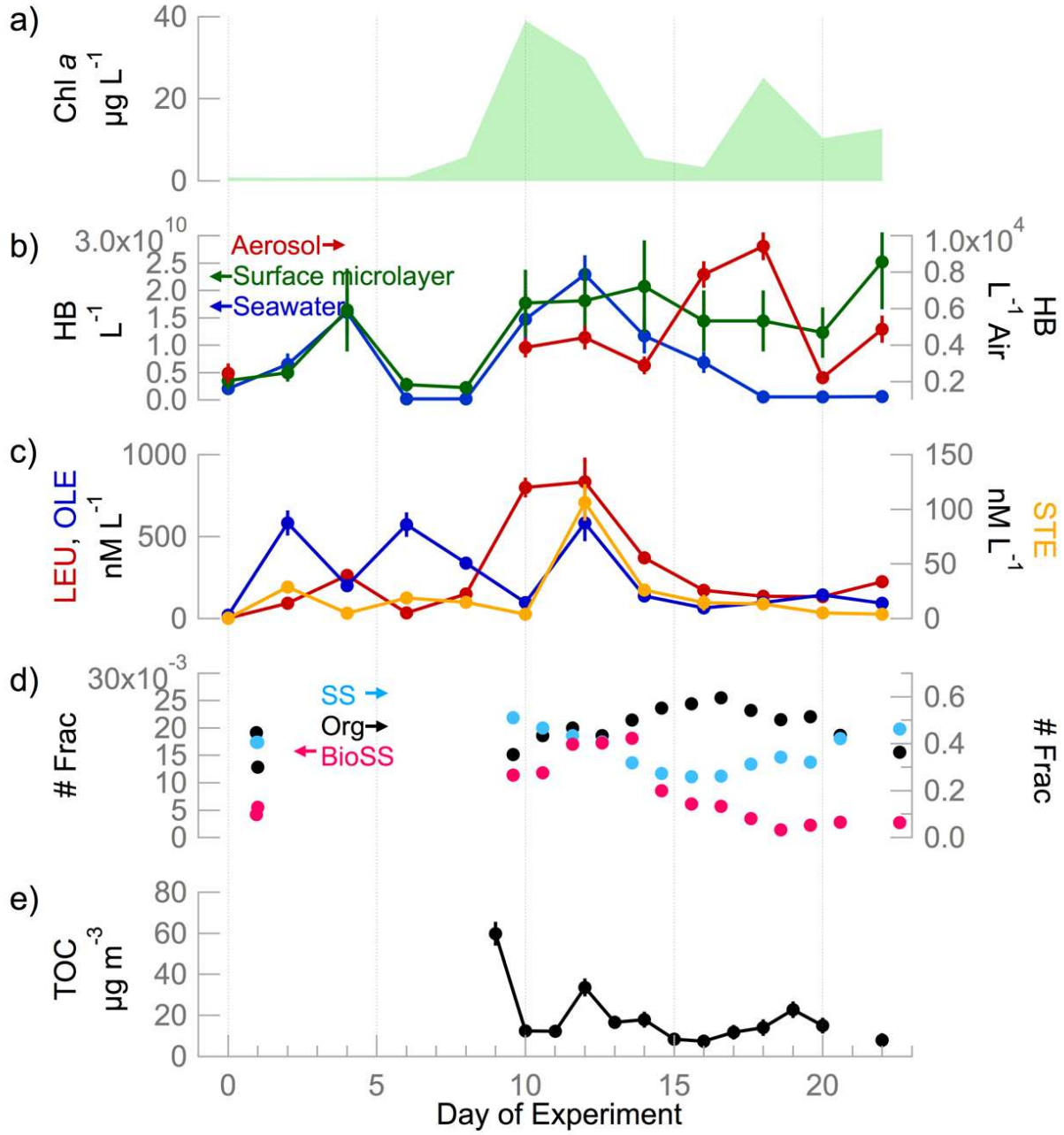

Figure 3.1-1 Timeline of (a) seawater Chl *a* concentrations and (b) Microscopy counts of HB in the bulk seawater (blue), SML (green), and aerosol (red; right axis). (c) Timelines of activity rates of LEU (protease, red), OLE (lipase, blue), and STE (lipase, orange) and (d) number fraction of mass spectral types measured during the MART study (*Sultana et al.,* 2017b). (e) Mass concentrations of TOC in the total suspended aerosol. Day 0 is 6 January 2014. This figure is modified from *McCluskey et al.* (2017) with additional data provided from *McCluskey et al.* (*submitted to J. Atmos. Sci.*).

an increase in the organic-rich (Org_{ATOFMS}) mass spectral type and a decrease in frequency of mass spectra dominated by sodium chloride ions (SS_{ATOFMS}) following the phytoplankton bloom suggested increasingly thick organic-enriched coatings on dried SSA particles (*Sultana et al.,* 2017a; *Sultana et al*., 2017b) and corresponded to a decrease in the $BioSS_{ATOFMS}$ number fraction.

This combination of offline and online measurements suggests that a small fraction of SSA during the MART study contained particulate cellular material without significant non-cellular organic coatings following the peak in Chl *a* between Days 12 and 15. After Day 15, aerosolized bacteria and cellular material were likely still transferred into the aerosol phase, and measured by offline microscopy, but they appear to have contained significant amounts of organic material and were not detected as the $BioSS_{ATOFMS}$ spectra type.

3.1.b IMPACTS study (Jan 2014)

3.1.b.i Bulk seawater and sea surface microlayer biology during IMPACTS

As shown in Figure 3.1-2, the IMPACTS study contained lower levels of Chl *a* compared to the MART study. Chl *a* concentrations indicate that two blooms also occurred during this study, where the first bloom of phytoplankton initiated around Day 10 and maximized on Day 14 (approximately 4 μg L^{-1}) and the second bloom initiated on Day 18 and remained elevated (Chl *a* approximately 5 μg L^{-}) through Day 25. HB counts from the bulk seawater, shown in Figure 3.1-2, indicate that peaks in HB abundance coincided with the two blooms and, similar to the MART experiment, the peaks in HB lagged the commencement of the two phytoplankton blooms. The concentrations of HB in the bulk water associated with the second bloom were twice those observed during the first bloom. Protease activity dynamics followed increases in Chl *a* and thus the phytoplankton bloom. Additionally, the lipase activities were highest during

the second bloom, coinciding with the highest concentration of HB in the bulk water. Interestingly, alkaline phosphatase and chitinase (AP and NAG) were also elevated after the first bloom, indicating intense phosphorous and carbon regeneration by microbes. In regard to the presence of an enriched SML, HB counts detected in the SML followed the dynamics of the SW throughout the duration of the study, indicating that HB were not as enriched in the SML in the IMPACTS study compared to the MART study.

3.1.b.ii Aerosol Chemistry

Aerosolized HB concentrations, evaluated via microscopy of collected aerosol, ranged from 5×10^4 to 2×10^5 HB L^{-1}. An increase in aerosolized HB (factor of 5) was observed on Day 14, possibly associated with a short-lived shift in the SML properties. The fractional contribution of $BioSS_{ATOFMS}$ signatures suggests relatively high transmission of microbes into SSA, with insignificant organic coatings present after particle drying. Silver-rich mass spectra had been identified in a previous wave channel study, and were attributed to aerosolized heterotrophic bacteria which had bioaccumulated trace silver material present as contamination in the wave channel (*Guasco et al.,* 2014). The fractional contribution of this mass spectra type with silver ion markers ($BioAg_{ATOFMS,}$) had a similar temporal trend to $BioSS_{ATOFMS}$.

A detailed evaluation of the organic contribution to SSA during the IMPACTS study has been published by *Wang et al.* (2015). ATOFMS and HR-ToF-AMS results indicate the presence of two distinct types of organics in the SSA, including an aliphatic-rich submicron organic and an oxygen-rich supermicron organic. Due to their short lifetime and aliphatic character, the aliphatic-rich organic type was likely associated with labile species, most likely lipids. Furthermore, Raman micro-spectroscopy results indicate that long-chain fatty acids were the dominant contributor to the organic submicron ($0.56 < D_p < 1$ μm) aerosol (up to 70%) (*Wang et*

al., 2015). Aliphatic-rich submicron organic aerosol peaked on Day 14 of the experiment, whereas the organic-rich supermicron organic type gradually increased throughout the study.

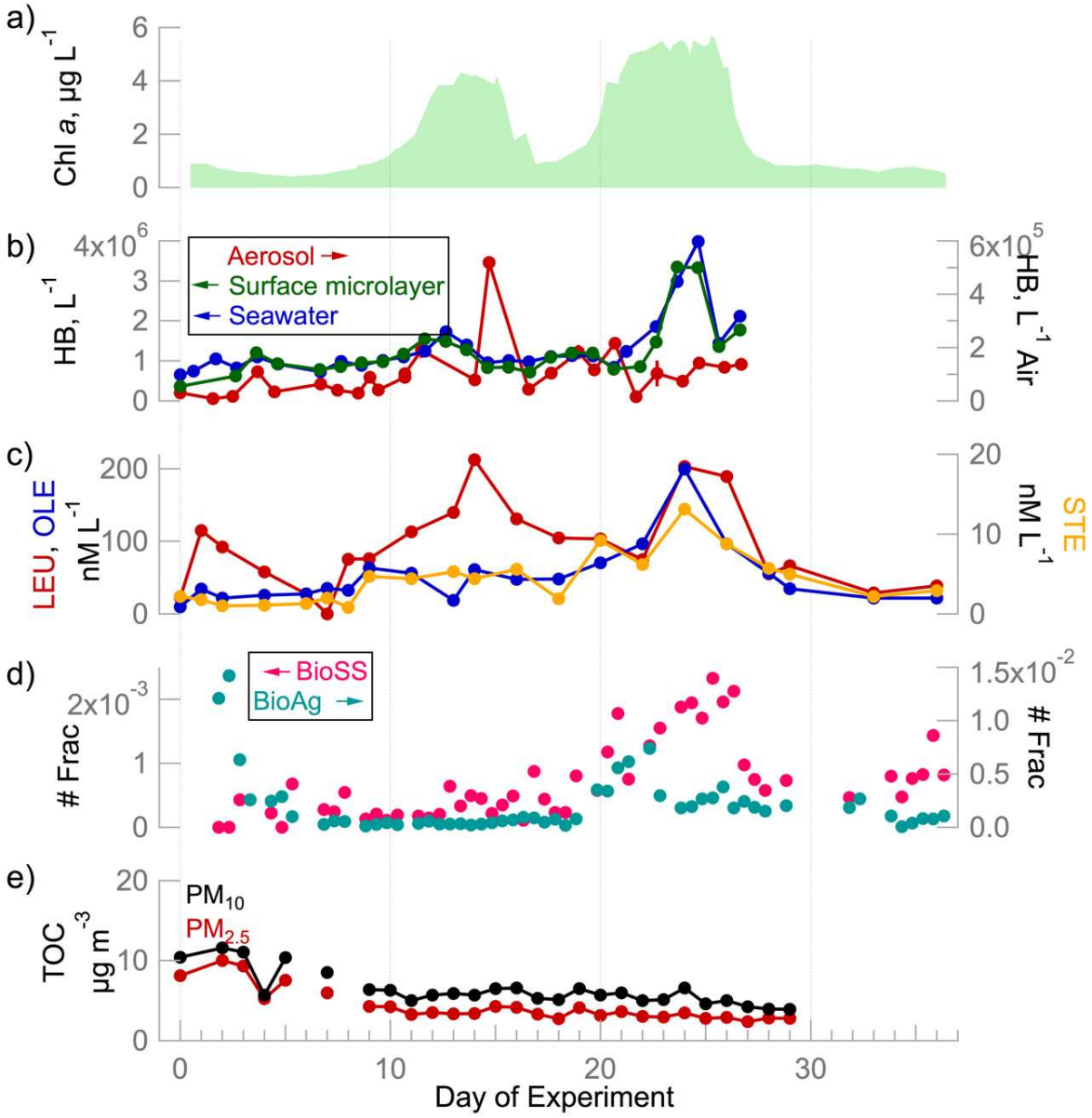

Figure 3.1-2. Timeline of (a) Chl *a* concentrations and (b) Microscopy counts of HB in the bulk seawater (blue), SML (green), and aerosol (red; right axis) during the IMPACTS study. Timelines of (c) activity rates of LEU (protease, red), OLE (lipase, blue), and STE (lipase, orange) and (d) number fraction of mass spectral types measured during the IMPACTS study (*Sultana et al.,* 2017b). (e) Mass concentrations of TOC in the total suspended aerosol. Day 0 is 3 July 2014. This figure is modified from *McCluskey et al.* (2017) with additional data provided from *McCluskey et al.* (submitted to *J. Atmos. Sci.*).

Section 3.2 Results from MART and IMPACTS laboratory experiments

Investigations of the characteristics of marine INPs during these two laboratory experiments included significant effort in probing all components of the complex system, including bulk seawater (SW), the sea surface microlayer (SML) and the aerosol (SSA). Section 3.2.a summarizes a comprehensive evaluation of INP number concentrations (n_{INPs}) against measured descriptors of biology and aerosol chemistry. Section 3.2.b describes the characteristics of ice nucleating entities that were present in the SW. Heat sensitivity of INPs in the SSA was determined (Section 3.2.c), and residuals of ice crystals formed by INPs present in the SSA were directly probed for their size and composition (Section 3.2.d). Finally, the most current approach for estimating marine organic INPs (*Wilson et al.*, 2015) was evaluated against the nascent SSA sampled during these studies.

3.2.a Trends in INP number concentration (indirect evidence for marine INP identity)

An unknown diversity of SSA constituents may contribute to the overall marine INP population. One approach to explore these various INP types is to examine trends in INPs active in various temperature regimes versus trends in other biological and chemical markers. We define three additional terms for this purpose: $n_{INPs,cold}$ refers to INPs active below -25 °C, $n_{INPs,mid}$ refers to INPs active between -25 and -15 °C and $n_{INPs,warm}$ refers to INPs active at temperatures warmer than -15 °C. To account for variations in aerosol number and size distribution, we also report INPs normalized by total number concentration of particles $D_p < 1.5$ μm (N_{tot}) and total surface area of particles $D_p < 1.5$ μm (SA_{tot}), respectively.

3.2.a.i MART

Timelines of n_{INPs} and Chl *a* for the MART experiment are shown in Figure 3.2-1. n_{INPs} measured by the IS on Day 9 were lower than Day 1. Changes in composition of the initial

phytoplanktonic, bacterial and viral communities during the growing stage of the bloom may also have led to the decrease in n_{INPs}. The interpretation of these differences is limited due to restrictions on aerosol production in the MART system during the growing phase. On Day 10, the warmest INP activity was observed by the IS at -14 °C and a modest peak in n_{INPs} was observed at -18 °C (increase in $n_{INPs,18°C}$ by a factor of 2). A more significant peak in $n_{INPs,mid}$ occurred on Day 16 (n_{INPs} at -22 °C increased by a factor of 30), lagging the peak in Chl *a* by 4 days. After Day 10, a steady decline in $n_{INPs,\ cold}$ was observed, with n_{INPs} ranging from 9.8 L^{-1} to 86 L^{-1} for INPs active at -30 °C.

To normalize for variability in aerosol number concentrations throughout the study, number fractions of INPs in the total aerosol particle population ($D_p < 1.5$ μm) are shown as a function of temperature (Figure 3.2-2). Variations in aerosol size distributions are accounted for in Figure 3.2-2b, where n_{INPs} were normalized by total aerosol surface area ($D_p < 1.5$ μm) to calculate nucleation site densities (n_s). These data confirm that the normalized temperature spectra of INPs from the MART before and after the bloom (Days 0 and 20) were similar, whereas the normalized spectra obtained on days during the bloom (Day 10 and 16) were clearly different. Thus, the aforementioned temporal dynamics of $n_{INPs,mid}$ and $n_{INPs,warm}$ during that interim period are not reflective solely of variations in aerosol production rates.

Overall, peaks in n_{INPs} were not directly related to Chl *a* concentrations, and the response in n_{INPs} across the range of temperatures was not uniform, supporting the expectation that the INP population was indeed comprised of diverse sub-populations that expressed themselves at different points throughout the chronosequence of each phytoplankton bloom. Positive trends in Org_{ATOFMS} corresponded to periods of increased $n_{INPs,mid}$, suggesting that sea spray organic matter were important potential contributors to the INP population within the MART system. Increased

aerosolized HB measured by offline microscopy coincided with the multi-day elevated values of $n_{INPs,mid}$ that were also observed after the peak in Chl *a* concentrations. Increased emissions of HB may also indicate that other microbes, such as diatoms, fragments of diatoms, or viruses, were enhanced in the aerosol phase on these days and were important contributors to the INP population. However, the presence of IN-active marine microbes was not immediately supported by ATOFMS measurements, because $BioSS_{ATOFMS}$ spectra types were found to decrease during the period of high $n_{INPs,mid}$. The decline in $BioSS_{ATOFMS}$ in conjunction with increased HB counts from offline microscopy counts, is interpreted as an increase in aerosolized microbes comprised significant organic coatings. While the total concentration of viruses (*Malfatti et al.* in prep) was not correlated with the abundance of INPs at any temperature range, suggesting they were not a dominant contributor to the overall INP population, this does not preclude a particular strain of phage possessing IN activity.

Evaluation of trends in enzyme activities within the bulk seawater can also elucidate contributions from biomolecules and microbes. For example, if a relationship between n_{INPs} and protease activity is observed, the growth of protease-producing HB are probably linked to the INP population. Similarly, a trend of n_{INPs} with lipase activity would suggest that a portion of the INP population is linked to the presence of microbes that degrade lipids. Evaluation of enzyme activity revealed little indication of any correlations with n_{INPs}. However, a slight increase in protease enzyme activity (in Figure 3.1-1) was coincident with a reduction in $n_{INPs,mid}$. Summarizing the MART study, measurements of HB and organic aerosol indicate that the most variable population of INPs, active between -25 and -15 °C, may have been non-cellular organic matter (i.e., biomolecules) or microbes. Direct investigations of the characteristics of INPs during the MART study are described in Sections 3.2.b, 3.2.c, and 3.2.d.

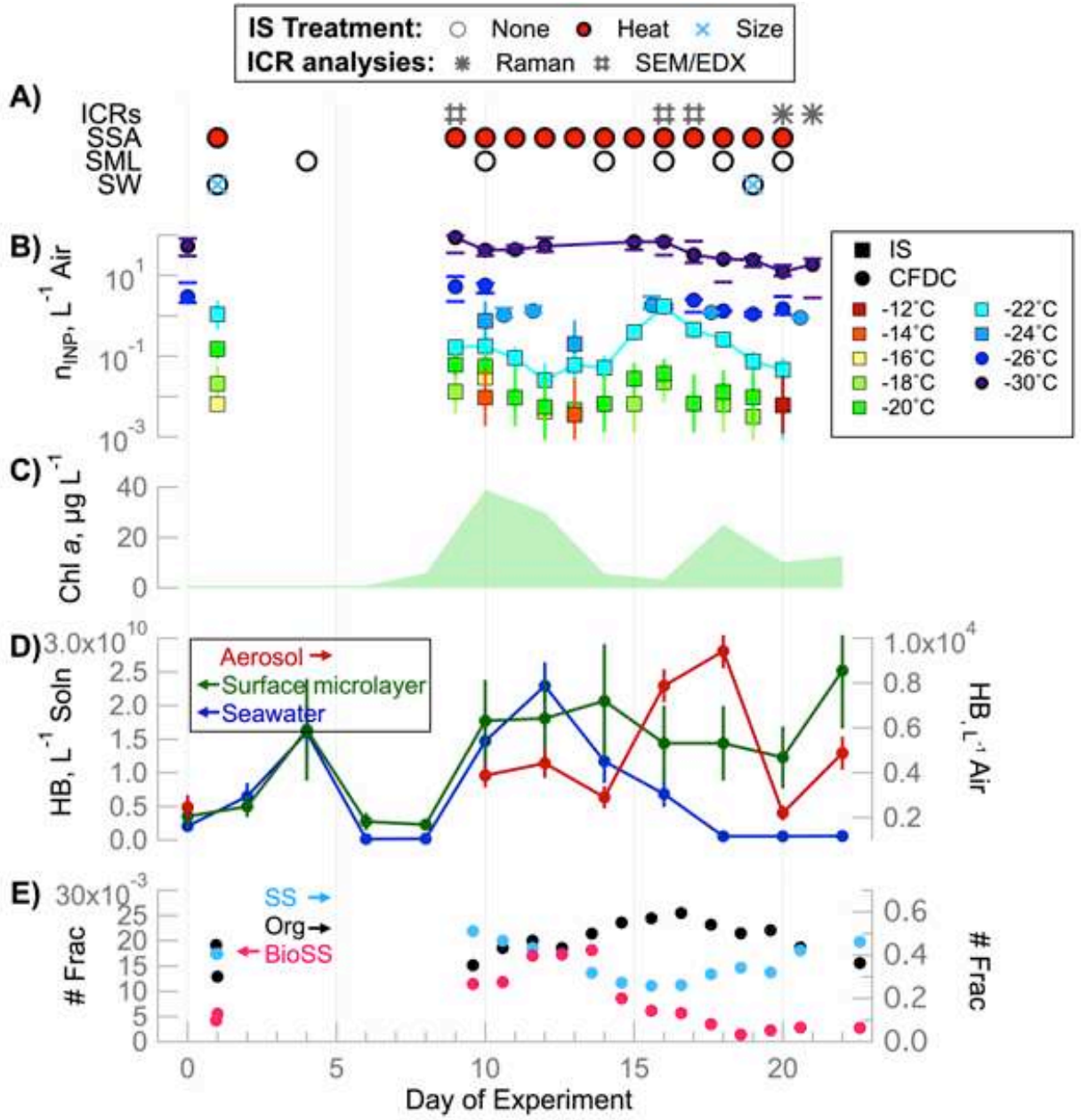

Figure 3.2-1. Timeline of (A) different tests performed on each day, including heat treatments (red filling), size filtering (blue cross) and collections of ice crystal residuals (ICRs) for Raman (asterisk) and SEM/EDX (Hash) analyses, during the MART study. Also shown are (B) ice nucleating particle (INP) number concentrations (*McCluskey et al.,* 2017), (C) Chlorophyll *a* concentrations, (D) counts of heterotrophic bacteria (HB) measured in the seawater (SW, blue), surface microlayer (SML, green) and aerosol (red) (*McCluskey et al.,* 2017) and (E) number fraction of mass spectral types measured during the MART study (*Sultana et al.*, 2017b). Figure from *McCluskey et al.* (*submitted to J. Atmos. Sci.*)

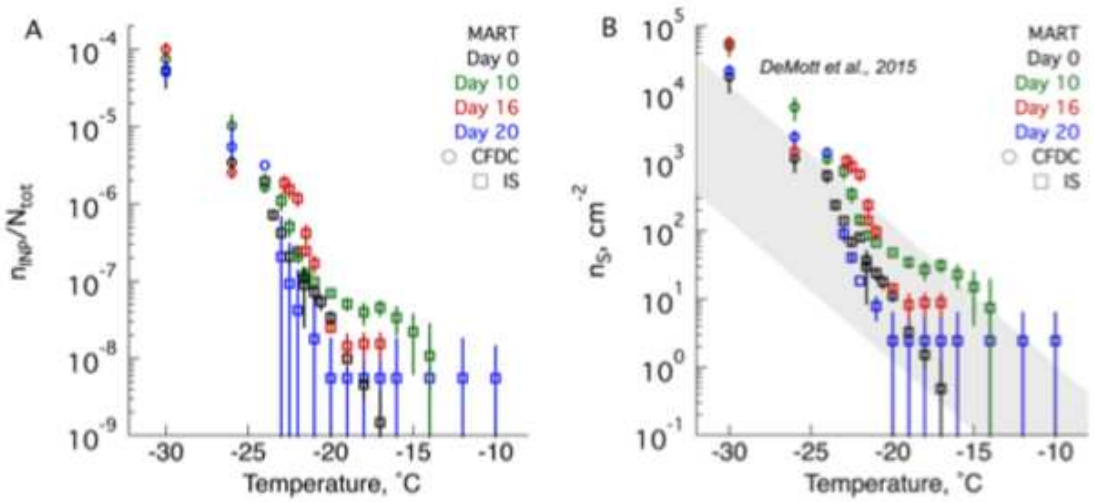

Figure 3.2-2. IN activity temperature spectra normalized by A) total aerosol number concentrations and B) total aerosol surface area (markers) for case study days of the MART study. Also shown in B is the range of nucleation site density values for marine aerosol reported by *DeMott et al.* (2016). This figure is from *McCluskey et al.* (2017).

3.2.a.ii IMPACTS

Timelines of n_{INPs} at various temperatures (-20 to -8 °C) and Chl *a* concentrations from the IMPACTS study are shown in Figure 3.2-3. Similar to the MART study, the most variable temperature regime of INPs captured throughout the duration of the blooms was $n_{INPs,mid}$. The first peak in $n_{INPs,mid}$ occurred on Day 14, with a sharp increase by a factor of 40 in $n_{INP,-22\,°C}$ from Day 13 to Day 14. A second peak in $n_{INPs,mid}$ was observed from Days 18-23, comprising an increase in $n_{INPs,\,-22°C}$ of a factor of 3 and lagging the first Chl *a* peak by 4 days. On Days 14, 20 and 22, coincident with the first and second n_{INPs} peaks, IN activity was observed at -8 °C, the warmest temperature observed for IN activity in both laboratory studies. $n_{INPs,cold}$ varied by an order of magnitude, with $n_{INPs,-30°C}$ reaching maxima on Days 15 and Day 26. Figure 3.2-4 shows normalized IN activity temperature spectra for focus days during the IMPACTS study, accounting for changes in aerosol generation, and revealing that, again, trends in $n_{INPs,cold}$, $n_{INPs,mid}$, and $n_{INPs,warm}$ were independent of particle emission variations.

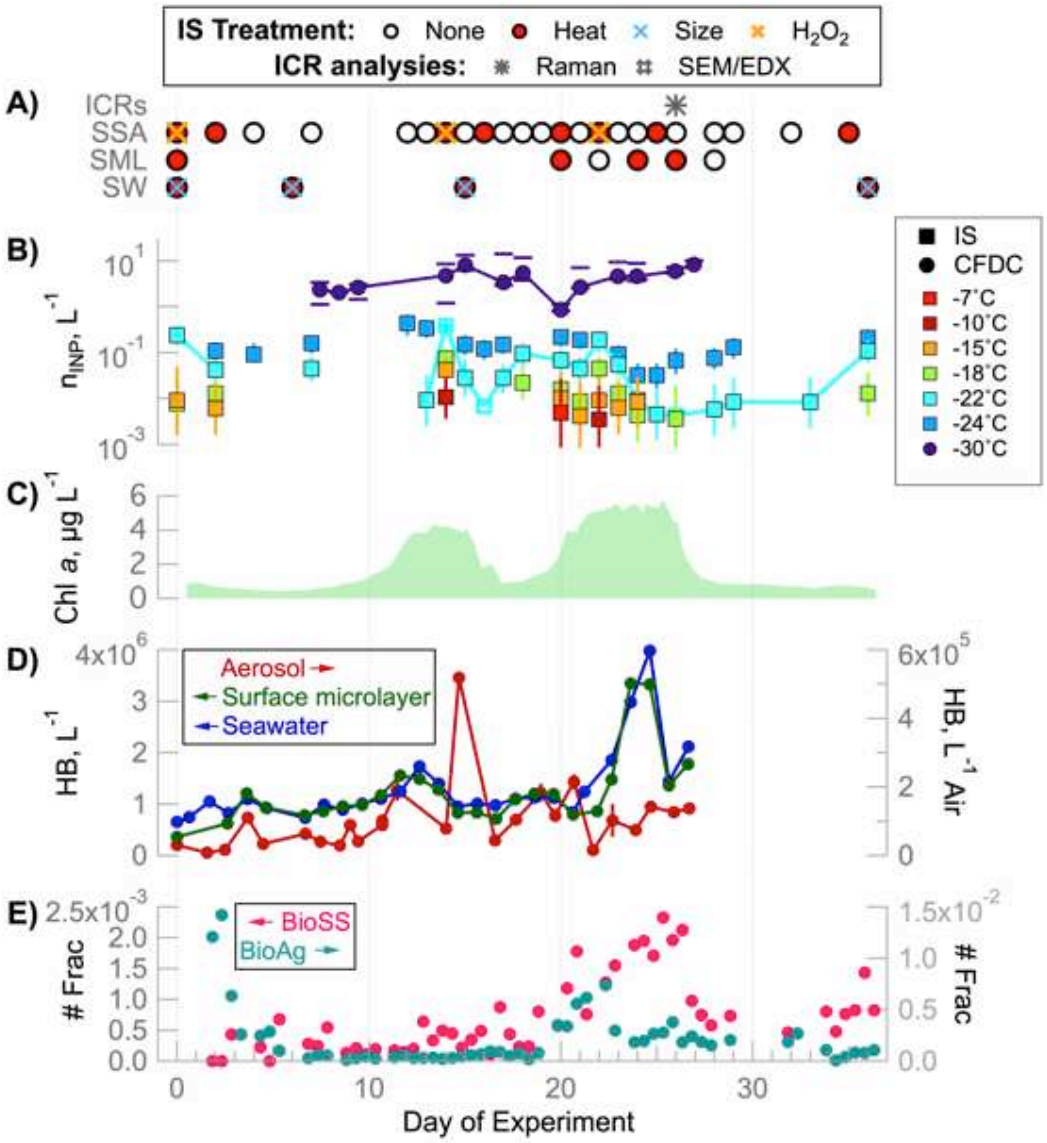

Figure 3.2-3. Timeline of (A) different tests performed on each day, including heat treatments (red filling), size filtering (blue cross), hydrogen peroxide digestion (orange cross) and collections of ice crystal residuals (ICRs) for Raman (asterisk) and SEM/EDX (hash) analyses. (B)-(E) are the same as Figure 3.2-1, but for the IMPACTS study. From *McCluskey et al.* (*submitted to J. Atmos. Sci.*).

On Day 14, peaks in $n_{INPs,warm}$ and $n_{INPs,mid}$ were elevated coincident with a higher fractional contribution of aliphatic-rich organics to the submicron aerosol detected by the HR-ToF-AMS (*Wang et al.,* 2015). In contrast, the oxygen-rich supermicron organic type gradually increased throughout the first bloom and leveled off and was not correlated with INP emissions. Although seemingly disconnected from abundances of HB in the bulk water and SML, days that

had higher levels of aerosolized HB also tended to have the highest concentrations of INPs active at the warmest temperature (-8 °C, Day 14). The positive contribution of both biomolecules (i.e., non-cellular organics) and microbes to the INP population on Day 14 was further supported by trends in enzyme activity; the peaks in $n_{INPs,mid}$ and $n_{INPs,warm}$ corresponded to a peak in protease activity, suggesting that protein-utilizing constituents (i.e. bacteria or diatoms) contributed to the INP population that was emitted on Day 14. The second peak in $n_{INP,mid}$ was not correlated with organic aerosol or aerosolized HB. Interestingly, in this episode, elevated protease and lipase activities were associated with a collapse in the second $n_{INPs,mid}$ peak (Days 18-23), suggesting that the INP population in this second peak may have also included protein-containing microbes and/or intact lipids. Finally, a positive relationship of $n_{INPs,cold}$ with lipase enzyme activity was observed, indicating that an increase in processed lipids, including fatty acids, may be associated with INPs active at colder temperatures.

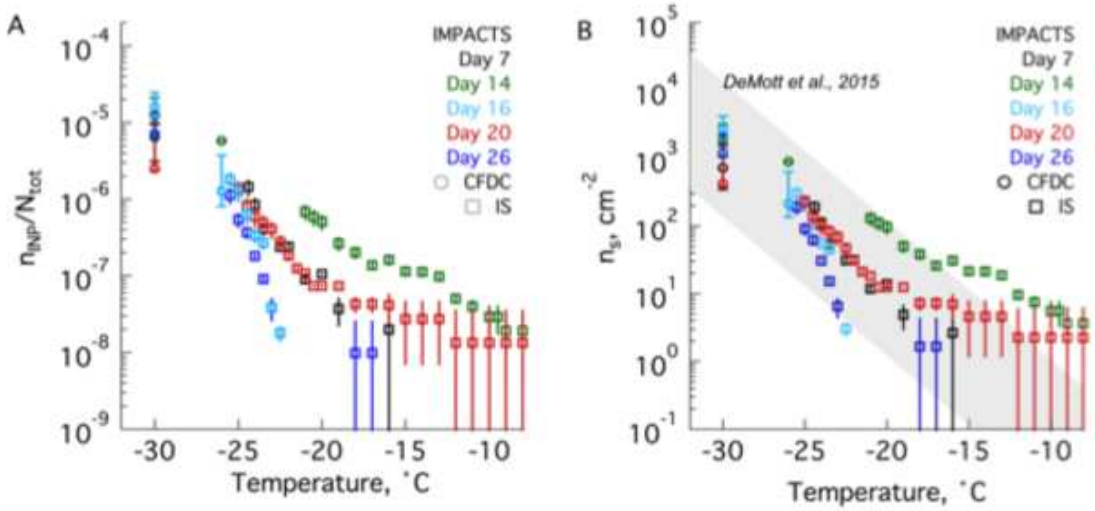

Figure 3.2-4. Same as Figure 3.2-2, but for IMPACTS study.

3.2.a.iii Summary of dynamics in n_{INPs} during MART and IMPACTS studies

No evidence was found to support a direct relationship between Chl *a* or total organics and $n_{INPs,}$ as suggested previously (*Prather et al., 2013*). However, a complex relationship

between INPs released as aerosol and the microbiology occurring in the seawater was observed. In general the MART and IMPACTS studies possessed similarities in the response of INP production to Chl *a*, in which $n_{INP,mid}$ was found to increase approximately 3-4 days after the collapse of the bloom. This trend scaled with the density of the bloom, where a 30-fold increase was observed during the MART study and only a 3-fold increase was observed in the IMPACTS study. However, tremendous complexity is evident, where slight alterations in the SML, on timescales shorter than 1 day, facilitate higher releases of both aliphatic-like organic aerosol and HB, increasing emissions of INPs active over a broad temperature range.

3.2.b Ice nucleating entities in seawater and sea surface microlayer

During the MART study, number concentrations of INEs active at -20 °C in the SW ($n_{INEs,SW}$) were 43 mL^{-1} on Day 0 and decreased by a factor of 25 to 1.7 mL^{-1} by Day 19 (Table 3.2-1; Figure 3.2-5). These concentrations were within the range previously reported in bulk seawater from other locations (*Schnell et al.,* 1974*; Schnell,* 1977). Filtration tests (0.2 μm filter) revealed that 50 to 100% of the INEs in SW active at -20 °C were present in the 0.2 μm filtrate (Table 3.2-1, Figure 3.2-5). Number concentrations of INEs in the SML ($n_{INEs,SML}$) were also measured on Days 4, 10, 14, 16, 18, and 20 of the MART study (Figure 3.2-6); $n_{INEs,SML}$ active at -20 °C were below the detection limit at the beginning of the study (Day 4) and reached a maximum on Day 16 (74 mL^{-1}).

During the IMPACTS study, $n_{INE,SW}$ was measured on Days 0, 6, 15 and 36 and ranged from > 54 mL^{-1} (Day 0) to 2 mL^{-1} (Day 15) at -20 °C (Table 3.2-2, Figure 3.2-5) throughout the course of the experiment. Heating tests revealed that 61 to 95% of INEs were heat labile on Days 0, 6 and 36. On Day 15, seawater INEs were not heat sensitive. IMPACTS SML samples were analyzed on Days 0, 20, 22, 24, 26 and 28. $n_{INEs,SML}$ at -20 °C ranged from 21 mL^{-1} (Day 26) to

100 mL^{-1} (Day 28) during IMPACTS (Figure 3.2-6). Heating tests, performed on SML samples collected on Days 0, 20, 24 and 26, showed that a statistically significant portion of the measured SML INEs were heat labile on Day 0 and Day 26 (Figure 3.2-7).

In both studies, direct DNA-based tests were used to screen SW and SML for the ice nucleation active (*ina*) gene, motivated by previous studies that had isolated ice nucleating bacteria (INB) from seawater collected from the SIO pier (*Fall and Schnell,* 1985). However, the *ina* gene was not detected in any of the samples tested and no evidence was found for the presence of known INB strains. While it is possible that INB strains of these species were present but possessed alleles of the *ina* gene that failed to be amplified, the primers used provide the broadest coverage available short of full metagenomic profiling.

3.2.c Contributions of heat labile material to aerosol INP populations

Heat treatments were applied to all SSA samples during the MART study and no significant change in IN activity was observed due to heating for most days (Table 3.2-1; Figure 3.2-8). However, during the observed peak periods of INP emissions, on Days 14, 15 and 17, heating lead to a significant increase (factor of 10 to 30) in n_{INPs} for temperatures -20 to -10 °C (Figure 3.2-8). An increase in INP activity on exposure to heating has not previously been reported and some possible explanations for this observation are discussed in Section 3.3.a.

During the IMPACTS study, smaller aerosol sample volumes were available (shorter sampling times were allowed) and thus heat treatments were only applied to select samples (Table 3.2-2). Except for Days 25 and 35, where no significant change was observed, heating resulted in a reduction in n_{INPs} at temperatures warmer than -25 °C (Figure 3.2-9). The highest contributions of heat labile INPs (i.e., proteinaceous or thermally unstable IN macromolecules (*Pummer et al.,* 2015; *Hill et al.,* 2014) to the INP population were observed on Days 14 and 20.

However, on Day 16 INPs were enhanced due to heating, similar to several samples collected during the MART study, and is discussed in Section 3.3.b. The H_2O_2 treatment, which was used to oxidize and denature all organic matter, was also applied on Days 0, 14 and 22 and n_{INPs} were statistically significantly reduced, with the largest impact observed on Day 14 (Figure 3.2-9).

3.2.d Characteristics of ice crystal residuals

To directly identify the types of particles responsible for ice nucleation from these mesocosm experiments, nucleated ice crystals were collected downstream of the CFDC and ice crystal residuals (ICRs) were probed with microscopic techniques to determine their morphology and chemical composition. During the MART study, ICRs were collected for SEM/EDS analyses on Days 9, 16 and 17, and 27 and 80 ICRs were analyzed for each sample (Table 3.2-3). These ICRs are material remaining after ice crystals (collected at approximately -30 °C) evaporate. The mode diameters of ICRs on Day 9, 16 and 17 were 250, 750 and 300 nm, respectively (Figure 3.2-10). The morphology analysis revealed that many ICRs (10-30%) were crystalline particles visibly coated (Type A, Figure 2.4-4) and a significant proportion (18-33%) of ICRs were considered heterogeneous (Type B, Figure 2.4-4). The majority (50-66%) of the ICRs collected were unclassified (Type C, Figure 2.4-4), due to their indistinct shape or limited resolution of the SEM. EDS elemental analyses are also summarized in Table 3.2-3. All ICRs that were classified as crystalline with coatings (Type A) contained NaCl and the majority of these had significant amounts of organic carbon. The primary diameter of these coated crystalline residuals ranged from 200 nm to over 2 μm, with an average diameter of 0.55-0.62 μm. We note that the residual material for this morphology type includes a coating that may lead to an over-estimate of the primary diameter (See Figure 2.4-4). ICRs classified as heterogeneous ranged from 0.22 to 1.8 μm (mean primary diameter 0.56-0.97 μm), and organic carbon was detected for nearly all ICRs

within this morphology type (40 out of 42), while NaCl was detected in only a few of these ICRs. Finally, unclassified ICRs had the smallest sizes (average diameters ranged from 0.3 to 0.48 μm), due to the contributions from ICRS that were unresolved because of their small size. However, several larger ICRs were also considered unclassified, illustrated by the maximum residual diameters for this morphology type.

The chemical composition of ICRs was also probed via Raman microspectroscopy on Days 20 and 21 of the MART study (Figure 3.2-11). These collections occurred following a period of elevated number concentrations of INPs active between -25 and -15 °C on Days 15-18 (Figure 3.2-1). Raman particle spectra revealed that over 90% (N = 50) of the ICR spectral signatures contained long chain fatty acids (Figure 3.2-11). In contrast, the Raman spectra for the total submicron ($0.56 < D_p < 1$ μm) aerosol particle population (shown for Day 18, the closest day with available data) were dominated by lipopolysaccharides (indicative of Gram-negative bacteria), and long- and short-chain fatty acids.

ICRs collected on Day 26 of the IMPACTS study were also analyzed with Raman microspectroscopy. Similar to the ICR samples from the MART experiment, the Day 26 IMPACTS SSA sample represented INPs present at the conclusion of a peak in INPs observed at temperatures ranging between -25 and -15 °C from Days 17 to 23. The most common Raman spectrum type, representing over 40% of the ICRs analyzed (N = 165) was siliceous material (Figure 3.2-11), indicative of diatomaceous cellular material. An additional ICR sample was collected from a MART, run coincidentally during the IMPACTS study, that contained fresh seawater (SW collection from SIO on 27 July 2014) and had no nutrient addition. The siliceous material in the ICRs isolated from SSA produced by this MART was similar to that observed in

ICRs isolated from SSA on Day 26 of the IMPACTS study (Figure 3.2-11). Polysaccharides and long- and short-chain fatty acids were also observed in the IMPACTS ICR populations.

Table 3.2-1. Number concentrations of ice nucleating entities (INEs) in seawater (SW) and sea surface microlayer (SML) and ice nucleating particles (INPs) in sea spray aerosol samples at -20 °C during the MART study. Number concentrations of INEs and INPs after heating or filtering are also shown. A "-" indicates the treatment was not performed on the sample; "ADL" and "BDL" indicate values above and below the detection limit, respectively. Also reported are the 95% confidence intervals, listed in parentheses. The SSA samples only included samples that were treated with heating or filtering.

Day	No treatment	95 °C for 20 min	0.2 μm filtrate
	Bulk seawater, $n_{INEs,\ SW}$(mL^{-1})		
1	43 (23-63)	-	20 (11-30)
19	1.7 (0.5-6.0)	-	2.7 (0.85-7.4)
	Sea surface microlayer, $n_{INEs,\ SML}$(mL^{-1})		
4	*BDL*	-	-
10	22 (11-40)	-	-
14	4.8 (1.3-12)	-	-
16	74 (45-110)	-	-
18	15 (7.3-31)	-	-
20	19 (8.7-37)	-	-
	Sea spray aerosol, n_{INPs} ($x10^{-2}$ L^{-1} Air)		
1	15 (8.6-24)	30 (15-51)	-
9	6.1 (3.0-11)	*ADL (>71)*	-
10	5.6 (2.4-12)	2.4 (.47-13)	-
11	0.95 (1.9-5.1)	*BDL (< 2.9)*	-
12	0.55 (0.072-3.6)	2.5 (1.8-6.2)	-
13	0.46 (0.4-3)	3.4 (0.98-12)	-
14	0.65 (0.13-3.5)	20 (9.3-39)	-
15	2.7 (1.1-6.8)	43 (24-70)	-
16	3.7 (1.5-8.5)	5.4 (4-13)	-
17	0.66 (0.13-3.5)	65 (35-100)	-
18	1.3 (0.38-4.5)	0.92 (0. 079-9.9)	-
19	0.94 (0.19-3.9)	0.90 (0. 077-9. 7)	-
20	0.61 (0.12-3.3)	0.92 (0.079-9.9)	-

Table 3.2-2 Same as Table 3.2-1, but for the IMPACTS study. An additional hydrogen peroxide (H_2O_2) digestion treatment was included. Full spectra for SW and SML from the IMPACTS study treatments are provided in Figure 3.2-5, Figure 3.2-6, and Figure 3.2-7. The SSA samples only included samples that were treated with heating or filtering. All SSA INP data are as reported by *McCluskey et al.,* (2017).

Day of IMPACTS	**Number concentrations of INEs and INPs (T = -20 °C)**			
	No treatment	95 °C for 20 min	0.2 μm filtrate	H_2O_2 digestion
	Bulk seawater, $n_{INEs,\ SW}(mL^{-1})$			
0	*ADL (> 54)*	7.3 (4-13)	6.8 (3.6-12)	-
6	10 (5.7-17)	0.55 (0.096-2.9)	0.53 (0.093-2.9)	-
15	2.0 (0.66-5.5)	2.3 (0.88-5.7)	*BDL (<5.5)*	-
36	2.9 (1.1-6.9)	0.58 (0.10-3.1)	1.1 (0.31-4.0)	-
	Sea surface microlayer, $n_{INEs,\ SML}$ (mL^{-1})			
0	27 (10-66)	*BDL (<0.64)*	-	-
20	34 (14-76)	34 (14-76)	-	-
22	75 (40-130)	-	-	-
24	66 (34-120)	13 (3.5-45)	-	-
26	100 (59-170)	*BDL (<0.64)*	-	-
28	21 (10-66)	-	-	-
	Sea spray aerosol, n_{INPs} $(x10^{-2}\ L^{-1}\ Air)$			
0	7.2 (0.36-14)	0.64 (0.11-0.34)	-	*BDL (< 3.8)*
2	0.02 (0.93-3.9)	*BDL (< 0.18)*	-	-
14	19 (11-29)	7.1 (3.4-12)	-	0.88 (0.72-3.8)
16	*BDL (<0.7)*	5.3 (2.5-11)	-	-
20	2.7 (1.2-5.7)	0.10 (0.017-0.53)	-	-
22	16. (8.3-22)	3 (1.7-3.6)	-	0.83 (0.14-4.4)
25	*BDL (< 0.26)*	0.26 (0.045-1.4)	-	-
35	8.4 (4.6-15)	0.49 (0.4-2.1)	-	-

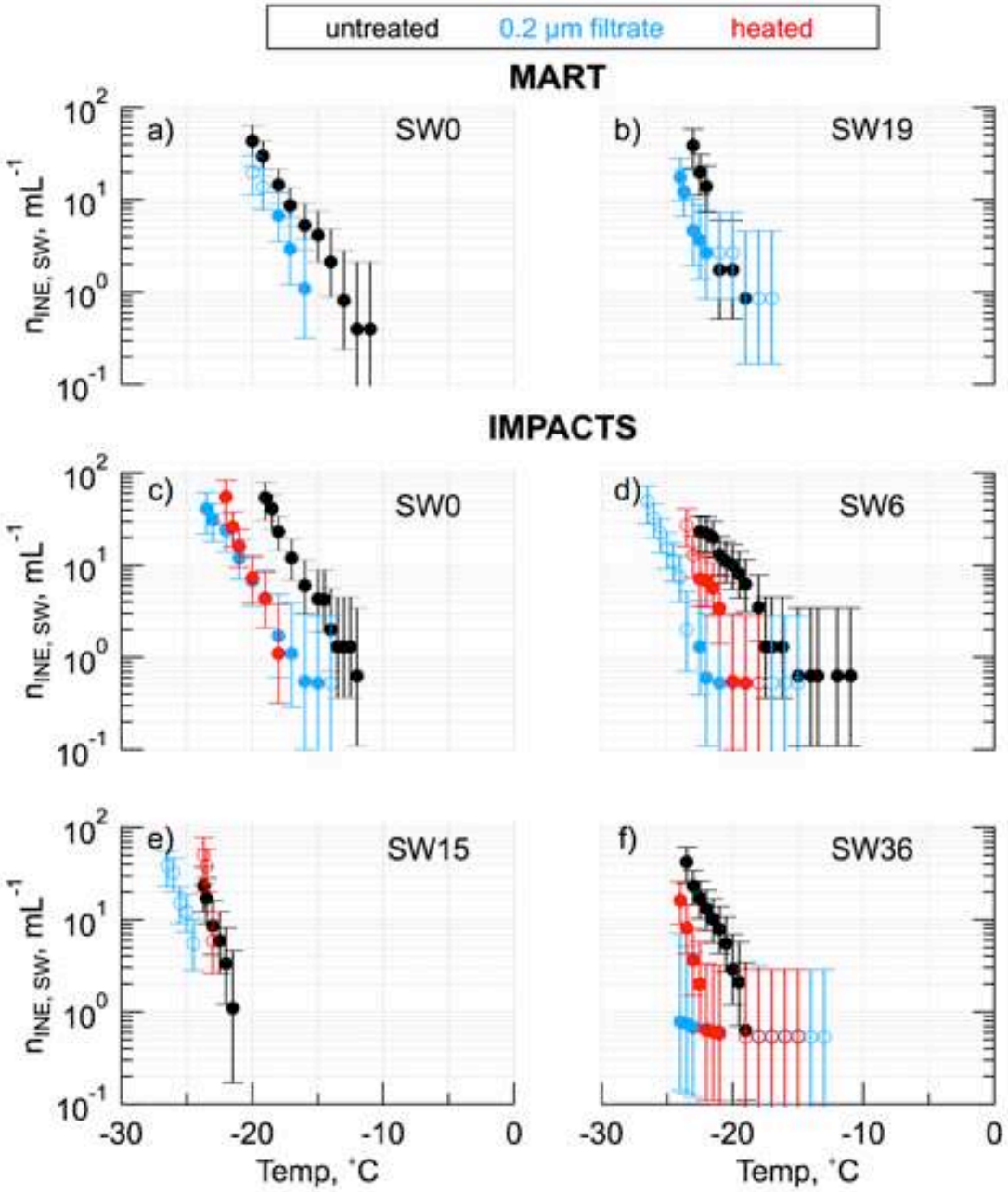

Figure 3.2-5. Temperature spectra of ice nucleating entity (INE) number concentrations in untreated bulk seawater samples (black) collected on a) Day 0 and b) Day 19 of the MART study and c) Day 0, d) Day 6 e) Day 15 and f) Day 36 of the IMPACTS study. Blue markers correspond to INE spectra obtained after filtering seawater through a 0.2 µm filter and red markers correspond to INE spectra obtained after heating (95 °C for 20 min) seawater. n_{INPs} determined from the treated samples that are statistically significantly different ($p < 0.05$) from unperturbed sample are shown as filled markers, while those that are not statistically different are shown as open markers. Vertical bars are the 95% confidence intervals for the IS measurements. Figure from *McCluskey et al.* (*submitted to J. Atmos. Sci.*).

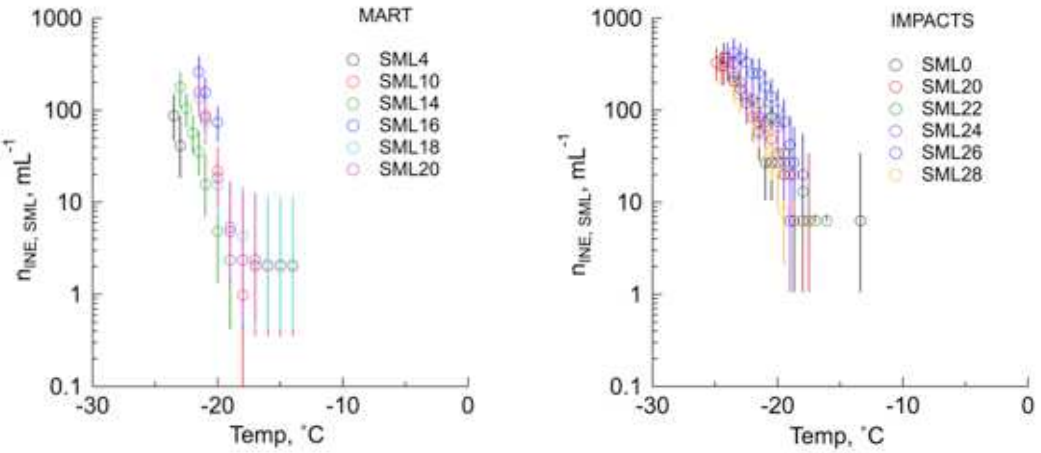

Figure 3.2-6. Temperature spectra of INE number concentrations in SML samples collected during the a) MART study and b) IMPACTS study labeled by day as SML[day#]. Vertical bars are the 95% confidence intervals for the IS measurements.

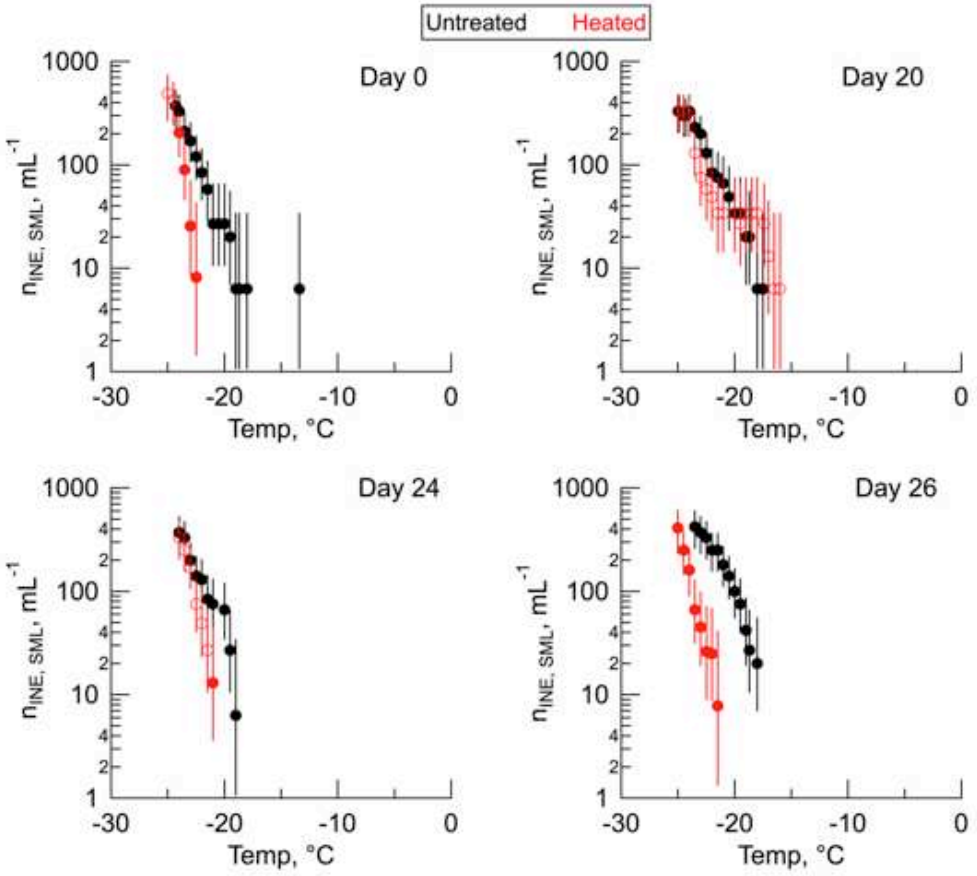

Figure 3.2-7. Temperature spectra of INE number concentrations in SML samples (black) collected on Day 0, Day 20, Day 24 and Day 26 of the IMPACTS study. Red markers correspond to INE spectra obtained after heating (95 °C for 20 min) SML samples. n_{INPs} determined from the heat treated samples that are statistically significantly different ($p < 0.05$) from unperturbed sample are shown as filled markers, while those that are not statistically different are shown as open markers.

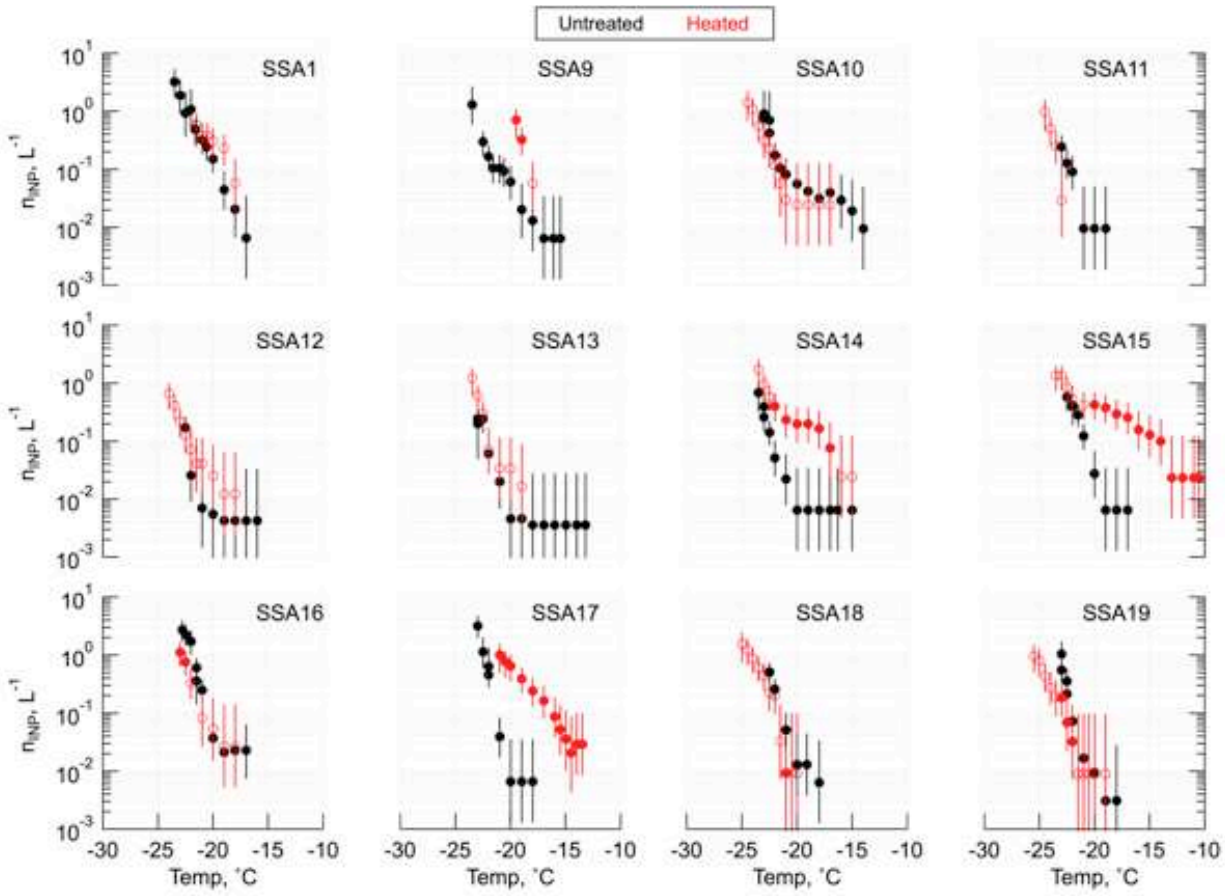

Figure 3.2-8. Temperature spectra of ice nucleating particle (INP) number concentrations for SSA samples collected during the MART study and labeled by day as SSA[day#]. Spectra for unperturbed samples are shown in black, while spectra for heated samples are shown in red. n_{INP} determined from the heat treated samples that are statistically significantly different ($p < 0.05$) from unperturbed sample are shown as filled markers, those that are not statistically different are shown as open markers. Vertical bars are the 95% confidence intervals for the IS measurements.

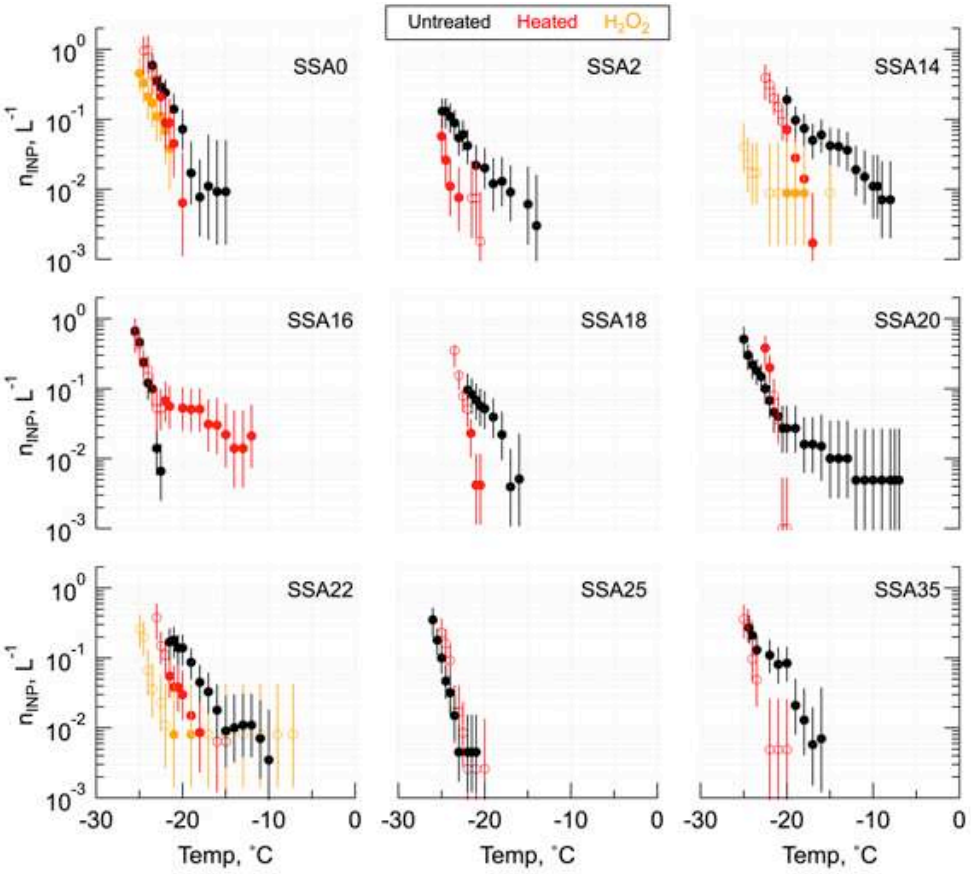

Figure 3.2-9. Temperature spectra of ice nucleating particle (INP) number concentrations for SSA samples collected during the IMPACTS study and labeled by day as SSA[day#]. Spectra for unperturbed samples are shown in black, spectra for heated samples are shown in red and spectra for hydrogen peroxide digested samples are shown in yellow. n_{INP} determined from the treated samples that are statistically significantly different ($p < 0.05$) from unperturbed sample are shown as filled markers, those that are not statistically different are shown as open markers. Vertical bars are the 95% confidence intervals for the IS measurements.

Table 3.2-3. Summary of SEM/EDS results from Day 9, 16 and 17 of the MART experiment for the three different morphology categories: Crystalline with coatings (Type A), Heterogeneous (Type B) and Amorphous/Unclassified (Type C). Number of ICRs that contained organic carbon (N_{org}) and sodium chloride (N_{NaCl}) are also provided for each morphology type.

	Day 9				Day 16				Day 17			
	A	**B**	**C**	**Total**	**A**	**B**	**C**	**Total**	**A**	**B**	**C**	**Total**
N	9	18	27	**54**	8	5	14	**27**	8	19	53	**80**
%	17	33	50		39	19	52		10	24	66	
N_{org}	9	18	14	**41**	3	5	3	**11**	8	17	41	**66**
N_{NaCl}	9	2	7	**18**	8	4	2	**14**	8	4	11	**23**

Morphology A is Crystalline with coating; B is Heterogeneous, C is Unclassified

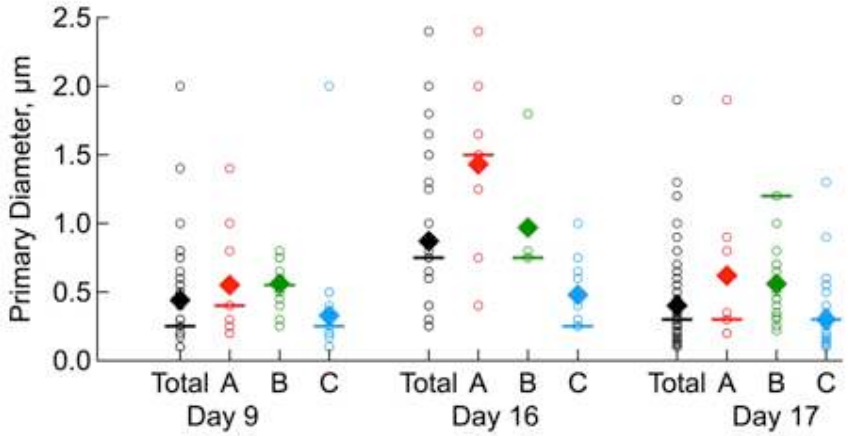

Figure 3.2-10. Primary diameters for total ICRs and ICRs in each morphology class (as defined in Table 3.2-3) for the MART study. Mean and mode primary diameters are shown as diamond and horizontal lines, respectively.

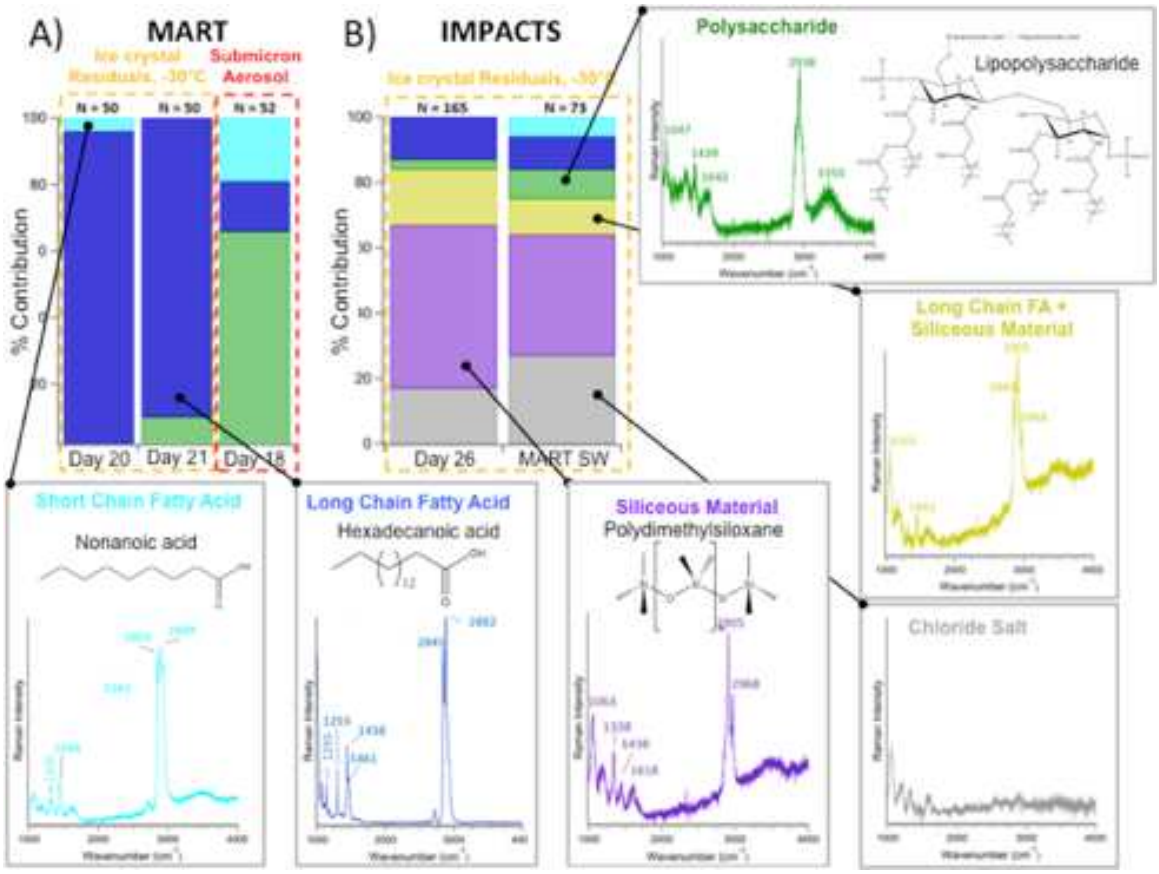

Figure 3.2-11. Contribution of Raman spectra types to collected ice crystal residuals (ICRs) during A) Day 20 (n=50) and 21 (n=50) of the MART study and B) Day 26 (n=165) and unperturbed fresh seawater SSA (n=73) (collected from a MART tank filled with fresh seawater on 27 July 2014) during the IMPACTS studies. Also shown is the contribution of Raman spectra types to the total submicron aerosol ($0.56 < D_p < 1.0$ µm) population during the MART study on Day 18 (n = 52).

Section 3.3 Discussion

3.3.a Ice nucleating material during MART study

In the MART study, filtering treatments revealed that a large fraction of the INEs were present in the 0.2 μm filtrate of seawater sample (Table 3.2-1,Figure 3.2-5). This finding is consistent with recent investigations that found material smaller than 0.2 μm was a major contributor to INEs in SML samples collected in the North Atlantic and Arctic Oceans (*Wilson et al.,* 2015) and over Canadian Arctic Ocean region (*Irish et al.,* 2017). INEs in the SML increased towards the end of the study ($n_{INE,SW}$ was 1.7 mL^{-1} on Day 19 and $n_{INE,SML}$ was >20 mL^{1} on Days 18 and 20). These measurements suggest that, along with other surface-active molecules and constituents, INEs are transferred from the bulk SW to the SML. Higher concentrations of INEs in SML compared to SW have been reported previously (*Wilson et al.,* 2015).

During the MART study, over 80% of the Raman spectra, for ICRs collected at -30 °C, were classified as containing long-chain fatty acids (Figure 3.2-11). The action of long-chain fatty acids as IN-active monolayers or crystallites has not been investigated extensively, but previous studies show contradictory results. *Gavish et al.* (1990) suggested potential IN activity of carboxylic acid monolayers, warmer than -20 °C, but these observations were made very close to the freezing point of pure water samples in their experimental setup. More recent studies of freezing of palmitic acid (*Qiu et al.,* 2017) and nonadecanoic acid (*Knopf and Forrester,* 2011) monolayers indicate a requirement for much lower temperatures, within several degrees Celsius of the homogeneous freezing limit, consistent with theoretical considerations (*Qiu et al.*, 2017). The SEM analyses on ICRs showed morphologies containing large amounts of crystalline and amorphous materials that included organics (Table 3.2-3). We therefore surmise that significant

amounts of long chain fatty acids may be released into SSA and are active as INPs at cooler temperatures (T < -30 °C). This is an ongoing area of research.

INP activity across the range of temperatures did not respond to heat treatments in a manner that would indicate the presence of proteinaceous INPs (Table 3.2-2, Figure 3.2-8). Notably, heating in some cases resulted in increased IN activity of the collected SSA over a range of temperatures warmer than -22 °C (by a factor of 10-30 at -20 °C) on Days 14, 15 and 17. This unique heating effect has not been reported previously. As such, we offer a few possible mechanisms that may lead to an increase in particulate surface area (i.e., more area available for ice nucleation sites) or that would reveal IN-active surfaces due to heating. Microbial cells may lyse in response to heating, dispersing their membranes and releasing intracellular material, such as viruses, cytoplasm, organelles and dissolved organic molecules. Some types of diatom membrane surfaces (*Knopf et al.,* 2011) and their contents (*Wilson et al.,* 2015) have been suggested to be IN active in laboratory studies and their contents may also be released after heating. *Junge and Swanson* (2008) report no IN activity down to -41 °C for a *Colwellia* infecting phage V 9. However, the IN ability of marine viruses and their heat sensitivity is largely unknown. Ice nucleation active molecules from the collected particles may dissolve into the sample solution after degradation from the heat treatment and, upon cooling, these coatings may be redistributed onto particles or even the suspension surface, leading to a higher proportion of particles coated with IN active organics, or islands of IN-active monolayers on the surface of aliquots tested in the IS. For example, certain alcohols are known to stimulate ice nucleation as monolayers (*Gavish and Popovitz-biro,* 1990; *Popovitz-Biro et al.,* 1991; *Popovitz-Biro et al.,* 1994; *Qiu et al.,* 2017).

Single particle chemistry data, provided by the ATOFMS, in combination with offline microscopy HB counts were used to interpret the heat treatment findings from the MART Study. As mentioned previously (Section 3.1.a.ii), $BioSS_{ATOFMS}$ spectra type, representative of cells or cellular fragments absent of significant organics, and offline microscopy HB counts that do not detect organic coatings, indicated that significant organic coatings were present on aerosolized HB and likely other microbes during the second half of the MART study. This is further supported by the observed decline in SS_{ATOFMS} as Org_{ATOFMS} increased. Thus, we hypothesize two possible mechanisms for the MART heating results: 1) the offline heat treatment of the SSA dissolved organic coatings from the collected particles, which were then redistributed onto all available particles, thereby increasing the surface area of IN-active organic coatings on particles or 2) heating SSA induced bursting of bacteria (or other microbes), thereby augmenting the number of particles with the IN-active non-cellular organic material.

The contribution of IN-active organic material to the INP population observed during the MART study is further supported by SEM/EDS analysis, revealing that most ICRs contained significant amounts of organic carbon and that >30% of ICRs included visible organic coatings. Since the INEs in the bulk seawater remained in the 0.2 μm filtrate (Figure 3.2-5), the INEs are likely agglomerating into larger particles upon ejection or are attaching to the surfaces of other non IN-active particles such as NaCl.

3.3.b Ice nucleating material during IMPACTS study

During IMPACTS, we observed a significant portion (>80%) of the INEs in the bulk seawater were removed after 0.2 μm filtering and were heat-labile, indicating that the INEs in the seawater were possibly microbial cells (Table 3.2-2, Figure 3.2-5). INEs in the SML were also heat labile. On days of elevated concentrations of INPs active at T = -25 to -15 °C (Day 14 and

22), the number concentrations of aerosol INPs were degraded by 18-37% in response to heating (Figure 3.2-9). The H_2O_2 treatments also revealed that the majority of all INPs on Days 14 and 22 were organic (i.e., not mineral or other refractory material). The fractional contribution of $BioSS_{ATOFMS}$ and $BioAg_{ATOFMS}$ signatures suggested relatively high transmission of microbes into SSA, with relatively insignificant organic coatings after particle drying. These particles corresponded to higher n_{INPs} active at temperatures warmer than -25 °C (Days 19 to 24, Figure 3.2-1, *McCluskey et al.,* 2017). The important contribution of microbes to the INP population during the IMPACTS study was further supported by the Raman analyses, which revealed that over 50% of the ICRs were siliceous, indicating the presences of IN active microbial material (e.g., diatoms) that dominated INPs even at -30 °C. However, qPCR of the *ina* gene in bulk seawater found no evidence of presently known INB strains throughout the IMPACTS study. Hence, attribution of specific marine microbes responsible for generation of INEs and therefore INPs remains as a topic for future research.

Heat-labile and microbe-like INPs were most commonly observed during the IMPACTS study. However, on Day 16, heat treatments revealed indication of the non-cellular organic INP type that was often observed during the MART study, where a significant increase in IN activity was observed after heating. A change in the heat sensitivity of IN material may be associated with sharp changes in the SSA composition, similar to those investigated by *Wang et al.*, 2015, where rapid changes in organic aerosol were attributed to microbial degradation processes that modulate the abundance of organics in the SML. This rapid change in the INP population exemplifies at least a few of the complex processes that govern the relationship between the surface microlayer, biological processes and the release of marine INPs.

3.3.c Two classes of marine INPs

The findings from this work show that the marine INPs generated in our lab studies consisted of two distinct populations. One population of marine INPs, referred to here as "dissolved organic carbon INPs", are particles that contain INEs that pass through a 0.2 μm filter (i.e. following format of oceanography literature, but with 0.2 μm cutoff); these INPs were not heat-labile in these studies and comprise ice nucleation active molecules that may occur within or coat particles, embed themselves within exopolymers of colloids, partition into the SML, and even arrange themselves in a favorable lattice structure that catalyzes ice nucleation. DOC INPs were preferentially detected after the peak in Chl *a* concentration for the MART phytoplankton bloom, consistent with increased production of organic aerosol that is commonly observed during a bloom's decay (e.g., *O'Dowd et al.,* 2015*, Lee et al.,* 2015*, Wang et al.,* 2015). Previous observations of DOC INE material (*Wilson et al.,* 2015; *Irish et al.,* 2017) and small carbonaceous INPs (*Rosinski et al.,* 1987) fall under the proposed marine DOC INP type. We note that viruses are also possible contributors to the DOC INP population. DOC INPs may be important contributors to the INP population in cases of dense phytoplankton blooms that occur in nature, where the SML is significantly enriched with IN-active molecules that are transferred into the aerosol phase during bubble bursting. It is clear that this category possesses sub-categories that may be of different chemical makeup and dominate under different biological conditions or under different cloud activation conditions.

The second INP population is termed "particulate organic carbon INPs" or "POC INPs", which are microbes that are IN-active, heat labile and emitted as intact cells or as cell fragments. The contribution of POC INPs depends on the abundance of microbe species that are IN-active, which was not quantified for these studies (apart from excluding the known INB as contributors).

Diatoms tested by *Knopf et al.* (2011) and phytoplankton cultures tested by *Schnell and Vali* (1974) and *Fall and Schnell* (1985) are examples of the proposed marine POC INP type.

Both of the proposed marine INP populations were detected in these two laboratory experiments and lagged phytoplankton biomass growth (i.e. Chl *a*) leading to increases in aerosolized IN-active POC (i.e., bacteria and/or diatom fragments) or to enrichment of IN-active molecules in the SML that coated SSA particles. Both INP types appear to have similar INP temperature regime, where INPs are active at temperatures warmer than -25 °C. We propose that future studies should aim to represent marine INPs in a manner that reflects two distinct types of organic matter: IN-active DOC and IN-active POC. Future studies should also aim to quantify the chemical classes of molecules and species of microbes that are IN-active. These findings will move us towards a mechanistic understanding of the production of INEs within a phytoplankton bloom life cycle and the transfer of INEs to the aerosol phase mediated by the SML.

3.3.d Evaluating existing parameterizations with laboratory-generated nascent SSA

Ultimately, a comprehensive determination and evaluation of the most important variables that are needed to predict ambient marine INP measurements should be completed, assuming of course the validity of our hypothesis regarding the origins of the INPs. Future observational campaigns will need to probe diverse regions and scenarios to adequately represent the key aspects of hemispheric, latitudinal, and regional differences in microbial diversity, seasonal variability and changes in INP activity associated with atmospheric processing of SSA, all of which are not represented in the MART and IMPACTS experiments. Hence, a marine INP parameterization was not developed based on these laboratory studies.

To put the findings from this work into context with the current proposed descriptions for atmospheric marine INPs, we compare our results to the recent parameterization proposed and

implemented by *Wilson et al.* (2015). In *Wilson et al.* (2015), SML collected from the North Atlantic and Arctic Ocean during summertime were used to determine a relationship between INPs and mass of total organic carbon in the SML. Their parameterization estimates the number concentrations of INPs present in the atmosphere based on two predictors: ambient temperature and mass of sea spray organic matter (*Wilson et al.,* 2015*).* The details of this parameterzation are presented in Chapter 4. TOC mass concentrations were measured for total suspended aerosol during the MART experiment (Figure 3.1-1), as described in Section 2.4.d.iii), and were used to estimate INP:TOC ratios in the aerosol phase during the MART study for INPs determined from the IS filters, as shown in Figure 3.3-1a. IMPACTS INP to TOC ratios were calculated with $PM_{2.5}$ and PM_{10} TOC mass concentrations and both of these values are presented to provide a range of values for this study, shown in Figure 3.3-1b. Unlike the MART study, where the IS filters were collected with minimal tubing, the IS filters collected during the IMPACTS study were likely more representative of $PM_{2.5}$ (see Section 2.4.a.ii). This analysis was only applied to the IS filter collections, since the upper size limit of the CFDC ($D_p < 1.5$ μm) may miss significant aerosol mass in the $PM_{2.5}$ fraction. While a few measurements, all of which were made during periods of the highest n_{INPs}, fell within an order of magnitude of the *Wilson et al.* parameterization, the majority of the data from this study were nearly two orders of magnitude lower than predicted by the relationship proposed by *Wilson et al.* (2015).

Assuming that INP number concentrations are proportional to total sea spray organic matter mass concentrations (i.e. organics are the only source of marine INPs), differences between our results and the predictions of *Wilson et al.* (2015) may be explained by the complex interplay between the seawater, SML and aerosol phase. During the process of bubble bursting, the SML entrains bulk seawater and the emitted aerosol becomes a mixture of SML and seawater

components. The enrichment factor for organics from the ocean to the aerosol can range across orders of magnitude (1 to >5000, *Burrows et al.,* 2013*; Quinn et al.,* 2015 and references therein). Results from these laboratory studies indicate that enrichment factors must be taken into account when estimating INP emissions. That is to say, if organics are the main constituents of marine INPs, the distribution of ice nucleation active organics among the emitted aerosol is likely an important feature needed to estimate n_{INPs}. In fact, recent work by *Wang et al.,* (2017) illustrated that jet drops and film drops contribute differently to sea spray organic matter and to INP emissions and that the contribution of jet and film drops to the total sea spray droplet distribution changes during a phytoplankton bloom. Another important difference between the *Wilson et al.* (2015) study and laboratory studies presented in this work was the origin of the seawater; the IN ability of organics in the MART study may have differed intrinsically from the material studied by *Wilson et al.* (2015).

In contrast to the relationship proposed by *Wilson et al.* (2015), the results from the MART mesocosm experiment indicated that n_{INPs} were independent of, or at least not well correlated with, total aerosol-phase organic carbon. Based on our findings, microbes and biomolecules may both be contributors to marine INP populations. Efforts to parameterize the connection between INP emissions and bulk seawater or SML biological activity will need to account for both of DOC and POC INP populations and their enrichment factors. An illustration of the complexity of the link between bulk water components and potential suspended INP components is demonstrated by *Malfatti et al.* (in prep) and from the HB counts from the IMPACTS study (Figure 3.1-2), where the abundance of HB found in the aerosol phase did not trend with the bulk seawater or the SML. We thus conclude that much work remains in understanding the numerous factors that modulate the abundance of INPs associated with SSA.

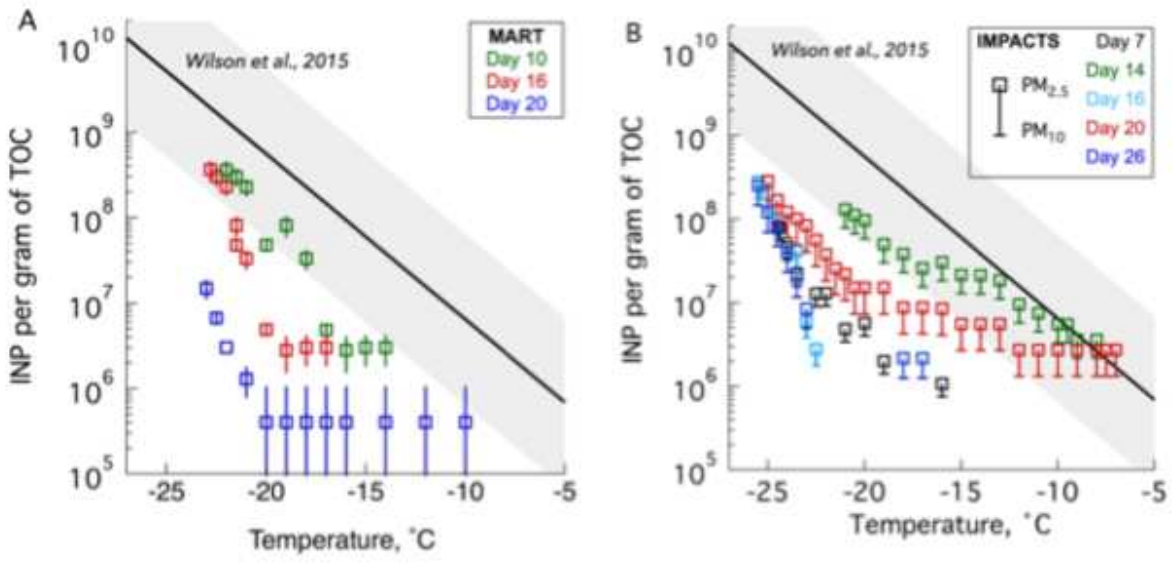

Figure 3.3-1. a) Ratio of INP to TOC in SSA generated on focus days of the MART experiment determined using INP data from the ice spectrometer measurements. Total suspended aerosol-phase TOC data were not available for Day 0 of the MART study. B) Ratio of INP to TOC in SSA during focus days of the IMPACTS study, for INP number concentrations determined using the ice spectrometer. INP to TOC ratios were estimated using $PM_{2.5}$ (square marker) and PM_{10} (line maker). On both figures, estimated INP to TOC ratios from *Wilson et al., (2015)* are shown (black line) and the shaded region outlines an order of magnitude spread above and below that parameterization.

Section 3.4 Summary of laboratory studies

Previous studies have investigated the identity of marine INPs via correlative analyses with aerosol composition and indicators of biological activity in the bulk seawater (e.g., *Prather et al.,* 2013*, Wang et al.,* 2015), through direct testing of potential INP material in the laboratory (e.g., *Knopf et al.,* 2011*, Rosinski et al.,* 1987), and via inference from compositional studies of surface microlayer samples (*Wilson et al.,* 2015).

We utilized the laboratory setting to isolate dynamic relationships between atmospheric INPs and seawater biological activity, described here by Chl *a*, abundances of microbes and enzyme activity, throughout the duration of two phytoplankton blooms. The data reported here demonstrate that links exists between marine biochemistry and the production of INPs. During phytoplankton blooms, we observed increases in n_{INPs}, typically those active at moderate

temperatures, following the peak in bulk water Chl *a* (i.e. after the peak in phytoplankton growth cycle). INPs active at various temperatures, indicative of various ice nucleating materials, had unique dynamics associated with the phytoplankton bloom, suggesting that the marine INP population is diverse. INPs active at warm temperatures (-8 °C) were observed on days of enhanced aerosolized heterotrophic bacteria, suggesting that microbes contributed to warm-temperature marine INPs. Aliphatic-like, submicron organic aerosol was found to correspond to INPs active at moderate and cold temperatures, a link supported by single particle chemistry and enzyme activity.

The identity of marine INPs was also probed using offline treatments that deactivated biological material (heating or hydrogen peroxide digestion), and isolated the contribution of dissolved organic matter (i.e. material that passes through a 0.2 μm filter) to the overall population of INEs in bulk seawater. Individual ice crystal residuals were also directly collected and analyzed to determine the chemical composition and size of INPs. We report a differentiation of two populations of marine INPs and suggested these two populations could be the basis for quantification of separate INP categories for modeling purposes: 1) DOC INPs are particles that were coated with or contained major masses of IN-active molecules (e.g., exudates, *Wilson et al.,* 2015) and were more common during the denser phytoplankton bloom that favored the production of organic coatings on particles and 2) POC INPs are IN-active bacteria, diatoms or grazers, which are represented in SSA as intact cells or cell fragments, that were more prominent following the decline in phytoplankton biomass and lacked significant organic coatings. These marine INP types were active at temperatures warmer than -25 °C.

These findings motivate future studies that focus on identifying individual molecules and microbes that contribute to both marine INP types, the mechanisms that govern their biochemical

production during phytoplankton blooms, and the transfer of these molecules and microbes into SSA. Specifically, studies should quantify specific molecules and microbes that are IN active in the SSA, SML, and SW. Equally important is to determine the biochemical mechanisms that produce the marine INEs in SW and to understand the surface active properties of the INE components and how these govern their participation in SML enrichment. Finally, future work should investigate the biotic and abiotic conditions that favor production of INPs (i.e., aerosolization of INEs).

CHAPTER 4: MEASUREMENTS OF MARINE INPS IN THE FIELD

Section 4.1 Overview of INP measurements made over remote oceans and coastal regions

A variety of measurements made over oceans and at a coastal location are used here to provide an overview of the abundance and variability of INPs in the marine boundary layer. Measurements at the Bodega Marine Laboratory (BML) were used to describe number concentrations of INPs (n_{INPs}) found in the marine boundary layer along the California coast during wintertime. Six ship campaigns, including MAGIC, ACAPEX-RB, Tangaroa, SHIPPO 2012 and 2014, and CAPRICORN are used to illustrate variability in n_{INPs} across the Pacific Ocean, from -72 °S to 60 °N. As aerosol surface area measurements, needed for calculation of nucleation site density, were not available in all of these campaigns, comparisons are presently restricted to n_{INPs} values.

4.1.a Results and Discussions

4.1.a.i CalWater-2015

During the CalWater-2015 campaign, n_{INPs} ranged from 0.001 to 0.2 L^{-1} of air for INPs active at -15 °C. Many n_{INPs} were consistent with the range reported by *DeMott et al.* (2016), which was representative of sea spray aerosol observed in laboratory-generated SSA and observations in the marine boundary layer. Aerosol population types in air masses arriving at the Bodega Marine Laboratory were determined using an unsupervised K-Means cluster analysis performed by *Atwood et al.* (in prep). The cluster analysis incorporated aerosol microphysical properties (size distributions, aerosol number concentrations, and CCN activation) and meteorological properties (wind conditions and HYSPLIT back trajectories). A marine

background aerosol population was observed from 17 to 21 February 2015 and another period identified as marine aerosol was observed from 26 February to 1 March 2015 (*Atwood et al.,* in prep). The primary wind direction for both periods was from the northwest and total aerosol number concentrations were 400 to 700 cm^{-3}. No measurements with the CFDC were made during these time periods, but 5 aerosol filters were collected and analyzed within these windows and those data are shown in Figure 4.1-1. The range of n_{INPs} observed at BML was in the upper range of other marine boundary layer surveys (*DeMott et al.,* 2016), but a detailed comparison to other locations requires normalization to aerosol concentrations or aerosol surface area, which is planned in future work.

Ship-based measurements from ACAPEX-RB are also shown in Figure 4.1-1 for two filters that represent a range of distances from the California coast. Measured n_{INPs} near the coastline (350-800 km offshore) were similar to the n_{INPs} measured at BML. However, three orders of magnitude variability in the number concentrations of INPs was observed between 3000 km offshore and the coastline (BML), where n_{INPs} ranged from 0.0016 to 1.4 L^{-1} of air for INPs active at -20 °C. Variable SSA production due to changes in wind speed is one of many factors that will change n_{INPs}. This factor was accounted for by normalizing n_{INPs} by aerosol surface area, reported by *Levin et al.* (in prep) and shown in Figure 4.1-2 for the ACAPEX-RB data, and indicated good agreement with previous measurements of INPs in the remote marine boundary layer (*DeMott et al.,* 2016). Additional analyses of these data (CalWater-2015, ACAPEX-RB, MAGIC, etc.), particularly regarding aerosol composition and surface area, will help to determine the influence of the many factors that may control the variability in n_{INPs}, including wind conditions (i.e., sea spray production), influences of land-based INP sources (e.g., mineral dust), changes in ocean biological activity, and many other factors.

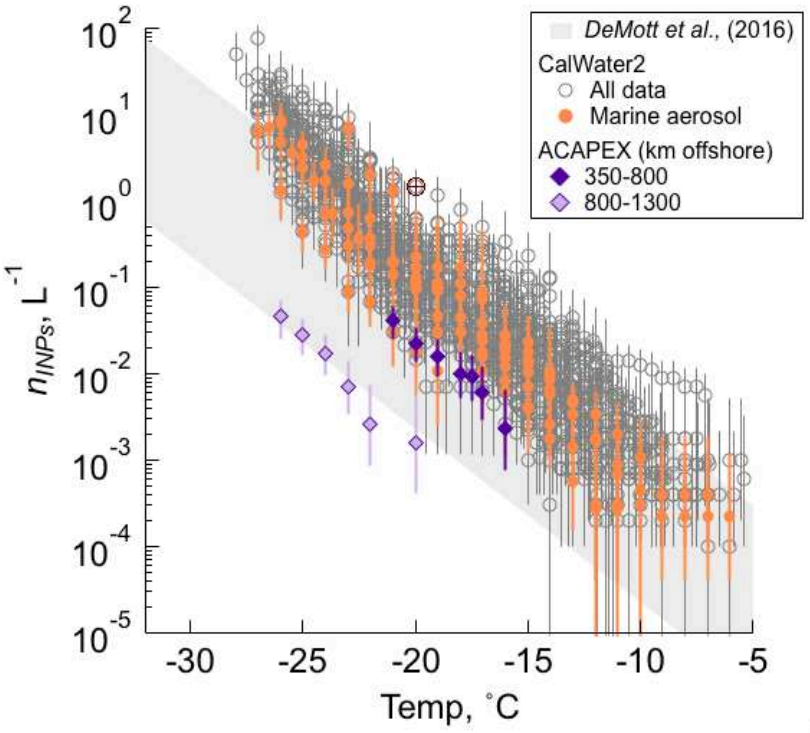

Figure 4.1-1. Number concentrations of INPs as a function of temperature observed during the Calwater-2015 campaign. All data are shown in dark grey. Three filters that corresponded to background marine aerosol, determined based on cluster analysis, are highlighted in orange. Ship-based measurements from ACAPEX-RB are also shown in purple (collected between 24 and 26 January 2015), where each shade corresponds to a different distance from the shoreline. Vertical bars are the 95% confidence intervals for the IS measurements.

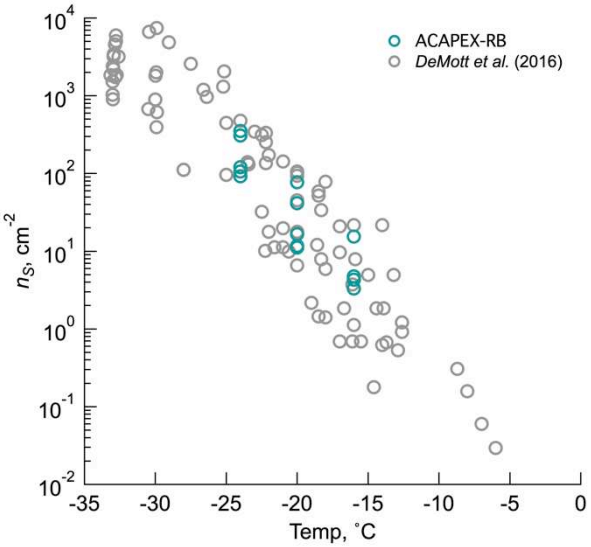

Figure 4.1-2. Nucleation site densities from ACAPEX-RB samples collected during an atmospheric river event (teal, from *Levin et al.,* in prep) and from *DeMott et al.* (2016).

4.1.a.ii INPs over the Pacific Ocean

Number concentrations of INPs (n_{INPs}) found in the marine boundary layer over the Pacific Ocean during six ship-based field campaigns are shown in Figure 4.1-3. Ocean surface Chl *a* concentrations for each study region are shown in Figure 4.1-4. Over three orders of magnitude variability in n_{INPs} at any one temperature was observed across all temperatures during these six campaigns. The highest n_{INPs} observed over the Pacific Ocean were measured during SHIPPO-2012 from a filter collected while the ship was traveling between Korea and Japan and passing through a strait located between two Japanese islands. It is likely that this filter was heavily influenced by terrestrial aerosol sources. Other samples collected during SHIPPO-2012 agreed with n_{INPs} observed during the other campaigns. ACAPEX n_{INPs} ranged over three orders of magnitude. In contrast, n_{INPs} comparable to the highest values observed during ACAPEX were not commonly observed during MAGIC, although the measurement region was similar. Chl *a* concentrations were higher over the Pacific Ocean as a whole during ACAPEX compared to MAGIC, suggesting possible increases in n_{INPs} due to higher ocean biological productivity, though ocean Chl *a* concentrations were similar for the ship track region. During the SHIPPO-2014 study, the highest n_{INPs} observed across all temperatures were measured on a filter collected closest to New Zealand, suggesting possible influence from terrestrial aerosol. While some variability in n_{INPs} was observed for INPs active at temperatures warmer than approximately -22 °C, nearly all n_{INPs} for INPs active at -25 °C and colder were within an order of magnitude of each other during the Tangaroa and CAPRICORN campaigns.

The Pacific Ocean ship-based data are summarized in Figure 4.1-5, in which measured n_{INPs} have been stratified into samples from the Northern and Southern Hemispheres. This summary clearly shows that n_{INPs} in the Northern Hemisphere were observed to have greater

variability and higher n_{INPs} compared to n_{INPs} observed over the Pacific Ocean in Southern Hemisphere. Data from the Northern Hemisphere are in better agreement with those reported by *DeMott et al.,* (2016), which include data exclusive to the Northern Hemisphere.

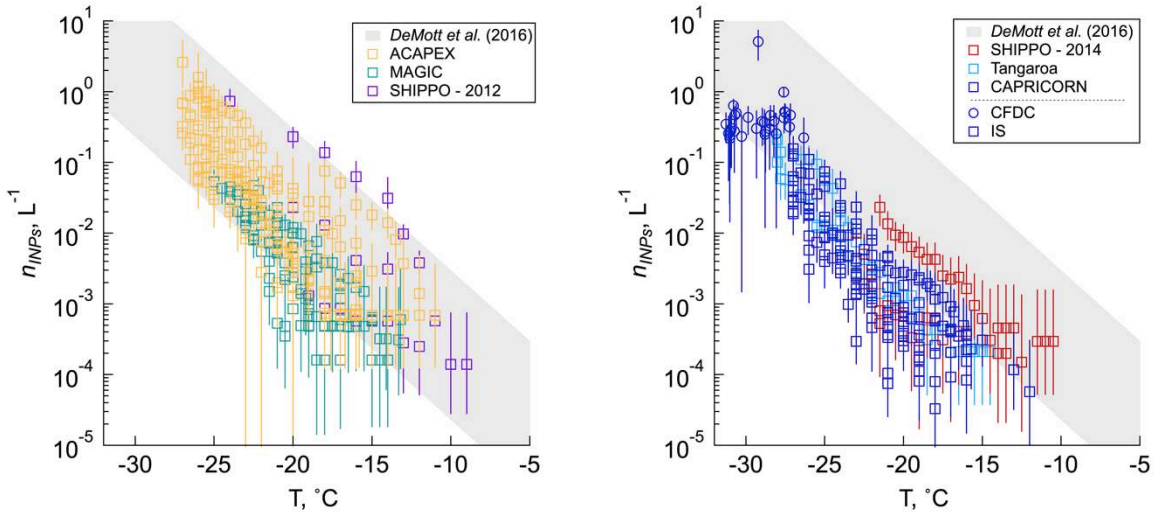

Figure 4.1-3. Number concentrations of INPs as a function of temperature observed during six ship measurement campaigns, including (left) ACAPEX (yellow), MAGIC (teal green), SHIPPO-2012 (purple), (right) SHIPPO-2014 (red), Tangaroa (light blue), and CAPRICORN (blue). Data are from both ice spectrometer (IS, square markers) and the continuous flow diffusion chamber (circle markers). Error bars for IS data represent 95% confidence intervals. Error bars for CFDC data show the errors estimated based on Poisson counting statistics.

4.1.b Main findings and future work

From the CalWater-2015 campaign, we found that n_{INPs} in the marine boundary layer at the BML were at the upper range of previously reported marine boundary layer INP measurements. This may be due to local and long-range influences that lead to aerosol populations that are not explicitly pristine SSA, as also suggested by observations made during a period of background marine air, for which measured n_{INPs} were on the lower end of the observed range at BML. Ship-based measurements from ACAPEX-RB, occurring in the midst of the CalWater-2015 campaign, indicate that the coastal region is associated with elevated n_{INPs} compared to the open ocean. This finding may be explained by higher SSA production near the

coast, higher Chl *a* concentrations, the presence of terrestrial INPs, or changes in ocean water composition (e.g., more terrestrial runoff into coastal waters that are the source of the observed particles). Additional analyses will be needed to discern the major influences from among these possibilities.

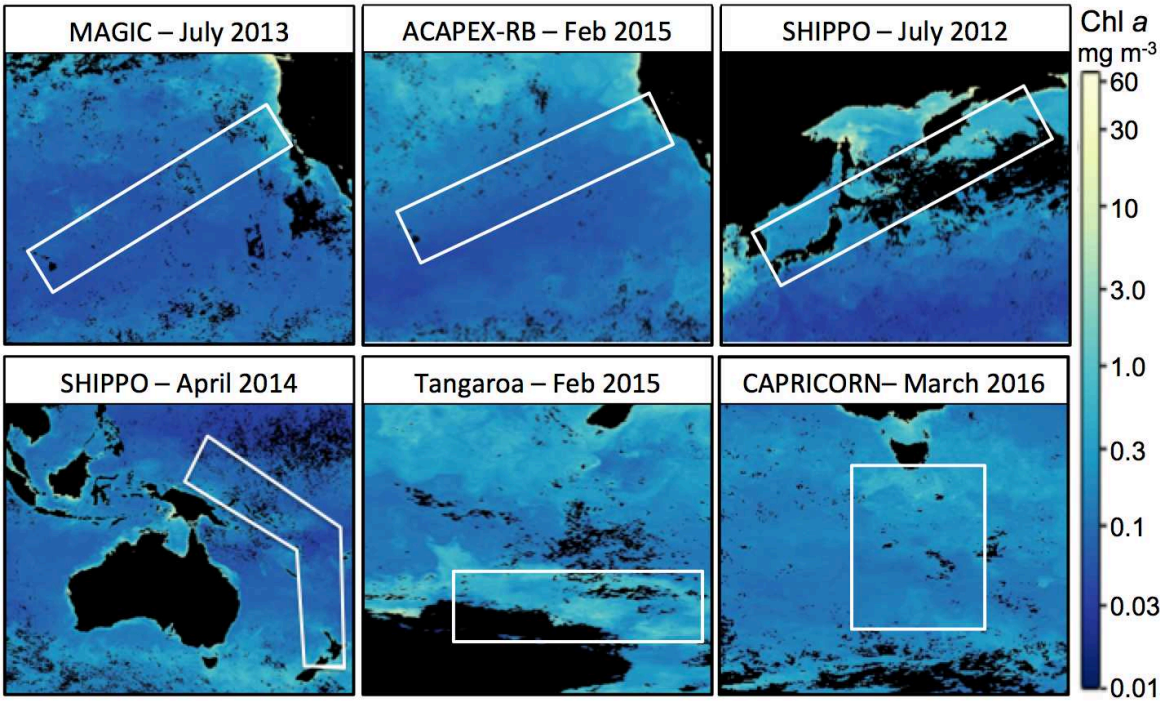

Figure 4.1-4. Ocean surface Chl *a* concentrations during the six ship-based campaigns. Only one month is shown for each campaign. Data are from AQUA/MODIS OceanColor.

The largely unexplained and vast range of n_{INPs} observed from this extensive survey over the Pacific Ocean and from the CalWater-2015 campaign supports the need for detailed investigations on marine INPs. During ACAPEX-RB, SHIPPO-2012, and SHIPPO-2014, the highest n_{INPs} were spatially closer to land, suggesting that the presence of terrestrial aerosol or higher coastal biological productivity and wave action are important factors for understanding INP populations in the marine boundary layer regions. This discussion has been limited to observed total number concentrations of INPs. Changes in SSA production (initiated by e.g., changes in wind speed) and subsequent changes in total number of aerosol (or total surface area)

have not been considered. Particularly due to the sensitivity of SSA production to wind speed, normalizing data by surface area or particle number concentrations can be helpful in reducing variability due only to changes in source and sink strengths, revealing underlying variability due to fundamental differences in the types and behaviors of INPs. Although these measurements only represent a portion of the hemisphere, these data suggest that the Northern Hemisphere marine boundary layer over the Pacific Ocean contains more abundant (by approximately a factor of 10) and more variable INP populations, in comparison to the Southern Hemisphere.

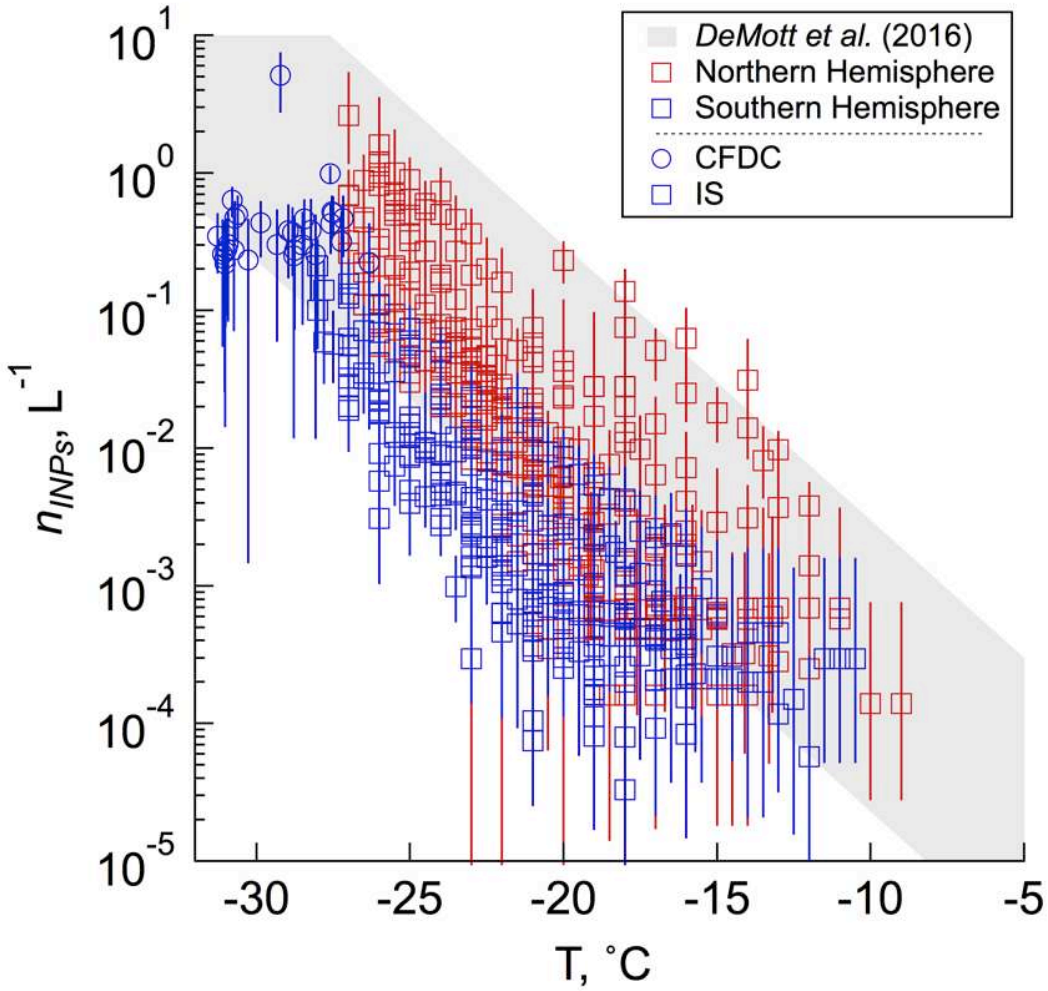

Figure 4.1-5. INP number concentrations as a function of temperature for ship-based measurements made over the Pacific Ocean. Data are separated into Southern Hemisphere (blue) and Northern Hemisphere (red). Vertical bars are the 95% confidence intervals for the IS measurements. Range of n_{INPs} reported by *DeMott et al.* (2016) is also shown.

Section 4.2 Marine and Terrestrial Organic Ice Nucleating Particles in Pristine Marine to Continentally-Influenced Northeast Atlantic Air Masses

4.2.a Project overview

Section 2.2.c describes the design of the Mace Head field project (MHD) in detail. Briefly, observations of aerosol composition, ice nucleation and meteorology were made on the west coast of Ireland at the Mace Head Research Station (MHD) during August of 2015. The goal of this study was to determine the ice nucleation properties of SSA at a remote coastal location that is often influenced by increased organic aerosol mass concentrations arising from offshore biological activity. Pairs of filters were collected, termed CLEAN sector (i.e., pristine marine air based on wind direction and very low black carbon concentrations) and ALL samples (i.e., all aerosol present at MHD, including pristine marine aerosol). Particular attention was given to samples collected during elevated organic aerosol events, detected by an aerosol mass spectrometer, to determine the contributions of marine and terrestrial organic aerosol to the INP population at this remote location.

4.2.b Results and Discussion

4.2.b.i Organic aerosol events during the campaign

Number concentrations of INPs active at -15 °C ($n_{INPs,-15\ °C}$, measured by the IS), submicron organic aerosol mass concentrations ([*Org*]), black carbon mass concentrations ([*BC*]) and meteorological (wind direction and speed) timelines are shown in Figure 4.2-1. Additional submicron aerosol chemistry, particulate matter mass concentrations ($PM_{2.5}$ and PM_{10}) and meteorology data are summarized in Table 4.2-1 and Figure 4.2-2. The study average [*Org*] was 0.33 (±0.38) μg m^{-3} and included three periods of elevated [*Org*] that were studied to investigate organic INPs at MHD.

The first marine organic event (M1) was sampled from 9 Aug 11:43 to 9 Aug 19:10 (Figure 4.2-1). HYSPLIT back trajectories and ocean surface Chl *a* concentrations (Figure 4.2-3) show that air originated from biologically active ocean regions during M1. [*Org*] increased to 0.85 (±0.20) μg m^{-3} during M1 and HR-ToF-AMS mass spectra for submicron particles (Figure 4.2-4) were similar to those previously observed in association with offshore biological activity (*Ovadnevaite et al.,* 2011). During M1, terrestrial chemical markers, including ammonium (NH_4), nitrate (NO_3) and *BC,* were lower or similar to the study average (Table 4.2-1, Figure 4.2-2). Particulate matter concentrations were elevated during M1, with $PM_{2.5}$ and PM_{10} mass concentrations of 3.42 (±1.06) μg m^{-3} and 15.65 (±2.37) μg m^{-3}, respectively. While [*Org*] was higher than the study mean, sea salt mass concentrations in submicron aerosol measured by the AMS during M1 (0.15 ±0.06 μg m^{-3}) were similar to the study average (0.15 ±0.16 μg m^{-3}), suggesting the presence of organic enriched submicron SSA. Observed changes in n_{INPs} during M1 are discussed below.

The second marine organic event (M2) was sampled from 12 Aug 19:52 to 14 Aug 09:47. Air during M2 was arriving from the marine sector (CLEAN sector wind direction is 190 to 300°, Figure 4.2-1), but BC concentrations (18 ±11 ng m^{-3}, Table 4.2-1) were slightly above the CLEAN sector threshold (15 ng m^{-3}). Based on HYSPLIT back trajectories and ocean surface Chl *a* concentrations (Figure 4.2-3), air masses associated with M2 originated from oceanic regions further north than M1 that were also biologically productive. During M2, average [*Org*] was 0.57 (±0.25) μg m^{-3} and submicron organic aerosol HR-ToF-AMS mass spectra were similar to those observed during M1. Terrestrial aerosol chemical constituents (NH_4, NO_3, *BC*) were similar to M1 and the study average (Table 4.2-1 and Figure 4.2-2). During M2, sea salt mass concentrations (0.12 ±0.13 μg m^{-3}) were similar to M1 and to the study average (0.15 ±0.16 μg

m^{-3}). With lower concentrations of [*Org*], M2 is considered a marine organic event with lower organic enrichment in submicron SSA compared to M1. HR-ToF-AMS mass spectra during M2 (Figure 4.2-4) contained higher signal from methanesulfonic acid (MSA, m/z 79), indicative of higher contributions from marine secondary organic aerosol (*Rinaldi et al.,* 2010), compared to M1. $PM_{2.5}$ and PM_{10} mass concentrations were 1.65 (±1.90) μg m^{-3} and 9.15 (±6.56) μg m^{-3}, respectively, which were lower than average values observed both during the study as a whole and during M1. Negative values of $PM_{2.5}$ as derived from TEOM data were observed during M2, which are due to very low mass concentrations with possible losses of particle water or semi-volatile species, as reported by *Charron et al.,* (2004). Notably, wind speeds were lower during M2 (4.18 ± 2.03 m s^{-1}) compared to M1 (7.92 ± 1.31 m s^{-1}) suggesting lower SSA generation (*Ovadnevaite et al.,* 2012).

Finally, a terrestrial organic event (T1) was sampled from 15 Aug 11:14 to 20 Aug 11:36. In Figure 4.2-3, HYSPLIT back trajectories illustrate that aerosol sampled during this event originated from ocean regions, but passed over southwest Ireland before arriving at MH. Average [*Org*] were elevated during T1 (0.75 ±0.53 μg L-1) and HR-ToF-AMS mass spectra collected for organic submicron aerosol during T1 (Figure 4.2-4) were representative of marine organic aerosol (MSA, m/z 79) mixed with contributions from refined (anthropogenic) hydrocarbons (C_nH_{2n+1}, m/z 43, 57 and 71). During T1, mass concentrations of submicron *NH_4, NO_3,* and *BC* were considerably higher than the study averages (Table 4.2-1 and Figure 4.2-2), indicating significant influence from land aerosol sources. T1 is considered a marine air mass with significant mixing with land-derived aerosol. In the CLEAN sector, mass concentrations of $PM_{2.5}$ (2.74 ±1.78 μg L-1) and PM_{10} (9.36 ±5.19 μg L-1) were similar to those observed during M2.

Table 4.2-1. Summary of INP number concentrations (n_{INPs}), aerosol chemistry, particulate matter (PM) and meteorology, showing averages and standard deviations for the entire study, and for the selected periods M1, M2 and T1. From *McCluskey et al., (a, in prep).*

		Study	M1	M2	T1
INP	ALL $n_{INPs,-15°C}$ (L^{-1})	0.0030 ± 0.0033	0.0077 (n = 1)*	0.0006 (n = 1)**	0.0076 ± 0.0018
	CLEAN $n_{INPs,-15°C}$ (L^{-1})	0.0011 ± 0.0014	0.0053 (n = 1)***	no sample	0.0006 (n = 1)****
Chemistry	NH_4 ($\mu g\ m^{-3}$)	0.06 ± 0.09	0.07 ± 0.02	0.04 ± 0.02	0.15 ± 0.15
	NO_3 ($\mu g\ m^{-3}$)	0.03 ± 0.04	0.02 ± 0.00	0.02 ± 0.01	0.07 ± 0.08
	SO_4 ($\mu g\ m^{-3}$)	0.39 ± 0.31	0.51 ± 0.18	0.47 ± 0.22	0.62 ± 0.49
	Org ($\mu g\ m^{-3}$)	0.33 ± 0.38	0.85 ± 0.20	0.57 ± 0.25	0.75 ± 0.53
	SS ($\mu g\ m^{-3}$)	0.15 ± 0.16	0.15 ± 0.06	0.12 ± 0.13	0.07 ± 0.07
	MSA ($\mu g\ m^{-3}$)	0.03 ± 0.02	0.03 ± 0.01	0.04 ± 0.02	0.04 ± 0.02
	BC ($ng\ m^{-3}$)	20.98 ± 53.19	10.43 ± 4.79	17.95 ± 10.88	56.57 ± 106.08
Particulate Matter	$PM_{2.5}$ ($\mu g\ m^{-3}$)	2.78 ± 2.00	3.42 ± 1.06	1.65 ± 1.90	2.74 ± 1.78
	PM_{coarse} ($\mu g\ m^{-3}$)	9.35 ± 4.74	12.24 ± 1.89	7.49 ± 5.17	6.62 ± 4.09
	PM_{10} ($\mu g\ m^{-3}$)	12.13 ± 6.05	15.65 ± 2.37	9.15 ± 6.56	9.36 ± 5.19
Meteorology	Temp (°C)	14.0 ± 1.3	14.5 ± 0.2	13.5 ± 1.2	14.85 ± 1.4
	RH (%)	80.4 ± 8.4	89.9 ± 0.9	78.1 ± 7.6	84.17 ± 7.9
	RR ($mm\ Hr^{-1}$)	-0.04 ± 2.68	0.01 ± 0.07	-0.21 ± 4.64	-0.12 ± 3.69
	Wind Speed ($m\ s^{-1}$)	6.74 ± 3.08	7.92 ± 1.31	4.18 ± 2.03	4.91 ± 2.46
	Wind Direction (°)	225.3 ± 56.2	200.5 ± 7.7	238.8 ± 37.9	188.85 ± 58.6

* no standard deviation; n_{INP} = 0.0077 L^{-1} with a 95% confidence interval of 0.0041 to 0.0137 L^{-1}

** no standard deviation; n_{INP} = 0.0006 L^{-1} with a 95% confidence interval of 0.0003 to 0.0014 L^{-1}

*** no standard deviation; n_{INP} = 0.0053 L^{-1} with a 95% confidence interval of 0.0033 to 0.0077 L^{-1}

**** no standard deviation; n_{INP} = 0.0006 L^{-1} with a 95% confidence interval of 0.0002 to 0.0021 L^{-1}

4.2.b.ii INP population influences at MHD

Average $n_{INPs,-15\ °C}$ measured by the IS was 0.003 (± 0.0033) L^{-1} of air for samples collected continuously (ALL), whereas average CLEAN sector $n_{INPs,-15\ °C}$ was 0.0011 (± 0.0014) L^{-1} of air. Figure 4.2-5 includes n_{INPs} temperature spectra for the ALL (Figure 4.2-5a) and CLEAN-sector (Figure 4.2-5b) samples analyzed by the IS during this study. Figure 4.2-5 also includes n_{INPs} measured by the HINC-EV (ALL) and DFPC (CLEAN), and illustrate that all methods presented in this study are in good agreement. Details on the intercomparison between the HINC-EV, DFPC and IS are provided by *Atkinson et al.* (In prep). Measured n_{INPs} at MHD are within the range of previous laboratory and field measurements of SSA, with many data falling at the lower range of temperature spectra identified as marine by *DeMott et al.* (2016).

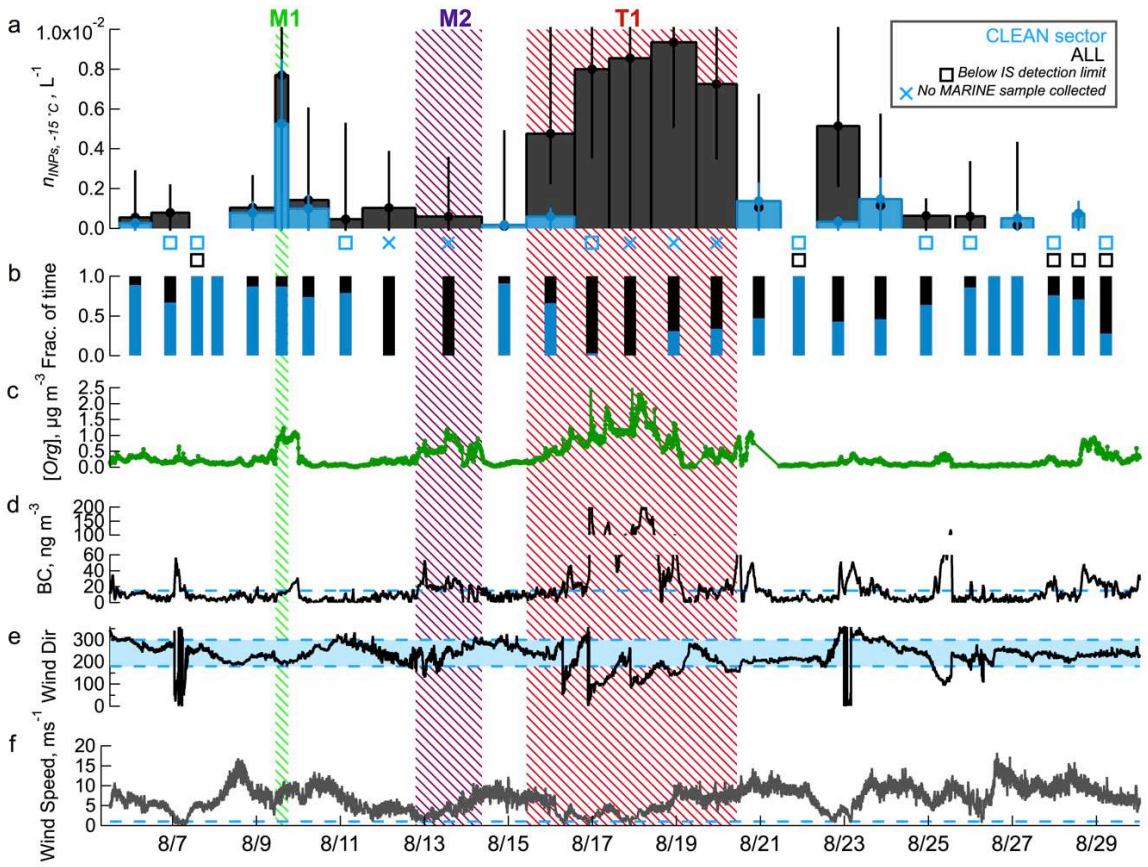

Figure 4.2-1. Timeline of a) INP number concentrations active at -15 °C ($n_{INPs,-15°C}$) for ALL (black) and CLEAN sector (blue) samples. Open square markers indicate measured $n_{INPs,-15°C}$ that were below detection limit. Cross markers indicate that a sample was not collected for that sampling period. b) Fraction of sampling time that was in the CLEAN sector (blue) versus non-clean sectors (black). c) Timeline of organic carbon mass concentrations measured by the AMS. d) Timeline of black carbon (BC) mass concentrations. e) timeline of wind direction (Wind Dir). f) timeline of wind speed. Green, purple and red shaddings correspond to organic events M1, M2, and T1. In d-e, thresholds used to define CLEAN sector periods are shown in light blue for BC, wind direction and wind speed. From *McCluskey et al., (a, in prep).*

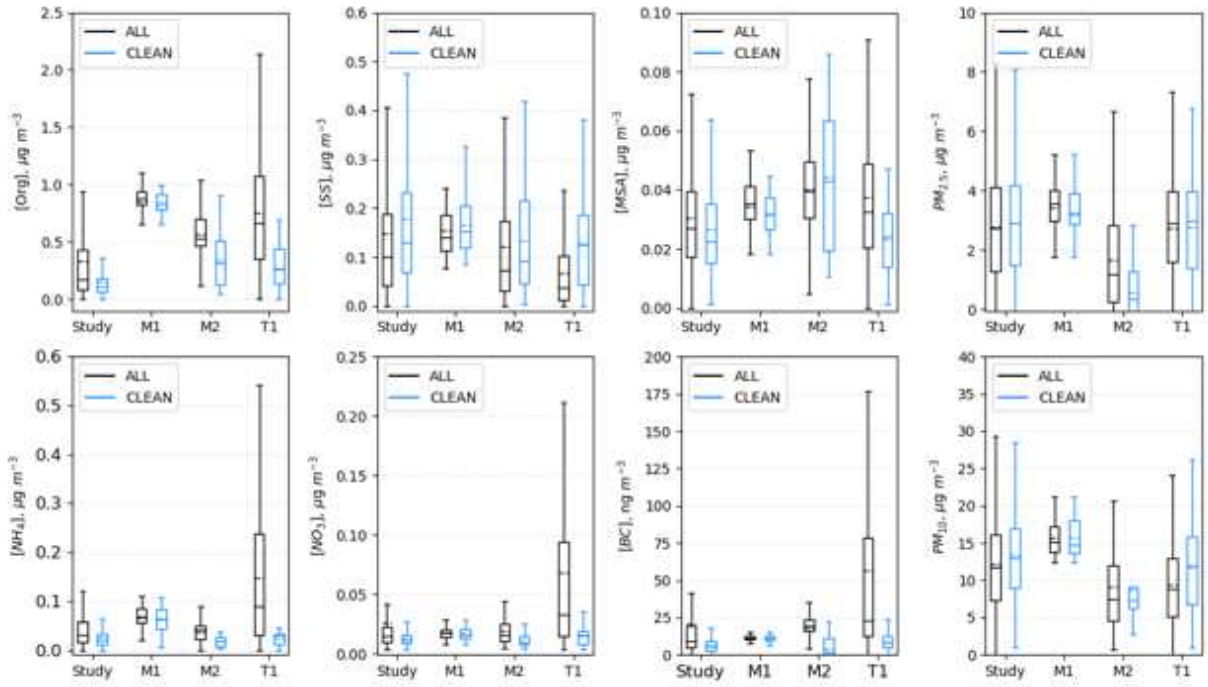

Figure 4.2-2.. Box and whisker plots for ALL (black) and CLEAN (blue) samples for the entire study, marine organic event 1 (M1), marine organic event 2 (M2) and the event with mixed marine and terrestrial air masses (T1). From *McCluskey et al., (a, in prep).*

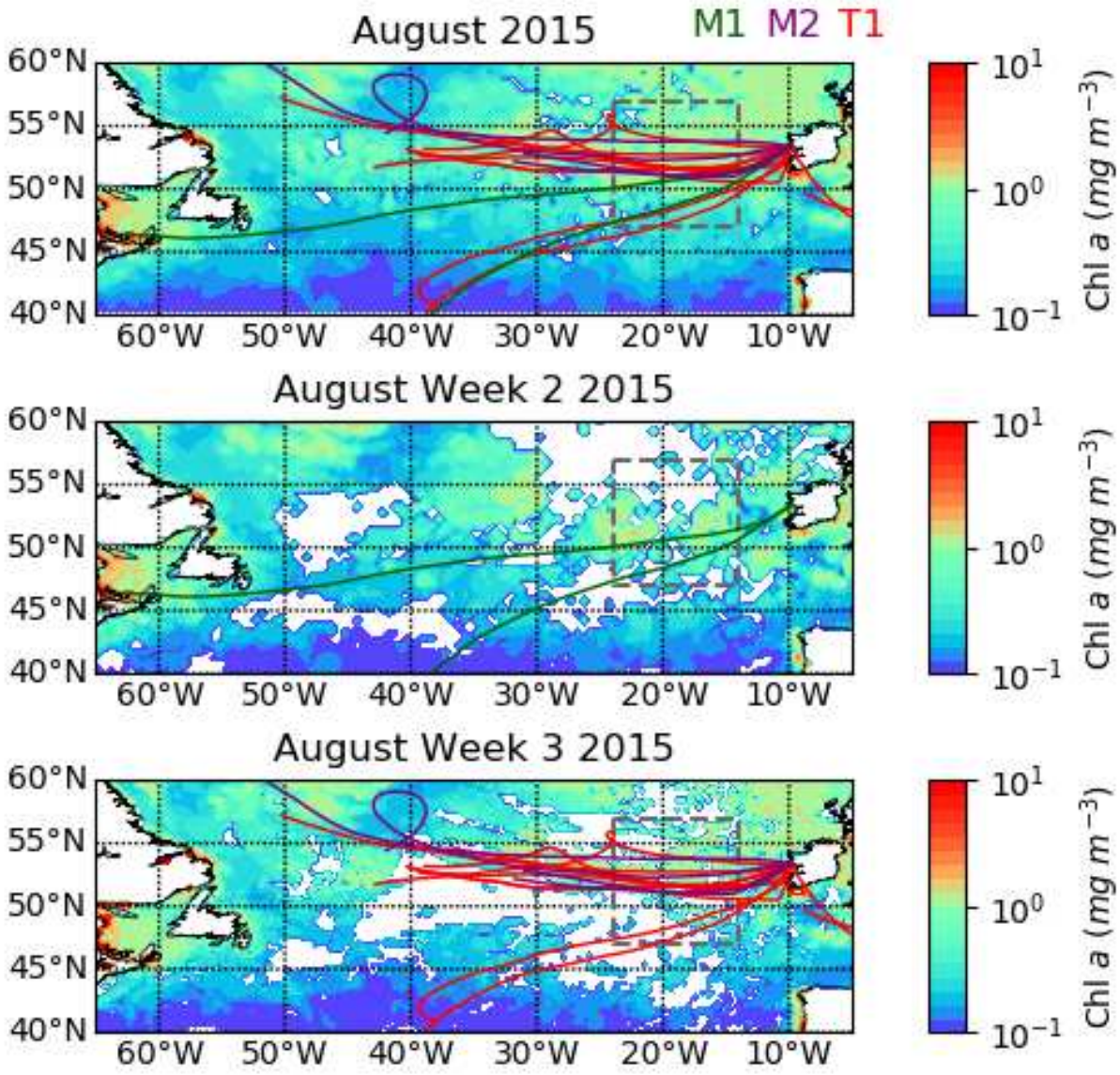

Figure 4.2-3. Ocean surface Chl *a* concentrations, retrieved from satellite during August 2015 (top), week 2 of August 2015 (middle) and week 3 of August 2015 (bottom). Green traces depict HYSPLIT back trajectories during the M1 event; Purple traces depict HYSPLIT back trajectories during the M2 event; Red traces depict HYSPLIT back trajectory during the T1 event. Grey dashed box outlines region used for lag correlation analysis. White regions indicate land regions or areas absent of data. From *McCluskey et al., (a, in prep).*

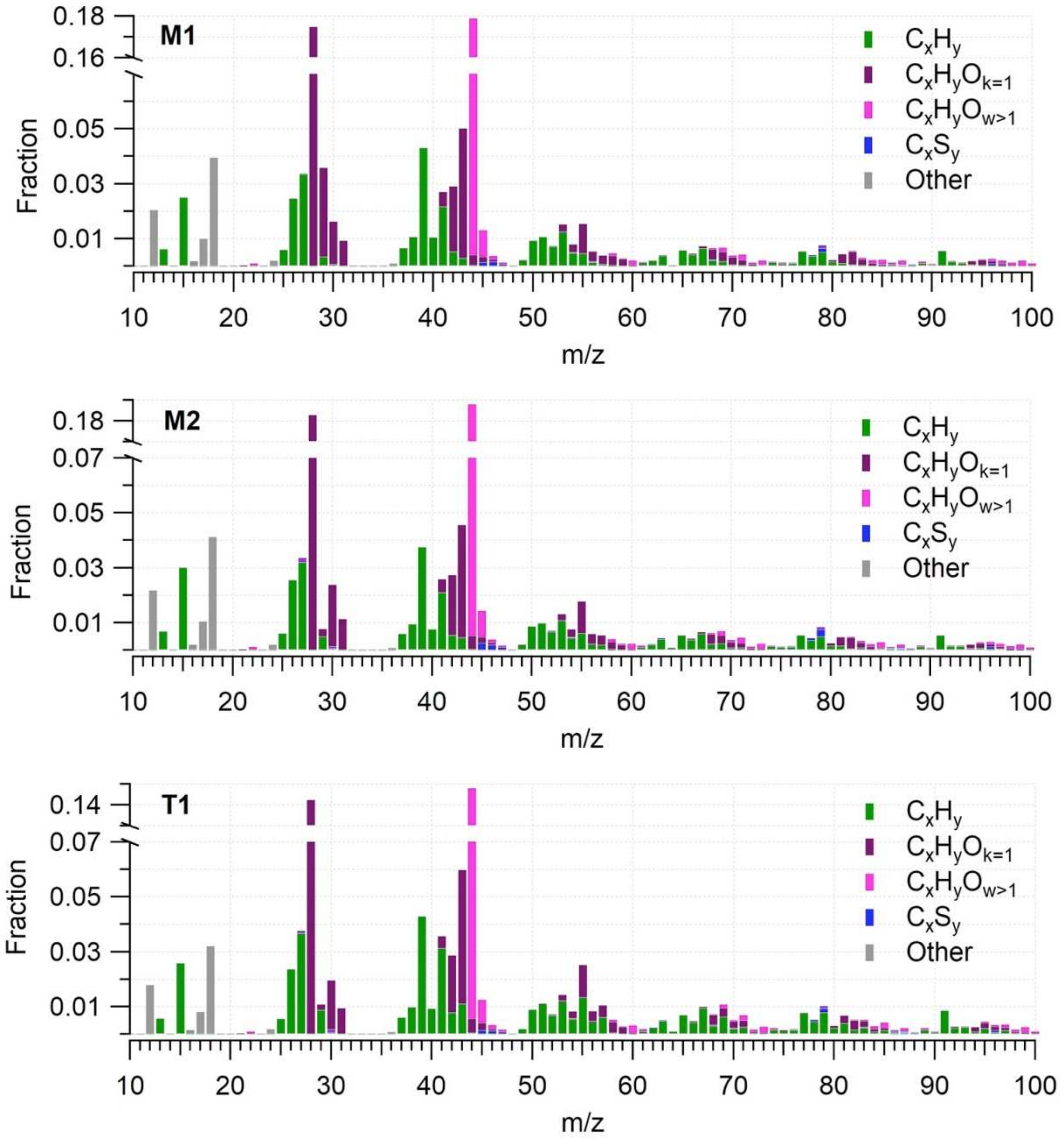

Figure 4.2-4. HR-ToF-AMS averaged organic mass spectra for (top) M1, (middle) M2, and (bottom) T1. From *McCluskey et al., (a, in prep).*

Samples collected over the entire study regardless of wind direction (Figure 4.2-5a) illustrate that n_{INPs} varied by a factor of 5-200 for any given temperature warmer than -30 °C, with progressively more variability at warmer temperatures (T > -20 °C). Variability was reduced when measurements were isolated to the CLEAN-sector (Figure 4.2-5 b), particularly at warmer temperatures, but n_{INPs} were still scattered over an order of magnitude. These findings remain true after accounting for variations in aerosol surface area (Figure 4.2-6).

Highlighted in Figure 4.2-5c-d are the organic events described previously (M1, M2, and T1) for the ALL and CLEAN sector samples, respectively. For the purpose of this discussion, measurements by the HINC-EV and DFPC for these events were limited to those made within the IS filter sampling periods. The presence of terrestrial INPs is evident during T1, where higher n_{INPs} across temperatures warmer than approximately -22 °C (Figure 4.2-5c) were observed in the ALL samples analyzed by the IS. No significant enhancement was observed in CLEAN sector samples collected during T1, suggesting the INP population was from a terrestrial source (Figure 4.2-5 d). No difference was observed for average n_{INPs} observed by the HINC at -30 °C during T1 compared to the rest of the study.

During the first marine event M1, n_{INPs} measured in the ALL and CLEAN-sector samples indicate elevated n_{INPs} at temperatures warmer than approximately -22 °C, but little change in n_{INPs} at colder nucleation temperatures. However, HINC measurements of n_{INPs} at -30 °C show higher n_{INPs} during M1. As mentioned previously, *BC* was slightly above the CLEAN sector threshold during M2 and thus a CLEAN sector sample was not collected during M2 for the IS. Despite this, the concentrations of n_{INPs} observed by the IS during M2 fell within the same range of temperature spectra observed in the CLEAN sector (Figure 4.2-5c). The two events differ slightly in aerosol composition, with HR-ToF-AMS mass spectra of submicron organic aerosol suggesting a higher contribution of secondary organic aerosol during M2 compared to M1. Wind speeds were lower during M2 compared to M1, likely leading to lower primary aerosol production during M2 compared to M1 (*Ovadnevaite et al.,* 2012).

Some previous studies have reported lower enrichments of organic matter in SSA associated with higher wind speeds (*Gantt et al.,* 2011; *Rinaldi et al.,* 2013) and have suggested that higher wind speeds lead to increased mixing of the ocean surface organic layer with sub-

surface water, reducing coverage of and organic enrichment in the SML, thereby reducing the amount of organic matter transferred to the aerosol. However, recent studies indicate that other processes, including chemical selectivity (*Cochran et al.,* 2016; *van Pinxteren et al.,* 2017) and film versus jet drop formation (*Wang et al.,* 2017), are additional important mechanisms that control the specific compounds or particulates that comprise the organic fraction of SSA, which will ultimately control the number of INPs. In particular, *van Pinxteren et al.* (2017) showed that a source function for predicting sea spray organic matter (*Rinaldi et al.,* 2013) under-predicted moderately high mass concentrations of sea spray organic matter derived from their study. They suggest that non-Chl *a* descriptors of biological productivity (e.g., bacteria abundance) or other meteorological parameters (e.g., sea surface temperature) may be important variables that can also change the makeup of organic marine aerosols. *McCluskey et al.* (Under Review, *J. Atmos. Sci*) demonstrated that the identity of marine INPs can include both IN active molecules and microbial constituents, depending on bloom conditions. While all the factors that lead to an increase in n_{INPs} during M1 but not in M2 are not known, it is possible that primary SSA production was more vigorous during M1 (higher wind speeds) than during M2 (lower wind speeds and more evidence for secondary organic aerosol). However, we note that wind speeds increased towards the end of the M2 period (Figure 4.2-1) and corresponding elevated n_{INPs} were not observed, suggesting that wind speed alone is a not a sufficient predictor of $n_{INPs.}$

4.2.b.iii Heat sensitivity and organic make up of INPs

INP population types were classified based on submicron aerosol composition, air mass back trajectories (Figure 4.2-3) and INP temperature spectrum shape (Figure 4.2-5). The most commonly observed INP temperature spectrum type (19 out of 25 sample pairs) is termed here as the Marine Organic INP population, as shown in Figure 4.2-7a, where n_{INPs} increase

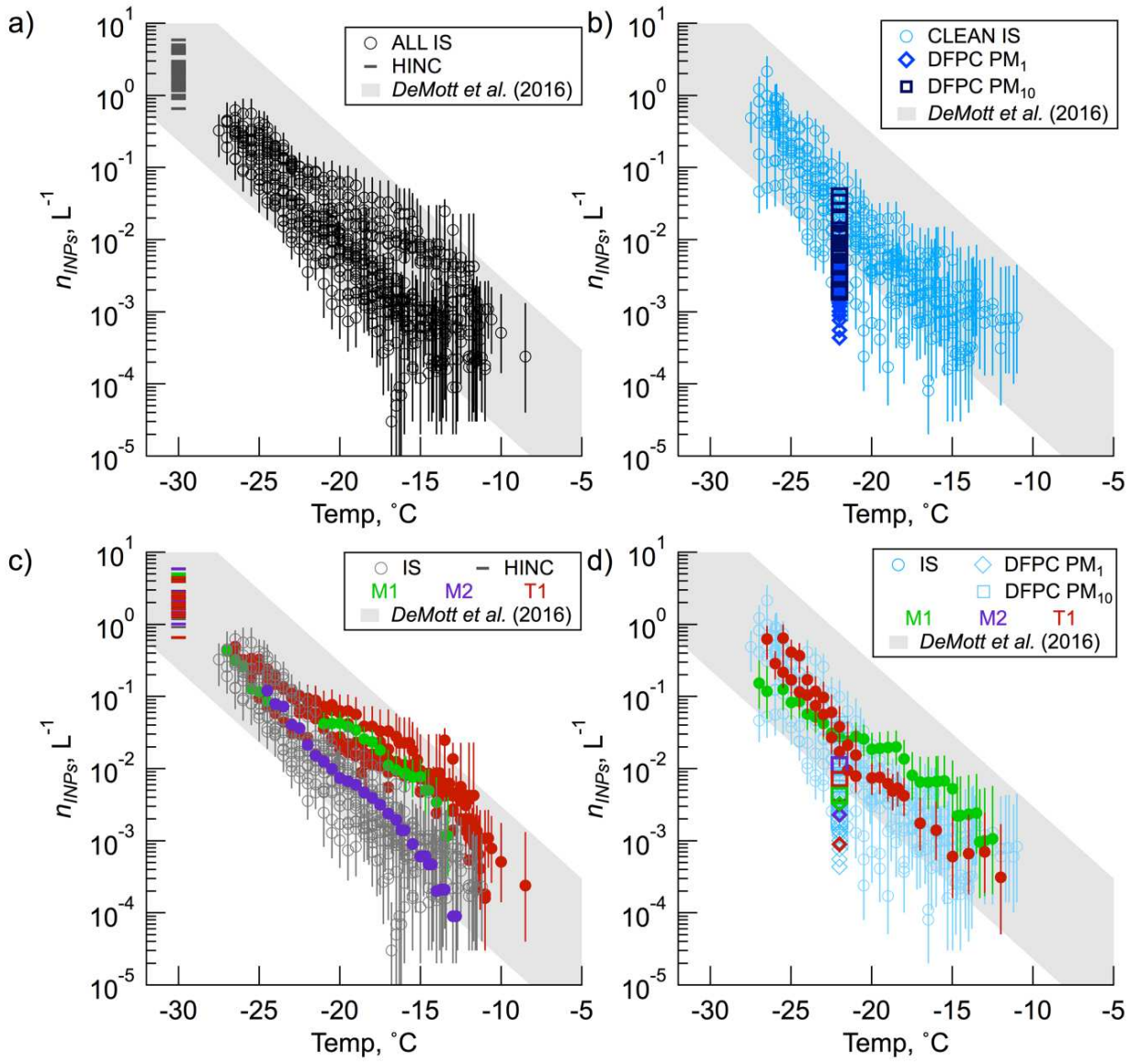

Figure 4.2-5. Panels a-c) show the three main INP spectrum types observed at MHD: (a,d) log-linear, (b,e) marine organic and (c, f) terrestrial organic. INP spectra resulting from offline treatments performed on samples that are representative of the three classes of INP populations are shown in d-f. d) 10-11 Aug, 2015 represents the log-linear INP spectrum type; e) 9 Aug, 2015 represents marine organic INP spectrum type; and f) 17-18 Aug, 2015 represents the terrestrial organic INP spectrum type. For d-f, blue and black markers correspond to CLEAN sector and ALL samples. Red markers correspond to the heat-treated samples (heat treatments were performed on either the CLEAN sector or ALL samples, which were nominally the same) and gold markers correspond to hydrogen peroxide digested samples. Filled markers indicate values in treated samples that are statistically significantly different from untreated samples. Vertical bars are the 95% confidence intervals for the IS measurements.

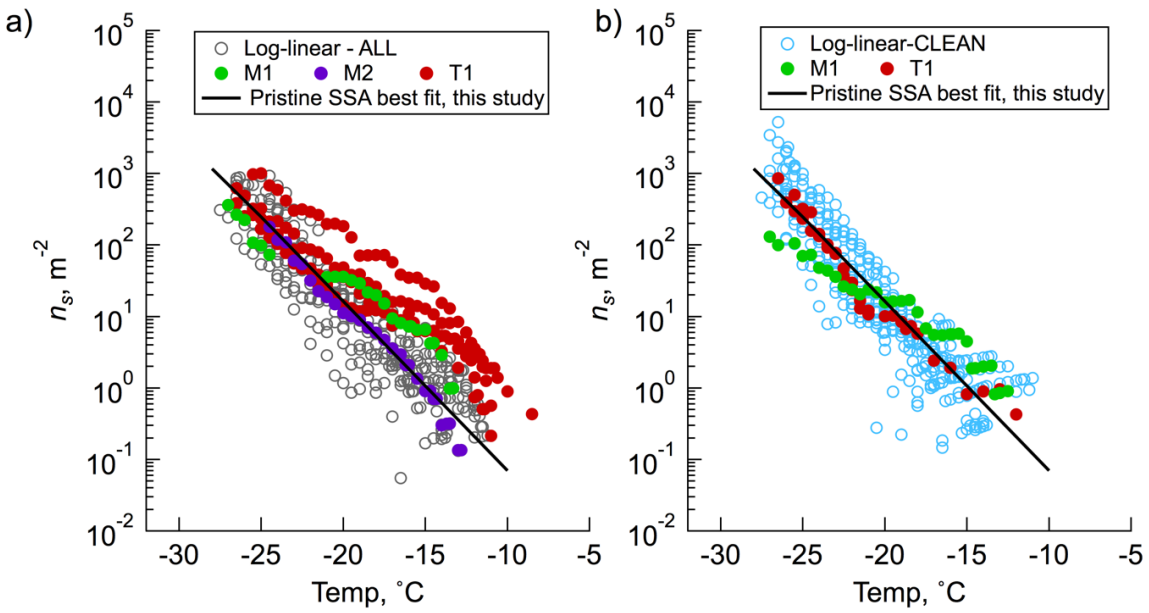

Figure 4.2-6. Nucleation site density as a function of temperature for (a) ALL samples measured by IS for M1 (green), M2 (purple), T1 (red) and all other samples (grey, open circles); (b) same as a, but for CLEAN samples. In both a and b, the ns parameterization for pristine sea spray aerosol in the CLEAN sector at MHD from this study is shown as a black line.

approximately log-linearly with decreasing temperature. The Marine Organic INP temperature spectrum type likely represents a regional INP population that is representative of a variety of sources, but the source apportionment is not attempted here. However, we note that the log-linear INP temperature spectrum type is found in both CLEAN sector and ALL samples, suggesting that a primary regional source is from the pristine marine sector. Heat treatments on one set of samples show that this population is heat-stable, with no statistically signficant difference observed between untreated and heated samples (Figure 4.2-7d). However, hydrogen peroxide digestion treatment of the Marine Organic INP type results in a significant reduction in INPs across all temperatures (Figure 4.2-7d), indicating not only that organic matter is a major component of the particles that serve as INPs but also that organic mass may be a possible predictor for determining the ice nucleation properties of aerosol at MHD when this type of aerosol dominates the INP population.

Figure 4.2-7b presents the subset of INP temperature spectra characterized by divergence from log-linearity, caused by an abundance of INPs active at temperatures warmer than approximately -22 °C. These spectra were observed only during M1, a period when HYSPLIT back trajectories indicated that aerosol arrived from pristine ocean regions (Figure 4.2-3). Chl *a* in the oceans below M1 back trajectories ranged from approximately 0.1 to 1 mg m^{-3} and HR-ToF-AMS mass spectra for submicron organic particles during this period (Figure 4.2-4) resembled organic particles arising from offshore biological activity (*Ovadnevaite et al.,* 2011). Thus, this INP population is defined as Augmented Marine Organic INPs, and was present for approximately 0.5 days during the study. This Augmented Marine Organic INP population was heat labile (Figure 4.2-7b), suggesting that most ice nucleation active material contained proteins or other biological material that is deformed or disaggregated by 95 °C heat, similar to the particulate organic carbon INPs previously observed in laboratory-generated SSA (*McCluskey et al.,* submitted to *J. Atmos. Sci.)*. Hydrogen peroxide treatments were not performed on M1 samples due to limited sample availability, so the total contribution of organic matter to these Augmented Marine Organic INPs is unknown.

Data from the T1 event provide evidence for an important source of terrestrial organic aerosol INPs (Figure 4.2-7c), characterized by INP temperature spectra that had elevated n_{INPs} across all temperatures warmer than approximately -22 °C. Distinct from the Marine Organic INP population, this elevated n_{INPs} feature was not observed in the CLEAN-sector INP temperature spectra. This INP population was observed on 5 out of 25 total study samples (total event duration of 6 days). HYSPLIT back trajectory analyses and the presence of elevated terrestrial chemical markers (NH_4, NO_3 and *BC*) indicate that the land was an important contributor to the aerosol during these sampling times. Offline treatments revealed that the

terrestrial type was also heat labile and largely comprised of organic matter (Figure 4.2-7f). The remaining INPs detected in the H_2O_2 treated sample suspensions from T1 are consistent with a higher base level of refractory and likely soil mineral particles. The terrestrial origin and impact of these treatments suggests that the INPs are from organic-rich soils, which have been reported as a potentially important source of INPs to the atmosphere (*O'Sullivan et al.,* 2014; *Tobo et al.,* 2014).

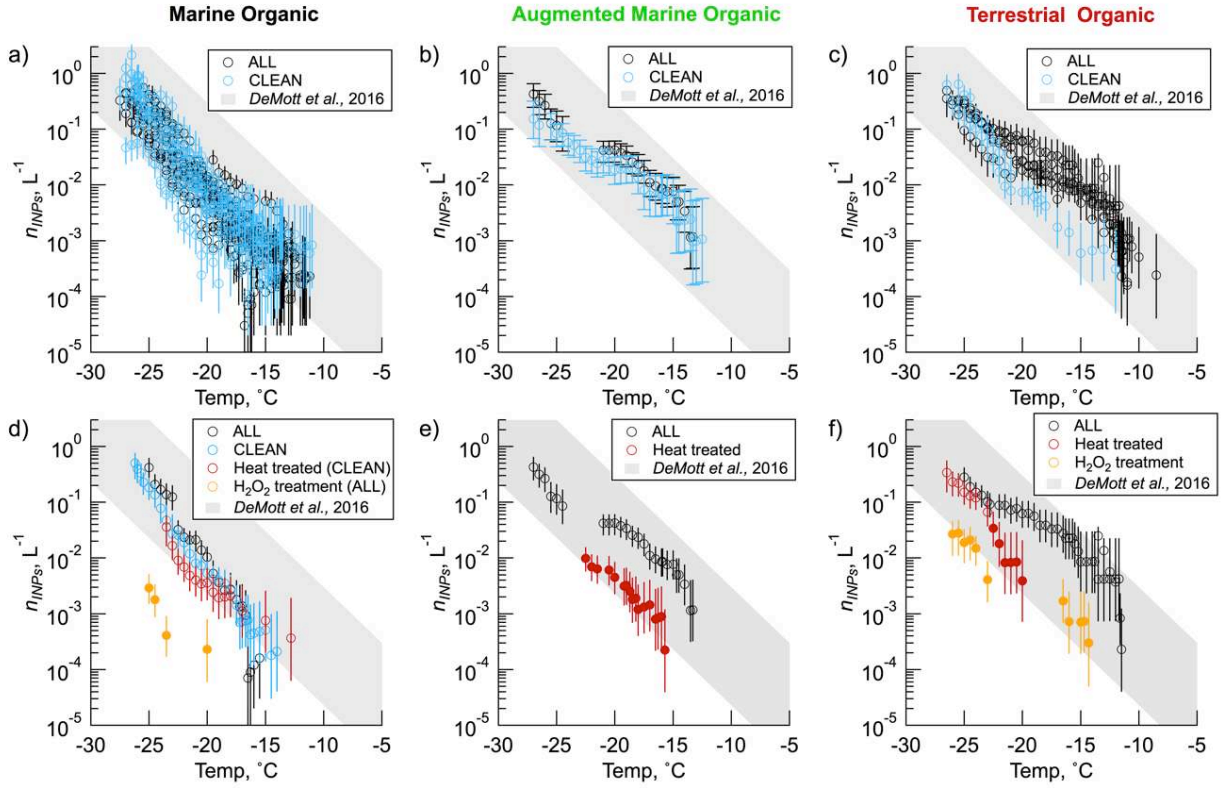

Figure 4.2-7. Panels a-c) show the three main INP spectrum types observed at MHD: (a,d) Marine Organic (b,e) Augmented Marine Organic and (c, f) Terrestrial Organic. INP spectra resulting from offline treatments performed on samples that are representative of the three classes of INP populations are shown in d-f. d) 10-11 Aug, 2015 represents the Marine Organic INP spectrum type; e) 9 Aug, 2015 represents the Augmented Marine Organic INP spectrum type; and f) 17-18 Aug, 2015 represents the Terrestrial Organic INP spectrum type. For d-f, blue and black markers correspond to CLEAN sector and ALL samples. Red markers correspond to the heat-treated samples (heat treatments were performed on either the CLEAN sector or ALL samples, which were nominally the same) and gold markers correspond to hydrogen peroxide digested samples. Filled markers indicate values in treated samples that are statistically significantly different from untreated samples. Vertical bars are the 95% confidence intervals for the IS measurements. From *McCluskey et al., (a, in prep).*

4.2.b.iv Predicting marine INPs at MHD

Previous studies have examined the relationship between marine organic aerosol and offshore biological activity at MHD (e.g., *O'Dowd et al.,* 2004, *Rinaldi et al.,* 2013, *O'Dowd et al.*, 2015). *Rinaldi et al.,* (2013) found that sub-micrometer organic aerosol arising from biological productivity lags Chl *a* concentrations by 8 days. A similar but somewhat shorter lag between n_{INPs} and Chl *a* is supported based on laboratory studies of nascent SSA (Chapter 3). Here, we use offshore Chl *a* concentrations, observed from satellite (sample box of 47 to 57 °N and 14 to 24 °W, shown in Figure 4.2-3), to determine the utility of Chl *a* as a predictor for marine organic n_{INPs} in nature. The relationship between Chl *a* and n_{INPs} (measured by the IS and DFPC for samples of air masses arriving from the CLEAN sector) is tested for lag-correlation coefficients calculated for 0 – 14 day lags.

Correlations between Chl *a* and INPs measured by the DFPC at -22 °C are shown in Figure 4.2-8 for both PM_1 and $PM_{1\text{-}10}$ ($1 < D_p < 10$ μm) samples, providing insight as to how these relationships may differ for submicron versus supermicron aerosol particles. INPs active at -22 °C, measured by the DFPC, in the PM_1 aerosol were positively lag correlated with Chl *a* after 8 days (R up to 0.37, but statistically insignificant). INPs active at -22 °C that were measured by the DFPC in the coarse aerosol fraction showed no suggestion of correlation with Chl *a* for any lag time. Although the correlations observed here are at best moderate, submicron INPs follow closely the trend showed by *Rinaldi et al.* (2013) for submicron primary marine organic aerosols, suggesting that the organic component has some role in influencing the ice nucleating properties of submicron SSA.

Lag-correlation results for INPs measured by the IS (total suspended particles, or TSP) at -18, -22 and -26 °C are shown in Figure 4.2-8. For INPs active at -18 and -22 °C in the TSP (IS),

the trend is opposite to that of sub-micron INPs observed by the DFPC, with moderate to poor correlations. However, INPs active at -26 °C show a trend somewhat consistent with PM_1 INP active at -22 °C, though these correlations are not statistically significant. Interestingly, n_{INPs} are statistically significantly anti-correlated after 11-13 days for INPs active at -18 and -22 °C and after 0-2 days for INPs active at -22 in PM_1 measured by the DFPC. These results suggest that, if there is a link between ocean biological productivity and INP emissions, the relationship between n_{INPs} and ocean surface Chl *a* is not simple.

This exercise illustrates that the relationship between n_{INPs} and Chl *a* in nature is different across different ice nucleation temperatures and may be sensitive to particle size. The lack of a clear relationship between n_{INPs} and Chl *a* found in this study is consistent with previous measures of nascent SSA by *McCluskey et al.* (2017) and summarized in Chapter 3. In the laboratory studies, INP temperature spectra collected over the course of phytoplankton blooms revealed that increases in n_{INPs} occurred only for INPs in specific temperature ranges, during peak INP emission periods. While determining the size of marine INPs remains an active area of research, many studies have illustrated that the organic enrichment in SSA from ocean biological activity is strongly dependent on particle size (e.g., *O'Dowd et al*., 2004, *Gantt and Meskhidze,* 2013). Future studies should aim to characterize size-dependent n_{INPs} across all temperatures (e.g., *Mason et al.,* 2015) during multiple marine organic events to investigate the relationship between Chl *a* and n_{INPs} across a range of temperatures of activity, Chl *a*, and marine organic aerosol concentrations. Improved correlations between n_{INPs} and Chl *a* may be obtained by extending the temporal coverage of the observations to include data collected during, before and after both low and high biological activity conditions.

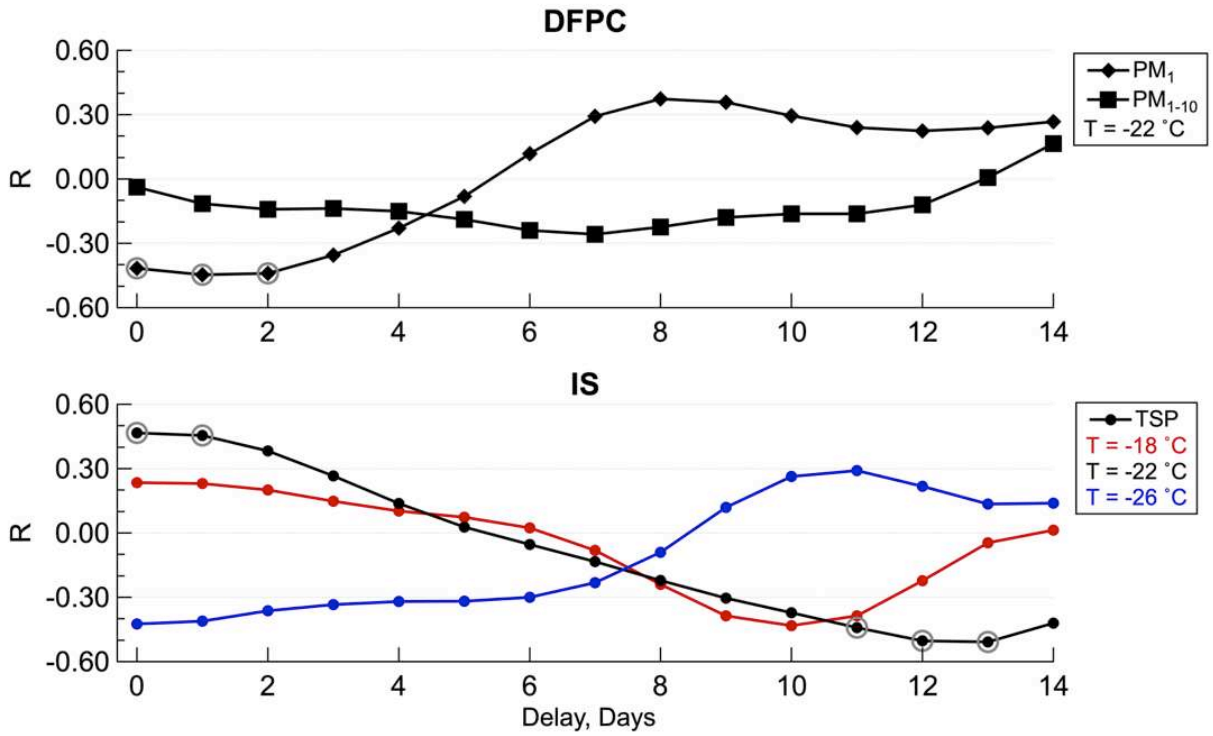

Figure 4.2-8. Correlation coefficients between Chl *a* and n_{INPs} as a function of the delay time, for (top) PM_1 and $PM_{1\text{-}10}$, measured by the Dynamic Filter Processing Chamber (T =-22° C and SS_w >1), and (bottom) TSP, Ice Spectrometer (T = -18, -22, and -26 °C). Grey circles indicate correlation coefficients significant at the 95% confidence level. From *McCluskey et al., (a, in prep)*.

At the time of the *Wilson et al.* (2015) study, concurrent ambient measurements of marine aerosol chemistry and n_{INPs} were not available to provide more insight into the relationship between TOC and INPs in ambient marine aerosol. The CLEAN sector observations made at MHD as part of this study provide the first opportunity to test how well the assumptions proposed in the *Wilson et al.* (2015) hold against ambient atmospheric aerosols and INPs, following the expression:

$$n_{INP} = (\exp(11.2186 - (0.4459 \times T))) \times TOC$$

where n_{INPs} is the ambient number concentration (m^{-3}) of INPs active at a given temperature (T, °C) and TOC (g of C per m^3 of air) is the total organic carbon mass concentration measured in the ambient aerosol. In order to match the definition of the TOC used by Wilson et al. to develop

this relationship, some approximations were made to estimate aerosol phase TOC for the MHD observations. We estimate *TOC*, termed here as TOC_{est}, from the submicron organic aerosol mass concentration measured by the HR-ToF-AMS ($[Org]_{HR\text{-}ToF\text{-}AMS}$) as follows:

$$TOM_{est} = [Org]_{HR-ToF-AMS} \times \frac{POM_{tot}}{POM_{sub}}$$

$$TOC_{est} = \frac{TOM_{est}}{OM:OC}$$

Supermicron aerosol significantly contributes to the total mass of sea spray organic matter (e.g., *Facchini et al.,* 2008); here, a factor of 2 is assumed for the ratio of total particulate matter to submicron particulate organic matter (POM_{tot}/POM_{sub}), following the best estimate reported by *Burrows et al.* (2013). A range of POM_{tot}/POM_{sub} (1.4 to 2.5) is also tested and used as lower and upper limits of predicted n_{INPs}. The OM:OC ratio of sea spray organic matter is assumed to be 2.0, determined based on measured OM:OC of 2.0 and 1.99 for M1 and M2 respectively, by the HR-ToF-AMS.

Results from this exercise are shown in Figure 4.2-9, where we compare the predicted n_{INPs} to observed n_{INPs} for INPs active at -15 and -20 °C in CLEAN sector samples. These estimates indicate that the *Wilson et al.* (2015) relationship predicts n_{INPs} measured in the CLEAN sector (i.e., pristine marine aerosol) within an order of magnitude for one third (9 out of 27) of the periods evaluated. A tendency to overpredict n_{INPs} is consistent with a comparison with INP observations in laboratory studies of nascent SSA (*McCluskey et al.,* 2017, Section 3.3.d) and experiments that found differing composition and organic volume fractions for jet drops versus film drops, indicating that the composition and ice nucleation ability of sea spray organic matter is not equal to the composition and ice nucleation ability of the SML (*Wang et al.,* 2017).

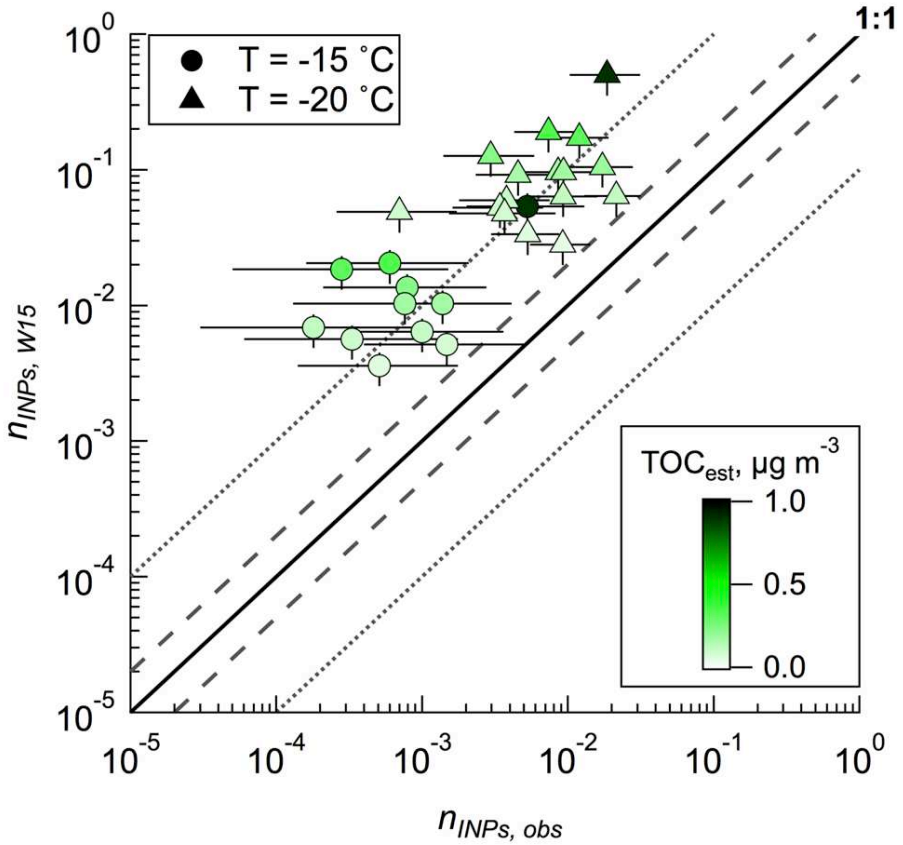

Figure 4.2-9. Predicted n_{INPs} (*Wilson* et al., 2015 compared to observed n_{INPs} at -15 °C (circle markers) and -20 °C (triangle markers) in total suspended aerosol from the CLEAN sector. Points are colored based on the estimated TOC. Vertical uncertainty bars describe the range in estimated n_{INPs} for the range of POM_{tot}/POM_{sub} reported in the literature. Horizontal bars on data points show uncertainties associated with the measurement (95% confidence interval). Lines indicate 1:1 (solid), a factor of 2 from 1:1 (dashed) and a factor of 10 from 1:1 (dotted). From *McCluskey et al., (in prep).*

The enhanced n_{INPs} observed during a period that was identified as a clean marine organic event (M1) were heat labile, suggesting that INPs associated with sea spray organic aerosol were impacted by ocean biological processes. Relating n_{INPs} to Chl *a* indicated a lack of a clear relationship between Chl *a* concentrations the emissions of ice nucleation active sea spray organic matter. Discrepancies between observed n_{INPs} and n_{INPs} estimated from the Wilson et al. relationship suggest that additional mechanisms impact the inclusion of INPs from the SML into sea spray organic matter. These exercises clearly demonstrate that much work remains in unraveling the intricacies that lead to periods of elevated n_{INPs} associated with sea spray organic

aerosol. However, progress in characterizing ice phase transitions in SSA-cloud interactions requires advancements in scientific understanding and numerical representation of the biological, physical, and chemical mechanisms controlling the emissions and ice nucleation properties of sea spray organic aerosol.

The CLEAN sector measurements at MHD during periods without significant enhancements in organic aerosol represent pristine SSA and were used to develop a parameterization that describes the typical INP population that is observed in the pristine marine boundary layer in the North Atlantic region. That is, only CLEAN sector Marine Organic INP temperature spectra (i.e., excluding Augmented Marine Organic INPs and Terrestrial Organic INPS) were used for this parameterization. We followed the approach of *Niemand et al.* (2012), where the nucleation site density is described as:

$$n_s(T) = \exp(a\ (T - 273.15) + b),$$

where n_s is the nucleation site density (m^{-2}), T is temperature (K), and a and b are fit parameters that were determined to be -0.545 and 1.0125, respectively, for our data. The exponential fit to the CLEAN Marine Organic INP spectra is shown in Figure 4.2-10, with a coefficient of determination of 0.821. This parameterization should be used to specify immersion freezing ice nucleation properties unique to SSA, and could be used to improve estimates of primary ice formation in numerical models that simulate SSA. However, we emphasize that this parameterization does not yet incorporate heat labile organic INPs, which were demonstrated as an important component of INP populations observed during the Augmented Marine Organic INP event. Extending this parameterization to include dependencies on ocean biological and organic matter should be possible with more observations and advanced understanding of the physico-chemical mechanisms that control the composition of sea spray organic matter.

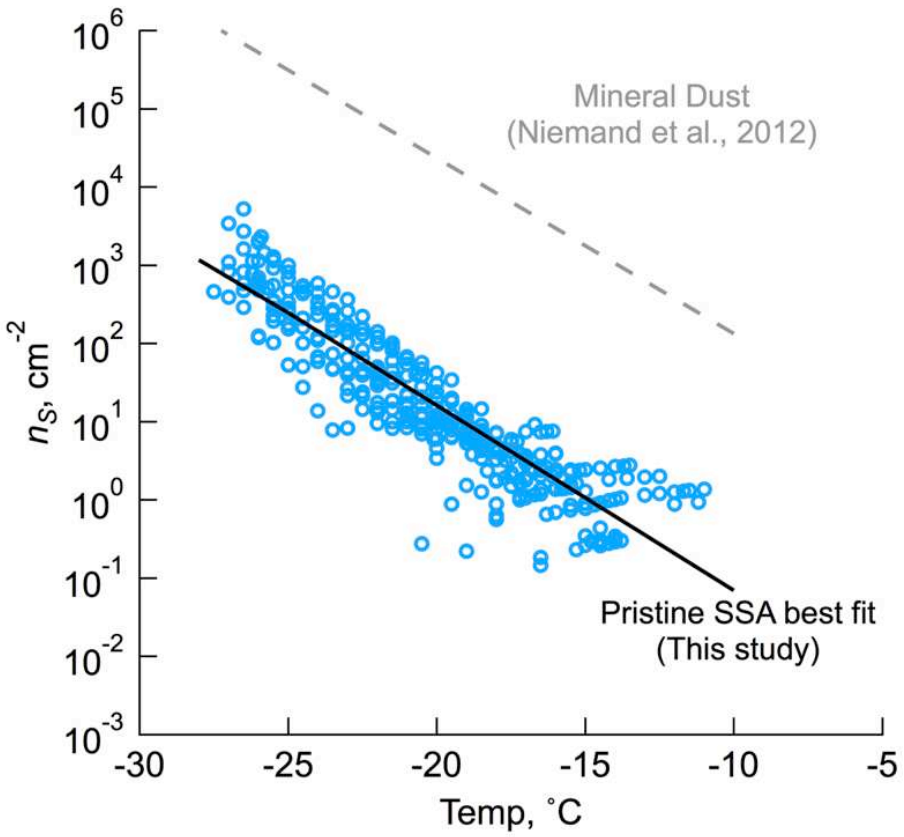

Figure 4.2-10. Nucleation site densities as a function of temperature measured in the CLEAN sector by the ice spectrometer. Exponential fit to the data (R^2 = 0.821) is also shown, following the approach by *Niemand et al.* (2012); equation for exponential fit for data is $n_s = \exp(-0.545(T-273.15)+1.0125)$, where n_s is nucleation site density (m^{-2}) and T is temperature (K). Also shown is the parameterization for mineral dust n_s proposed by *Niemand et al.* (2012).

4.2.c Summary

In August 2015, three ice nucleation measurement methods were deployed at the Mace Head Research Station (MHD), a remote coastal location at which marine organic aerosol arising from offshore biological activity is commonly observed. Observed INP number concentrations (n_{INPs}) at MHD were within previously reported measurements for marine regions, with the largest variability in number concentrations occurring for ice nucleation temperatures warmer than -22 °C. To investigate factors contributing to the variability in n_{INPs}, three periods of

elevated organic aerosol mass concentrations were examined for changes in meteorology, off-shore biological activity, aerosol chemistry, and properties of INPs (heat sensitivity and organic makeup). The first marine organic event (M1) was associated with higher numbers of n_{INPs} active at temperatures warmer than -22 °C. INPs observed during M1 were heat labile, suggesting the presence of protein-containing primary marine organic INPs. A second marine organic event (M2) was observed during the study, but was associated with no change in observed INPs, potentially due to differences in organic composition that may have been a consequence of lower wind speeds, biological processes that are not described fully by Chl *a* (e.g., bacteria abundances) or other variables that are currently unknown. Finally, marine aerosol that was significantly influenced by terrestrial aerosol (T1) was associated with increased n_{INPs}, and the INP population that was present during this period was heat labile and was largely made up of organic material.

Offshore ocean Chl *a* and organic aerosol mass concentrations were explored as possible predictors for the changes in n_{INPs} associated with marine organic aerosol events. Lag correlation analyses show a lack of a clear relationship between n_{INPs} and Chl *a,* and the utility of Chl *a* as a predictor for INP emissions likely requires detailed evaluations on how this relationship changes across different ice nucleation temperatures and particle sizes. Predictions of n_{INPs} based on organic carbon mass concentrations (*Wilson et al.,* 2015) showed some merit, but generally over predicted marine n_{INPs} by a factor of 4-100 in this study. While our current understanding of the many factors that control the abundance of INPs in sea spray heat labile organic aerosol is inadequate to numerically describe their behavior, we propose a parameterization that describes the nucleation site density of the typical marine organic INP population observed in the marine boundary layer at MHD.

Section 4.3 Ice nucleating particles over the Southern Ocean

4.3.a Study overview/approach

The Clouds, Aerosols, Precipitation, Radiation, and atmospheric Composition Over the southeRn ocean (CAPRICORN) campaign was conducted from March 13 to April 15 in 2016 onboard the RV Investigator (V02-2016). The research voyage occurred south of Australia during the late summer and early Austral fall season (Figure 4.3-1). The objective of this study was to characterize n_{INPs} in the marine boundary layer over the Southern Ocean region. These data serve as the first measurements of their kind in nearly four decades, as discussed below. Ocean surface Chl *a* concentrations indicate that a moderate, but representative, range of Chl *a* concentrations (up to 2 mg m^{-3}) were present during the study (Figure 4.3-1) and were used to explore the role of biological productivity on the observed INP populations.

In addition to surveying atmospheric n_{INPs}, number concentrations of ice nucleating entities (n_{INEs}, *Vali et al.,* 2015) were measured in seawater samples collected during the voyage. These measurements were used to characterize the source potential, or the number of INEs in seawater that potentially contribute to the INP population via bubble bursting, of the Southern Ocean. Specifically, seawater samples were collected in mesoscale oceanic eddies, which are ocean dynamical feature analogous to atmospheric low and high pressure systems. Oceanic eddies have large spatial (100 km) and time (weeks to months) scales (*McGillicuddy et al.,* 2016), and are ubiquitous features in the Southern Ocean (*Frenger et al.,* 2015*)*. These prevalent ocean features impact biological productivity by allowing or prohibiting advection of ocean waters containing anomalous amounts of phytoplankton and nutrients (*Gaube et al.,* 2014). As described by *Moreau et al.* (2017), the cold core (CC) eddy sampled during this study developed from the Sub Antarctic Front and was identified based on distinct negative sea surface height

anomalies, with an eddy diameter of approximately 190 km. Additional SW samples were collected in a region that weakly depicted a warm-core eddy (WC), with moderate positive sea surface high anomalies (*Moreau et al.,* 2017). CTDs were used to collect seawater samples for numerous analyses; near-surface SW samples (collection depths of <15 m) were used in this work for detection of INEs and Chl *a*. The CC and WC sampling approach facilitated the assessment of the Southern Ocean source potential and inferred composition of INEs at varying levels of biological productivity.

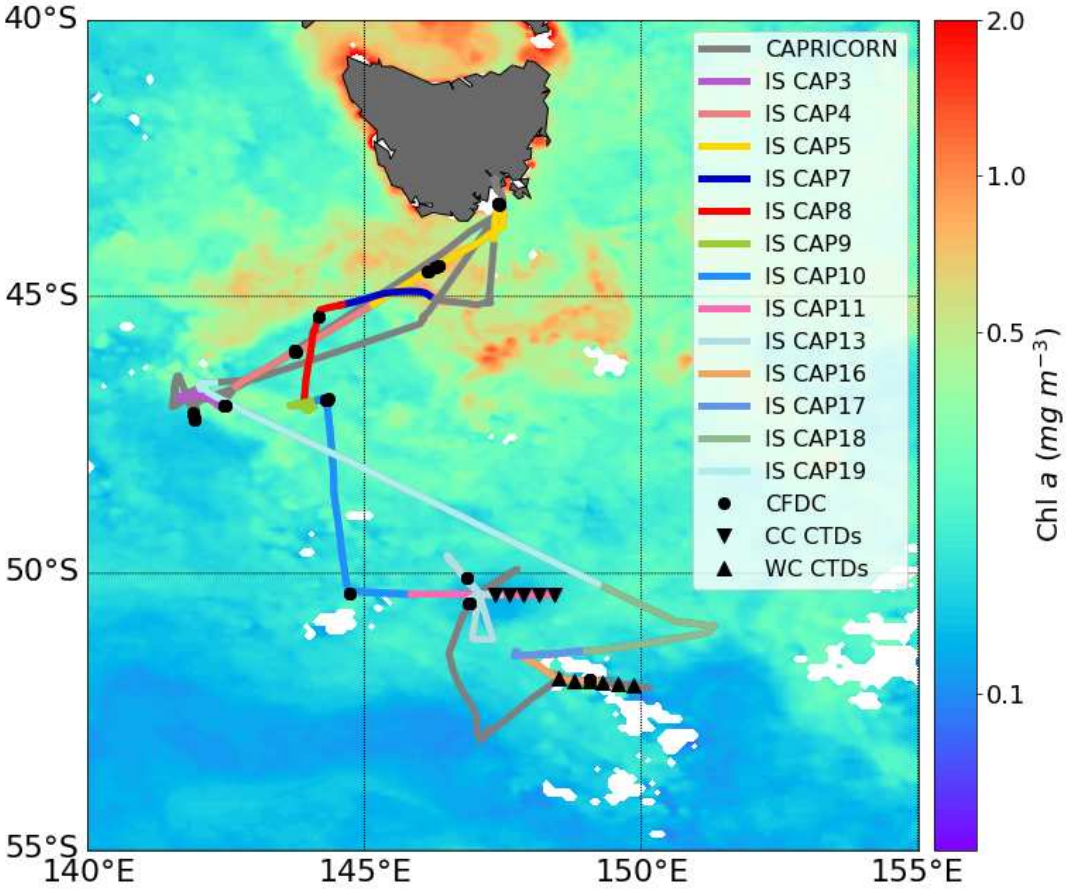

Figure 4.3-1. Map of ocean surface Chlorophyll a concentrations detected by satellite (4 km, level 3 Moderate Resolution Imaging Spectroradiometer aboard NASA's Aqua satellite) for March 2016. Grey trace indicates the CAPRICORN voyage track. Color traces depict individual Ice Spectrometer (IS) collection periods. Circle markers show sampling locations for measurements made by the Continuous Flow Diffusion Chamber (CFDC). CTD deployments for the cold core (CC, downward pointing triangle makers) and the "warm core" (WC, upward pointing triangle markers) are also shown.

4.3.b Results and Discussion

4.3.b.i INPs measured during CAPRICORN

Temperature spectra from CFDC and IS measurements during the CAPRICORN campaign are shown in Figure 4.3-4. n_{INP} ranged from 0.25 to 2.8 m^{-3} for INPs active at -20 °C, with an average concentration of 0.86 +/- 0.78 m^{-3}. We note that n_{INPs} measured during CAPRICORN are much lower than reported herein for the other measurement campaigns, and thus, n_{INPs} are discussed in units of per m^{-3} instead of L^{-1} to ease readability. Diesel-electric engines provided power and propulsion to the ship and waste was incinerated while at sea. These activities emitted combustion aerosol, included particles such as black carbon and other particulate organic carbon. Detailed characterization of particle composition from this aerosol source was not completed in this study. The ice nucleation activity of combustion particles is still an active area of research (e.g., *Schill et al.,* 2017), but it is possible that these particles may have influenced measurements in this remote region (i.e., extremely low n_{INPs}) and thus we investigated the influence of ship exhaust on ice nucleation measurements. Linear regression analysis between n_{INPs} and average exhaust flag (i.e., fraction of time potentially influenced by ship exhaust, see Section 2.2.d) shows a statistically significant positive relationship between n_{INPs} and estimated contribution from exhaust, illustrated in Figure 4.3-2. A summary of the correlation coefficients, slope and p-values are provided in Figure 4.3-3, revealing that the trend is statistically significant (p-value <0.05) for n_{INPs} measured between -20 °C and -25 °C. The highest impact of exhaust was an increase in n_{INPs} by up to a factor of approximately 2. Samples with 20% or less exhaust are considered here to be clean. The bias possible from 20% exhaust is insignificant compared to the values measure (e.g., possible increase due to 20% exhaust is approximate 0.0005 L^{-1} at -20 °C). Consequently, n_{INPs} are segregated into non-influenced

samples (exhaust less than 20% of the sampling duration) and samples with potential contributions from exhaust (exhaust greater than 20%).

For measurements with less than 20% of sampling time influenced by exhaust, n_{INP} ranged from 0.25 to 0.75 m^{-3} for INPs active at -20 °C, with an average concentration of 0.4 +/- 0.16 m^{-3}. Observed n_{INPs} varied by less than a factor of 3 for exhaust-free samples across all temperatures, which is the lowest variability observed for marine environments thus far. Similar to findings from the CAICE studies, n_{INPs} measured by the CFDC and IS were in good agreement, despite being measured in different locations (CFDC sampled from the air sampling inlet (see Methods) and the IS sampled total suspended particles on an open-face filter approximately 23 meters above the ocean surface). This agreement suggests that the aerosol sizes containing the majority of INPs were successfully transferred to the CFDC via the sampling inlet and concentrator inlet. The CAPRICORN n_{INPs} are at the lower range of n_{INPs} of those reported for several different ocean regions (*DeMott et al.,* 2016), shown in in Figure 4.3-4. Shown in Figure 4.3-5, normalizing the data by aerosol surface area reveals that the ice nucleation site density (n_s) during the study were similar to n_s measured at MHD, though nearly all n_s observed during CAPRICORN were lower than the best fit line to the MHD observations. The lower n_s observed during CAPRICORN compared to MHD may be due to higher wind speeds present over the Southern Ocean; higher wind speeds may lead to an increased production of coarse mode sea salt particles, which would increase the total aerosol surface area without increase non-sea salt aerosol, resulting in a lower n_s. A comparison of sea spray aerosol production and the resulting size-dependent organic mass fractions in these two regions is of interest for future research.

Observed n_{INPs} from this study (maximum n_{INPs} = 2.8 m^{-3} at -20 °C) were at least a factor of 100 lower than those reported by *Bigg* (1973) (> 200 m^{-3} at -20 °C for -40 to -55 °S). The measurements reported by *Bigg* (1973) were made from filters collected onboard the U.S. Antarctic Research Program RV *Eltanin* from 1969 to 1972. Pairs of filters were collected every 12 hours, collecting 300 and 3000 L of air. One meter of spiraled brass tubing was used to remove rain and larger sea salt particles from the sampled air. Filters were analyzed for n_{INPs} by exposing the filter membrane to supercooled temperatures and supersaturation, similar to the approach utilized in the DFPC (see MHD study).

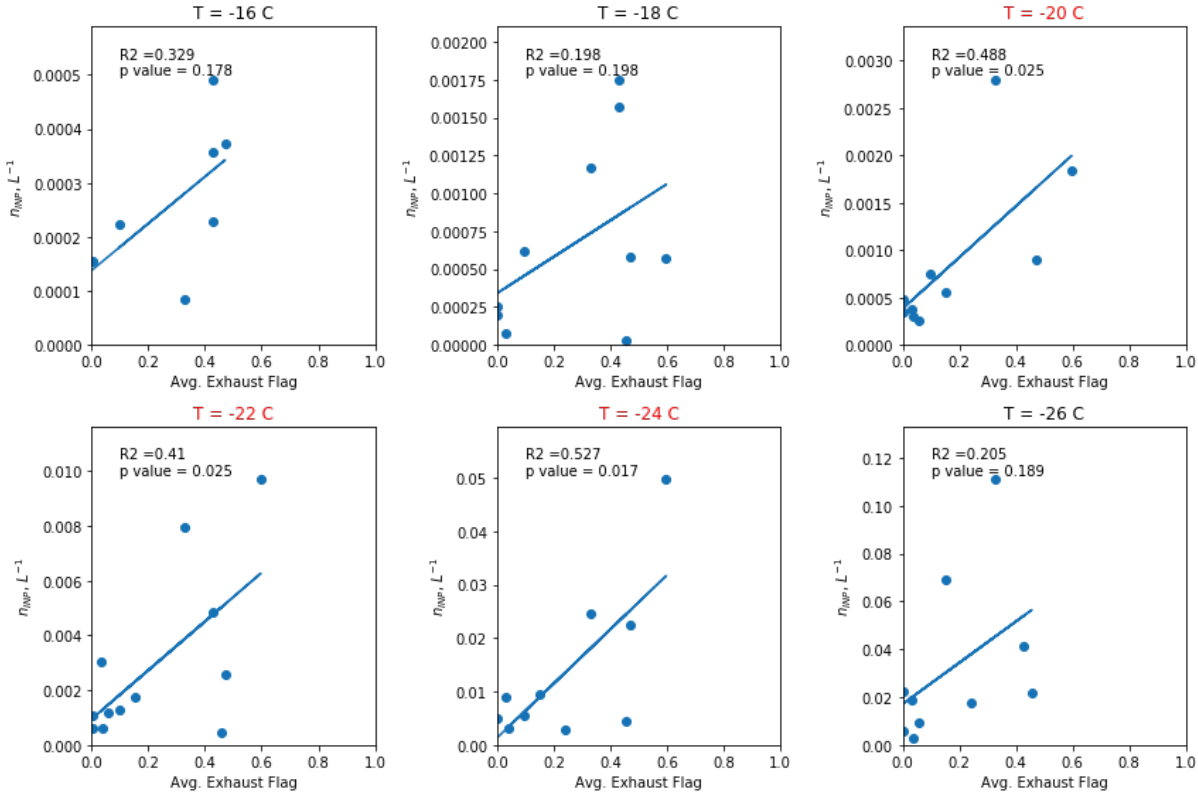

Figure 4.3-2. Linear regression analysis between n_{INPs} and average CAPRICORN exhaust flag value (fraction of time with potential exhaust contamination). R^2 and p values are also reported for each temperature

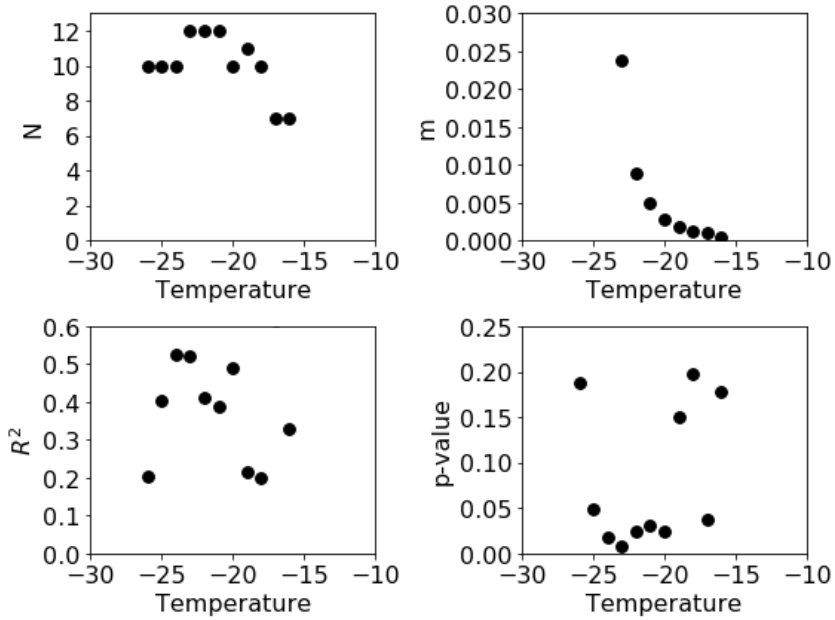

Figure 4.3-3. Summary of results for linear regression analysis for n_{INPs} and CAPRICORN exhaust flag value: Top Left is the number of values used to calculate fit. Top Right is the slope of the linear regression. Bottom left is the correlation coefficient and Bottom Right is the p-value determined for each regression analysis.

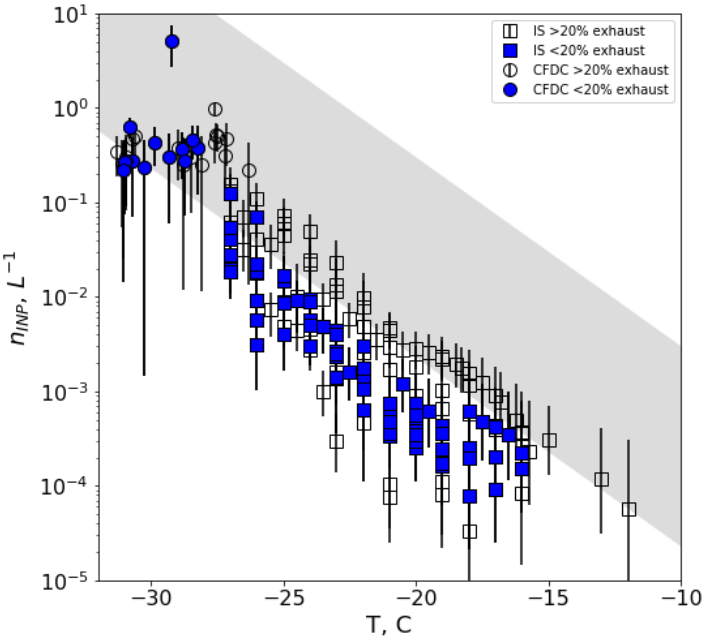

Figure 4.3-4. INP temperature spectra for aerosol measured during CAPRICORN by the IS (square markers) and the CFDC (circle markers). Error bars for IS data represent 95% confidence intervals. Error bars for CFDC data show the errors estimated based on Poisson counting statistics. Filled blue and open black markers indicate samples with exhaust detection for less than 20% and more than 20% of the sampling time, respectively.

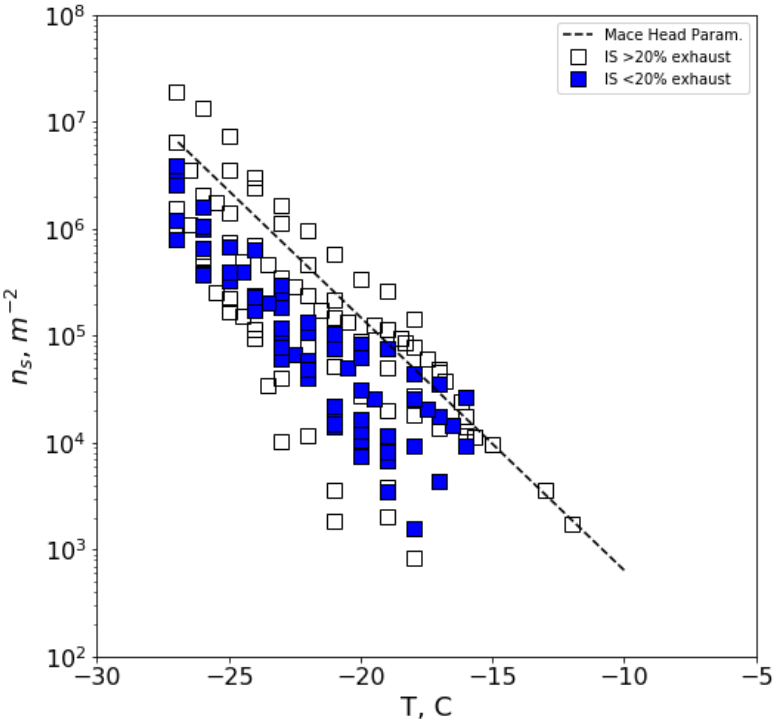

Figure 4.3-5.Ice nucleation site density (n_s) for IS measurements during CAPRICORN. Data are colored by estimated exhaust contributions, where samples collected with less than 20% exhaust are highlighted in blue. Also shown is the parameterization derived from data collected at MHD (Section 4.2.b.iv)

There are many possible explanations for the drastic observed differences between CAPRICORN and historical measurements. First, we note that the ability to detect extremely low levels of n_{INPs} is a result of an advanced understanding of materials that nucleate ice and advances in making artifact-free measurements of low concentrations of INPs. We note that *Bigg* (1973) evaluated filters that were set aside during the voyages to determine IN concentrations associated with the filters themselves, reporting that these blank filter concentrations corresponded to approximately 10% of the observed concentrations (0.1 m^{-3}, 1 m^{-3}, and 10 m^{-3} at -10 °C, -15 °C, and -20 °C, respectively). However, the extent to which these blank filters were exposed to other aspects of the method (loading filters into holder, handling, etc) is unknown, and we now understand that these aspects may lead to substantial errors for measuring low concentrations of INPs (e.g., *Twohy et al.,* 2016). Additionally, care was taken in this study to

account for contamination due to exhaust. *Bigg* (1973) notes that samples discolored from collection of exhaust were not included in his analyses, but we note that all filters analyzed in our study did not have visible discoloring, suggesting that a visual screening of exhaust would not fully account for exhaust influences. Erroneously high n_{INPs} due to sampling contaminations are a possible reason for the discrepancies between these studies, but such speculation is impossible to confirm.

An important difference between the CAPRICORN study and the extensive survey conducted by *Bigg* (1973) is the study season and duration. n_{INP} reported by Bigg were annual means of n_{INPs} based on 3 years of data, whereas n_{INP} reported here are only for late summer and early fall of a single year. It is possible that transported INPs (e.g., terrestrial aerosol containing dust) are important contributors to the Southern Ocean INP population that are seasonally dependent. In fact, one interpretation of the data observed by *Bigg* (1973) was that the n_{INPs} maxima he observed arrived due to subsidence or sedimentation of INPs transported in the upper troposphere from distant land sources (*Bigg*, 1973). A seasonal maximum may be missing from the CAPRICORN data. We note that, while observed seasonal variability in n_{INPs} has not been reported for this region, modeling studies of iron deposition from dust particles over the Southern Ocean indicate a seasonal maximum of dust transport during austral summer (*Ito and Kok,* 2017). Modeling studies of seasonal variability in the abundance of marine and terrestrial aerosol are underway as part of Chapter 5. However, these analyses are currently limited to more recent periods, due to the lack of aerosol emission inventories during the periods that *Bigg* (1973) explored the Southern Ocean region.

Finally, Figure 4.3-6 shows a timeline of n_{INPs} reported from 1955 to 1989 from *Bigg* (1990), suggesting a decreasing trend in n_{INPs} over 3 decades at Cape Grim, Tasmania and

measurements made on ship and remote ground sites south of 60 °S. Also shown in Figure 4.3-6 are the observed n_{INPs} measured at -15 °C and -16 (±0.5) °C during CAPRICORN. We find that the recent low CAPRICORN measurements are consistent with the long-term trend reported by *Bigg* (1990). Barring any influences of the above-mentioned concerns regarding measurement artifacts, the data suggests that n_{INPs} have decreased with time over the Southern Ocean. In fact, changes occurring in the Southern Ocean have been explored from the point of view of oceanographers, revealing a statistically significant 10% decrease in iron deposition (i.e., dust deposition) and a corresponding reduction in ocean biological activity between years 1997-2002 and 1979-1986 (*Gregg et al.,* 2003). A decline in dust transport to the region would correspond to a decline in a known terrestrial source of INPs (e.g., *DeMott et al.,* 2015). Additionally, *Gregg et al.* (2003) reported that increases in wind stress have been observed in the high latitude regions, which would lead to a deepening of the ocean upper mixed layer, thereby reducing light availability for biological productivity. This is an ongoing area of research, but we note that *Bigg* (1990), himself, stated "it is clearly important to verify the present extremely low ocean values in the southern latitude since it might either be a response to or cause of climatic change".

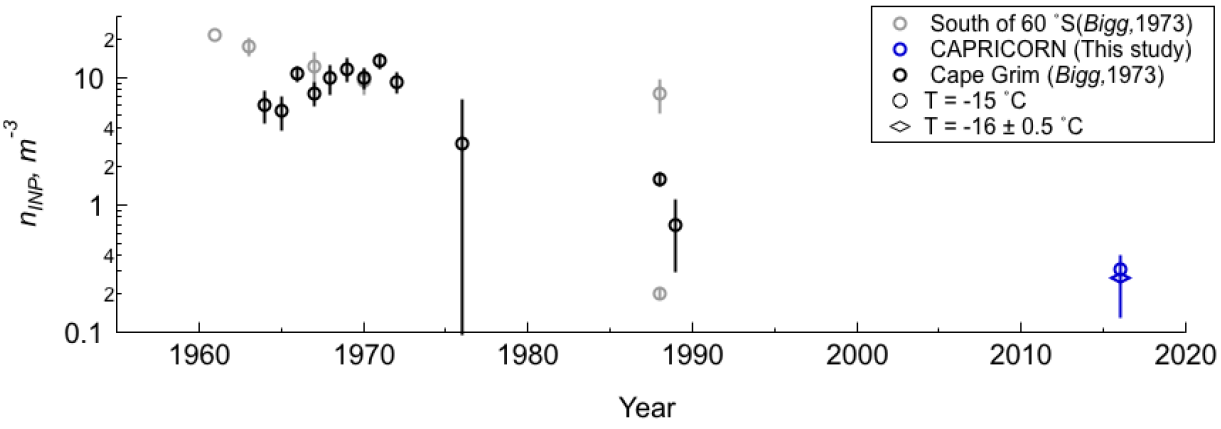

Figure 4.3-6. Timeline of n_{INPs} reported for T = -15 °C by *Bigg* (1973) at Cape Grim (black) and various remote ship and ground stations south of 60 °S (grey). CAPRICORN n_{INPs} for -15 °C (blue circles) and -16 °C are also shown. Vertical bars are reported standard deviations from *Bigg* (1990) and calculated standard deviations.

4.3.b.ii Characteristics of INPs observed during CAPRICORN

The contribution of terrestrial and marine air masses to the INPs observed during CAPRICORN is evaluated using radon (^{222}Rn) concentrations. A study by *Chambers et al.* (2014) reported average concentrations of ^{222}Rn up to 150 mBq m^{-3} in Antarctica and that ^{222}Rn concentrations greater than 400 mBq m^{-3} were considered high ^{222}Rn events and were found to originate from land. ^{222}Rn concentrations observed during CAPRICORN are shown in Figure 4.3-7. n_{INPS} and n_s spectra colored by ^{222}Rn concentration are shown in Figure 4.3-8 and Figure 4.3-9, respectively. Linear regression analyses of n_{INPs} and ^{222}Rn are shown for a range of temperatures in Figure 4.3-10. No statistically significant correlation was found. The warmest temperature with measureable IN activity (-12 °C) was for a sample with highest ^{222}Rn concentrations that was collected while the RV Investigator was located near land (CAP5, see Figure 4.3-1). However, CAP5 was likely influenced by exhaust for >50% of the sampling period, suggesting that the increase in n_{INPs} could be due to terrestrial and/or exhaust sources. Overall, based on low ^{222}Rn concentrations (less than 100 mBq m^{-3}), we conclude that terrestrial air masses were largely absent from the measured aerosol and n_{INPs} reported here are representative of oceanic sources.

Offline treatments, like those performed in CAICE laboratory and MHD studies, were performed on selected samples from this study to determine the contribution of heat labile and organic INPs to the total INP population. These treatments were performed on two samples that were potentially influenced by exhaust for less than 20% of sampling time (CAP 3 and CAP 18, Figure 4.3-1) and on two samples that had significant contribution from exhaust (CAP 7 and CAP 16, Figure 4.3-1), as shown in Figure 4.3-11. n_{INPs} detected during CAP3 were some of the lowest n_{INPs} observed during the study, over a region with relatively moderate Chl *a*

concentrations; INPs detected on CAP3 were not heat labile or organic (on the basis of peroxide digestion). Contrastingly, CAP18 was collected over a region that corresponded to similar Chl *a* concentrations and INPs were heat-stable, but were comprised entirely of organic material (no freezing detected for H_2O_2 treated sample). CAP16 was collected over a region that was also investigated as a pseudo-warm cold eddy (see Section 4.3.b.ii) and INPs were found to be heat stable and largely comprised of organic material, though some IN activity remained, similar to levels of n_{INPs} observed from CAP3. Finally, CAP7 was collected over ocean regions with highest ocean surface Chl *a* concentrations and INPs appear to be largely comprised of heat labile INPs, though the contribution from organic matter is unknown. These treatments collectively reveal that organic matter and heat-labile material contributed to the INP population measured during CAPRICORN, similar to the findings from laboratory studies (Chapter 3).

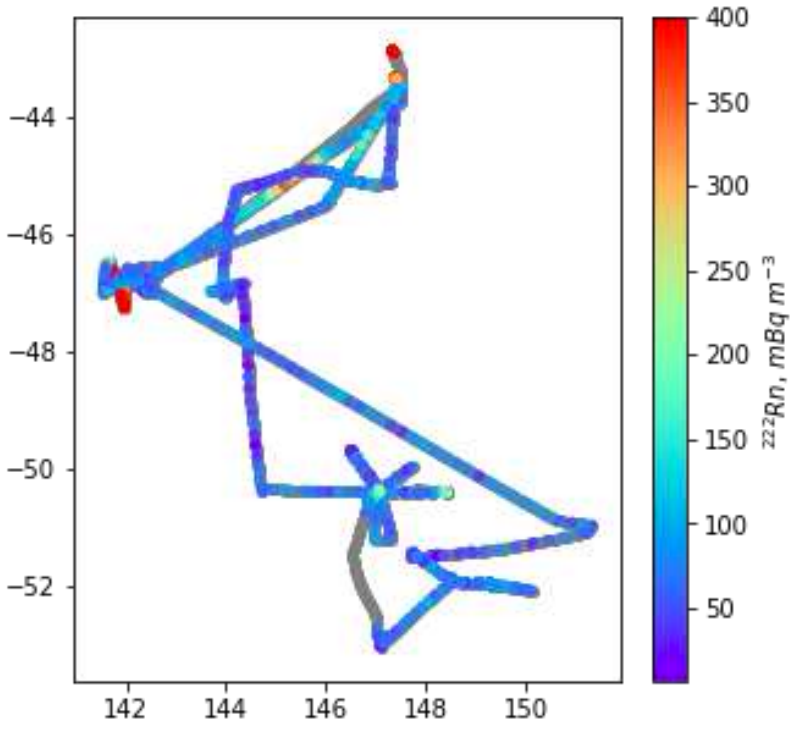

Figure 4.3-7.Radon (^{222}Rn) concentrations measured during CAPRICORN. Values over 400 mBq m^{-3} are also show as red.

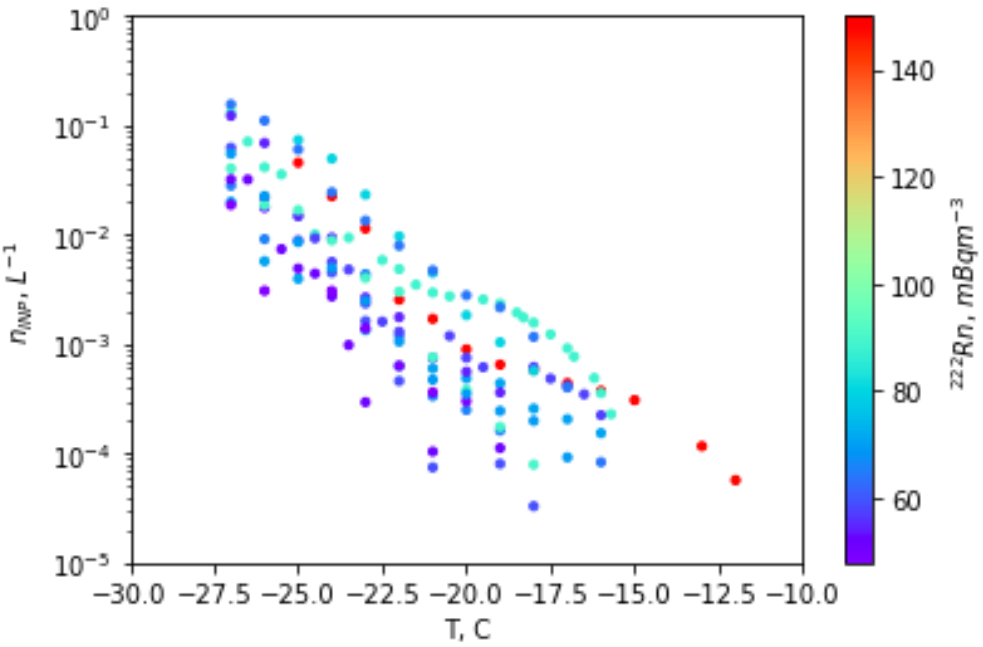

Figure 4.3-8. INP temperature spectra for all CAPRICORN samples, colored by average ^{222}Rn concentrations.

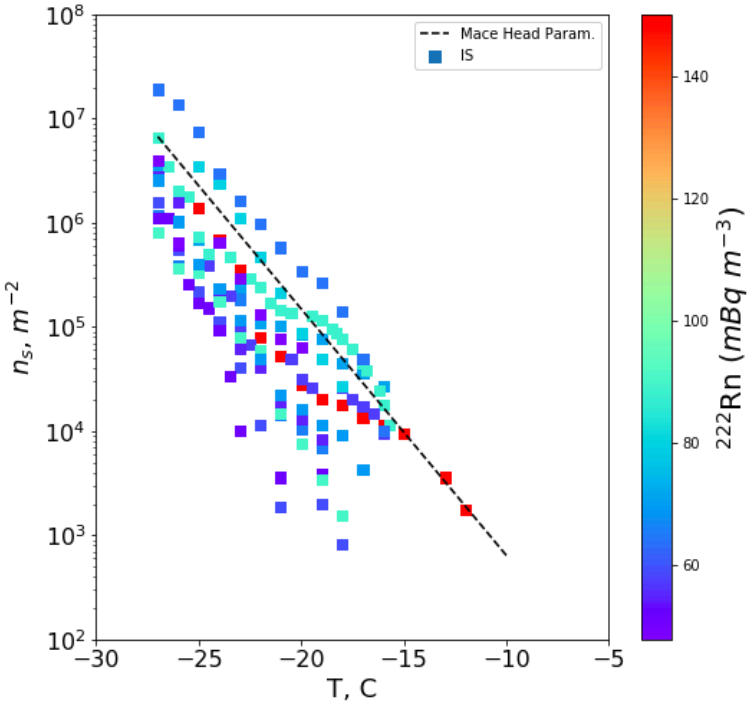

Figure 4.3-9. Ice nucleation site densities (n_s) for CAPRICORN IS samples, colored by ^{222}Rn concentrations.

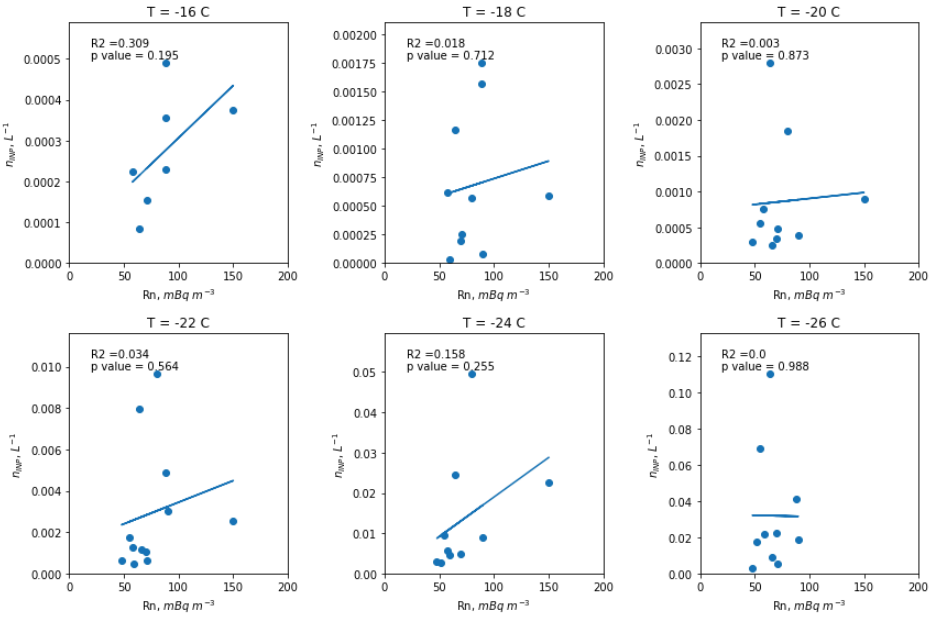

Figure 4.3-10. Linear regression analysis between n_{INPs} and ^{222}Rn. R^2 and p values are also reported for each temperature.

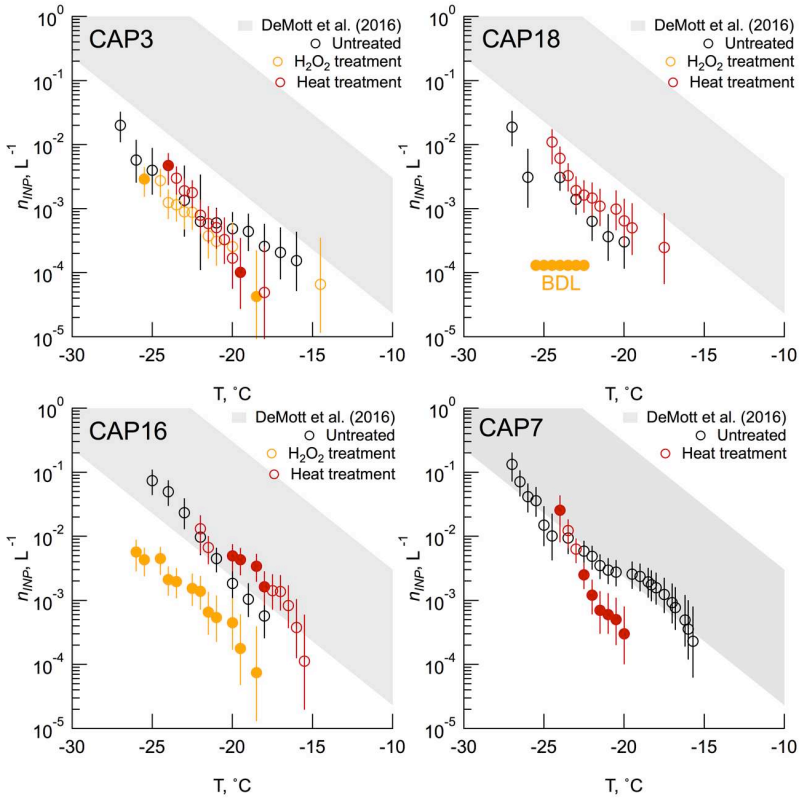

Figure 4.3-11. INP spectra for untreated (black), heated (red) and H_2O_2 treated (gold) samples. H_2O_2 treatment was not performed on CAP7. Treated values that are statistically significantly different from untreated values are indicated by filled circles. Vertical bars are the 95% confidence intervals for the IS measurement.

4.3.b.iii Southern Ocean INP source potential

Sampling of seawater near the ocean surface (5-15 m, i.e., not the sea surface microlayer) was used to evaluate the INP source potential of Southern Ocean seawater in two ocean features. The cold core (CC) eddy investigated in this study contained low Chl *a* concentrations in the eddy center (0.33 mg m^{-3}) with higher Chl *a* concentrations at the eddy peripherals (0.74 mg m^{-3}) (*Moreau et al.,* 2017), shown in Figure 4.3-12. SW samples were also collected from CTDs that were deployed in a region that weakly depicted a warm-core eddy, with positive sea surface high anomalies and fairly homogeneous Chl a concentrations (0.54 mg m^{-3} to 0.71 mg m^{-3}) that were higher compared to the CC eddy. Six CTDs were deployed from edge to center in both features, enabling characterization of horizontal changes in INE concentrations through varying biologically productive water.

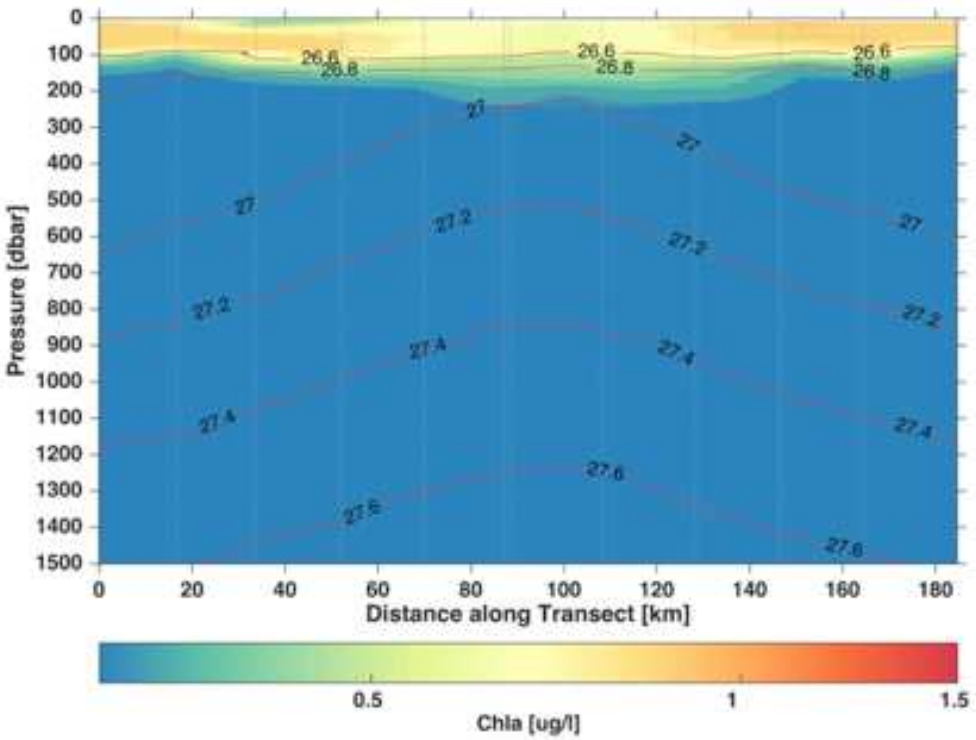

Figure 4.3-12. Chl *a* concentrtaions measured during triaxus transit from edge to edge of the Cold Core eddy (figure from Sebastian Moreau).

Ice nucleating entities (INEs) found in seawater samples from the CC eddy are reported in Figure 4.3-13. n_{INEs} during CAPRICORN were lower than those observed during the CAICE laboratory studies of SW collected from the SIO pier; n_{INEs} for -20 °C were less than 3 mL^{-1} during CAPRICORN and were over 40 mL^{-1} for the first day of the IMPACTS and MART studies (Figure 3.2-5). Data in Figure 4.3-13 are colored based on Chl *a* concentrations that were measured from the same CTD bottle to illustrate changes in INE temperature spectra as a function of Chl *a*. We note that, while Chl *a* concentrations were highest at the eddy center no clear difference was observed between n_{INPs} measured in surface water at the core compared to the eddy edge. All surface SW samples from the WC region are also shown in Figure 4.3-13 and no observed difference is found across all temperatures. As a result of recent CAICE laboratory studies, we now understand that SW n_{INEs} typically increase following the peak in Chl *a* concentrations, suggesting that SW INEs are generated during the decay phase of a phytoplankton bloom. Thus, we expect that the lack of observed changes in n_{INEs} found in these SW samples may be due to a lack of samples from a decaying phytoplankton bloom.

4.3.b.iv Characteristics of Southern Ocean seawater INEs

Offline heat and 0.2 μm filtering treatments, similar to the analyses performed on SW samples from the CAICE laboratory studies, were performed on SW samples that were collected in the CC eddy and the WC region. These results are shown in Figure 4.3-14. The majority of SW INEs were heat stable and smaller than 0.2 μm, similar to the DOC INP type observed from the MART and IMPACTS studies (Section 3.2.b). Two samples collected in the warm core region contained INEs that were both heat labile and larger than 0.2 μm, similar to the POC INP reported from CAICE studies (Section 3.2.b). However, the contribution of the POC INP type is small. These results suggest that the INEs observed in this study dominated by the DOC INP

type. The transfer of these INEs to the aerosol phase will likely differ from that observed in laboratory studies and other ocean regions. Specifically, the Southern Ocean is considered to roughest ocean on earth (*Young*, 1999) and this may correspond to a modest reduction in surfactant enrichment (persistent high wind stress and mixing of ocean surface waters).

4.3.c Summary

Modeling studies (*Burrows et al.*, 2013) and historical measurements (*Bigg*, 1973) and their interpretations (*Schnell and Vali,* 1976) suggested that INPs over the Southern Ocean are influenced by ocean biological productivity and serve as an important component to the aerosol-cloud interactions in this remote region. Measurements made during the month-long CAPRICORN study provide the first evaluation of the Southern Ocean as a source of INPs in nearly four decades. A flag developed based on wind direction, BC and CN concentrations indicated that ship exhaust could be an important source of contamination for ship-based n_{INPs} measurements. We find that ambient n_{INPs} were low compared to n_{INPs} observed in the marine boundary layer over various oceans (*DeMott et al.,* 2016) and were over two orders of magnitude lower than annual averaged n_{INPs} reported from an extensive 3-year survey by *Bigg* (1973) for the same region. Ignoring possible contamination issues that may have occurred at the time for these challenging INP measurements, reasons for this large discrepancy include 1) seasonal variability that would have been measured during Bigg's 3-year survey, but were absent from this month-long campaign or 2) long term decadal decreasing trend in n_{INPs} over the Southern Ocean (*Bigg,* 1990). Modeling studies are used to address the present-day seasonality in aerosol over the Southern Ocean region, but simulations for estimating long term decadal trends are not currently feasible due to unknowns in aerosol emissions during those time periods.

Observed n_{INPs} did not vary more than a factor of 3 for INPs active at -20 °C. Offline treatments of INPs collected during CAPRICORN reveal that the INP population is diverse for this region, with measureable contributions from both organic matter and heat-labile material to the INP populations. The source potential of the Southern Ocean was evaluated by measuring n_{INEs} in near surface SW, revealing n_{INEs} that were up to a factor of 10 lower than those observed in SW collected from the SIO pier. While n_{INEs} were lower in the Southern Ocean waters probed in this study, we note that offline treatments indicate that the INEs were dominated by the DOC INE type that was reported by *McCluskey et al.* (*Submitted to J. Atmos. Sci.*) and discussed in Chapter 3.

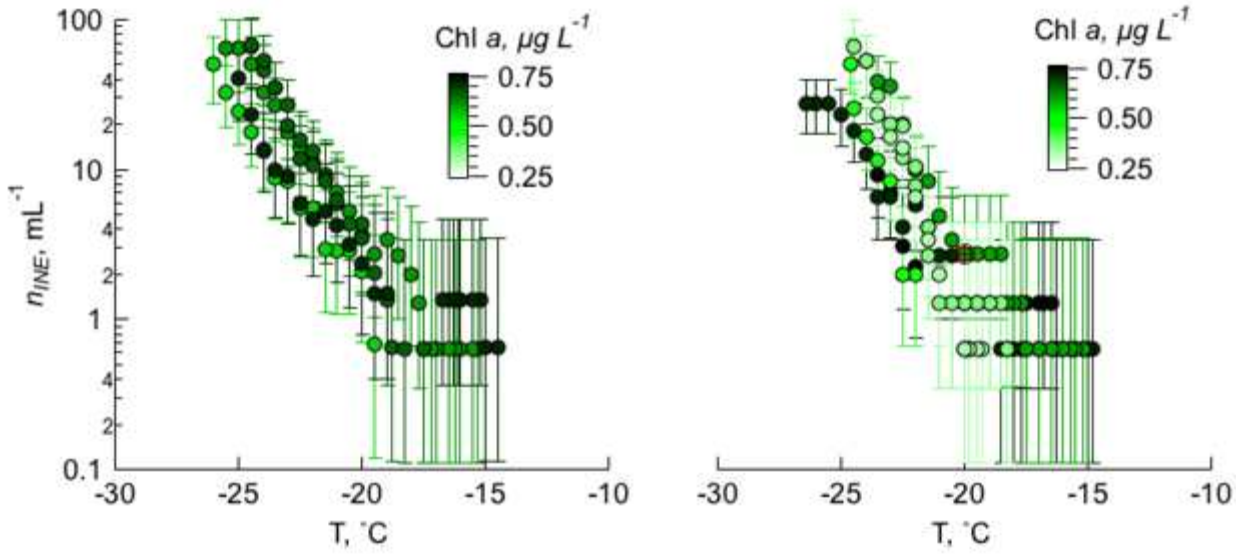

Figure 4.3-13. INE temperature spectra of near ocean surface water collected in the (left) WC eddy and (right) CC eddy. Marker color corresponds to the measure Chl *a* concentration for SW samples collected from the same CTD deployment. Vertical bars are the 95% confidence intervals for the IS measurements.

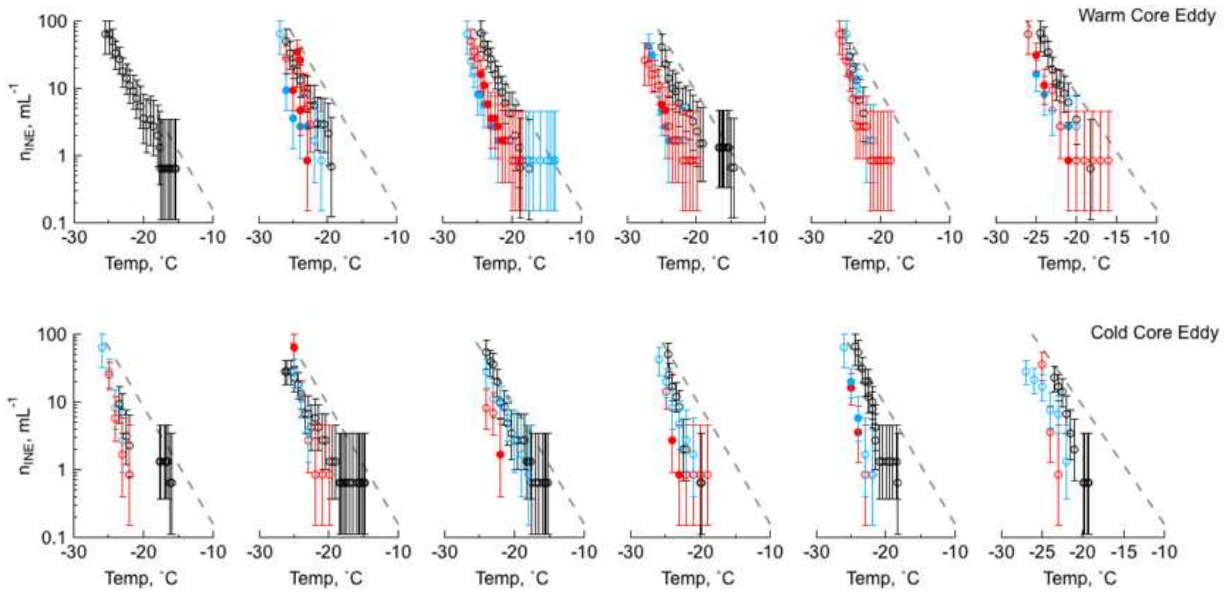

Figure 4.3-14. INE spectra for untreated (black), heat treated (red) and filtered seawater samples for (top) warm core region and (bottom) cold core eddy. Results are shown for samples collected from eddy or region edge (left) to center (right). For treated spectra (red and blue), filled markers indicate that the INE number concentration is statistically significantly different from the untreated sample (black). Vertical bars are the 95% confidence intervals for the IS measurements. Dashed line corresponds to n_{INEs} observed in SW from the SIO pier (CAICE studies). –

CHAPTER 5: MODEL PREDICTION OF MARINE INPS

Nudged model simulations with CAM5 and OCEANFILMS were performed to simulate concentrations of aerosol species for August 2015 that were subsequently used to estimate n_{INPs}. The goal of this study is to evaluate the utility of currently available marine INP parameterizations by comparing estimated n_{INPs} to observed n_{INPs}. In this chapter, we present preliminary and qualitative results that evaluate the model performance against observations at the Mace Head Research Station (MHD). In Section 5.1, we discuss a comparison between simulated and observed wind conditions and mass concentrations of particulate matter with diameters smaller than 10 μm (PM_{10}). Section 5.2 describes the approaches for estimating n_{INPs}. Discussion of preliminary findings and future work are provided in Section 5.3 and Section 5.4, respectively.

Section 5.1 Model and observation comparison of wind conditions and aerosol mass concentrations at MHD

Two model grid points were used in this study to extract simulated aerosol concentrations, shown in Figure 5.1-2. The nearest grid point to MHD (green star) is shown as a red circle, which is located along the coastline of Ireland (MH). Due to the model resolution and possible loss of accuracy in simulating transport and concentration gradients near the poorly resolved coastline, we also evaluated output from a second grid point, located west of MHD (MH-west, blue circle). Model output was evaluated against observations made during the Mace Head campaign (Section 3.2). These *in situ* observational data included wind speed, wind direction, PM_{10} mass concentrations, and observed n_{INPs} (for INPs active at all temperatures

reported for the IS measurement) that were measured from the ALL filters. All results reported here are preliminary.

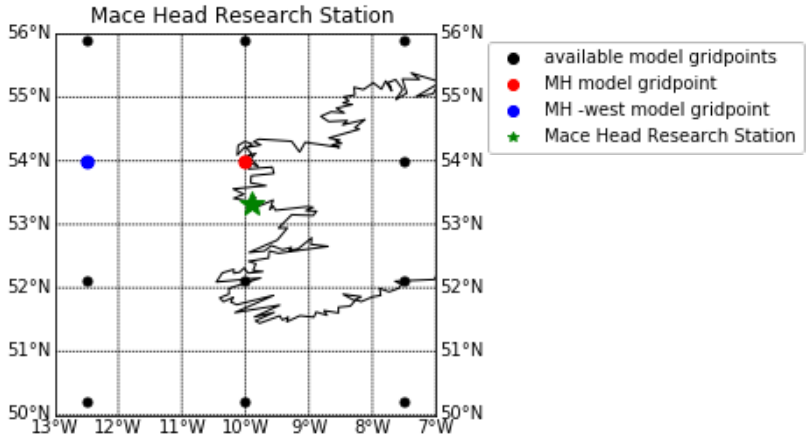

Figure 5.1-1.Map of Mace Head Research Station (MHD, green star), model grid box midpoint closest to MHD (red point) and model grid point west of MHD (blue point).

Wind speed and direction are shown in Figure 5.1-2 to evaluate simulated wind conditions near MHD. The range of simulated wind speeds over the month of August is within the range of observations, with maximum observed wind speeds of approximately 20 m s^{-1}. Wind speeds for the MH grid point are consistently higher than those over ocean (MH-west grid point). The simulated wind directions were similar to observed conditions during periods when observed winds were arriving from the west (i.e., SSA). For simplicity, the MH-west location was chosen as the most similar grid point to the wind and aerosol conditions present at MHD during this study period. All further analyses will used the MH-west location for model-observation comparisons.

A timeline of observed and simulated aerosol mass concentrations (PM_{10}) are shown in Figure *5.1-3* for the study period. A comparison between the modeled and observed PM_{10} (Figure *5.1-4*) reveals that the model tends to underestimate PM_{10} mass concentrations during the

study period (B_n = -0.29). To incorporate the model skill in representing the correct aerosol mass concentrations, B_n of the modeled PM_{10} was calculated for IS filter periods (Figure *5.1-5*).

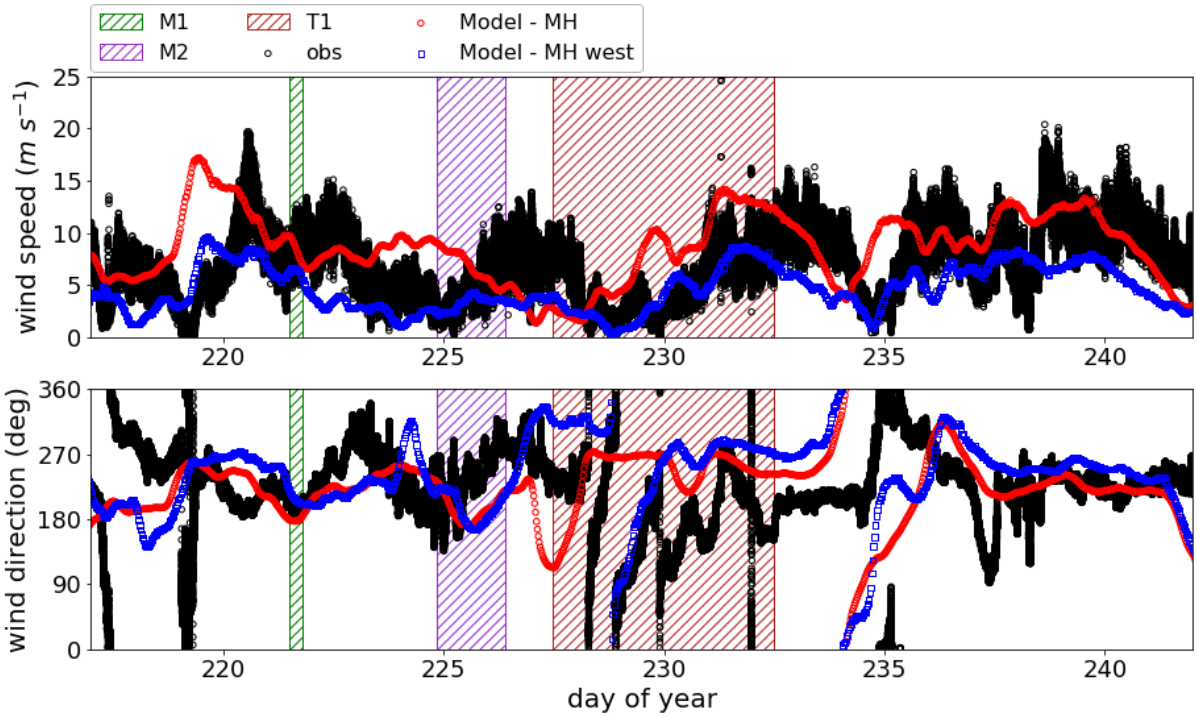

Figure 5.1-2. Timeline of wind speed (top) and wind direction (bottom) at MHD during the study period. Black points show observations from Mace Head Research Station. Red and blue points are simulated for grids point closest to MHD and west of MHD, respectively. Hashed shaded regions illustrate the study focus periods: M1, M2, and T1.

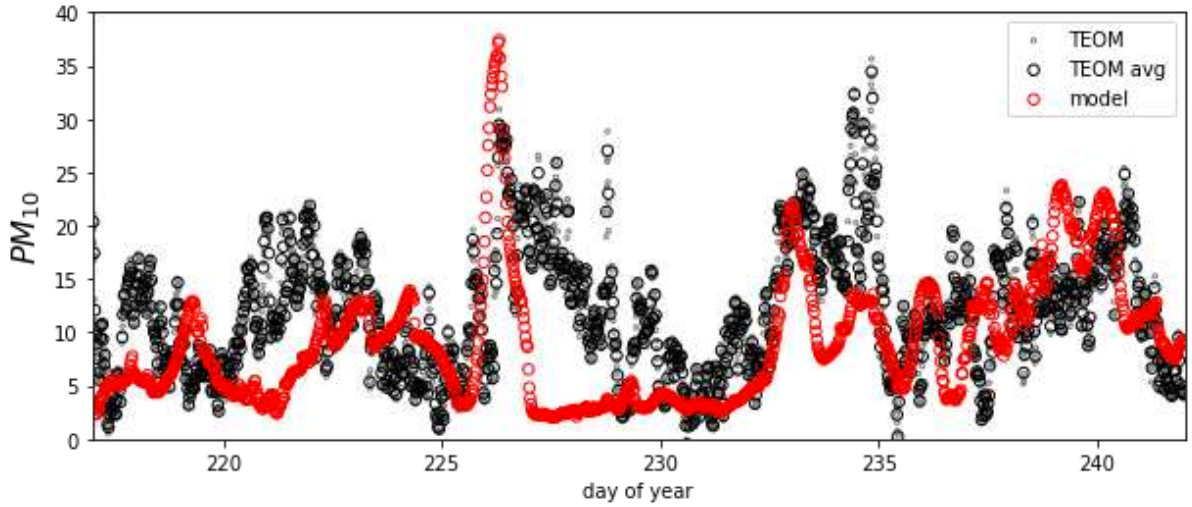

Figure 5.1-3. Timeline of mass concentrations of particles with diameters smaller than 10 microns (PM_{10}, in µg per m^3 of air) measured by a TEOM (black) and simulated by the model at the MH-west location (red).

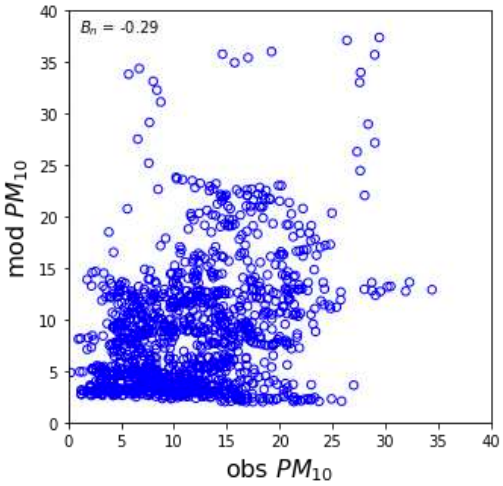

Figure 5.1-4. Comparison between modeled (MH-west location) and observed PM_{10} mass concentrations.

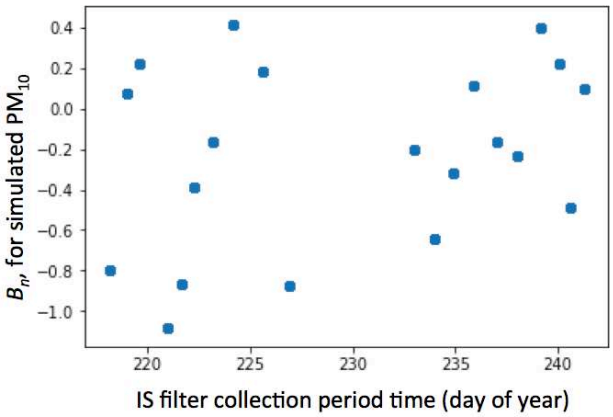

Figure 5.1-5. Modified normalized mean bias of simulated PM_{10} for each IS filter collection period (excluding samples collected during the period of elevated terrestrial organic INPs).

Section 5.2 Estimating n_{INPs} from model output

In this study, three methods were used to estimate n_{INPs} based on simulated aerosol and are summarized in Table 5.2-1. (1) Mass concentrations of marine organic matter (OM, total mass of organic material including non-carbon elements), predicted by OCEANFILMS, were used in the *Wilson et al.* (2015) relationship (W15), in which grams of total organic carbon (TOC) are related to n_{INPs} active at a particulate temperature (see Sections 3.3.d and 4.2.b.iv). (2) Sea salt and marine organic matter were used as estimates of the total mass of SSA, which was then converted to total aerosol SSA surface area, for the parameterization that was reported in

Section 4.2.b.iv (*McCluskey et al.,* a, in prep, M17). M17 predicts nucleation site density for pristine sea spray aerosol and was developed based on data collected at MHD for clean marine periods that had low concentrations of submicron organic aerosol. This approach is proposed as an estimate of n_{INPs} in sea spray organic aerosol that does not contain the heat labile INPs that were reported for the first marine organic event (M1, see Section 4.2.b.i). (3) Simulated dust aerosol concentrations and size distributions were used to estimate total number concentrations of dust particles with diameters larger than 500 nm for use in a parameterization for n_{INPs} associated with mineral dust (D15, *DeMott et al.,* 2015). The current version of MAM4 does not include an aerosol species that could be related to organic-rich soils, for estimation of terrestrial organic INPs, so it is not possible for the model to capture n_{INPs} that would arise from the transport of organic-rich soil particles. Thus, this study excludes measurements made during the terrestrial organic INP event that was identified and described in Section 4.2.b.ii. Finally, (4) contributions from both SSA and mineral dust were estimated combining contributions estimated by M17 with D15 (i.e., M17+D15). A global map of dust and SSA mass concentrations is shown in Figure *5.2-1*.

Table 5.2-1. Summary of approaches used to estimate n_{INPs} for different aerosol types.

Acronym	**INP type short description**	**Description of parameterization**	**CESM model output variable used in n_{INPs} estimates**
W15	Marine organic aerosol	Predicts INPs per gram of total organic carbon, derived from SML samples collected from N. Atlantic and Arctic Oceans	Marine organic matter (converted to TOC, assuming OC/OM of 2)
M17	Sea spray aerosol	Predicts INPs per surface area of sea spray aerosol, as derived from aerosol measurements made at MHD in the CLEAN sector. Does not account for INPs associated with marine organic events nor heat-labile INPs	Total surface area of sea spray aerosol (sea salt and marine organic matter)
D15	Mineral dust	Predicts n_{INPs} based on n_{500nm} of mineral dust, derived from laboratory and field measurements	Total number concentration of dust particles with diameters larger than 500 nm.

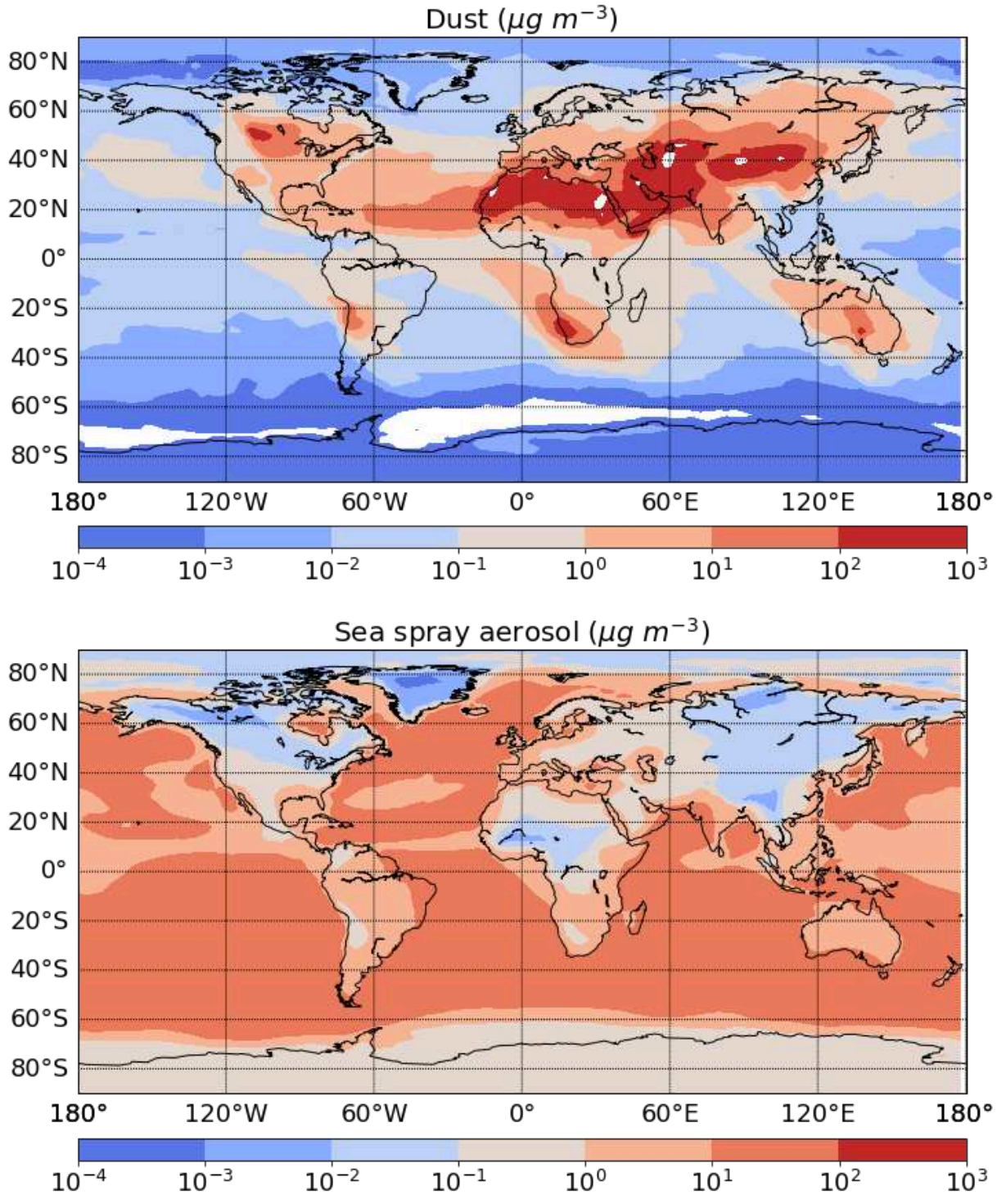

Figure 5.2-1. Map of simulated mass concentrations of mineral dust (top) and sea spray aerosol (bottom) for August 2015.

Section 5.3 Overview of simulated aerosol and estimated n_{INPs} at MHD

Estimates of n_{INPs} based on simulated aerosol and INP parameterizations are shown in Figure *5.3-1* for the MHD study period (excluding the terrestrial organic event). Estimates of INPs associated with mineral dust (using D15) were lower than observed n_{INPs} (B_n = -1.42), indicating that the mineral dust was not a significant contributor to the simulated INP population. The W15 approach for estimating INPs associated with marine organic aerosol overestimates n_{INPs} compared to observations, with a B_n of 1.12. This finding is consistent with analyses in Section 4.2.b.iv, where n_{INPs} estimated using the W15 relationship and total organic carbon aerosol mass concentrations (estimated by submicron organic matter mass concentrations measured by the HR-ToF-AMS) were higher than observed. The M17 approach for estimating INPs associated with SSA lead to an underestimation (B_n = -1.18) of n_{INPs} compared to MHD observations for W15. However, combining INPs associated with SSA (M17) and mineral dust (D15) led to the best agreement between modeled and observed n_{INPs}, where 86 percent of the estimated n_{INPs} were within a factor of 10 of observed n_{INPs} and B_n was minimized to -0.82.

Comparisons between model estimates of n_{INPs} and observed n_{INPs} were improved after accounting for biases between modeled and observed PM_{10} mass concentrations. Modified normalized mean bias for model estimated n_{INPs} was calculated for samples that corresponded to good model agreement, defined here as samples for which the B_n of modeled PM_{10} was within 20% of observations (i.e., $-0.2 < B_n$ for $PM_{10} < 0.2$). This exercise results in a reduction of the B_n for n_{INPs} estimated from the M17+D15 approach with a B_n of -0.33, as summarized in Table *5.3-1* and shown in Figure *5.3-2*.

The low bias of simulated n_{INPs} at MHD suggests that the simulated aerosol composition and abundance may not be in adequate agreement with the observed aerosol and that the

estimated INP population may be missing an important INP source that is not described by M17 and D15. The limitations of these parameterizations will be evaluated and reported in the final publication.

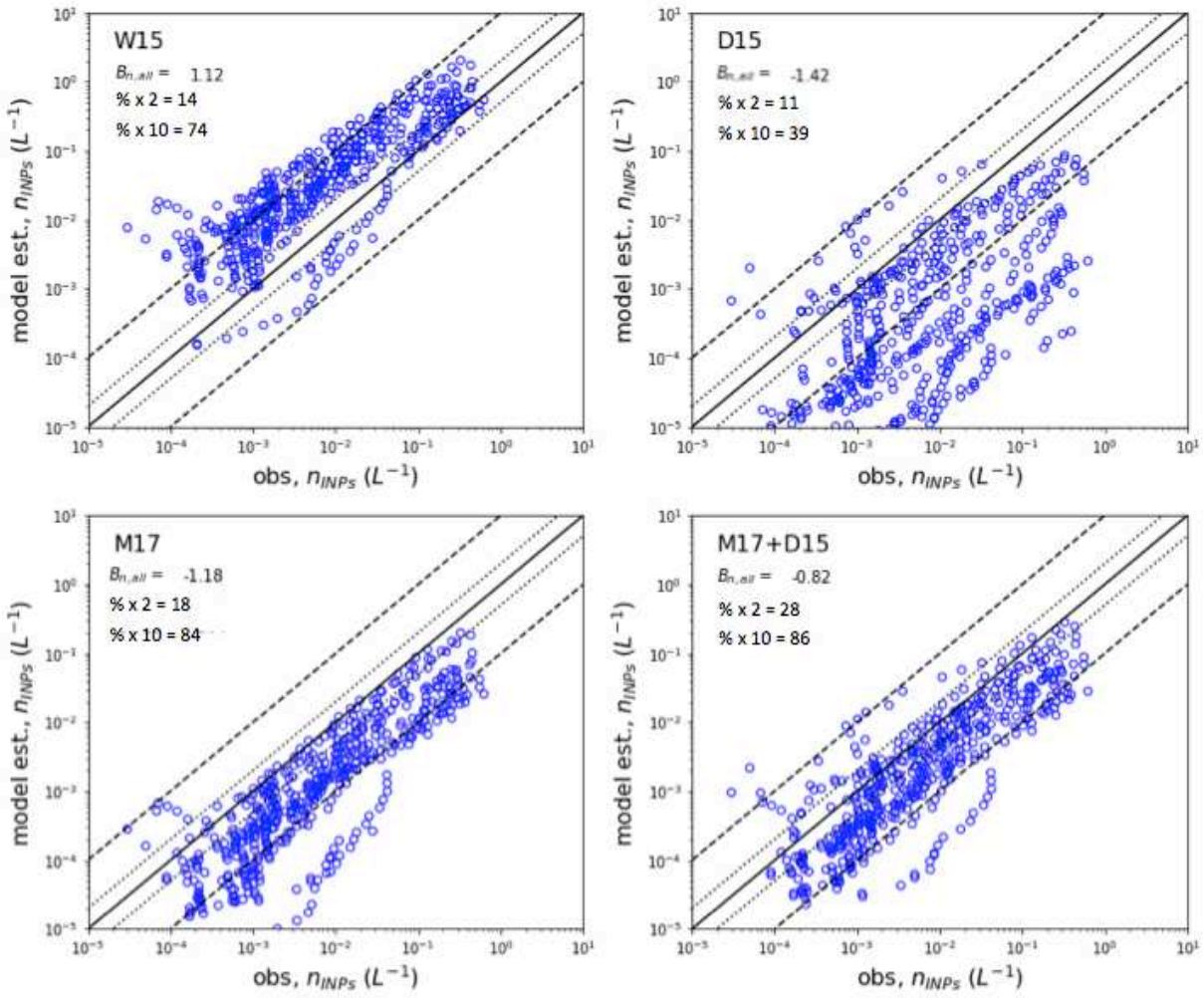

Figure 5.3-1. Scatter plots comparing modeled estimates of n_{INPs} and observed n_{INPs} for INPs associated with marine organic matter (W15), mineral dust (D15), sea spray aerosol (M17), and combined concentrations from sea spray aerosol and mineral dust (M17 + D15). Observed values are n_{INPs} measured by the ice spectrometer at all temperatures for filters collected at the MHD (excluding samples of the terrestrial organic event). Metrics listed in each panel are modified normalized mean biases (B_n), percentage of data points that are predicted within a factor of 2 (% x 2), and percentage of data points that are predicted within a factor of 10 (% x 10).

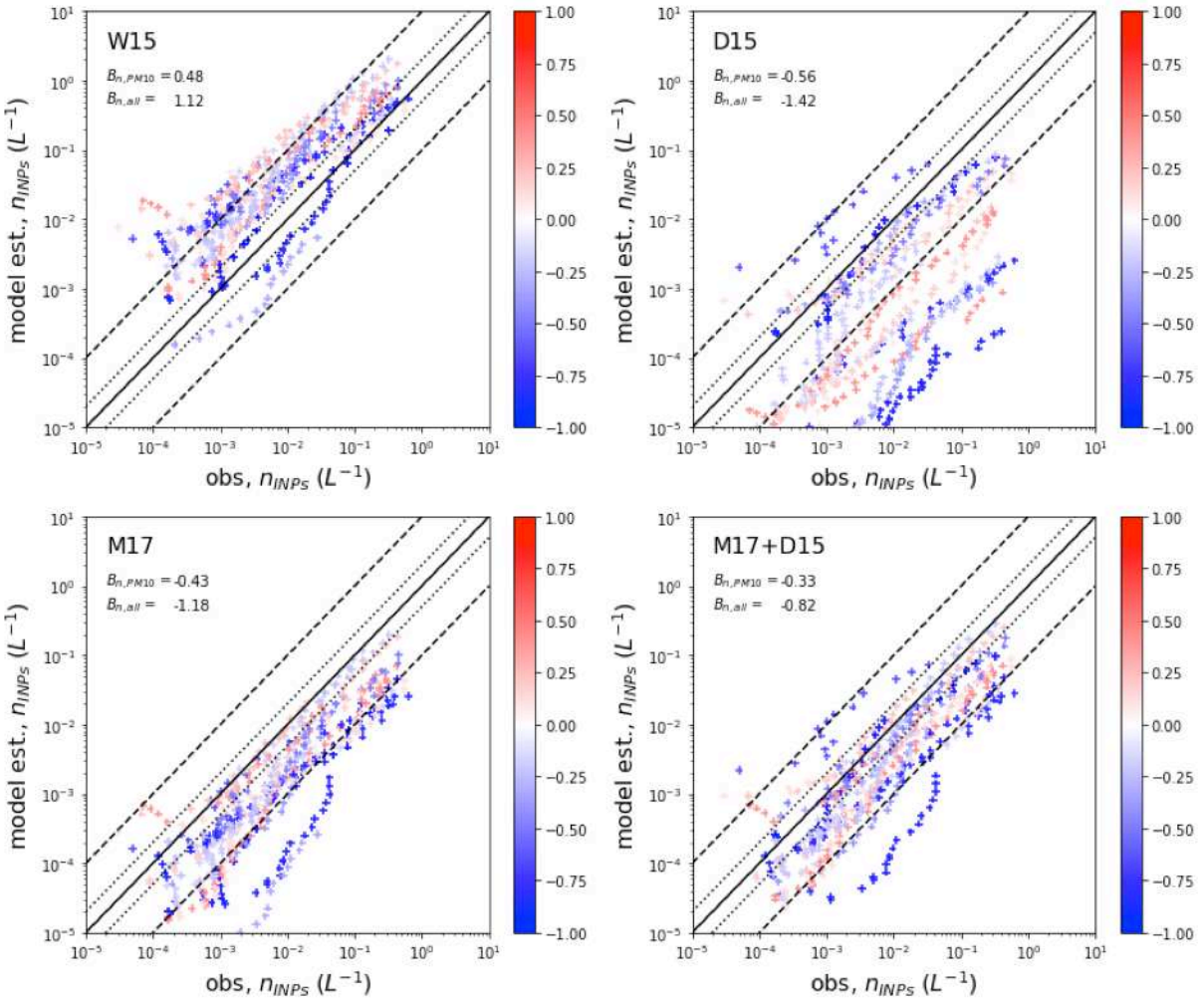

Figure 5.3-2. Same as Figure 5.3-1, but colored based on the modified normalized mean biases of simulated mass concentrations (PM_{10}) at MHD during the observation period. Metrics listed in each panel are modified normalized mean biases calculated for n_{INPs} estimated for sample periods in which the model was within 20% of observed PM_{10} mass concentrations ($B_{n,\ PM10}$) and modified normalized mean bias for all data point shown ($B_{n,\ all}$).

Table 5.3-1. Summary of modified normalized mean bias (B_n) and percentage of estimated n_{INPs} within a factor of 2 and within a factor of 10 of observed n_{INPs} for the MHD. $B_{n,\ PM10}$ is also reported, which is the modified normalized mean bias for comparison periods in which the model estimated PM_{10} mass concentrations within 20% of observations (i.e., $-0.2 < B_n$ for PM10 < 0.2).

Approach	% factor of 2	% factor of 10	B_n	$B_{n,\ PM10}$
W15	14	74	1.12	0.48
M17	11	84	-1.18	-0.56
D15	18	39	-1.42	-0.43
M17+D15	28	86	-0.82	-0.33

Section 5.4 Future work

One unique aspect of the observations at MHD is that CLEAN sector samples provide a "filter" for the data that isolates marine INPs from non-marine INPs, providing good test cases for parameterizations that are specifically aimed at representing solely a marine source of INPs. Therefore, an additional useful exercise will be to evaluate these same comparisons after selecting model output based on wind speed, wind direction and black carbon concentrations, like the clean sector sampler.

This approach for evaluating n_{INPs} estimated by these different parameterizations and relationships will also be applied to modeled aerosols over the Southern Ocean region, where CAPRICORN observations will be used to compare to simulated winds and to n_{INPs} estimated based on simulated aerosol. Specifically, comparing W15 and M17, which were developed for the North Atlantic and Arctic Ocean regions (W15) and air masses arriving from the North Atlantic Ocean (M17), to measurements made over the Southern Ocean, will be useful for determining the applicability of M17 and W15 for predicting abundances of INPs the Southern Hemisphere. Finally, the OCEANFILMS model will be used to identify the role of seasonal shifts in marine aerosol concentrations and compositions, and hence of INPs, in the region surrounding MHD and the Southern Ocean study region. Seasonal variability in aerosol and therefore n_{INPs} is one possible explanation for the discrepancies in observed n_{INPs} during CAPRICORN compared to those reported by *Bigg* (1973), and will be explored in that future work.

CHAPTER 6: SUMMARY

Historical measurements supported a hypothesis that INPs were connected to ocean biological activity (*Bigg,* 1973, *Schnell and Vali*, 1976). More recently, in an exploratory study by *Burrows et al.* (2013), organic matter arising from ocean biological activity was investigated as a biogenic INP source. *Burrows et al.* implemented a state of the science representation of marine organic aerosol and its ice nucleation properties, based on historical measurements, into a global climate model to determine the potential impact of marine biogenic INPs. They concluded that marine biogenic INPs may be an important contributor to INP populations for clouds over remote oceans, such as the Southern Ocean, that are not influenced by terrestrial aerosol. However, their exploratory study highlighted the gap in the scientific understanding of INPs present in SSA, including their composition and the factors that control their variability. In this work, this gap was addressed with numerous investigations of marine INPs in the laboratory and in the marine boundary layer across a number of oceanic and coastal regions. The understanding gained through these studies and the database of new observations of marine INPs that they produced, were used to evaluate the current best model estimates of marine INPs and provided insight for development of a new framework for advancing mechanistic numerical representation of marine INPs.

Since the historical studies that lead to the hypothesized link between INPs and marine biology, advancements have been made in knowledge regarding sea spray organic aerosol. Specifically, we understand that the composition of particles emitted from the ocean is complex, and depends on the composition of SW and the SML. We also know that specific organic species are incorporated into the aerosol phase depending on their water solubility, surface activity and

on the type of droplet that the particle originated from (i.e., jet versus film drop). That is, the composition and physical properties (e.g., surface tension and bubble size distribution) of the interfaces between SW, SML and air are all important factors for understanding sea spray organic matter. Following this framework for understanding sea spray organic aerosol, use of a laboratory platform through CAICE was fundamental for probing IN activity of all aspects of this complex interface. SW, SML and SSA were extensively characterized during the MART and IMPACTS laboratory experiments. The detailed observations from these studies, including biology, aerosol composition and ice nucleation ability of SW, SML and SSA, revealed that marine INP emissions are in fact linked to biological activity, where n_{INPs} and n_s measured across all temperatures (T > -30 °C) changed during both phytoplankton bloom experiments. Specifically, n_{INPs} active at temperatures warmer than -25 °C peaked following the peak in Chl *a* in both MART and IMPACTS studies, suggesting that the decay phase of a phytoplankton bloom is particularly important for producing SSA with enhanced IN activity. The timing of peak n_{INPs} suggests that INP emissions could be influenced by biochemical processes that occur during the decay phase (related to phytoplankton death or HB growth) and by enrichment of organic matter in SML. Integrating all analyses of INPs and INEs leads to two proposed classes of marine INPs: (1) DOC INPs are defined as particles that are coated with or contain major masses of IN-active molecules and (2) POC INPs are defined as IN-active bacteria, diatoms or grazers, which are represented in SSA as intact cells or cell fragments. These marine INP types were active at temperatures warmer than -25 °C.

Laboratory studies of marine INPs allow for detailed characterization of multiple components of this complex problem. However, at least for the studies reported in this work, laboratory studies inherently lack many aspects of nature, of which a few may be mentioned

here. SSA production, while essentially consistent in laboratory-generated nascent SSA, varies with wind speed. Enrichment of organic matter in SML compared to SW also varies in nature, depending on biological activity and wind stress. Distributions of phytoplankton species vary regionally and seasonally over natural oceans and thus laboratory experiments only represent a very small sample of the world's ocean biota. Atmospheric chemical aging and particle drying of SSA may alter the composition and IN properties of SSA that actually reach cloud level. For these reasons, observations of INPs present in the marine boundary layer were made in various remote ocean and coastal regions. Some of these measurements also served as the first survey of natural INPs in these regions in four decades. Looking solely at number concentrations of INPs, over three orders of magnitude variability was observed in marine boundary layer samples collected over the Pacific Ocean over various seasons. This range in n_{INPs} (factor of over 1000 at -22 °C) far exceeds the range observed in the laboratory studies (factor of 30-40 at -22 °C).

Greater variability and higher n_{INPs} were observed in the Northern Hemisphere versus the Southern Hemisphere. To explore these hemispheric differences, detailed evaluations of INPs present in the marine boundary layer and their variability were conducted at a North Atlantic Ocean coastal site (MHD) and over the Southern Ocean (CAPRICORN). At MHD, variability in n_{INPs} measured in the clean sector (i.e., pristine marine air) was less than the variability in n_{INPs} measured in all air masses. The majority of INPs in pristine marine aerosol samples were found to contain heat-stable organic matter. A log-linear increase in active site density (n_s) with decreasing temperature was proposed as a parameterization for pristine marine heat stable organic INPs. An organic aerosol event, which occurred during a period of relatively high wind speeds and in an air mass that had passed over a region of high offshore biological activity, corresponded to the highest n_{INPs} and n_s observed in the clean sector; these INPs were also heat

labile, suggesting the presence of the POC INP type proposed from the CAICE lab studies. Also at MHD, terrestrial INPs, found to be largely composed of heat labile organic matter and interpreted as having a source from organic-rich soils, were observed. Both marine and terrestrial heat-labile organic INPs were the main contributors to the maximum n_{INPs} and n_s observed in the marine boundary layer at MHD. During CAPRICORN, n_{INPs} varied by a factor of 3 at temperatures warmer than -20 °C and n_{INPs} were 100 times lower than the annual averaged n_{INPs} reported by *Bigg* (1973) for the same region. Offline analyses indicated that refractory, heat-stable organic, and heat-labile material all contributed to the observed INPs. INEs in near-surface SW samples were used to evaluate the source potential of the Southern Ocean, but no clear relationship was found between n_{INEs} and Chl *a*. Offline treatments indicated that the dominant INE type was similar to the DOC INPs found in the laboratory studies. SW n_{INEs} were up to a factor of 10 lower than n_{INEs} found in SW samples collected from California coastal water (i.e., seawater collected for CAICE studies), consistent with lower n_s found over the Southern Ocean compared to n_s observed from ACAPEX-RB off the coast of California. Observations from these three studies, summarizing the contrasts between hemispheres, are shown in Figure 6.1-1.

These field observations provide an updated survey of INPs found over oceans, which is needed to evaluate modeling approaches for predicting marine organic INPs. *Wilson et al.* (2015) developed an approach for estimating marine INPs, where the ratios of INEs to total organic carbon measured in SML samples collected over the North Atlantic and Arctic Ocean were directly applied to the sea spray organic matter simulated by a global climate model. When applied to data presented in this dissertation, this approach was found to lead to an over prediction of INPs for n_{INPs} observed in nascent SSA (laboratory) and natural SSA (MHD). Of note is that n_{INPs} estimated by W15 agreed better with observed n_{INPs} during the IMPACTS study,

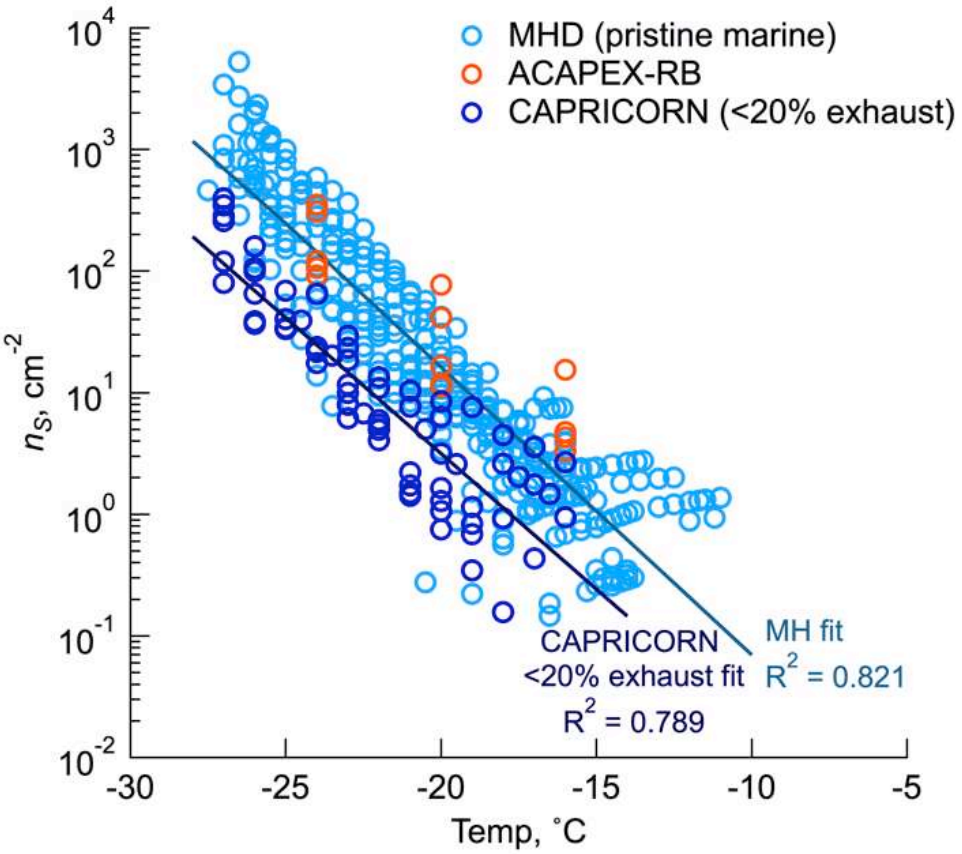

Figure 6.1-1. Nucleation site densities observed at Mace Head Research Station (MHD), onboard the RV Ron Brown (ACAPEX-RB), and onboard the RV Investigator (CAPRICORN). Exponential fits are provided for CAPRICORN and MHD.

which had an INP population dominated by POC INPs. That is, observations from the experiment with larger, heat-labile INPs were in better agreement with the TOC-based approach suggested by W15. Nudged global modeling simulations were also performed for the MHD study period, where marine INPs active at all measured temperatures were estimated by W15 and also by the parameterization developed in this work from MHD observations (M17). Preliminary results indicate that observed n_{INPs} are bounded by M17 (lower estimate) and W15 (upper estimate) for the MHD, if marine organics are considered as the only contributing INPs. An evaluation of W15 and M17 for marine organic INPs versus the augmented marine organic INP populations was not possible due to the poor agreement between simulated and observed mass

concentrations of total particles. Regardless, best agreement between model estimates and observations of marine INP populations at MHD was achieved by estimating contributions from both mineral dust (using the *DeMott et al.* (2015) parameterization) and from sea spray aerosol with the M17 parameterization.

Whereas previous studies have neglected the presence of multiple INP components, this work has contributed findings that provide insights for the development of a new framework for studying marine INPs and has highlighted areas that require more research. Specific compounds and species that contribute to DOC and POC constituents should be identified, which would allow links to be established between INP types and specific organic components of SW and the SML. A recent study by *Wang et al.* (2017) identified different organic volume fractions and IN properties in jet versus film drops. In a similar vein, the contribution of the DOC INPs and POC INPs to jet versus film drops could be quantified for repeated experiments with natural seawater over the course of many bloom experiments and under various wind conditions. Such a study would lead to a robust description of DOC INPs and POC INPs as a function of droplet distribution and biological activity, which can be translated to surface bubble size distributions and thus nascent SSA size distributions. All of this could then be implemented into a model, like OCEANFILMS, that predicts SSA production (i.e., nascent SSA as a function of wind speed) and sea spray organic aerosol as a function of SW organic composition, determined by an ocean biogeochemical model. Finally, a fundamental gap in knowledge regarding mixed phased clouds over the Southern Ocean is the importance of primary versus secondary ice formation. Secondary ice formation is a complex phenomenon in itself, and will be the subject of future investigations in upcoming field campaigns in the Southern Ocean region. This work addresses primary ice formation, and will serve to provide global climate and cloud resolving model simulations with

constraints on the abundance of immersion freezing INPs (i.e., the numbers of particles available to initiate primary ice formation) present in remote marine boundary layer regions. With improved representation of the uniquely low baseline ice nucleation activity of SSA, particularly in the Southern Hemisphere, modeling studies can begin to investigate the sensitivity of modeled cloud phase distributions to variations in n_{INPs} due to changes in SSA production and biological activity.

REFERENCES

Agresti, A., and B. A. Coull, 1998: Approximate Is Better than "Exact" for Interval Estimation of Binomial Proportions. *The Amer. Stat.*, **52**, 119, doi:10.2307/2685469.

Azam, F., T. Fenchel, J. G. Field, J. S. Gray, L. A. Meyer-Reil, and F. Thingstad, 1983: The ecological role of water-column microbes in the sea. *Mar. Ecol. Prog. Ser.* 10, 257-263.

— —, and F. Malfatti, 2007: Microbial structuring of marine ecosystems. *Nature Reviews Microbiology*, **5**, 782–791, doi:10.1038/nrmicro1747.

Atkinson J.D., and Coauthors, *In prep*.: Summertime Ice Nucleating Particle Observations on the North-East Coast of the Atlantic.

Atwood et al., in prep, Classification of aerosol population type and cloud condensation nuclei properties in a coastal California littoral environment.

Barker, D. R., and H. Zeitlin, 1972: Metal-Ion Concentrations in Sea-Surface Microlayer and Size-Separated Atmospheric Aerosol Samples in Hawaii, *J. Geophy. Res.,***77** (27), 5076-5086.

Belosi, F., M. Rinaldi, S. Decesari, L. Tarozzi, A. Nicosia, G. Santachiara, 2017: Ground level ice nuclei particle measurements including Saharan dust events at a Po Valley rural site (San Pietro Capofiume, Italy), *Atmos. Res.*, **186**, 116-126, doi:10.1016/j.atmosres.2016.11.012.

Bigg, E. K. 1973: Ice nucleus concentrations in remote areas*, J. Atmos. Sci.*, **30**, 1153–1157.

— —, 1990: Long-term trends in ice nucleus concentrations, *Atmos. Res.,* **25**, 409-415.

Blanchard DC, Woodcock AH (1957) Bubble formation and modification in the sea and its meteorological significance. *Tellus* 9:145–158.

Blanchard DC (1963) The electrification of the atmosphere by particles from bubbles in the sea. *Prog Oceanogr* 1:73–202.

de Boer, G., H. Morrison, M. D. Shupe, and R. Hildner, 2011: Evidence of liquid dependent ice nucleation in high-latitude stratiform clouds from surface remote sensors: Liquid Induced Ice Nucleation. *Geophys.l Res. Let.*, **38**, doi:10.1029/2010GL046016.

Burrows, S. M., C. Hoose, U. Pöschl, and M. G. Lawrence, 2013: Ice nuclei in marine air: biogenic particles or dust? *Atmos. Chem. and Phys.*, **13**, 245–267, doi:10.5194/acp-13-245-2013.

— —, O. Ogunro, A. A. Frossard, L. M. Russell, P. J. Rasch, and S. M. Elliott, 2014: A physically based framework for modeling the organic fractionation of sea spray aerosol from bubble film Langmuir equilibria. *Atmos. Chem. and Phys.*, **14**, 13601–13629, doi:10.5194/acp-14-13601-2014.

— —, S. M.,. R. Easter, X. Liu, P. Ma, H. Wang, S. M. Elliot, B. Singh, K. Zhang, P. J. Rash, *in prep*: OCEANFILMS organic sea spray emissions – Part1: implementation and impacts on clouds

Carslaw, K. S., and Coauthors, 2013: Large contribution of natural aerosols to uncertainty in indirect forcing. *Nature*, **503**, 67–71, doi:10.1038/nature12674.

Chambers, S. D., S.-B. Hong, A. G. Williams, J. Crawford, A. D. Griffiths, and S.-J. Park, 2014a: Characterising terrestrial influences on Antarctic air masses using Radon-222 measurements at King George Island. *Atmos. Chem. and Phys.*, **14**, 9903–9916, doi:10.5194/acp-14-9903-2014.

Charron, A., R. M. Harrison, S. Moorcroft, J. Booker, 2014: Quantitative interpretation of divergence between PM and PM mass measurement by TEOM and gravimetric (Partisol) instruments, *Atmos. Env.*, **38**, 3, 415-423, doi:10.1016/j.atmosenv.2003.09.072.

Cochran, R. E., and Coauthors, 2016: Analysis of Organic Anionic Surfactants in Fine and Coarse Fractions of Freshly Emitted Sea Spray Aerosol. *Environ.l Sci. & Tech.*, **50**, 2477–2486, doi:10.1021/acs.est.5b04053.

Collins, D. B., and Coauthors, 2014: Direct aerosol chemical composition measurements to evaluate the physicochemical differences between controlled sea spray aerosol generation schemes. *Atmos. Meas. Techn.*, **7**, 3667–3683, doi:10.5194/amt-7-3667-2014.

Creamean, J. M., and Coauthors, 2013: Dust and Biological Aerosols from the Sahara and Asia Influence Precipitation in the Western U.S. *Science*, **339**, 1572–1578, doi:10.1126/science.1227279.

Cunliffe, M., and Coauthors, 2013: Sea surface microlayers: A unified physicochemical and biological perspective of the air–ocean interface. *Prog. in Ocean.*, **109**, 104–116, doi:10.1016/j.pocean.2012.08.004.

Czerwieniec, G. A., and Coauthors, 2005: Stable Isotope Labeling of Entire Bacillus atrophaeus Spores and Vegetative Cells Using Bioaerosol Mass Spectrometry, *Anal. Chem.,* **77** (4), 1081-1087, doi: 10.1021/ac0488098

DeCarlo, P. F., Kimmel, J. R., Trimborn, A., Northway, M. J., Jayne, J. T., Aiken, A. C., Gonin, M., Fuhrer, K., Horvath, T., Docherty, K. S., Worsnop, D. R., and Jimenez, J. L.: Field-deployable, high-resolution, time-of-flight aerosol mass spectrometer, *Anal Chem,* **78**, 8281-8289, doi:10.1021/Ac061249n, 2006.

DeMott, P. J., and Coauthors, 2010: Predicting global atmospheric ice nuclei distributions and their impacts on climate. *Proceedings of the National Academy of Sciences*, **107**, 11217–11222.

——, and Coauthors, 2016: Sea spray aerosol as a unique source of ice nucleating particles. *Proceedings of the National Academy of Sciences*, **113**, 5797–5803.

——, and Coauthors, 2017: Comparative measurements of ambient atmospheric concentrations of ice nucleating particles using multiple immersion freezing methods and a continuous flow diffusion chamber. *Atmos. Chem. and Phys.*, **17**, 11227–11245, doi:10.5194/acp-17-11227-2017.

Ducklow, H. W., 2000: Bacterial production and biomass in the oceans. In D. L. Kirchman (ed.) *Microbial Ecology of the Ocean*, 1st end. Wiley-liss, pp. 85-120.

Eller, P. M., and M. E. Cassinelli, 1999: Elemental carbon (diesel particulate): Method 5040. NIOSH Manual of Analytical Methods, National Institute for Occupational Safety and Health, 9 pp.

Exton, H. J., Latham, J., Park, P. M., Perry, S. J., Smith, M. H. and Allan, R. R. (1985), The production and dispersal of marine aerosol. *Q.J.R. Meteorol. Soc.,* 111: 817–837. doi:10.1002/qj.49711146909

Facchini, M. C., and Coauthors, 2008: Primary submicron marine aerosol dominated by insoluble organic colloids and aggregates. *Geophys. Res. Let.*, **35**, doi:10.1029/2008GL034210.

Fall, R. and R. C. Schnell, 1985: Association of an ice-nucleating pseudomonad with cultures of the marine dinoflagellate, Heterocapsa niei. *J. Mar. Res.*, **43**, 257-265.

Fergenson, D. P., and Coauthors, 2004: Reagentless Detection and Classification of Individual Bioaerosol Particles in Seconds, *Anal. Chem.,* **76** (2), 373-378, doi:10.1021/ac034467e.

Frenger, I., M. Münnich, N. Gruber, and R. Knutti, 2015: Southern Ocean eddy phenomenology: SOUTHERN OCEAN EDDIES. *J. Geophys. Res.: Oceans*, **120**, 7413–7449, doi:10.1002/2015JC011047.

Fuentes, E., H. Coe, D. Green, G. de Leeuw, and G. McFiggans, 2010: On the impacts of phytoplankton-derived organic matter on the properties of the primary marine aerosol – Part 1: Source fluxes. *Atmos. Chem. and Phys.*, **10**, 9295–9317, doi:10.5194/acp-10-9295-2010.

Gantt, B., and N. Meskhidze, 2013: The physical and chemical characteristics of marine primary organic aerosol: a review. *Atmos. Chem. and Phys.*, **13**, 3979–3996, doi:10.5194/acp-13-3979-2013.

——, ——, M. C. Facchini, M. Rinaldi, D. Ceburnis, and C. D. O'Dowd, 2011: Wind speed dependent size-resolved parameterization for the organic mass fraction of sea spray aerosol. *Atmos. Chem. and Phys.*,, **11**, 8777–8790, doi:10.5194/acp-11-8777-2011.

Gavish, M., Popovitz-Biro, R., Lahav, M., and Leiserowitz, L. 1990: Ice nucleation by alcohols arranged in monolayers at the surface of water drops, *Science*, **250**, 973-975.

Gard, E., J. E. Mayer, B. D. Morrical, T. Dienes, D. P. Fergenson and K. A. Prather, 1997: Real-Time Analysis of Individual Atmospheric Aerosol Particles: Design and Performance of a Portable ATOFMS. *Anal. Chem.,* **69** (20), 4083–4091, doi: 10.1021/ac970540n.

Gaube, P., D. B. Chelton, P. G. Strutton, and M. J. Behrenfeld, 2013: Satellite observations of chlorophyll, phytoplankton biomass, and Ekman pumping in nonlinear mesoscale eddies: Phytoplankton And Eddy-Ekman Pumping. *J. Geophys. Res,: Oceans*, **118**, 6349–6370, doi:10.1002/2013JC009027.

Ghil, M., M. R. Allen, M. D. Dettinger, K. Ide, D. Kondrashov, M. E. Mann, A. W. Robertson, A. Saunders, Y. Tian, F. Varadi, and P. Yiou, 2002: Advanced spectral methods for climatic time series, *Rev. Geophys.,* **40**(1), 1003, doi:doi:10.1029/2000RG000092.

Gregg, W. W., M. E. Conkright, P. Ginoux, J. E. O'Reilly, and N. W. Casey, 2003: Ocean primary production and climate: Global decadal changes: OCEAN PRIMARY PRODUCTION AND CLIMATE. *Geophys. Res. Let.*, **30**, doi:10.1029/2003GL016889.

Griffiths, A. D., S. D. Chambers, A. G. Williams, and S. Werczynski, 2016: Increasing the accuracy and temporal resolution of two-filter radon–222 measurements by correcting for the instrument response. *Atmos. Meas. Tech.*, **9**, 2689–2707, doi:10.5194/amt-9-2689-2016.

Grythe, H., Ström, J., Krejci, R., Quinn, P., and Stohl, A., 2014: A review of sea-spray aerosol source functions using a large global set of sea salt aerosol concentration measurements. *Atmos. Chem. and Phys.*, **14**(3), 1277.

Guasco, T. L., and Coauthors, 2014: Transition Metal Associations with Primary Biological Particles in Sea Spray Aerosol Generated in a Wave Channel. *Environ. Sci. Tech.*, **48**, 1324–1333, doi:10.1021/es403203d.

Hill, T. C. J., B. F. Moffett, P. J. DeMott, D. G. Georgakopoulos, W. L. Stump, and G. D. Franc, 2014: Measurement of ice nucleation-active bacteria on plants and in precipitation by quantitative PCR. *Appl. Environ. Microbiol.,* **80**, 1256-1267, doi: 10.1128/AEM.02967-13.

Hinds, W. C., 1999: *Aerosol Technology: Properties, Behavior, and Measurement of Airborne Particles*. 2nd ed. Wiley, 504 pp.

Hiranuma, N., and Coauthors, 2015: A comprehensive laboratory study on the immersion freezing behavior of illite NX particles: a comparison of 17 ice nucleation measurement techniques. *Atmos. Chem. and Phys.*, **15**, 2489–2518, doi:10.5194/acp-15-2489-2015.

Hoffman, E. J. and R. Duce. 1974: The organic carbon content of marine aerosols collected on Bermuda, *J. Geophys. Res.*, **79**, 4474–4477.

Holm-Hansen, O., C. J. Lorenzen, R. W. Holmes, and J. D. H. Strickland, 1965: Fluorometric determination of chlorophyll, *J. Conseil.,* 30(1), 3-15.

Hoppe, H. G., 1983: Significance of exoenzymatic activities in the ecology of brackish water: Measurements by means of methylumbelliferyl-substrates. *Mar. Ecol. Prog. Ser.,* 11, 299–308, doi:10.3354/meps011299.

Huang, Y., A. Protat, S. T. Siems, and M. J. Manton, 2015: A-Train Observations of Maritime Midlatitude Storm-Track Cloud Systems: Comparing the Southern Ocean against the North Atlantic. *J. Climate*, **28**, 1920–1939, doi:10.1175/JCLI-D-14-00169.1.

Humphries, R., I. McRoberts, W. Ponsonby, J. Ward, M. Keywood, Z. Loh, P. Krummel, and J. Harnwell, *in prep*: Identification of platform exhaust on the RV Investigator.

Hurrell, J. W., and Coauthors, 2013: The Community Earth System Model: A Framework for Collaborative Research. *Bulletin of the American Meteorological Society*, **94**, 1339–1360, doi:10.1175/BAMS-D-12-00121.1.

Irish, V. E., and Coauthors, 2017: Ice-nucleating particles in Canadian Arctic sea-surface microlayer and bulk seawater. *Atmos. Chem. and Phys.*,**17**, 10583–10595, doi:10.5194/acp-17-10583-2017.

Ito, A., and J. F. Kok, 2017: Do dust emissions from sparsely vegetated regions dominate atmospheric iron supply to the Southern Ocean?, *J. Geophys. Res. Atmos.,* **122**, 3987–4002, doi:10.1002/2016JD025939.

Jimenez, J. L., Jayne, J. T., Shi, Q., Kolb, C. E., Worsnop, D. R., Yourshaw, I., Seinfeld, J. H., Flagan, R. C., Zhang, X. F., Smith, K. A., Morris, J. W., and Davidovits, P.: Ambient aerosol sampling using the Aerodyne Aerosol Mass Spectrometer, *J Geophys Res-Atmos*, **108**, 8425, doi:10.1029/2001JD001213, 2003.

Junge K. and B. D. Swanson 2008: High-resolution ice nucleation spectra of sea-ice bacteria: implications for cloud formation and life in frozen environments. *Biogeosciences,* **5**, 865–873. doi:10.5194/bg-5-865-2008.

Kanji, Z. A., and Abbatt, J. P. D., 2009: The University of Toronto Continuous Flow Diffusion Chamber (UT-CFDC): A Simple Design for Ice Nucleation Studies, *Aero. Sci. Tech.*, **43**, 730-738, 10.1080/02786820902889861.

Kay, J. E., L. Bourdages, N. B. Miller, A. Morrison, V. Yettella, H. Chepfer, and B. Eaton, 2016: Evaluating and improving cloud phase in the Community Atmosphere Model version 5 using spaceborne lidar observations: CAM Cloud Phase Evaluation with CALIPSO. *J. Geophys. Res. Atmos.*, **121**, 4162–4176, doi:10.1002/2015JD024699.

Kirchman, D. L., 2008: Microbial Ecology of the Oceans, 2nd ed., Wiley, New Jersey.

Knopf, D. A., and S. M. Forrester, 2011: Freezing of Water and Aqueous NaCl Droplets Coated by Organic Monolayers as a Function of Surfactant Properties and Water Activity, *J. Phys. Chem.,* **115**, 5579-5591, dx.doi.org/10.1021/jp2014644.

Knopf, D. A., P. A. Alpert, B. Wang, and J. Y. Aller, 2011: Stimulation of ice nucleation by marine diatoms. *Nat. Geosci.*, **4**, 88–90, doi:10.1038/ngeo1037.

Lacher, L., and Coauthors, *Under Review*: The Horizontal Ice Nucleation Chamber HINC: INP measurements at Conditions Relevant for Mixed-Phase Clouds at the High Altitude

Research Station Jungfraujoch, *Atmos. Chem. Phys. Discuss.*, doi: 10.5194/acp-2017-474, in review.
Lamarque, J.-F., and Coauthors, 2010: Historical (1850–2000) gridded anthropogenic and biomass burning emissions of reactive gases and aerosols: methodology and application. *Atmos. Chem. Phys.*, **10**, 7017–7039, doi:10.5194/acp-10-7017-2010.
Langer, G., Rodgers, J., 1975. An experimental study of ice nuclei on membrane filters and other substrata. *J. App. Meteor.* **14**, 560–571.
Leck, C., and E. K. Bigg, 2007: Comparison of sources and nature of the tropical aerosol with the summer high Arctic aerosol. *Tellus B,* doi:10.1111/j.1600-0889.2007.00315.x.
Lee, C., and Coauthors, 2015: Advancing Model Systems for Fundamental Laboratory Studies of Sea Spray Aerosol Using the Microbial Loop. *J. Phys. Chem. A*, **119**, 8860–8870, doi:10.1021/acs.jpca.5b03488.
Levin, E. J. T., and Coauthors, 2017: Spatial and temporal distributions of ice nucleating particles during the Atmospheric Radiation Measurement (ARM) Cloud Aerosol Precipitation Experiment (ACAPEX), in preparation for submission to *J. Geophys. Res.*
Lorenzen, C. J., 1966: A method for the continuous measurement of in vivo chlorophyll concentration, *Deep Sea Res. Oceanogr. Abstr.,* 13(2), 223-227.
Mace, G. G., R. Marchand, Q. Zhang, and G. Stephens, 2007: Global hydrometeor occurrence as observed by CloudSat: Initial observations from summer 2006: Cloudsat Hydrometeor Occurrence. *Geophys. Res. Let.*, **34**, doi:10.1029/2006GL029017.
Mårtensson, E. M., E. D. Nilsson, G. de Leeuw, L. H. Cohen, and H.-C. Hansson, 2003: Laboratory simulations and parameterization of the primary marine aerosol production: The Primary Marine Aerosol Source. *J. Geophys. Res. Atmos.*, **108**, doi:10.1029/2002JD002263.
Malfatti, F., T. Tinta, Y. Zhou, C. M. Sultana, C. Lee, A. Rotter, J. L. Axson, D. B. Collins, M. V. Santander, M. Celussi, L. I. Aluwihare, F. Azam and K. A. Prather, *in prep*: Active microbial enzymes in sea spray aerosols: A new atmospheric reaction pathway.
Maltrud, M. E., R. D. Smith, A. J. Semtner, R. C. Malone, 1998: Global eddy-resolving ocean simulations driven by 1985-1995 atmospheric winds, *J. Geoph. Res.* **103**, 30825-30853.
Martin, A. C., and Coauthors, 2017: Transport of pollution to a remote coastal site during gap flow from California's interior: impacts on aerosol composition, clouds, and radiative balance. *Atmos. Chem. Phys.*, **17**, 1491–1509, doi:10.5194/acp-17-1491-2017.
Mason, R., and Coauthors, 2015: Ice nucleating particles at a coastal marine boundary layer site: correlcations with aerosol type and meteorological conditions. *Atmos. Chem. Phys.,* **15**, 12547-12566, doi:10.5194/acp-15-12547-2015.
McCluskey, C. S., and Coauthors, 2014: Characteristics of atmospheric ice nucleating particles associated with biomass burning in the US: Prescribed burns and wildfires: Biomass burning ice nucleating particles. *J. of Geophys. Res. Atmos.*, **119**, 10458–10470, doi:10.1002/2014JD021980.
——, and Coauthors, 2017: A Dynamic Link between Ice Nucleating Particles Released in Nascent Sea Spray Aerosol and Oceanic Biological Activity during Two Mesocosm Experiments. *J. Atmos. Sci.*, **74**, 151–166, doi:10.1175/JAS-D-16-0087.1.
——, T. C. J. Hill, C. M. Sultana, O. Laskina, J. Trueblood, M. V. Santander, C. M. Beall, J. M. Michaud, K. A. Prather, V. Grassian, P. J. DeMott, A mesocosm double feature: Insights into the chemical makeup of marine ice nucleating particles, *submitted to J. Atmos. Sci.*

——, J. Ovadnevaite, M. Rinaldi, J. Atkinson, F. Belosi, D. Ceburnis, S. Marullo, T. C. J. Hill, U. Lohmann, Zamin. A. Kanji, C. O'Dowd, S. M. Kreidenweis, P. J. DeMott, *a in prep*, Marine and Terrestrial Organic Ice Nucleating Particles in Pristine Marine to Continentally-Influenced Northeast Atlantic Air Masses.

——, R. Humphries, S. Moreau, L. Cravigan, A. M. Rauker, T. C. J. Hill, A. Protat, P. J. DeMott, *b in prep*, Ice Nucleating Particles Over the Remote Southern Ocean.

McCoy, D. T., D. L. Hartmann, M. D. Zelinka, P. Ceppi, and D. P. Grosvenor, 2015: Mixed-phase cloud physics and Southern Ocean cloud feedback in climate models. *J. Geophys. Res. Atmos.*, **120**, 9539–9554, doi:10.1002/2015JD023603.

McGillicuddy, D. J., 2016: Mechanisms of Physical-Biological-Biogeochemical Interaction at the Oceanic Mesoscale. *Annual Review of Marine Science*, **8**, 125–159, doi:10.1146/annurev-marine-010814-015606.

Middlebrook, A. M., Bahreini, R., Jimenez, J. L., and Canagaratna, M. R., 2012: Evaluation of composition-dependent collection efficiencies for the aerodyne aerosol mass spectrometer using field data, *Aerosol Sci Tech*, **46**, 258–271, doi:10.1080/02786826.2011.620041.

Miyazaki, Y., K. Kawamura, and M. Sawano, 2010: Size distributions and chemical characterization of water-soluble organic aerosols over the western North Pacific in summer. *J. Geophys. Res.*, **115**, doi:10.1029/2010JD014439.

Monahan, E., D. Spiel, and K. Davidson (1986), A model of marine aerosol generation via whitecaps and wave disruption, in Oceanic Whitecaps and Their Role in Air–Sea Exchange, pp. 167–174, D. Reidel, Norwell, Mass.

Mongin, M., R. Matear, and M. Chamberlain, 2011: Seasonal and spatial variability of remotely sensed chlorophyll and physical fields in the SAZ-Sense region. Deep Sea Research Part II: *Topical Studies in Oceanography*, **58**, 2082–2093, doi:10.1016/j.dsr2.2011.06.002.

Moore, J. K., and M. R. Abbott, 2000: Phytoplankton chlorophyll distributions and primary production in the Southern Ocean. *J. Geophys. Res.,* **105**, 28 709–28 722, doi:10.1029/1999JC000043

Moreau, S., and Coauthors, 2017: Eddy-induced carbon transport across the Antarctic Circumpolar Current: Eddy-Induced Carbon Transport. *Global Biogeochemical Cycles*, doi:10.1002/2017GB005669.

Murray, B. J., D. O'Sullivan, J. D. Atkinson, and M. E. Webb, 2012: Ice nucleation by particles immersed in supercooled cloud droplets. *Chemical Society Reviews*, **41**, 6519, doi:10.1039/c2cs35200a.

Niemand, M., and Coauthors, 2012: A Particle-Surface-Area-Based Parameterization of Immersion Freezing on Desert Dust Particles. *J. Atmos. Sci.,* 69, 3077–3092, https://doi.org/10.1175/JAS-D-11-0249.1

O'Dowd, C. D., and Coauthors, 2004: Biogenically driven organic contributions to marine aerosol. *Nature*, **431**, 676-680, doi: 10.1038/nature02959.

——, and Coauthors, 2015: Connecting marine productivity to sea-spray via nanoscale biological processes: Phytoplankton Dance or Death Disco? *Sci. Rep.*, **5**, 14883, doi:10.1038/srep14883.

Oppo, C., S. Bellandi, N. Degli Innocenti, A. M. Stortini, G. Loglio, E. Schiavuta, and R. Cini, 1999: Surfactant components of marine organic matter as agents for biogeochemical fractionation and pollutant transport via marine aerosols. *Marine Chemistry*, **63**, 235–253.

O'Sullivan, D., and Coauthors, 2014: Ice nucleation by fertile soil dusts: relative importance of mineral and biogenic components, *Atmos. Chem. Phys.,* **14**, 1853-1867, https://doi.org/10.5194/acp-14-1853-2014.

Ovadnevaite, J., and Coauthors, 2011: Detecting high contributions of primary organic matter to marine aerosol: A case study, *Geo. Res. Lett.,* **38**, L02807.

——, D. Ceburnis, M. Canagaratna, H. Berresheim, J. Bialek, G. Martucci, D. R. Worsnop, and C. O'Dowd, 2012: On the effect of wind speed on submicron sea salt mass concentrations and source fluxes. *J. Geophys. Res. Atmos.*, **117**, D16201, doi:10.1029/2011JD017379.

——, de Leeuw, G., Ceburnis, D., Monahan, C., Partanen, A. I., Korhonen, H., & O'Dowd, C. D., 2014: A sea spray aerosol flux parameterization encapsulating wave state. *Atmos. Chem. Phys.*, *14*(4), 1837.

Patterson, J. P., and Coauthors, 2016: Sea Spray Aerosol Structure and Composition Using Cryogenic Transmission Electron Microscopy. *ACS Central Science*, **2**, 40–47, doi:10.1021/acscentsci.5b00344.

Pósfai, M., J. Li, J. R. Anderson, and P. R. Buseck, 2003: Aerosol bacteria over the Southern Ocean during ACE-1. *Atmospheric Research*, **66**, 231–240, doi:10.1016/S0169-8095(03)00039-5.

Prather, K. A., and Coauthors, 2013: Bringing the ocean into the laboratory to probe the chemical complexity of sea spray aerosol. *Proceedings of the National Academy of Sciences*, **110**, 7550–7555, doi:10.1073/pnas.1300262110.

Prenni, A. J., P. J. Demott, D. C. Rogers, S. M. Kreidenweis, G. M. Mcfarquhar, G. Zhang, and M. R. Poellot, 2009: Ice nuclei characteristics from M-PACE and their relation to ice formation in clouds. *Tellus B*, **61**, 436–448, doi:10.1111/j.1600-0889.2009.00415.x.

Pruppacher, H. R., and J. D. Klett, 1997: Microphysics of Clouds and Precipitation, 2nd ed., Springer, New York.

Pummer, B. G., and Coauthors, 2015: Ice nucleation by water-soluble macromolecules. *Atmos. Chem. Phys.*, **15**, 4077–4091, 2015.

Qiu, Y., N. Odendahl, A. Hudait, R. H. Mason, A. K. Bertram, F. Paesani, P.J. DeMott, and V. Molinero, 2016: Ice nucleation efficiency of hydroxyilated organic surfaces is controlled by their structural fluctuations and mismatch to ice, *J. Amer. Chem. Soc.*, **139**, 3052-3064, doi:10.1021/jacs.6b12210.

Quinn, P. K., D. J. Coffman, J. E. Johnson, L. M. Upchurch, and T. S. Bates, 2017: Small fraction of marine cloud condensation nuclei made up of sea spray aerosol. *Nature Geoscience*, **10**, 674–679, doi:10.1038/ngeo3003.

Rinaldi, M., and Coauthors, 2009: On the representativeness of coastal aerosol studies to open ocean studies: Mace Head–a case study. *Atmos. Chem. Phys.*, **9**, 9635–9646.

——, and Coauthors, 2010: Primary and Secondary Organic Marine Aerosol and Oceanic Biological Activity: Recent Results and New Perspectives for Future Studies, *Adv. in Meteor,* doi:10.1155/2010/310682

——, and Coauthors, 2013: Is chlorophyll-a the best surrogate for organic matter enrichment in submicron primary marine aerosol?, *J. Geophys. Res. Atmos.*, **118**, 4964–4973, doi:10.1002/jgrd.50417.

Rogers, D. C., P. J. DeMott, S. M. Kreidenweis, and Y. Chen, 2001: A continuous-flow diffusion chamber for airborne measurements of ice nuclei. *Journal of Atmospheric and Oceanic Technology*, **18**, 725–741.

Rogers, D. C., 1988: Development of a continuous flow thermal gradient diffusion chamber for ice nucleation studies. *Atmos. Res.*, **22**(2), 149-181.

Romay, F. J., D. L. Roberts, V. A. Marple, B. Y. H. Liu, and B. A. Olson, 2002: A High-Performance Aerosol Concentrator for Biological Agent Detection. *Aerosol Science and Technology*, **36**, 217–226, doi:10.1080/027868202753504074.

Rosinski, J., P. L. Haagenson, C. T. Nagamoto, and F. Parungo, 1987: Nature of ice-forming nuclei in marine air masses. *J. Aerosol Sci.*, 18, 291-309, doi:10.1016/0021-8502(87)90024-3.

Sabbaghzadeh, B., R. C. Upstill-Goddard, R. Beale, R. Pereira, and P. D. Nightingale, 2017: The Atlantic Ocean surface microlayer from 50°N to 50°S is ubiquitously enriched in surfactants at wind speeds up to 13 m s^{-1}: Atlantic Ocean Surfactants. *Geophys.l Res. Let.*, **44**, 2852–2858, doi:10.1002/2017GL072988.

Santachiara, G., L. Di Matteo, F. Prodi, and F. Belosi, 2010: Atmospheric particles acting as Ice Forming Nuclei in different size ranges. *Atmos. Res.*, **96**, 266–272, doi:10.1016/j.atmosres.2009.08.004.

Schill, G. P., and Coauthors, 2016: Ice-nucleating particle emissions from photochemically aged diesel and biodiesel exhaust: Diesel Exhaust Ice-Nucleating Particles. *Geophys. Res. Let.*, **43**, 5524–5531, doi:10.1002/2016GL069529

Schnell, R. C., and G. Vali, 1974: Freezing nuclei in marine waters. *Tellus*, **27**, 321–323. doi:10.1111/j.2153-3490.1975.tb01682.x

——, and G. Vali, 1976: Biogenic ice nuclei: Part I. Terrestrial and marine sources, *J. Atmos. Sci.*, **33**(8), 1554-1564.

——, 1977: Ice Nuclei in Seawater, Fog Water and Marine Air off the Coast of Nova Scotia: Summer, 1975. *J. Atmos. Sci.*, **34**, 1299-1305.

Stein, A.F., Draxler, R.R, Rolph, G.D., Stunder, B.J.B., Cohen, M.D., and Ngan, F., (2015). NOAA's HYSPLIT atmospheric transport and dispersion modeling system, *Bull. Amer. Meteor.* Soc., 96, 2059-2077, doi: 10.1175/BAMS-D-14-00110.1.

Stokes, M. D., G. B. Deane, K. Prather, T. H. Bertram, M. J. Ruppel, O. S. Ryder, J. M. Brady, and D. Zhao, 2013: A Marine Aerosol Reference Tank system as a breaking wave analogue for the production of foam and sea-spray aerosols. *Atmos. Meas. Tech.*, **6**, 1085–1094, doi:10.5194/amt-6-1085-2013.

Sultana, C. M., D. B. Collins, and K. A. Prather, 2017a: Effect of Structural Heterogeneity in Chemical Composition on Online Single-Particle Mass Spectrometry Analysis of Sea Spray Aerosol Particles. *Environ. Sci. & Tech.*, **51**, 3660–3668, doi:10.1021/acs.est.6b06399.

——, H. Al-Mashat, and K. A. Prather, 2017b: Expanding Single Particle Mass Spectrometer Analyses for the Identification of Microbe Signatures in Sea Spray Aerosol. *Anal. Chem.*, doi:10.1021/acs.analchem.7b00933.

Tobo, Y., and Coauthors, 2013: Biological aerosol particles as a key determinant of ice nuclei populations in a forest ecosystem: Biological Ice Nuclei In Forest. J. *Geophys. Res. Atmos.*, **118**, 10,100-10,110, doi:10.1002/jgrd.50801.

——, and Coauthors, 2014: Organic matter matters for ice nuclei of agricultural soil origin, *Atmos. Chem. Phy.,* **14**(16), 8521-8531, doi: 10.5194/acp-14-8521-2014.

Trenberth, K. E., and J. T. Fasullo, 2010: Simulation of Present-Day and Twenty-First-Century Energy Budgets of the Southern Oceans. *J. Climate*, **23**, 440–454, doi:10.1175/2009JCLI3152.1.

Twohy, C. H., and Coauthors, 2016: Abundance of fluorescent biological aerosol particles at temperatures conducive to the formation of mixed-phase and cirrus clouds. *Atmos. Chem. and Phys.*, **16**, 8205–8225, doi:10.5194/acp-16-8205-2016.

Vali, G., 1971: Quantitative evaluation of experimental results on the heterogeneous freezing nucleation of supercooled liquids. *J. Atmos. Sci.,* **28**, 402–409, doi:10.1175/1520-0469(1971)028,0402:QEOERA.2.0.CO;2.

Vali, G., P. J. DeMott, O. Möhler, and T. F. Whale, 2015: Technical Note: A proposal for ice nucleation terminology. *Atmos. Chem. and Phys.*, **15**, 10263–10270, doi:10.5194/acp-15-10263-2015.

van Pinxteren, M, et al 2017 The influence of environmental drivers on the enrichment of organic carbon in the sea surface microlayer and in submicron aerosol particles – measurements from the Atlantic Ocean. *Elem Sci Anth,* 5: 35, DOI: https://doi.org/10.1525/elementa.225

Verheggen, B., and Coauthors, 2007: Aerosol partitioning between the interstitial and the condensed phase in mixed-phase clouds. *J. Geophys. Res.*, **112**, doi:10.1029/2007JD008714.

von der Weiden, S. L., F. Drewnick, and S. Borrmann, 2009: Particle Loss Calculator–a new software tool for the assessment of the performance of aerosol inlet systems. *Atmos. Meas. Tech*, **2**, 479–494.

Wang, X., and Coauthors, 2015: Microbial Control of Sea Spray Aerosol Composition: A Tale of Two Blooms. *ACS Central Science*, **1**, 124–131, doi:10.1021/acscentsci.5b00148.

——, and Coauthors, 2017: The role of jet and film drops in controlling the mixing state of submicron sea spray aerosol particles. *Proceedings of the National Academy of Sciences*, **114**, 6978–6983, doi:10.1073/pnas.1702420114.

Wilson, T. W., and Coauthors, 2015: A marine biogenic source of atmospheric ice-nucleating particles. *Nature*, **525**, 234–238, doi:10.1038/nature14986.

Wurl, O., E. Wurl, L. Miller, K. Johnson, and S. Vagle, 2011: Formation and global distribution of sea-surface microlayers. *Biogeosciences*, **8**, 121–135, doi:10.5194/bg-8-121-2011.

Xu, L., L. M. Russell, and S. M. Burrows, 2016: Potential sea salt aerosol sources from frost flowers in the pan-Arctic region: Salt Aerosol Sources From Frost Flowers. *J. Geophys. Res. Atmos.*, **121**, 10,840-10,856, doi:10.1002/2015JD024713.

Young, I. R., 1999: Seasonal variability of the global ocean wind and wave climate. *International Journal of Climatology*, **19**, 931–950.

Zelenyuk, A., D. Imre, L. A. Cuadra-Rodriguez, and B. Ellison, 2007: Measurements and interpretation of the effect of a soluble organic surfactant on the density, shape and water uptake of hygroscopic particles. *Journal of Aerosol Science*, **38**, 903–923, doi:10.1016/j.jaerosci.2007.06.006.

Zhang, Z.B., Liu, L.S., Wu, Z.J., Li, J., Ding, H.B., 1998. Physicochemical studies of the sea surface microlayer – I. Thickness of the sea surface microlayer and its experimental determination. *J. Colloid Interface Sci.,* **204**, 294–299.

APPENDIX I. ICE SPECTROMETER MEASUREMENT DETAILS

Details for the ice spectrometer can be found in Section 2.4.a.ii, but each step of the IS process is outlined here. First, filters are pre-cleaned by soaking filters in 10% H_2O_2 for 10 and 60 minutes, respectively, and three rinses with deionized water. The deionized water used for cleaning was 18 mΩ, 0.2 μm pore filtered. Finally, filters rinsed in deionized water that had been passed through a 0.02 μm pore Anotop syringe filter (Whatman). Cleaning was also applied to the filter holders used in the CAICE studies. Filters and filter holders were then placed on aluminum foil in a laminar flow hood under high-efficiency filtered airflow to dry. Open-faced Nalgene analytical filter units (Nalgene Nunc Int.) were used for all other studies presented in this work. These open-faced filters were pre-packed with the pre-cleaned filters, which were overlaid on top of the existing 0.45 μm filter, placed in Ziplock® bags and shipped to each field location for sampling. After collection, filters were removed from filter holders with sterile tweezers (Figure S *1*a) and stored in sterile petri dishes (sealed with Parafilm) and stored frozen (-20 °C) until they were processed.

Photos of filter processing by the IS are provided in Figure S *1*. After collection, filters were removed from the storage petri dishes using sterile tweezers. Filters were immersed into 5 mL of deionized water (0.02 μm pore filtered). For some samples, 6 mL of deionized water (0.02 μm pore filtered) was used to generate larger sample volumes. The re-suspension volumes are included in the final calculations of n_{INPs}. To release particles from filters, an end-over-end shaker (Rototorque, Cole-Palmer) was used to shake the immersed filters for 20 minutes (Figure S *1*b). The resulting liquid is the filter sample suspension. A sample suspension may also be a sample of bulk seawater or sea surface microlayer, which does not require the filter removal or

shaking steps. The sample suspensions were then dispensed (50 μL aliquots) into 24 or 32 wells of a PCR tray (96-well plate, μCycler) that were then inserted into the IS aluminum blocks, shown in Figure S *1*c. During an IS "run", coolant is circulated through copper pipes embedded within heat exchange plates that encase the sides and base of the IS, cooling the IS over its effective range, from 0 °C to -27 °C, at 0.33 °C min^{-1}. Insulation also surrounds the IS, as shown in Figure S *1*c. As the temperature of the IS decreases, wells containing INPs active at the supercooled temperature freeze, resulting in an opaque well (Figure S *1*d). Frozen wells are counted at 0.5 – 1 °C intervals and were used to determine n_{INPs} as a function of temperature, following methods developed by *Vali* (1971). For each IS run, deionized (0.02 μm pore filtered) water is also dispensed into 24 or 32 wells to measure the background present in the IS. This is depicted in Figure S *1*d, where the left 3 columns of wells contain deionized (0.02 μm pore filtered) water (DI well array) and the right 3 columns of wells contain a filter sample suspension (Sample well array). For each measured temperature, the number of frozen wells in the DI well array are subtracted from the number of frozen wells in the Sample well array.

The detection limit of the ice spectrometer ranged from 0.00013 to 0.0014 L^{-1} for the MHD study and from 0.00005 to 0.00012 L^{-1} for the CAPRICORN study. Since the detection of a freezing event is binary (a well is frozen or not frozen), the first frozen well is equal to the detection limit. This detection limit describes the minimum level of INP number concentrations measureable by the IS, accounting for the number of wells used in the IS (typically 32 wells for these studies), the volume of liquid used in each well (typically 50 microliters for these studies), the volume of water used to re-suspend the sample (typically 6 mL for aerosol samples) and the volume of air sampled for each filter. The variability in detection limits for this work is mainly

due to variability in the volume of air sampled per filter, where higher sample volumes correspond to lower detection limits.

Method blanks were collected during each study as described here. Filter holders were loaded with a cleaned filter and placed into the sampling apparatus (e.g., connected to the sampling lines or placed onto the ring stand). For the open-faced filter holders, the cap to the holder was removed briefly. The filter holders were then placed back into their storage bag and filter removal and processing followed the sample filter protocol as outlined above. During the CAICE studies, 3 blanks were collected and analyzed, shown in Figure S 2. INP measurements of the rinse water from these blank samples were subtracted from the counts made on collected samples prior to computation of volumetric concentrations of INPs in air.

During the Mace Head campaign, 7 blanks were collected and corrected frozen fractions are shown in Figure S 3. Due to slightly higher background concentrations during this campaign and the higher number of blanks, a different approach for correcting for method background was used. To determine the study average background INPs, we combined all blank filters by summing the number of wells that froze across all blanks (i.e., 7*32), shown in Figure S 4 and tabulated in Table S 1. To correct data, blank INP per filter (estimated blank frozen fraction using the exponential fit, shown in Figure S 4, and multiplying by the number of wells in the sample) was subtracted from the INP per filter detected from the filter. The corrected INP per filter was then converted back to INP per L of air by dividing by the total volume of air sampled by the filter. Finally, the 95% confidence intervals were also corrected by simply multiplying the initial (uncorrected) confidence interval by the ratio of uncorrected to corrected INP per L. Measurements were thrown out if corrected INP number concentrations or their $95^{\%}$ confidence interval was below zero. An example of the change in INP per L due to this correction is

provided in Figure S 5 for one of the cleanest samples collected during the MHD campaign. The same procedure for correcting samples for blanks was followed for the CAPRICORN study, where 4 blanks were collected, shown in Figure S 6. To illustrate the difference between the INPs present on the filter without air sampled through them (i.e., blank filters) and the filters from a measurement campaign, simulated INP number concentrations for the upper and lower quartile of sample volumes collected during the MHD and CAPRICORN studies are shown in Figure S *7* and Figure S *8*, respectively. Method blanks for the heating, size and H_2O_2 treatments are provided in Figure S 9.

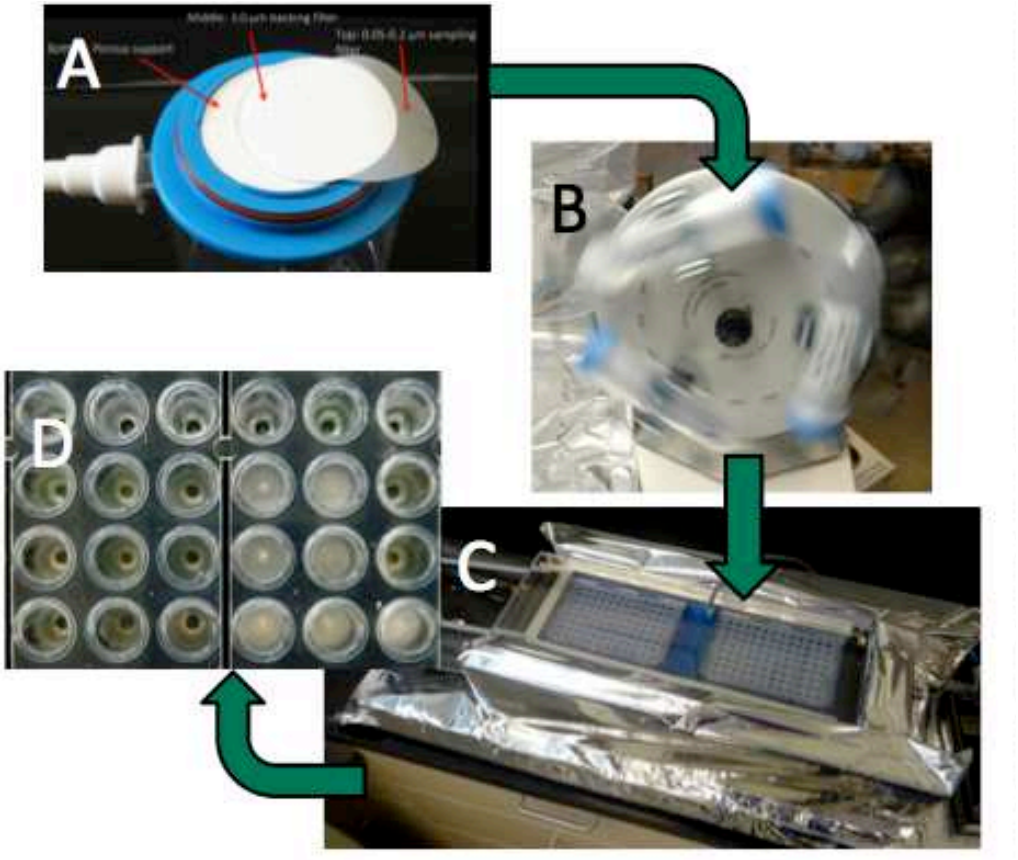

Figure S 1. Photos of the IS spectrometer analysis process: A) filter removal from an open-faced filter holder; B) making sample suspension by shaking filters in deionized water using an end-over-end shaker (Rototorque, Cole-Palmer); C) two 96-well PCR plates, containing sample solutions, in the IS; D) a selection of wells, where the left 3 columns of wells contain deionized water and the right 3 columns contain a sample solution. Opaque wells are frozen wells.

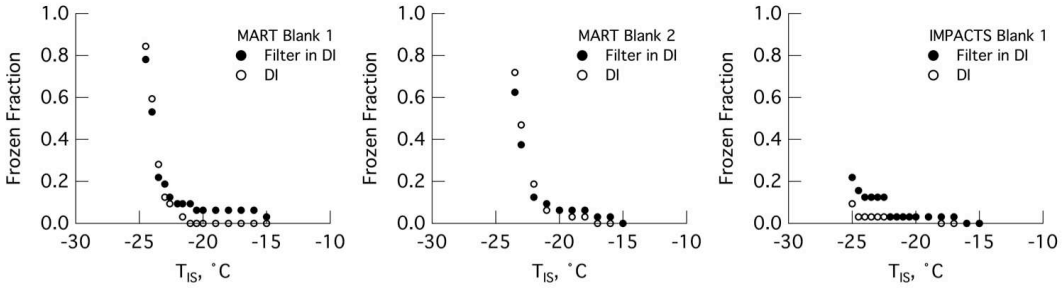

Figure S 2. Frozen fraction temperature spectra for blank filters suspended in DI water (filled circle markers) and DI water alone (open circle markers). Error bars are not shown for clarity, but there were no significantly differences between numbers of INPs per mL for DI with and without blank filters.

Table S 1. Tabulated values for each blank (1-7), total frozen wells across all temperatures, and average frozen fractions (i.e., total/7*32).

TEMP	BLANK1	BLANK2	BLANK3	BLANK4	BLANK5	BLANK6	BLANK7	TOTAL	TOTAL/(7*32)
-13	0	0	1	0	0	0	0	1	0.0045
-13.5	0	0	1	0	0	0	1	2	0.0089
-14	0	0	1	0	0	0	2	3	0.0134
-14.5	0	0	1	0	0	0	2	3	0.0134
-15	0	0	1	0	0	1	2	4	0.0179
-15.5	0	0	1	1	0	1	3	6	0.0268
-16	0	0	1	2	0	1	3	7	0.0313
-16.5	0	0	1	2	0	1	2	6	0.0268
-17	0	0	1	2	0	2	2	7	0.0313
-17.5	0	0	1	2	0	1	2	6	0.0268
-17.7	0	0	1	3	0	0	2	6	0.0268
-18	0	0	1	2	0	1	2	6	0.0268
-18.5	0	0	2	2	0	1	2	7	0.0313
-19	0	0	2	2	0	0	4	8	0.0357
-19.5	0	1	3	2	0	0	5	11	0.0491
-20	0	2	2	3	0	1	5	13	0.0580
-20.5	0	2	4	3	0	2	6	17	0.0759
-21	0	2	5	5	0	2	6	20	0.0893
-21.5	0	3	8	5	0	2	6	24	0.1071
-22	0	3	7	4	0	2	6	22	0.0982
-22.5	0	5	8	4	0	4	8	29	0.1295
-23	0	5	9	5	0	7	10	36	0.1607
-23.5	0	6	11	5	0	7	11	40	0.1786
-24	1	7	12	6	0	10	13	49	0.2188
-24.5	4	11	12	6	0	9	15	57	0.2545
-25	5	13	13	9	1	10	16	67	0.2991
-25.5	7	16	14	13	2	9	17	78	0.3482
-26	8	18	18	18	4	11	18	95	0.4241
-26.5	13	17	19	17	6	12	21	105	0.4688
-27	15	22	20	20	9	14	20	120	0.5357

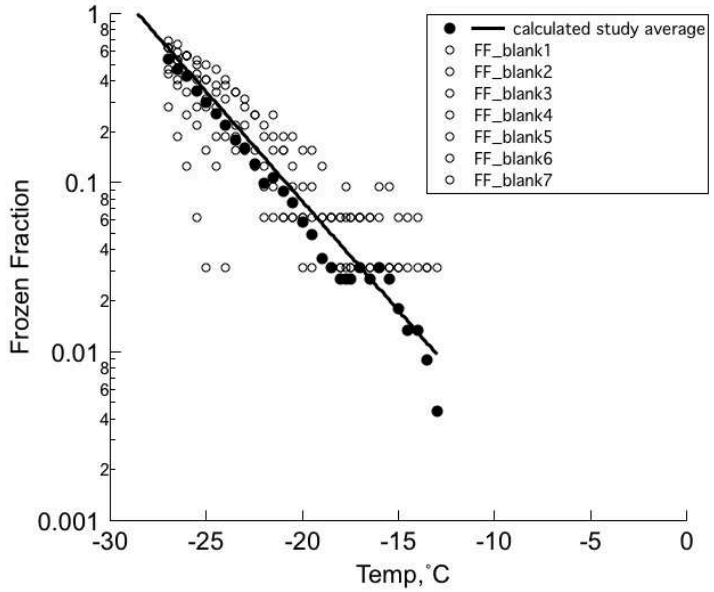

Figure S 3. Frozen fraction temperature spectra for blanks collected during the MHD campaign. Frozen fractions are corrected for DI background measured on the same day that the blank filter was analyzed.

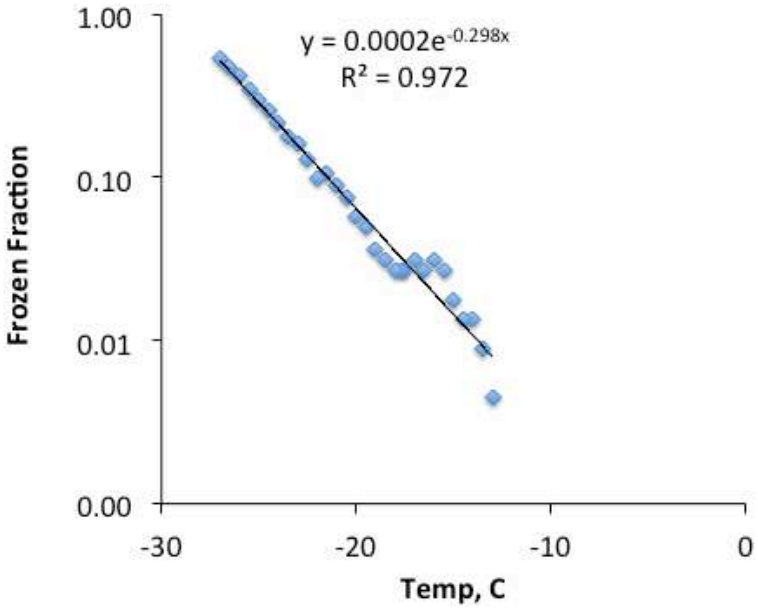

Figure S 4. Average frozen fractions found on blank samples (calculated by summing the frozen wells across all 7 blanks and dividing by 32*7). The blank line indicates the exponential fit to data.

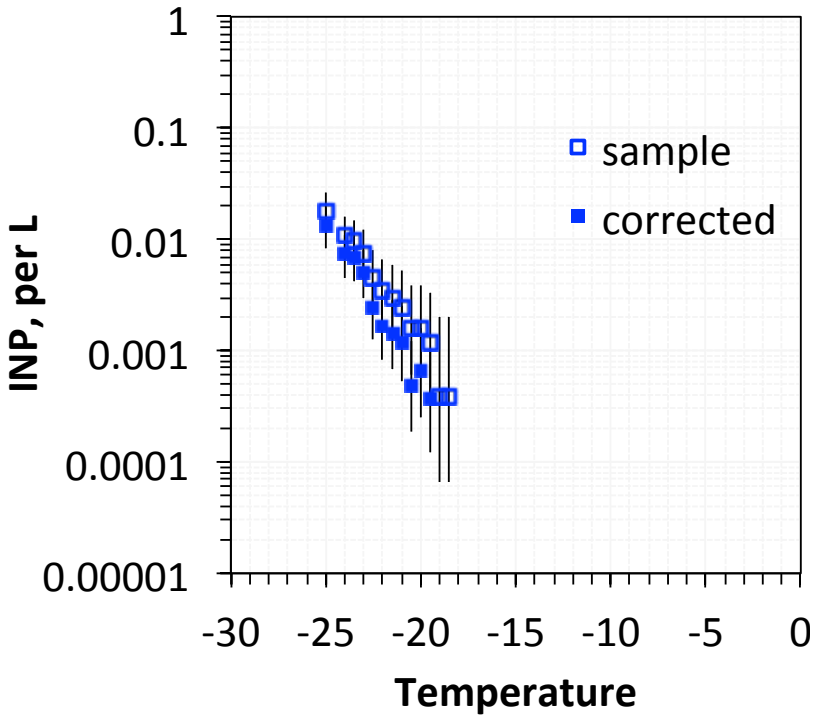

Figure S 5. Example of the change in nINPs that results from correcting for blank filters. This filter (#21) was one of the cleanest samples during the MHD study and thus is most sensitive to blank contamination.

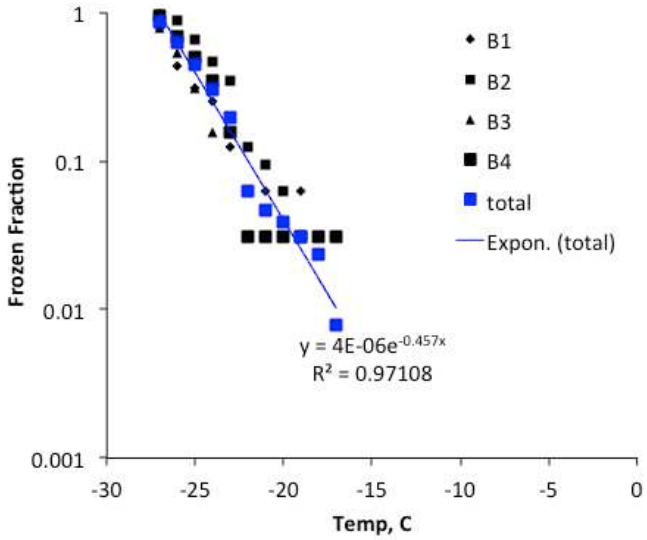

Figure S 6. Frozen fraction temperature spectra for blanks collected during the CAPRICORN campaign. Frozen fractions are corrected for DI background measured on the same day that the blank filter was analyzed. Blue markers indicate the average frozen fractions found on blank samples (calculated by summing the frozen wells across all 4 blanks and dividing by 32*4). The blue line indicates the exponential fit to data.

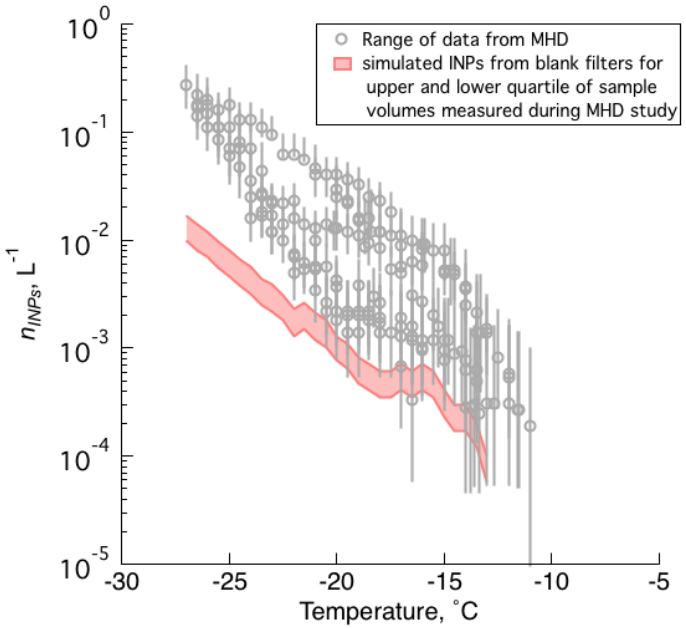

Figure S 7. INP temperature spectra for a range of samples collected at MHD (NOT corrected for blanks described by Figure S 2). Vertical error bars represent the 95% confidence interval. Red swath shows the INP concentrations simulated based on INPs present on BLANK filters for the upper (7506 L) and lower (4194 L) quartile of sample volumes from the MHD study.

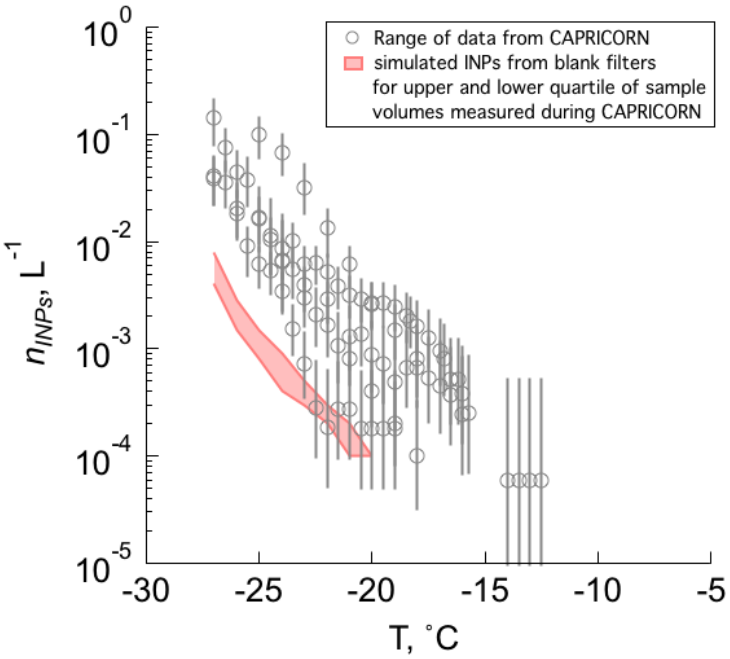

Figure S 8. INP temperature spectra for a range of samples collected during CAPRICORN (NOT corrected for blanks described by Figure S 2). Vertical error bars represent the 95% confidence interval. Red swath shows the INP concentrations simulated based on INPs present on BLANK filters for the upper (71463 L) and lower (37003 L) quartile of sample volumes from the MHD study.

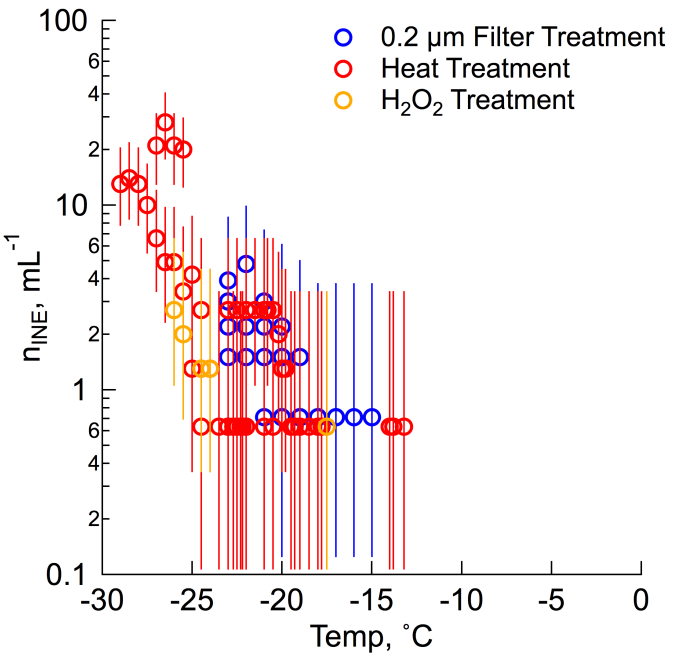

Figure S 9. Temperature spectra of ice nucleating particle (INE) number concentrations for heat (red), filter (blue), and H2O2 (orange) treatments of purified water (i.e., DI water heated or filtered).

APPENDIX II. AEROSOL CONCENTRATOR FACTORS

Aerosol concentrator factors are provided for the IMPACTS and CAPRICORN studies in

Table S 2. Concentrator factors for the IMPACTS study

IMPACTS Experimental day fraction	CF
7.44	*
8.43	*
9.44	14.70
14.02	11.50
15.03	6.40
17.00	3.60
18.02	8.40
20.01	7.50
21.01	9.20
22.97	6.60
23.96	3.50
25.97	4.80
26.95	6.10
Study Avg	**7.48**
Study Stdev	3.38

* No concentrator used

Table S 3. Concentrator factors for the CAPRICORN study.

date	CF
20160316	123.7
20160319	86.4
20160321	46.67
20160322	129.3
20160323	120.6
20160325	96.5
20160328	97.8
20160329	116.3
20160402	76.2
20160403	87.6
20160408	77.7

APPENDIX III. FREEZING POINT DEPRESSION EFFECTS

Salts present in seawater samples lead to a freezing point depression (FPD) effect that leads to a freezing temperature that is lower than the freezing temperature of the same sample absent of salts. Previous studies of seawater ice nucleating entities have accounted for the FPD effect by applying a 2 °C correction (*Schnell et al.,* 1977; *Schnell,* 1974) or by accounting for changes in water activity (*Wilson et al.,* 2015). Here, we tested changes in freezing temperature due to seawater.

Seawater that was collected from the SIO Pier on 7 January 2014 was filtered through a 0.2 μm filter. The filter was then cut in half using a sterile glass razor. One half of the filter was suspended in filtered, deionized (18 MΩ and filtered through a 0.02 μm pore Anotop syringe filter, Whatman, GE Healthcare Life Sciences) water. The other half of the filter was suspended in filtered seawater (0.02 μm pore Anotop syringe filter, Whatman, GE Healthcare Life Sciences). The two samples were then analyzed using the ice spectrometer, shown in Figure S 10. Ice nucleating entities (INEs) that were re-suspended in filtered seawater froze at colder temperatures compared to INEs re-suspended in DI water. The difference in freezing temperatures between the DI and seawater samples was greater than 2 °C and was not uniform with temperature. These data suggest a combined effect of freezing point depression and a direct inhibitory effect of salt on INEs. This combined effect was not quantified and thus a FPD correction was not applied to the seawater and SML data reported. To compare to previous studies, we estimate INE concentrations using the 2 °C correction that was used these early studies (*Schnell,* 1974; *Schnell et al.,* 1977).

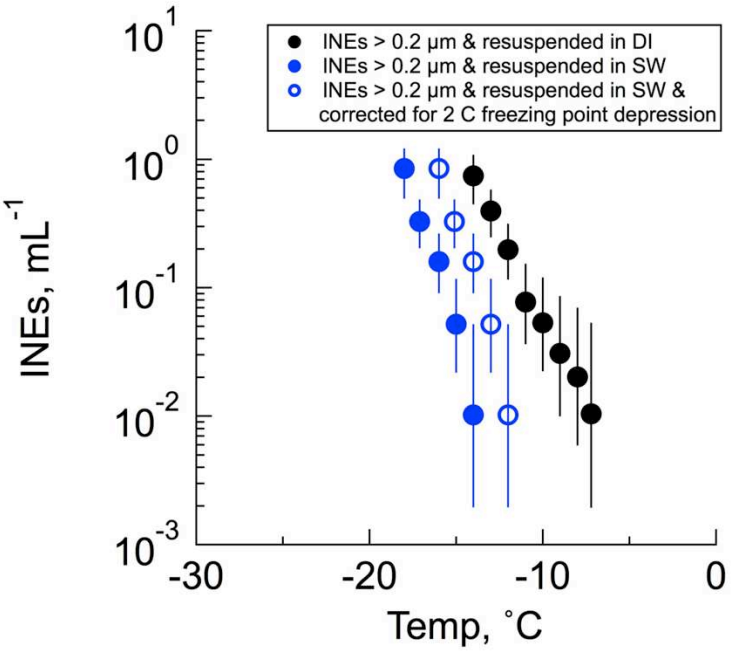

Figure S 10.INE number concentrations observed for material collected onto a 0.2 µm filter from seawater collected from the SIO pier on 7 January 2014. Material was re-suspended in distilled water (blue) and filtered seawater (red). Filled circles correspond to measured values, while open circles correspond to an estimated freezing point depression effect correction of 2 °C.

APPENDIX IV. HYSPLIT BACK TRAJECTORIES

The NOAA HY-SPLIT Trajectory Model was used to determine the origin of air masses during periods of elevated organic aerosol. GCAS 1 degree meteorological data was used for all of the back trajectories. Trajectories were forecasted 72 hr backwards from the end times listed in Table S 4 and were intended to represent filter collections during the three main organic events. The end height used for these back trajectories was 500 m.

Table S 4. Summary of end times for all HYSPLIT back trajectories used in this study.

Trajectory ID	**Trajectory end time (UTC)**
M1A	20:00:00 09 Aug 2015
M1B	13:00:00 09 Aug 2015
M2A	10:00:00 14 Aug 2015
M2B	22:00:00 13 Aug 2015
M2C	10:00:00 13 Aug 2015
M2D	22:00:00 12 Aug 2015
T1A	12:00:00 20 Aug 2015
T1B	00:00:00 20 Aug 2015
T1C	12:00:00 19 Aug 2015
T1D	00:00:00 19 Aug 2015
T1E	12:00:00 18 Aug 2015
T1F	00:00:00 18 Aug 2015
T1G	12:00:00 17 Aug 2015
T1H	00:00:00 17 Aug 2015
T1I	12:00:00 16 Aug 2015
T1J	00:00:00 16 Aug 2015
T1K	12:00:00 15 Aug 2015

APPENDIX V. INSTRUMENTATION CONTACT INFORMATION

Table S 5. Contact and affiliation information for the observational data in the studies referenced in this work: CAICE Marine aerosol reference tank (MART), Investigation into Marine PArticle Chemistry and Transfer Science (IMPACTS), CalWater-2015, Mace Head Research Station (MHD) and Clouds, Aerosols, Precipitation Radiation and atmospherIc Composition Over the southeRN ocean (CAPRICORN).

	CAICE - MART	**CAICE - IMPACTS**	**CalWater-2015**	**MHD**	**CAPRICORN**
CFDC	C. McCluskey[1]	C. McCluskey[1]	C. McCluskey[1]	-	C. McCluskey[1]
IS*	C. McCluskey[1]	C. McCluskey[1]	C. McCluskey[1]	C. McCluskey[1]	C. McCluskey[1]
HINC	-	-	-	J. Atkinson[2]	-
DFPC	-	-	-	F. Belosi[3]	-
ATOFMS	C. Sultana[4]	C. Sultana[4]	G. Cornwell[4]	-	-
Bulk TOC	B. Stone[5]	B. Stone[5]	-	-	-
AMS	-	-	-	J. Ovadnevaite[6]	-
SMPS	C. Lee[4]	C. Lee[4]	S. Atwood[1]	J. Ovadnevaite[6]	-
APS	C. Lee[4]	C. Lee[4]		J. Ovadnevaite[6]	-
TEOM	-	-		Darius	-
Neph	-	-	-	-	C. McCluskey[1]
Chl *a*	F. Malfatti[7]	F. Malfatti[7]	-	Matteo Rinaldi[3]	S. Moreau[6]
Enzyme act.	F. Malfatti[7]	F. Malfatti[7]	-	-	-
HB counts	F. Malfatti[7]	F. Malfatti[7]	-	-	-

1. Department of Atmospheric Science, Colorado State University, Fort Collins, CO, USA.
2. Institute of Atmospheric and Climate Science, ETH Zurich, Switzerland
3. Institute of Atmospheric Sciences and Climate, CNR, Bologna, Italy
4. Department of Chemistry, University of California San Diego, La Jolla, California, USA 92093
5. Department of Chemistry, University of Iowa, Iowa City, Iowa, USA 52242
6. School of Physics, National University of Ireland Galway, Galway, Ireland
7. OGS (Istituto Nazionale di Oceanografia e di Geofisica Sperimentale), Trieste, 34100, Italy